Universitat de València

Instituto de Investigación Sanitaria La Fe
Universitat de València

PHD Program in Physiology
Department of Physiology
Faculty of Medicine and Dentistry

Metabolomic approach to physiological circumstances and pathological conditions in neonatology

***Doctoral Thesis** presented by*

José David Piñeiro Ramos

Directed by:

Dra. Julia Kuligowski
Dr. Máximo Vento Torres

Tutored by:

Dra. Mª Rosario Salvador Palmer

Valencia, October 2022

Dña. Julia Kuligowski, Investigadora Posdoctoral MIGUEL SERVET, del Grupo de Investigación en Perinatología del Instituto de Investigación Sanitaria La Fe de Valencia,

D. Máximo Vento Torres, Investigador Principal del Grupo de Investigación en Perinatología del Instituto de Investigación Sanitaria La Fe de Valencia,

CERTIFICAN:

Que la presente memoria, titulada "Metabolomic approach to physiological circumstances and pathological conditions in neonatology", corresponde al trabajo realizado bajo su dirección por **D. José David Piñeiro Ramos**, para su presentación como Tesis Doctoral en el Programa de Doctorado en Fisiología de la Universitat de València.

Y para que conste firman el presente certificado en Valencia, a 26 de octubre de 2022.

Julia Kuligowski Máximo Vento Torres

A mis padres, a mi hermano Alex y a Alf

Agradecimientos

Quien me conoce ya sabe que no me gustan este tipo de cosas, pero no haría bien si no agradeciera a las diferentes personas que me han ayudado a llegar hasta aquí.

Al grupo de investigación en perinatología, por haberme acogido durante todos estos años, sobre todo a Julia y a Max, mis directores, que me han guiado por todo el camino y me han ayudado siempre que lo he necesitado.

A la Universitat de València, por darme la posibilidad de hacer realidad la consecución de este trabajo y, en especial, a Rosario que me ha guiado siempre que lo he necesitado.

A mis padres, por el apoyo que me ha ido dando durante todos estos años.

A Alex, mi hermano, por estar siempre ahí, tanto en los buenos como en los malos momentos.

A mis amigos, en especial a Toni y Paco, personas que han estado ahí pasara lo que pasara.

Y a todas y cada una de las personas, que no hace falta que nombre, pero que saben perfectamente que les estoy totalmente agradecido.

Mi más sincera gratitud.

Índice

De acuerdo con las regulaciones aprobadas por la Escuela de Doctorado y el Comité Académico del Programa de Doctorado en Fisiología de la Universitat de València, la presente Tesis Doctoral se ha estructurado en el formato de compendio de publicaciones. El núcleo de la tesis está compuesto por cuatro artículos originales de primer autor, publicados en revistas Q1 y Q2 según la base de datos "*Journal Citation Reports*". Además de un tercer artículo (capítulo 3) en proceso de publicación.

Metabolic Phenotypes of Hypoxic-Ischemic Encephalopathy with Normal vs. Pathologic Magnetic Resonance Imaging Outcomes. **Piñeiro-Ramos JD**, Núñez-Ramiro A, Llorens-Salvador R, Parra-Llorca A, Sánchez-Illana Á, Quintás G, Boronat-González N, Martinez Rodilla J, Kuligowski J, Vento M, The Hypotop Study Group. **Metabolites**. 2020 Mar 14;13(3):109. doi10.3390/metabo10030109.
Factor de impacto en Journal Citation Reports (JCR) 2021: 5.581
Categoría y posición (JCR) 2021: Biochemistry & Molecular Biology 90/297, Q2.

Noninvasive monitoring of evolving urinary metabolic patterns in neonatal encephalopathy. **Piñeiro-Ramos JD**, Núñez-Ramiro A, López-Gonzálvez Á, Solar-García A, Albiach-Delgado A, Martinez Rodilla J, Llorens-Salvador R, Sanjuan-Herraez D, Quintás G, Barbas C, Kuligowski J, Vento M, The Hypotop Study Group. **Pediatric Research.** 2021 May 5. doi: 10.1038/s41390-021-01553-z.
Factor de impacto en Journal Citation Reports (JCR) 2021: 3.953
Categoría y posición (JCR) 2021:Pediatrics 26/130, Q1

Effect of donor human milk on host-gut microbiota and metabolic interactions in preterm infants. **Piñeiro-Ramos JD**, Parra-Llorca A, Ten-Doménech I, Gormaz M, Ramón-Beltrán A, Cernada M, Quintás G, Collado MC, Kuligowski J, Vento M. **Clinical Nutrition**. 2021 Mar; 40(3):1296-1309. doi: 10.1016/j.clnu.2020.08.013.
Factor de impacto en Journal Citation Reports (JCR) 2021: 7.643
Categoría y posición (JCR) 2021: Nutrition & Dietetics 13/90, Q1

A reductive metabolic switch protects infants with transposition of great arteries undergoing atrial septostomy against oxidative stress. **Piñeiro-Ramos JD**, Rahkonen O, Korpioja V, Quintás G, Pihkala J, Pitkänen-Argillander O, Rautiainen P, Andersson S, Kuligowski J, Vento. **Antioxidants**. 2021 Sep 22:10(10):1502. doi: 10.3390/antiox10101502.
Factor de impacto en Journal Citation Reports (JCR) 2021: 7.675
Categoría y posición (JCR) 2021: Chemistry, medicinal 4/63, D1

La tesis también incluye un resumen global que consiste en un capítulo de introducción que expone los antecedentes descritos en la bibliografía científica y su contextualización sobre las diferentes patologías y condiciones fisiológicas del recién nacido y del recién nacido prematuro junto con un enmarque de la metodología empleada, concretamente metabolómica, técnica ómica emergente que juega un papel principal en el desarrollo de la tesis. Un capítulo con la hipótesis y objetivos de la presente Tesis Doctoral, un capítulo que estipula la metodología realizada para la consecución de los objetivos, un capítulo que contiene los principales resultados y un capítulo final que expone las conclusiones generales junto con el trabajo futuro, justificando la aportación original.

Resumen global

Introducción

La aparición de la medicina personalizada como campo en auge, tiene como objetivo mejorar el diagnóstico, la respuesta terapéutica, así como el pronóstico de cualquier enfermedad. El acceso a biomarcadores, basándose en métodos de análisis molecular de cualquier índole, incluyendo pruebas a nivel genético, proteico o metabólico, abre la puerta a ajustar cualquier tratamiento a las necesidades de cada paciente de manera individual y, por lo tanto, mejorar el pronóstico posterior. Los desarrollos tecnológicos, combinados con las mejoras en técnicas bioinformáticas, han revolucionado la metodología bioanalítica permitiendo el análisis "ómico" a cualquier nivel, desde mutaciones del genoma, metilación del DNA, expresión de RNA codificante y no codificante, así como proteínas y metabolitos. Estas nuevas tecnologías generan y agrupan esta información con el fin de obtener una visión global del sistema de estudio.

La metabolómica, la metodología usada mayoritariamente en esta tesis doctoral, es la más reciente de las técnicas ómicas y ha emergido con fuerza desde principios de la década de los noventa [1]. El término *metabolome*, introducido por Oliver et al en 1998, hace referencia al estudio sistemático de todas las moléculas de bajo peso molecular pertenecientes a huellas metabólicas que existen en los seres humanos y otros sistemas vivos [2]. Es una herramienta de investigación emergente integrada en la biología de sistemas, que aporta información dinámica y que permite estudiar el conjunto de metabolitos presentes en un medio biológico, lo que la convierte en una herramienta fundamental

en diferentes campos tales como la fisiología, el estudio de enfermedades, el descubrimiento de nuevos fármacos, la nutrición y la biomedicina. El fenotipado metabólico es de especial utilidad en la fase de generación de hipótesis y para la búsqueda de nuevos biomarcadores en matrices biológicas. Los metabolitos endógenos al igual que otras sustancias provenientes del medioambiente, de la nutrición, de los tóxicos y/o fármacos son típicamente estudiados en análisis metabolómicos. Para la detección de estas sustancias, los análisis metabolómicos se dividen en tres vertientes diferenciadas; en análisis metabolómico no dirigido, semi-dirigido y dirigido.

Los métodos analíticos basados en una estrategia de metabolómica dirigida fueron de los primeros en desarrollarse y consisten en la cuantificación de un número relativamente pequeño de metabolitos, típicamente de una o varias vías metabólicas y/o bioquímicas relacionadas entre sí, conocidos *a priori*. Existe una gran cantidad de literatura en la que se describen protocolos optimizados para la preparación y el análisis de clases específicas de metabolitos en múltiples matrices biológicas. Las principales ventajas de utilizar este enfoque de estudios de metabolómica dirigida son su especificidad, reproducibilidad, alta sensibilidad y alto rendimiento.

Por otro lado, el desarrollo de técnicas analíticas de alto rendimiento cada vez más sensibles ha renovado el interés en la metabolómica no-dirigida. Se utilizan varias plataformas analíticas complementarias para analizar los cambios en las concentraciones y flujos metabólicos. Entre ellas se encuentra la resonancia magnética nuclear ^{1}H (^{1}H-RMN) [3], espectrocopía ^{13}C-RMN [4], espectrometría

de masas de infusión directa (DI)-MS [5], cromatografía de gases (GC)-MS [6], electroforesis capilar (CE)-MS [7] y cromatografía líquida (LC)-MS [8]. Debido a la gran diversidad de propiedades fisicoquímicas y concentraciones que varían en varios órdenes de magnitud entre los metabolitos endógenos, no existe una única técnica analítica que permita medir completamente el perfil cualitativo o cuantitativo del metaboloma. A pesar de ello, la LC-MS se está convirtiendo en la principal tecnología aplicada en el campo debido a su mayor sensibilidad, selectividad, capacidades de detección, rango dinámico y rendimiento en comparación con las otras técnicas. Los métodos de LC-MS no-dirigidos apuntan a la detección global de todos los metabolitos de bajo peso molecular en las muestras de estudio. La capacidad de detección de LC-MS conducen a enormes cantidades de datos y esto hace que la instrumentación evolucione rápidamente hacia equipos más sofisticados. Una de las principales dificultades del desarrollo de métodos analíticos siguiendo una estrategia metabolómica no-dirigida radica en la naturaleza heterogénea de los metabolitos de cualquier sistema biológico, de los cuales presentan un amplio intervalo de polaridades, tamaños moleculares, carga a pH fisiológico, etc. Esta gran diversidad de propiedades químicas de los metabolitos y los amplios rangos de concentración en los que pueden encontrarse en las muestras biológicas estudiadas, hace necesaria la utilización conjunta de distintos métodos para abarcar completamente su estudio [9].

En LC-MS es posible determinar la relación de la masa frente a la carga de las moléculas presentes en una muestra (*m/z*). Primeramente, la cromatografía líquida separa componentes mediante diferentes mecanismos de interacción entre una fase estacionaria y una fase móvil.

La fase móvil normalmente está compuesta por dos disolventes de diferente polaridad. Se usa un gradiente para que la polaridad se incremente o se disminuya según se desee. La fase estacionaria es frecuentemente una columna solida donde moléculas de 18 hidrocarburos, están unidos a una superficie de sílice porosa y que efectúa la retención de diversos analitos. En cuanto a la espectrometría de masas, esta medida se lleva a cabo mediante la ionización de las moléculas, separación de los iones resultantes de acuerdo con su relación *m/z* y detección de las abundancias de los mismos. El desarrollo de técnicas de ionización suave como el electrospray (*Electrospray Ionization, ESI*) y la utilización de detectores de alta resolución como el detector de tiempo de vuelo (*Time Of Flight, TOF*) o los basados en la trampa de iones *Orbitrap* han permitido el estudio de biomoléculas con exactitudes de masa inferiores a 1 ppm en m/z y límites de detección por debajo del rango nanomolar (nM) para algunos compuestos [10,11]. Dada la gran resolución y sensibilidad de la instrumentación actual empleada en los estudios metabolómicos, se puede llegar a generar miles de señales analíticas para cada muestra, con la dificultad que conlleva su manejo e interpretación [12,13]. Por este motivo, como se muestra en la **ilustración 1**, el procesamiento y análisis de los datos obtenidos en metabolómica es un reto [14] y el desarrollo de herramientas bioinformáticas ha sido una pieza clave para el avance de la interpretación e integración de los resultados obtenidos [15]. Por otro lado, el uso del análisis estadístico multivariante está muy extendido en metabolómica, principalmente aplicado a la selección de los metabolitos más importantes de entre todos los detectados, que permiten diferenciar distintos grupos de muestras. También existe otra dificultad asociada y reside en la identificación de los metabolitos a partir de las señales

generadas por las diferentes técnicas analíticas. Se suele llevar a cabo mediante la comparación de los datos experimentales con bases de datos tanto generadas a partir de patrones puros y, así como librerías espectrales ya establecidas [16].

De manera más reciente, se han descubierto la presencia y estabilidad de unos pequeños RNAs no codificante, denominados microRNAs que se encuentran de manera intracelular pero también de manera circulante en diferentes biofluidos. Esto ha abierto nuevas líneas de investigación para estudiar su uso como biomarcadores, e incluso como dianas terapéuticas. Los microRNAs son una familia de RNAs pequeños no codificantes, con una longitud entre 19 y 25 nucleótidos, que juegan un papel muy importante en la regulación de la expresión génica postranscripcional. Estos pequeños moléculas, tienen la habilidad de unirse a la región 3'UTR de los mensajeros pudiendo así silenciarlos mediante la escisión o la desadenilación [17]. Se ha descubierto que estos microRNAs juegan un papel muy importante a nivel del desarrollo y función del sistema nervioso central y por lo tanto en el desarrollo de enfermedades neurológicas. Todo ello, hace sospechar, que podrían tener un papel importante en el diagnóstico de lesiones cerebrales, como ya se han descrito en muchas otras situaciones patológicas como el infarto de miocardio o paro cardiorrespiratorio, entre otros [18,19].

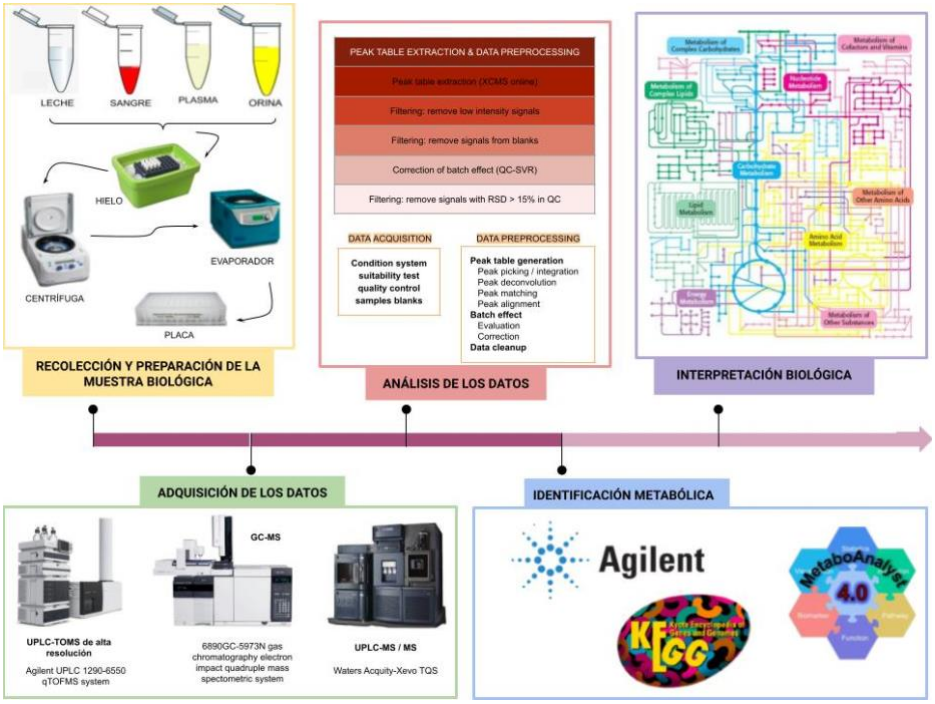

Ilustración 1. Diagrama de flujo donde se representan las partes más importantes de un estudio metabólomico.

Sin embargo, sea cual sea la modalidad utilizada, esta Tesis Doctoral, se enfrenta a muestras englobadas a la población neonatal. A día de hoy, la asfixia perinatal asociada a encefalopatía hipóxico-isquémica o la prematuridad, son aspectos fisiopatológicos a los cuales se enfrenta la neonatología por su importancia en cuanto a la incidencia, mortalidad y morbilidad. Aún así, pocos estudios sobre la evolución del metaboloma se han llevado a cabo con niños con EHI durante la hipotermia terapéutica [20,21]. Pero no solamente en situaciones en las que la EHI juega un papel principal. En el caso de la nutrición del prematuro o en intervenciones tan delicadas como la septostomía auricular con balón graduado (del inglés *Ballon Atrial Septostomy, BAS*) en recién nacidos con transposición de grandes arterias (del inglés, *Transposition of Great Arteries*, TGA), la búsqueda de biomarcadores,

mejores métodos de diagnóstico o mejores tratamientos son necesarios para la viabilidad de estos delicados pacientes.

Aun así, al estudiar una cohorte de pacientes tan delicado, conlleva a una serie de inconvenientes que hay que tener muy en cuenta. Por un lado, la obtención de la muestra puede ser muy complicada debido a procedimientos invasivos en estos pacientes tan delicados frente a la obtención de la misma muestra en una persona adulta. Por otro lado, muchas veces la obtención de la muestra se produce en situaciones extremadamente complejas. Escenarios donde se produzca un parto prematuro o patologías muy importantes en perinatología como la asfixia perinatal, hacen que estos pacientes se encuentren en una unidad de cuidados intensivos (UCIN), en una camilla de reanimación o durante complejos tratamientos como puede ser la hipotermia terapéutica y en consecuencia, la obtención de las muestras sea más complicado de lo habitual.

Encefalopatía hipóxico-isquémica

Una de las patologías que son objeto de estudio en el ámbito neonatal y parte importante de esta Tesis Doctoral es la encefalopatía hipóxico-isquémica (EHI). Esta patología es uno de los contribuyentes más importantes a la discapacidad neurológica en la edad pediátrica, donde en países desarrollados la incidencia es de alrededor de 1,6 por 1000 recién nacidos, mientras que el riesgo es 10 veces más alto en países subdesarrollados. La EHI es un proceso evolutivo de daño causado que se puede dividir en varias fases. El primer insulto isquémico y/o hipóxico, es la consecuencia neurológica de la alteración del flujo sanguíneo y/o el intercambio gaseoso durante el parto [22,23]. La

disminución de la perfusión cerebral y la oxigenación desencadenan una secuencia de alteraciones metabólicas cerebrales que provoca que se active el metabolismo anaeróbico y concluye en el descenso de la producción de adensín trifosfato (ATP) mientras que paralelamente se produce un aumento de los niveles de ácido láctico. Esto va a provocar una cascada de mecanismos moleculares que serán nocivos para el recién nacido. La falta de producción de ATP conlleva que las bombas sodio potasio (Na^+/K^+) dependientes de ATP empiecen a fallar, provocando el fallo del transporte a través de membrana provocando la acumulación de diferentes iones y la aparición de edemas citotóxicos [23]. La excitotoxicidad empieza a aparecer entre las neuronas cerebrales, en la cual empiezan a liberarse diferentes neurotransmisores como el glutamato. La peroxidación de los ácidos grasos libres a causa de los radicales libres de oxígeno provocan un mayor daño celular. Por lo que el conjunto del fallo energético, la acidosis provocada junto con la liberación de glutamato y la peroxidación lipídica conllevan a la muerte celular y caracterizan la fase de insuficiencia primaria de la EHI. El tiempo en el que se produce el daño y la intervención clínica son imprescindibles para la recuperación. Esta tiene una ventana temporal de unos 30-60 minutos después del insulto isquémico de la primera fase.

Posteriormente, en la reanimación, el proceso pasa por una fase latente que dura hasta 6 horas en la cual se observa una recuperación del metabolismo oxidativo, inflamación y activación de cascadas apoptóticas. La fase secundaria, caracterizada por insuficiencia energética que intensifica la lesión cerebral debido a la formación de edemas citotóxicos, la excitotoxicidad provocada, la aparición de convulsiones y el fallo energético asociado que afecta a la actividad

mitocondrial, provocado la muerte celular. Por último, en la reperfusión, se consigue aumentar los niveles de oxígeno en las mitocondrias, pero debido al sistema de oxidación inmaduro de los recién nacidos, se produce una muerte celular tardía, remodelado de las células neuronales dañadas y una astrogliosis que se pueden dar a los meses del daño [23]. Todos estos eventos vienen ilustrados en la **ilustración 2**. Los recién nacidos que han sufrido EHI tienen una mayor incidencia de afecciones graves como parálisis cerebral, deterioro cognitivo, restricción del crecimiento y epilepsia [24]. Mejoras en la reanimación, incluida la comprensión de los papeles relacionados con el estrés oxidativo (OS), la introducción de la hipotermia terapéutica (del inglés, *Therapeutic Hypothermia*, TH) como tratamiento estándar y el empleo de nuevas técnicas de monitorización representan los principales hitos en la gestión de la EHI. Esta terapia terapéutica ha supuesto un punto de inflexión en cuanto al pronóstico de pacientes con EHI. Además, los estudios con RMN muestran que el daño cerebral hipóxico-isquémico se caracteriza por un daño en estructuras cerebrales de la sustancia gris, donde los ganglios basales, el tálamo o partes del córtex son de las más afectadas. Aquellos recién nacidos con afectaciones en estas estructuras pueden presentar parálisis cerebral y epilepsia, afectando de manera más grave a nivel motor. Por lo tanto, la EHI juega una problemática fundamental en la medicina perinatal. Consiguientemente, la búsqueda de nuevos biomarcadores de diagnóstico y pronóstico precoces y precisos puede permitir anticiparse a estos acontecimientos y sería de gran ayuda reconociendo una transición hacia estrategias de tratamiento personalizado.

Ilustración 2. Cascada de eventos celulares sobre la encefalopatía hipóxico-isquémica donde se representa los sucesos patológicos a lo largo del tiempo.

Nutrición y prematuridad

La nutrición en el ámbito de la prematuridad también es objeto de estudio en esta Tesis Doctoral. Actualmente la prematuridad es la principal causa de mortalidad neonatal en países desarrollados y en cuanto a morbilidad a largo plazo, se ha relacionado con un peor neurodesarrollo, mayores tasas de ingresos hospitalarios y dificultados de aprendizaje y socioemocionales [25]. Aunque las muertes neonatales en prematuros disminuyeron en los últimos 20 años en países desarrollados, la prematuridad aún se considera una de las principales causas de mortalidad neonatal. La prevalencia de complicaciones graves como la retinopatía del prematuro (ROP), la displasia broncopulmonar (DBP), la enterocolitis necrotizante (ECN) o la leucomalacia periventricular (LPV) se han mantenido prácticamente sin cambios o incluso aumentada en neonatos muy prematuros [26,27]. Es una población especialmente vulnerable, por lo que una nutrición adecuada forma parte importante en estos momentos cruciales para la viabilidad del recién nacido prematuro. Diversos estudios han puesto en relieve que

la leche materna (LM) es el mejor alimento para los recién nacidos y lactantes por sus múltiples beneficios, incluyendo la prevención de infecciones, un mejor desarrollo neurológico y visual y la prevención de enfermedades crónicas [26,28]. A su vez, la LM es un complejo y dinámico biofluído que influye directamente en la colonización de la microbiota intestinal y la maduración del sistema inmune. Su composición única y específica para la especie humana aporta numerosos compuestos esenciales para el crecimiento y desarrollo como proteínas, lípidos y/o anticuerpos que no pueden ser administrados mediante leche de fórmula artificial. También aporta una amplia gama de compuesto como carbohidratos, oligosacáridos (prebióticos), microorganismos (probióticos), ácidos grasos, inmunoglobulinas, citoquinas, anticuerpos, lisozimas, lactoferrina y otros factores inmunomoduladores [29]. Cuando no existe posibilidad de proporcionar LM de madre propia o ésta es insuficiente, organizaciones como la Academia Americana de Pediatría (AAP), la Sociedad Europea de Gastroenterología, Hepatología y Nutrición pediátrica (ESPGHAN), o la Organización Mundial de la Salud (OMS) recomiendan como la alternativa más beneficiosa para el recién nacido prematuro la alimentación con leche materna donada (LMD). Uno de los beneficios más importantes demostrados de la LMD es el efecto protector frente la inflamación intestinal aguda, también conocida como ECN. Además, existen evidencias de que la LMD favorece la tolerancia alimentaria y, a largo plazo, tiene un efecto protector cardiovascular [30]. La preservación de la LMD mediante pasteurización proporciona además otros beneficios potenciales relacionados con la presencia en la LMD de oligosacáridos y ácidos grasos poliinsaturados de cadena larga, con destacada actividad antiinflamatoria e inmunomoduladora [31]. En

Noruega, todos los recién nacidos que no disponen de leche de madre propia reciben LMD. Desde un punto de vista económico, el estudio de coste-efectividad, centrándose exclusivamente en el ahorro al prevenir casos de ECN, favorece el uso de LMD [32].

Por otro lado, las primeras semanas de vida constituyen el periodo más dinámico desde el punto de vista bacteriano en el ecosistema gastrointestinal. Está descrito que la diferencia entre el tipo de parto (i.e., vaginal o cesárea) influye en la colonización neonatal [33], pero no está descrito como la diferente alimentación materna puede también influenciar la presencia de un tipo de bacterias u otra. Esta presencia resulta crítica para la modulación inicial del sistema nervioso como para el funcionamiento de importantes rutas metabólicas y/o la creación de un ambiente reductor que permita el desarrollo posterior de bacterias anaerobias estrictas.

El Banco de Leche Materna del Centro de Transfusión de la Comunidad Valenciana (CTCV) centraliza la gestión de leche materna de la Comunidad Valenciana y es uno de los dieciséis existentes a escala nacional.

En las instalaciones del banco de leche se recibe, procesa y distribuye la LMD altruistamente donada por madres, para que se beneficien los recién nacidos hospitalizados que la necesiten, a los que se ofrece gratuitamente bajo prescripción médica. Sin embargo, el uso de la LMD también tiene una serie de limitaciones. La LM sin fortificar, de madre propia o donada, no permite alcanzar la tasa de crecimiento extrauterino deseada si se compara con fórmula o con LM fortificada

[34]. Además, la variabilidad de la composición de la LM dificulta conocer exactamente la composición de componentes bioquímicos y nutricionales que aporta al recién nacido. También la influencia de los métodos de conservación y procesamiento (pasteurización) en las características de la leche o la posibilidad de transmitir infecciones son otros de los aspectos a tener en cuenta [35]. Para minimizar el impacto de estas limitaciones se han puesto a punto protocolos que regulan de forma precisa cada uno de los pasos del proceso de donación de LM y métodos de análisis de la composición de la LMD de manera que la LMD sea una alternativa válida a la LM de madre propia, cuando esta no está disponible.

Transposición de grandes arterias

Por último y también como objeto de estudio de esta Tesis Doctoral, se ha profundizado sobre otra patología implicada en el recién nacido. El procedimiento TGA, también conocida como transposición completa, es una malformación cardíaca congénita caracterizada por una concordancia auriculoventricular y discordancia ventrículoarterial. Se estima que su incidencia está sobre los 35000-5000 nacimientos y presenta sobre el 5-7% de todas las patologías congénitas que afectan al corazón [36]. Su fisiopatología consta de una malformación dependiente del ductus arterioso (DA) y del foramen oval (FO). Sin estas dos conexiones cardiovasculares, las circulaciones sistémicas y pulmonares cursan en paralelo, sin poder hacer el intercambio gaseoso a nivel pulmonar, por lo que se produce una situación hipoxémica que requiere tratamiento. La BAS sigue siendo un procedimiento esencial en recién nacidos con TGA. Esta intervención solo se realiza en centros de

referencia y consigue una mezcla intercirculatoria restrictiva que mejora considerablemente la oxigenación y previene un daño multiorgánico. Esta intervención implica la reducción de la hipoxia generada por el circuito sanguíneo cerrado y un aumento en la saturación de oxígeno [37]. Aunque gracias a todo esto, la mortalidad asociada a esta patología ha disminuido [38] y muy poco se sabe sobre el impacto que tienen estos procedimientos sobre el recién nacido.

Como ya se ha comentado, la intervención septostómica ayuda a promover la mezcla la sangre desoxigenada con la oxigenada a nivel auricular en pos de la supervivencia del recién nacido, si bien es cierto esta intervención provoca un aumento repentino en la oxigenación de la sangre arterial estimulando la aparición de estrés oxidativo, muy nocivo para la fisiología del recién nacido. Sin embargo, son muy escasos los trabajos de cómo afecta a nivel metabolómico los cambios producidos por esta intervención. Además, puede ser relevante qué cambios metabólicos relacionados con el oxígeno pueden verse afectados para buscar nuevas estrategias de prevención, diagnóstico y tratamiento.

Hipótesis y objetivos

La hipótesis de partida en la que se basa la presente Tesis Doctoral es la caracterización exhaustiva del metaboloma del recién nacido que proporciona información de utilidad para el estudio de diferentes situaciones fisiológicas y patológicas en el periodo neonatal.

Para ello, el objetivo tratará de proporcionar herramientas preparadas para llevar a cabo estudios metabolómicos integrales que aborden preguntas de investigación relevantes en el campo de la perinatología, como el descubrimiento e identificación de biomarcadores para la medicina personalizada y la exploración de una respuesta holística a nivel fenotípico.

Para ello se estudiarán diferentes situaciones clínicas relevantes para la salud del recién nacido:

- Descubrimiento de biomarcadores para la predicción temprana de lesión cerebral neonatal.
- Evaluación del impacto de la dieta en el crecimiento y desarrollo de los recién nacidos prematuros.
- Cambios metabólicos en recién nacidos con cardiopatías congénitas asociadas a la intervención quirúrgica.

Los artículos que conforman la presente Tesis Doctoral, en el formato de compendio de publicaciones, se han dividido en tres secciones donde se desarrollan los diferentes trabajos realizados en cada uno de ellos.

En la primera sección, titulada "*Biomarcadores para la predicción temprana de lesión cerebral neonatal*" se incluyen los trabajos donde se profundiza en la determinación de biomarcadores

precoces en una cohorte de recién nacidos con EHI. En el caso de las determinaciones en plasma, se desarrolla una metodología donde se combina, por un lado, LC-TOFMS y GC-MS y el desarrollo de diferentes métodos mediante LC-MS/MS para la determinación cuantitativa de un panel de biomarcadores que abarcan los metabolitos de la ruta de la biosíntesis de esteroides, biomarcadores de hipoxia, metabolitos de la ruta de triptófano. Asimismo, se analiza mediante GC-MS la determinación cuantitativa de metabolitos implicados en el metabolismo energético. Del mismo modo, se evalúa la expresión de microRNAs mediante secuenciación de última generación. Por otro lado, utilizando muestras de orina, se combina metodología que engloba LC-TOFMS, CE-MS y la determinación de un panel de aminoácidos.

En la segunda sección titulada "*Evaluación del impacto de la dieta en el crecimiento y desarrollo de los recién nacidos prematuros*" se incluye el trabajo donde se intenta esclarecer la relación entre la nutrición y el metaboloma urinario de los recién nacidos prematuros y la leche materna. Para ello se desarrollaron metodologías de LC-TOFMS para la orina de los recién nacidos prematuros, así como la leche empleada y secuenciación de la expresión de rRNA 16S bacteriano mediante plataforma *Illumina* en las muestras de heces de los prematuros.

En la tercera sección titulada "*Monitorización del cambio metabólico en neonatos con cardiopatías congénitas tras una intervención quirúrgica*" las muestras de plasma obtenidas de niños con cardiopatías congénitas se emplearón metodología LC-TOFMS, así como la determinación de un panel de biomarcadores relacionados con la peroxidación lipídica mediante LC-MS/MS.

Metodología

La metabolómica, en su vertiente no dirigida, forma la columna vertebral en el desarrollo de los diferentes trabajos presentados en la presente memoria de la tesis doctoral. Todas las metodologías de metabolómica desarrolladas en esta tesis, exceptuando el capítulo 3, parten desde un enfoque no dirigido. Posteriormente en algunos casos, se han añadido otras metodológicas ómicas, en su mayoría diferentes enfoques metabolómicos o la combinación con otras técnicas ómicas donde todas ellas han sido resumidas en la **Tabla 1**. Para ello, todas las metodologías aplicadas en los diferentes trabajos que presenta esta tesis han sido adaptados para trabajar con el menor volumen posible, así como diferentes preprocesados necesarios para poder emplear este tipo de metodología en los pequeños volúmenes de muestra habitualmente obtenidos del neonato.

Tabla 1. Resumen de la metodología utilizada en los diferentes capítulos de la presente tesis doctoral.

Sección	Capítulo	Metodología	Modalidad y biofluido
Biomarcadores para la predicción temprana de lesión cerebral neonatal	Metabolic Phenotypes of Hypoxic-Ischemic Encephalopathy with Normal vs. Pathologic Magnetic Resonance Imaging Outcomes	Metabolómica no dirigida Metabolómica dirigida	Análisis metabolómico no dirigido LC-QTOFMS en plasma. Cuantificación de succinato y piruvato por GC-MS en plasma.
	Non-invasive monitoring of evolving urinary metabolic patterns in Hypoxic-ischemic encephalopathy	Metabolómica no dirigida Metabolómica dirigida	Análisis metabólomico no dirigido LC-QTOFMS en orina. Análisis semidirigido por CE-TOFMS en orina. Cuantificación de aminoácidos por UPLC-MS en orina.
	Targeted Metabolomics data and miRNA-seq assessment from HIE newborns during hypothermia treatment	Metabolómica dirigida Secuenciación de microRNAs	Cuantificación de metabolitos de la ruta de biosíntesis de esteroides, biomarcadores de hipoxia, metabolitos de la ruta del triptófano por UPLC-MS en plasma. Cuantificación de metabolitos del metabolismo energético por GC-MS Secuenciación de microRNAs por Illumina en plasma.
Evaluación del impacto de la dieta en el crecimiento y desarrollo de los recién nacidos prematuros	Effect of donor human milk on host-gut microbiota and metabolic interactions in preterm infants	Metabolómica no dirigida Secuenciación 16S rRNA	Análisis metabolómico no dirigido por LC-QTOFMS en orina y leche. Secuenciación de 16S rRNA por Illumina en heces.
Monitorización del cambio metabólico en neonatos con cardiopatías congénitas tras una intervención quirúrgica	A reductive metabolic switch protects infants with congenital heart defect undergoing atrial septostomy against oxidative stress.	Metabolómica no dirigida Metabolómica dirigida	Análisis no dirigido por LC-QTOFMS en plasma. Cuantificación de biomarcadores de peroxidación lipídica en plasma.

Metabolómica no dirigida

Teniendo en cuenta las diferentes partes que forman la Tesis Doctoral, la sección "*Biomarcadores para la predicción temprana de lesión cerebral neonatal*" que comprenden los capítulos 1, 2 y 3, las muestras se obtuvieron de una cohorte dentro del ensayo clínico multicéntrico español HYPOTOP [39]. Es en esos pacientes donde, en el capítulo 1, un total de 188 muestras de sangre fueron procesadas, se resuspendieron las muestras con una disolución con patrones internos y se inyectaron en un sistema UPLC-TOFMS Agilent 1290 Infinity UHPLC. Para la separación cromatográfica se usó una columna UPLC Acquity BEH C_{18} (2.1 mm × 100 mm, 1.7 μm, Waters, Wexford, Ireland) con un caudal de trabajo de 400 μL min^{-1}. Se usaron diferentes condiciones para el gradiente de fase móviles. Los datos obtenidos del espectrómetro de masas en modo *full-scan MS* se emplearon con un rango de 100 a 1700 m/z con una frecuencia de escáner de 6 Hz, funcionando en modo de ionización tipo *electrospray* positivo.

Por otro lado, en la metodología aplicada en el capítulo 2, un total de 293 muestras de orina también de la cohorte HYPOTOP fueron procesadas y se inyectaron en el sistema Agilent 1290 Infinity UPLC el cual iba equipado con una columna UPLC BEH C_{18} (100 × 2.1 mm, 1.7 μm, Waters, Wexford, Ireland) para la separación cromatográfica. Se usó un gradiente de fase móvil A y B. Los datos obtenidos en modo full scan MS se obtuvo con un rango de *m/z* comprendido entre 100 y 1700 m/z en modo de ionización *electrospray* positivo.

En lo que atañe al estudio sobre la nutrición y la prematuridad, incluido en la sección "*Evaluación del impacto de la dieta en el*

crecimiento y desarrollo de los recién nacidos prematuros", el procesado de las muestras de recién nacidos prematuros de orina que se llevó a cabo en el capítulo 4, un total de 40 muestras fueron procesadas. Además, un total de 27 muestras de leche, fueron también procesadas. En ambos tipos de muestra se utilizó un sistema 1290 Infinity UPLC de Agilent Technologies (Santa Clara, CA, USA). El análisis de las muestras fue diferente dependiendo de la matriz biológica. En el caso de las muestras de orinas, la separación cromatográfica se utilizó una columna UPLC BEH C_{18} (100 × 2.1 mm, 1.7 μm) de Waters (Wexford, Ireland). El caudal de trabajo se estableció en 400 μL min^{-1} y se utilizó un gradiente binario de fases móviles A y B. En cuanto a las muestras de leche, se empleó una columna Kinetex C18 (50 × 2.1 mm, 1.7 mm) de Phenomenex (Torrance, CA, USA) con un gradiente binario de fases móviles A y B. Todos los parámetros de análisis restantes se establecieron como se describe para el análisis de orina.

Por último, la sección "*Monitorización del cambio metabólico en neonatos con cardiopatías congénitas tras una intervención quirúrgica*", dentro del capítulo 5, se emplearon 12 muestras de plasma del estudio prospectivo de recién nacidos con TGA pertenecientes al *Children´s Hospital, Helsinki University Hospital*. Las muestras fueron procesadas e inyectadas en un equipo Agilent Technologies (Santa Clara, CA, USA) 1290 Infinity UPLC y para la separación cromatográfica se utilizó una columna UPLC Acquity BEH C_{18} (2.1 × 100 mm, 1.7 μm, Waters, Wexford, Ireland). Se utilizó un gradiente binario de fase móvil A y B. Los datos obtenidos del espectrómetro de masas en modo *full-scan MS* se consiguieron con un rango de 100 a 1700 m/z, funcionando en modo de ionización tipo *electrospray* positivo. El procedimiento también se

llevó a cabo en modo de ionización *electrospray* negativo repitiendo el mismo procedimiento que con el modo de ionización *electrospray* positivo.

Es muy importante tener en cuenta, que el análisis de los datos en el contexto de la metabolómica no dirigida ha tenido un peso importante en los diferentes capítulos que conforman esta tesis doctoral. En los diferentes estudios, los datos crudos procedentes del UPLC-TOFMS fueron convertidos a formato mzXML usando Protewizard antes de generar una tabla de picos usando el software XCMS. Los parámetros seleccionados para la extracción y el alineamiento de la tabla de picos se basaron en la precisión/exactitud del tiempo de retención (TR) y la m/z de patrones internos seleccionados. Después de la detección, deconvolución e integración cromatográfica de las muestras identificándolas mediante m/z y TR se obtuvieron diferentes matrices de muestras vs variables. Además, la integración automática fue evaluada comparándola con la integración manual de los patrones internos.

Por otro lado, es muy típico que en los datos obtenidos a partir de experimentos de LC-MS a gran escala, se pueden distinguir diferentes fuentes de varianza, que además de la variación biológica, se puede observar variación instrumental que se origina a partir de cambios menores como el volumen de inyección o cambios graduales en la respuesta instrumental durante la medición de lotes de muestras. Por lo que, cabe destacar que en los diferentes capítulos de la tesis doctoral, se llevó una corrección del efecto intra lote utilizando el algoritmo *Radial Basis Function Kernel for a Support Vector Regression based correction (QC-SVR)*.

Para el resto de cálculos se empleó la hoja de cálculo Microsoft Excel 2016 de Microsoft (Redmon, EE.UU) y el software matemático MATLAB de Mathword (Natrick, EE.UU) a través de scripts y funciones propias desarrolladas así como funciones incluidas en el paquete PLS_Toolbox de Eigenvector Reserach Inc (Wenatchee, EE.UU). Por último, se necesitó de las herramientas online proporcionadas por MetaboAnalyst 4.0 así como de la herramienta de integración AMON.

Metabolómica dirigida

Otra de las metodologías importantes dentro de esta tesis doctoral, es la metabolómica en su vertiente dirigida, es decir, la cuantificación de diferentes compuestos mediante la generación de una calibración de patrones y posteriormente la interpolación de cada uno de los compuestos medidos. Esta metodología ha servido dentro de esta tesis doctoral, como sustento y confirmación de la existencia y cuantificación de diferentes compuestos con el objetivo de encontrar biomarcadores útiles dentro de cada una de las patologías estudiadas. Cada uno de los métodos cuantitativos que se desarrollan en ambos capítulos tiene sus propias peculiaridades sobre el procesado de la muestra. Se han empleado diferentes preprocesados con el objetivo de hacer las muestras compatibles con las diferentes técnicas instrumentales empleadas. Así como la preconcentración de la muestra debido al menor volumen obtenido de estos delicados pacientes, la adición de patrones internos, la estabilización del compuesto o eliminación de la matriz innecesaria.

Dentro de la sección "*Biomarcadores para la predicción temprana de lesión cerebral neonatal*" se utilizaron métodos cuantitativos. En el capítulo 2, un total de 237 muestras de orina pertenecientes al ensayo clínico HYPOTOP se utilizaron para la cuantificación de una batería de aminoácidos. 70 µL de agua (Optima LC-MS, Fisher Scientific) se añadieron junto a 5 µL de orina. Estas muestras se prepararon con una derivación (AccQ TagTM Ultra Derivatization Kit, Waters), siguiendo las instrucciones facilitadas. Se prepararon muestras de blanco y QC que se mezclaron a lo largo de la secuencia. El equipo utilizado fue un sistema 1290 Infinity UPLC de Agilent Technologies (Santa Clara, CA, USA) con una columna cromatográfica UPLC CORTECS C18 (150 × 2.1 mm, 1.6 µm) de Waters (Milford, MA, USA). El modo de ionización utilizado fue *electrospray* positivo. El caudal de trabajo fue de 500 µL min^{-1} con un gradiente binario. Tanto la adquisición como el procesado de los datos se realizó con el software MassHunter Workstation (versión B.07.00, Agilent).

Sin embargo, en el caso de la determinación de los compuestos del metabolismo intermediario energético del capítulo 1 y el capítulo 3, las muestras tuvieron que procesarse mediante dos pasos de oximación-sililación y procesadas mediante un método validado para GC-MS para posteriormente inyectarlas en un equipo de cromatografía de gases *6890 GC 5973N electron impact quadrupole MS* system de Agilent (Santa Clara, EEUU.) equipado con una columna HP-5MS de *Agilent Technologies* (Santa Clara, Ca, USA). La cromatografía de gases se llevó a cabo con una corriente de He constante y un caudal de 1200 µL min^{-1}

junto con una temperatura de inyección de 260 °C junto con un volumen de inyección de 1 µL.

Por otro lado, en el capítulo 3, un total de 359 muestras de plasmase utilizaron del ensayo clínico HYPOTOP donde se evaluaron un total de 34 compuestos divididos en 4 métodos cuantitativos y validados. Para la cuantificación de 10 compuestos de la ruta de biosíntesis de esteroides, se siguieron los diferentes pasos protocolizados mediante el kit comercial CHS^{TM} MSMS Steroids Kit de PerkinElmer (Waltham, MA USA). Se utilizaron 100 µL de muestras plasmáticas que después de varios pasos de procesado de la muestra y se analizaron mediante un Sistema *Acquity-Xevo TQS* usando una columna C8 (2.1 × 10 mm, 1.7 µm, Waters, Wexford, Ireland). Por otro lado, para la determinación de biomarcadores de hipoxia, se desarrolló un método cuantitativo en el que se consiguieron analizar 7 compuestos diferentes. Para ello, 10 µL de muestra se añadieron a 7µL de una mezcla de patrones internos. Posteriormente las muestras fueron centrifugadas y evaporadas hasta llevar a sequedad mediante *miVac centrigual vacuum concentrator*. El análisis se llevó a cambio mediante un sistema *Acquity* UPLC-MS/MS acoplado a un detector de espectrometría de masas Xevo-TQ operando con un modo de ionización del tipo *electrospray* positivo (ESI^+) (Waters, Manchester, UK). La columna cromatográfica usada fue un *Acquity* UPLC BEH C_8 (100 × 2.1 mm, 1.7 µm) con una fase móvil.

En el caso de la determinación de compuestos de la ruta del triptófano, 23 metabolitos se consiguieron medir, añadiendo 50 µL de muestra en 150 µL de CH_3OH para la precipitación proteica. Posteriormente las muestras fueron centrifugadas en varias tandas y

llevadas a sequedad mediante *miVac centrigual vacuum concentrator*. Las muestras fueron resuspendidas en disolución con una mezcla de patrones internos. El equipo utilizado para el análisis fue *Acquity-Xevo TQS system* de Waters (Milford, MA, USA) y la columna cromatográfica usada fue *Acquity* HSS T3 C_{18} (100 x 2.1 mm, 1.8 µm). Se usó un gradiente de fases móviles A y B.

Además se llevó a cabo la determinación de compuestos del metabolismo intermediario cuya metodología se ha descrito anteriormente.

En la última sección la última sección "*Monitorización del cambio metabólico en neonatos con cardiopatías congénitas tras una intervención quirúrgica*" también se llevó a cabo una metodología de metabolómica dirigida, en el capítulo 5, un total de 63 muestras se obtuvieron de un estudio prospectivo con pacientes con TGA en el *Children´s Hospital, Helsinki University Hospital.* El método cuantitativo desarrollado para la medición de compuestos relacionados con la peroxidación lipídica, las muestras se sometieron a una extracción en fase sólida (del inglés, *Solid Phase Extraction, SPE*) mediante una fase estacionaria Discovery® C18 de la casa comercial MerK (Darmstadl, Alemania). Finalmente, las muestras se inyectaron en un sistema *Acquity-Xevo TQS* de Waters (Milford, MA, USA).

En el caso de los métodos dirigidos, el análisis de los datos se llevó a cabo mediante diferentes software según el sistema de medición utilizado, las muestras que se inyectaron en los sistemas de LC-MS/MS se utilizó el softwares MassLynx™ de Waters (Milford, MA, EEUU)

mientras que las muestras analizadas por GC-MS se utilizó el software MassHunter Workstation de Agilent (Santa Clara, EEUU) para la integración cromatográfica, la generación de los calibrados y las interpolaciones tanto de los datos obtenidos.

Además, como ya se ha comentado en el punto 3.1, para los cálculos oportunos se emplearon la hoja de cálculo Microsoft Excel de Microsoft (Redmond, EEUU), así como el software de programación MATLAB en sus versiones actualizas a través de scripts y funciones desarrolladas por el laboratorio, así como funciones incluidas en el paquete PLS Toolbox 8.0 de Eigenvector Research Inc (Wenatchee, EEUU).

Otras metodologías

A parte de la metabolómica, como metodología "ómica" central de esta tesis, también se han utilizado otras metodologías complementarias que han servido para cubrir un espectro diferente de compuestos que pueden dar una información complementaria. En este caso, dentro de la sección "*Biomarcadores para la predicción temprana de lesión cerebral neonatal*" se utilizó la transcriptómica para la secuenciación de los microRNAs plasmáticos del capítulo 3. Las muestras de plasma de los diferentes recién nacidos se extrajeron el RNA siguiendo las pautas de kit comercial *miRNeasy serum/plasma* de Qiagen (Hilden, Alemania). Se utilizaron 100 µL de muestra donde, después de todos los pasos estipulados en el manual, se obtuvieron 14 µL de RNA. Posteriormente, las muestras de RNA sufrieron una serie de pasos antes de proceder a la secuenciación. Primero de todo, se determinó la integridad del RNA mediante 3 métodos distintos. Después del control

de calidad necesario, se construyeron las librerías mediante el kit *Small RNA sample Pre Kit*. . Por último, se procedió a la secuenciación mediante la plataforma Illumina (San Diego, EEUU). Todos los pasos de secuenciación se llevaron a cabo en la empresa Novogene (Beijín, China). Una vez obtenidos los datos crudos, se realizó una colaboración junto con la universidad de Cranfield (Cranfield, UK) para el procesamiento de los datos obtenidos. Un total de 1788 microRNAs se obtuvieron de la cohorte inicial.

Además, en la sección "*Evaluación del impacto de la dieta en el crecimiento y desarrollo de los recién nacidos prematuros*", en el capítulo 4, para las muestras fecales de 40 recién nacidos prematuros se obtuvo el DNA fecal mediante el aislamiento de DNA usando el kit *MasterPure Complete DNA & RNA Purification kit* (Epicentre, MA, EEUU) para posteriormente proceder a la secuenciación de la región V3-V4 del rRNA 16S mediante el equipo *MiSeq-Illumina* (San Diego, EEUU). Ulteriormente, los datos de secuenciación fueron tratados mediante el paquete QIMME versión 1.9.0 en R.

Resultados

Siguiendo con la estructura planteada en la tesis, en la sección "*Biomarcadores para la predicción temprana de lesión cerebral neonatal*" se obtuvieron diferentes resultados. En el análisis metabolómico realizado sobre muestras de sangre, se analizaron muestras del plasma de una cohorte de 55 recién nacidos asfixiados que desarrollaron una moderada/severa EHI donde esas muestras fueron obtenidas entre el nacimiento y la aplicación de la TH. Se llevó a cabo una evaluación de la utilidad del lactato, piruvato y el ratio piruvato/lactato para la predicción de resultados. Para evaluar el potencial del lactato, piruvato y el ratio lactato/piruvato en sangre antes del inicio de la TH y 24, 48 y 72 horas prediciendo resultados patológicos de RMN, se observó que los recién nacidos con RMN patológico tenían los niveles de lactato significativamente elevados a 24 y 48 horas, mientras que el piruvato aumentaba a las 72 horas (prueba de la U de Mann-Whitney, $\alpha = 0.05$). Sin embargo, no se encontraron diferencias significativas en el ratio lactato/piruvato. Para el enfoque no dirigido de las muestras de plasma, se construyó un análisis de componentes principales (PCA, del inglés *Principal Component Analysis*) y se vio una fuerte estratificación de los diferentes tiempos el metaboloma. Además, para confirmar el incremento de los metabolitos plasmáticos relacionados con la EHI relacionados con el tiempo, se realizó un mapa de calor (del inglés, *heat map*). Aunque no se observaron patrones al inicio de la TH, se observaron diferencias a las 24, 48 y 72 horas. Por último, se quiso averiguar a qué rutas metabólicas pertenecían estas variables detectadas. 11 rutas metabólicas fueron detectadas, de las cuales la mayoría fueron alteradas al cabo de 48 y/o 72 horas.

Por otro lado, se realizó otro abordaje metabolómico en la matriz biológica de orina, donde un total de 55 recién nacidos con EHI y tratamiento mediante TH de la cohorte HYPOTOP fueron incluidos. En total fueron 293 muestras de orinas las que se utilizaron para desarrollar el estudio desde un punto de vista no dirigido de las cuales se recogieron antes del inicio de la TH y 12, 24, 48, 72 y 96 horas. Usando como referencia las primeras muestras de orina, se observó que la mayoría de las señales detectadas mostraban una tendencia decreciente con el tiempo (prueba de la U de Mann-Whitney, $\alpha = 0.05$). Se observó que los cambios más pronunciados se generaron durante las primeras 48 h después del inicio de la TH, mientras que el recalentamiento se observó que no tuvo prácticamente ningún efecto a nivel metabolómico. Estas primeras observaciones, se volvieron a ver en un mapa de calor donde se representaban las concentraciones de los metabolitos con una correlación positiva con el tiempo. Utilizando la herramienta en línea MetaboAnalyst 4.0 y gracias a la anotación que el algoritmo *mummichog* realizó utilizando las variables metabólicas detectadas (prueba de la U de Mann-Whitney, $\alpha = 0.05$), 398 variables se manejaron para ver qué rutas metabólicas estaban alteradas. Se observaron que 32 rutas metabólicas alteradas en los diferentes tiempos. Con las 398 variables se generó un modelo predictivo PLSDA con 4 variables latentes para discernir entre la huella metabólica de recién nacidos que presentaron un RMN normal (puntuación 0) frente a un RMN patológico (puntuación 1, 2 o 3) entre las 24 y las 96 horas tras el inicio de la TH. Estos modelos fueron significativos (500 permutaciones) y se construyeron diferentes curvas ROC (del inglés, *Receiver Operating Characteristic*) multivariantes para confirmar la importancia del modelo creado.

Por lo que respecta al capítulo 3, 359 muestras de plasma de recién nacidos del estudio HYPOTOP fueron analizadas empleando 4 métodos cuantitativos validados por LC-MS. 34 compuestos fueron detectados en más del 90% de las muestras y 1788 microRNAs fueron secuenciados mediante NGS de segunda generación. Con el total de 34 compuestos medidos, se compararon concentraciones entre los grupos de los recién nacidos con RMN patológico y recién nacidos con RMN normal, y se encontraron diferencias significativas entre los grupos de estudio (prueba de U de Mann-Whitney, $\alpha = 0.05$). Se observaron incrementos de concentración en el grupo de recién nacidos con RMN patológica en algunos compuestos de las diferentes rutas metabólicas. Por otro lado, se detectaron y anotaron 1788 microRNAs en las muestras de plasma. Se encontraron intensidades de 29 microRNAs que estaban alteradas significativamente (prueba de U de Mann-Whitney, $\alpha = 0.05$) junto con un *Fold Change* (FC) > 1 comparando los recién nacidos con RMN patológico y RMN normal.

En lo que concierne al estudio sobre la nutrición y la prematuridad, incluido en la sección "*Evaluación del impacto de la dieta en el crecimiento y desarrollo de los recién nacidos prematuros*", varias muestras de diferente índole fueron analizadas; 15 y 12 muestras de LM y LMD, respectivamente, de madres de recién nacidos prematuros recogidos del banco de leche. Asimismo, se reclutaron 20 recién nacidos prematuros que recibieron exclusivamente LM y otros 20 recién nacidos prematuros que recibieron exclusivamente LMD, de los cuales se obtuvieron muestras de orina y fecales para los diferentes análisis del estudio. En cuanto al análisis de las muestras de leche, se realizó un

abordaje metabolómico no dirigido mediante LC-QTOFMS. De un total de 7109 variables detectadas, se encontraron diferencias significativas en 1034 variables (prueba de la U de Mann-Whitney, $\alpha = 0.05$) y diferencias significativas para 21 y 199 variables con log_2FC (del inglés, *Fold Change*) <1 y >1 respectivamente. Se quiso observar que rutas metabólicas podrían estar alteradas para una interpretación funcional. El análisis generado por la herramienta en línea MetaboAnalyst 4.0 junto con el algoritmo *mummichog* proyectó 13 vías donde más de dos metabolitos cambiaban significativamente (test exacto de Fisher, $\alpha = 0.05$). Por otro lado, y ya centrándose en el recién nacido prematuro, se quiso analizar los perfiles de la microbiota asociada, analizando las muestras fecales. Se observaron como existían diferencias significativas en la diversidad beta según la leche suministrada (PCoA, permanova con *p*-valor = 0,04). Además, se observó un aumento en la abundancia de los miembros de la familia Staphylococcaceae y Pasteurellaceae en el grupo de prematuros que se alimentaron con LMD, aunque las diferencias significativas no se mantuvieron después de la corrección mediante FDR (del inglés, *False Discovery Rate*). Del mismo modo, se identificaron cambios en 10 rutas metabólicas mediante la predicción funcional de las rutas KEGG (prueba de la U de Mann-Whitney, $\alpha = 0.05$), pero tampoco fueron significativas después de la corrección mediante FDR. En el análisis metabolómico de las muestras de orina de estos recién nacidos prematuros de las 10450 variables detectadas, 849 mostraron diferencias significativas enfrentando ambos grupos de estudio (prueba de la U de Mann-Whitney, $\alpha = 0.05$) así como 21 y 343 variables mostraron log_2FC < -1 y > 1 respectivamente. Del mismo modo, 32 rutas metabólicas fueron detectadas y solamente 2 de ellas mostraron alteraciones significativas comparando ambos grupos de estudio (*gamma p*-value

<0.05). Utilizando estos resultados que arrojó el algoritmo *mummichog,* 331 variables fueron asignadas a hormonas esteroideas, de las cuales, comparando su intensidad entre los dos grupos, se obtuvieron 19 variables que mostraban diferencias significativas. Todas ellas, aumentadas en el grupo de recién nacidos prematuros alimentados con LM comparado con el grupo de LMD. Del mismo modo, se procedió a hacer lo mismo con las variables anotadas incluidas en la ruta del metabolismo de pirimidinas. 101 variables fueron anotadas a dicha ruta, sin embargo, ninguna de ellas mostró alteraciones significativas enfrentando a los dos grupos de estudio. Ante estos interesantes resultados, y para esclarecer el origen de las alteraciones en las rutas metabólicas identificadas en las muestras de orina, se realizó un análisis integrativo de los diferentes datos ómicos. Teniendo la ruta de la biosíntesis de hormonas esteroides como eje central de esta parte del análisis, se observó que, en las muestras de leche, 73 variables fueron asignadas a dicha ruta utilizando el algoritmo *mummichog*, siendo 10 de ellas alteradas significativamente entre los dos grupos de estudio ($log_2FC> 1$) de manera que todas las variables alteradas pertenecían a la leche materna. Por otro lado, se correlacionaron las variables metabólicas anotadas como hormonas esteroideas en LM y orina (Coeficiente de correlación de Pearson). En las muestras de leche, los niveles de hormonas esteroideas mostraron una fuerte correlación entre ellas (R = 0,9) mientras que la correlación disminuyó entre muestras de orina entre sí (R = 0,5) y entre muestras de orina y muestras de leche (R = 0,38). Sin embargo, las abundancias relativas de las especies que conforman la microbiota mostraron correlaciones débiles entre ellos mismos (R =-0,1) con los niveles de esteroides presentes en orina y las muestras de leche (R = 0). Por último y para explorar si la alteración de

las rutas detectadas en las muestras de orina, podrían ser causadas por la microbiota intestinal, se empleó una herramienta integrativa denominada AMON (del inglés, *Annotation of Metabolite Origins via Network*) que permite el análisis de las interacciones presentes entre los datos del microbioma intestinal y el metaboloma, es decir determina el grado en el que los compuestos anotados en el metaboloma urinario de los recién nacidos prematuros pueden haber sido producidos por bacterias presentes en las muestras fecales, producidas por el propio recién nacido prematuro, producido por ambos o por el contrario, por ninguno de ellos. Del conjunto de rutas metabólicas, se observó como el impacto de la ruta de biosíntesis de hormonas esteroideas, la herramienta lo atribuye al metabolismo humano con *p* valores de 0.0005 para el metabolismo humano y 1 para el microbiano. Sin embargo, los metabolitos de la ruta del metabolismo de pirimidinas, está más pronunciado por el metabolismo bacteriano con p valores de 0,0005 para el metabolismo humano, mientras que un $7 \cdot 10^{-8}$ para el metabolismo bacteriano.

Por último, e incluido en la última sección "*Monitorización del cambio metabólico en neonatos con cardiopatías congénitas tras una intervención quirúrgica*", se realizó un análisis metabolómico aplicado a recién nacidos con TGA. En este caso, un total de 12 pacientes fueron incluidos en el estudio, empero uno de ellos pereció y dos no requirieron BAS. A nivel clínico y de manera monitorizada, se midieron diferentes parámetros que sirvieron para combinarlos con los parámetros analíticos medidos y donde se pudieron hacer las comparaciones correspondientes. Medidas como la saturación de oxígeno periférica preductal (SpO_2, del inglés *peripheral oxygen saturation*,), saturación regional de oxígeno del tejido cerebral ($rcSO_2$, del inglés, *regional cerebral tissue oxygen*

saturation,), extracción fraccionada de oxígeno tisular (FTOE del inglés, *fractional tissue oxygen extraction*,), espectroscopía de infrarrojo cercano (NIRS del inglés, *near infrared spectrocopy*), extracción de oxígeno cerebral (CEO_2 del inglés, *cerebral oxygen extraction*), saturación de oxígeno (SaO_2 del inglés, *saturation oxygen*) y saturación de oxígeno venoso central (ScO_2 del inglés central *venous oxygen saturation*) sirvieron para obtener información de todos los recién nacidos del estudio. En cuanto a los parámetros analíticos, fueron dos vertientes los que se realizaron. Por un lado, se procedió a la cuantificación de biomarcadores de peroxidación lipídica, de los cuales se cuantificaron los parámetros totales de neurofuranos, isofuranos y neuroprostanos, pero no se encontraron cambios significativos (prueba de la U de Mann-Whitney, $\alpha = 0.05$) así como correlaciones entre los distintos parámetros totales y la FTOE obtenida (coeficientes de correlación de Pearson > 0,5). Por otro lado, se realizó un análisis metabolómico no dirigido en plasma con la intención de ver qué era lo que sucedía en estos recién nacidos a lo largo de diferentes tiempos antes y después del BAS. Con las variables obtenidas después del procesamiento de los datos, se construyó un PCA para ver cómo se distribuían las muestras en función de su covarianza. Se pudo observar como el tiempo de recogida de las muestras antes y los diferentes tiempos después del BAS estaba impactando en el metaboloma plasmático, por lo tanto, se pudo ver como el metaboloma plasmático era dependiente del tiempo. Posteriormente, utilizando la FTOE como parámetro clínico el cual indica el balance entre el consumo y suministro de oxígeno, se construyó un modelo correlacionándolo con los cambios en el metaboloma plasmático observado. Dicha correlación se plasmó en un mapa de calor y se pudieron observar dos grupos diferenciados

(correlación Pearson < 0.05). Por último, se realizó un análisis de rutas gracias a la herramienta en línea MetaboAnalyst 4.0 en el cual y se observó que 4 rutas metabólicas se alteraron significativamente correlacionando las variables del metaboloma plasmático con la FTOE.

Conclusiones y trabajo futuro

A partir de los resultados obtenidos en los distintos estudios metabolómicos en el área neonatal, englobados en la presente Tesis Doctoral, es posible extraer las siguientes conclusiones:

- El análisis de las alteraciones en el metaboloma plasmático de los recién nacidos con EHI sometidos a TH permite discriminar aquellos con una mayor probabilidad de mostrar un patrón patológico en RMN.
- Existe una asociación significativa entre el daño por EHI, establecido a partir de resultados de RMN, y cambios longitudinales en el metaboloma urinario de recién nacidos. Se ha observado como la TH influye significativamente en el paciente, del mismo modo se ha podido monitorizar el perfil metabolómico de pacientes con EHI moderada y grave y abre una nueva perspectiva para una posible monitorización de pacientes en la UCIN, así como respaldar la predicción temprana de resultados.
- La determinación cuantitativa de los compuestos de la biosíntesis de esteroides, ruta metabólica del triptófano, biomarcadores de hipoxia y los intermediarios energéticos, junto con la secuenciación de los microRNAs han revelado aspectos fisiológicos interesantes y pueden servir como base para profundizar en la fisiopatología de la EHI.
- La composición de la LMD difiere con la LM, además la alimentación de la LMD tiene un impacto significativo en el fenotipo metabolómico y la microbiota de los recién nacidos prematuros. Los resultados obtenidos ayudan a entender el origen de los cambios observados en función de las rutas metabólicas afectadas, aunque las

implicaciones a corto y largo plazo deben evaluarse con estudios adicionales.

- El análisis del metaboloma de recién nacidos con TGA permite observar diferencias en el suministro y consumo de oxígeno a nivel cerebral durante la hipoxia y la normoxia. La evaluación combinada de los biomarcadores de peroxidación lipídica y el análisis metabolómico no dirigido proporciona información valiosa para comprender la fisiopatología de esta compleja enfermedad.

Los resultados y conclusiones alcanzadas permiten generar nuevas líneas de investigación en el área neonatal, entre las que se incluye:

- La nueva información obtenida mediante los resultados de las baterías de compuestos, la identificación de nuevas rutas metabólicas alteradas, al igual que la secuenciación de microRNAs en recién nacidos con EHI, podría usarse en el futuro para mejorar la capacidad diagnóstica temprana y tratar selectivamente a los recién nacidos en función de su condición de severidad.
- La identificación de nuevas estrategias para la optimización y personalización de la nutrición neonatal a través de la modificación de la composición de la LMD (fortificación dirigida), así como de posibles cambios en las pautas de la recogida, procesamiento y conservación de la LMD.
- La realización de un estudio prospectivo observacional en el que se compare posibles situaciones de hipoxia postnatal dependientes del conducto arterioso junto con la comparación del perfil metabolómico no dirigido antes y después de la

instauración de prostaglandinas para la dilatación del conducto arterioso. La información obtenida puede ser válida para la evaluación de mecanismos de adaptación a la hipoxia y a la normoxia post intervención.

List of abbreviations

aEEG amplitude-integrated electroencephalography

AMON Annotation of Metabolite Origins via Networks

ASO arterial switch operation

BAS Balloon atrial septostomy

CE-ESI TOFMS capillary electrophoresis–electrospray–time-of-flight mass spectrometry

CEO_2 cerebral oxygen extraction

CI confidence interval

DHM donor human milk

ESI^- negative electrospray ionization

ESI^+ positive electrospray

FC fold changes

FDR false Discovery rate

FTOE fractional tissue oxygen extraction

GA Gestational age

GC-MS gas chromatography-mass spectrometry

HIE Hypoxic-Ischemic Encephalopathy

HM Human Milk

HMO Human milk oligosaccharide

IQR interquartile range

IS internal standards

IPA isopropanol

KEGG Kyoto Encyclopedia of Genes and Genomes

KO KEGG Orthology identifier

LC-TOFMS Liquid Chromatography-Time of flight Mass Spectroscopy

MRI magnetic resonance imaging

MS mass spectrometry

MTBE methyl tert-butyl ether

NADPH nicotinamide adenine dinucleotide phosphate

NE neonatal encephalopathy

NEC necrotizing enterocolitis

NICHD National Institute of Child Health and Human Development

NICUs Neonatal Intensive Care Units

NIRS near infrared spectroscopy

NRN Neonatal Research Network

OMM own mother's milk

OS oxidative stress

OTU Operational taxonomic unit

PC principal component

PCA Principal Component Analysis

PCoA Principal Coordinates Analysis

PERMANOVA permutational multivariate analysis of variance

PGE1 prostaglandin E1

PICRUSt Phylogenetic Investigation of Communities by Reconstruction of Unobserved States

PLSDA partial least squares discriminant analysis

PPP pentose phosphate pathway

PRPP phosphoribosyl pyrophosphate

QC quality control

R pearson correlation coefficients

$rcSO_2$ regional cerebral tissue oxygen saturation

ROC Receiver operating characteristic

ROS reactive oxygen species

SD standard desviation

SpO_2 preductal peripheral oxygen saturation

TGA Transposition of the great arteries

TH therapeutic hypothermia

UDP-glucoronate uridine diphosphate glucoronate

UHPLC-TOFMS ultra-high-performance liquid chromatography–quadrupole time-of-flight mass spectrometry

List of tables

List of figures

Abstract

In this PhD Thesis different physiological and pathological situations that are relevant to the neonatal field have been assessed. Hypoxic-Ischemic encephalopathy (HIE) is a neurologic sequela of perinatal asphyxia. In this Thesis, the aim was to improve prediction of outcomes of HIE, which would be of key importance for developing personalized treatment strategies and reduce neonatal mortality and morbidity. Furthermore, breastfeeding is the gold standard for nutrition of the term and preterm infants. For preterm infants whose mothers are unable to provide of own mothers' milk (OMM), pasteurized donor human milk (DHM) is the preferred alternative. In this Thesis, metabolic signature of preterm infants has been studied to unscramble the effect of nutrition on their metabolism. Likewise, transposition of the great arteries (TGA) is a congenital heart disease characterized by hypoxemia and abnormal circulation is responsible for brain alteration and long-term neurodevelopmental delay. Atrial septostomy causes a sudden increase in arterial blood oxygenation leading to complex metabolic changes. In this Thesis, the metabolic switch in infants with TGA after atrial septostomy were assessed to shed light on the effect of the changes in the cerebral oxygenation.

On the one hand, the purpose of studies are focused in determination novel biomarkers in plasma and urine samples of newborns with different severity of asphyxia employed LC-TOFMS, LC-MS/MS, CE-MS, GC-MS and microRNA expression. Also, in a cohort of preterm infants, the metabolic signatures have been analyzed

to understand the relationship between nutrition and the urinary metabolome of premature newborns fed with human milk and donor human milk employed LC-TOFMS in urine and milk samples and the expression of gene microbiota in stool samples. Finally, in a cohort of newborns with congenital heart disease, we studied the metabolic switch in infants with TGA after atrial septostomy in order to shed light on the effect of the changes in the cerebral oxygenation. Plasma samples were measured employing LC-TOFMS and LC-MS/MS to identify biomarkers of oxidative stress.

In infants with moderate/severe HIE the altered metabolomic pathway and the metabolite panel with microRNA assessment might support prediction of long-term neurodevelopmental outcomes of perinatal brain injury. Observed changes in the nutritional approach could be potentially attributed to i) diet-dependent changes in the colonization pattern of preterm infants that might affect hormone production, ii) changes in the hormone levels in human milk and/or iii) the effect of pasteurization on DHM hormone levels. Based on the results, futures studies for assessing the impact of maternal nutrition as well as treatment and storage on human milk composition are encouraged. In TGA cohort, we observed correlation of metabolic features with cerebral tissue oxygen extraction (FTOE) and affected pathway with significant differences. Although the number subjects include are limited and require validation in follow-up studies, the results shown an important role of oxidative stress in the physiopathology of these infants.

Hypothesis and objectives

This Doctoral Thesis is developed from the starting hypothesis, in which it intends to the exhaustive characterization of the metabolome of the newborn, which provides useful information for the study of different physiological and pathological situations in the neonatal period.

Thus, the aim will be to provide tools to carry out comprehensive metabolomics that address relevant research questions in the field of perinatology, such as the discovery and identification of biomarkers for personalized medicine and the exploration of a holistic response at the global phenotype.

For this, different clinical relevant situations to the health of the newborn have been proposed to study:

- Discovery of biomarkers for the early prediction of neonatal brain injury.
- Assessment of the impact of diet on the growth and development of preterm infants.
- Metabolic changes in newborns with congenital heart disease associated with surgery.

Section I. Biomarkers for early prediction of neonatal brain injury

Chapter 1. Metabolic Phenotypes of Hypoxic-Ischemic Encephalopathy with Normal vs. Pathologic Magnetic Resonance Imaging Outcomes

1.1 Abstract

Hypoxic-Ischemic Encephalopathy (HIE) is one of the most relevant contributors to neurological disability in term infants. We hypothesized that clinical outcomes of newborns with HIE can be associated with changes at plasma metabolic level enabling the detection of brain injury. Plasma samples of a cohort of 55 asphyxiated infants who evolved to moderate/ severe HIE were collected between birth and completion of therapeutic hypothermia (TH). Samples were analyzed employing a quantitative gas chromatography–mass spectrometry method for the determination of lactate and pyruvate and an untargeted liquid chromatography–time-of-flight mass spectrometry method for metabolic fingerprinting. Brain injury was assessed employing magnetic resonance imaging (MRI). A critical assessment of the usefulness of lactate, pyruvate, and pyruvate/ lactate for outcome prediction was carried out. Besides, metabolic fingerprinting identified a dynamic perturbation of eleven metabolic pathways, including amino acid and purine metabolism, and the steroid hormone biosynthesis, in newborns with pathologic MRI outcomes. Although data suggest the usefulness of lactate and pyruvate monitoring during 72 h for discerning outcomes, only the steroid hormone biosynthesis pathway was significantly altered

in early plasma samples (i.e., before the initiation of TH). This study highlights pathways that might potentially be targeted for biomarker discovery or adjuvant therapies to be combined with TH.

1.2 Introduction

Hypoxic-Ischemic Encephalopathy (HIE) is the neurological consequence of impaired blood flow and/or gas exchange during birth [40]. Decreased cerebral perfusion and oxygenation trigger a sequence of acute cerebral metabolic alterations that characterize the primary energy failure phase of HIE. After resuscitation, the process undergoes a latent phase that lasts up to 6 h. This stage is followed by a secondary energy failure phase that enhances cerebral injury and may last for days, weeks, or even months [23].

HIE is one of the most relevant contributors to neurological disability in the pediatric age. In high-income countries, the incidence of HIE is around 1.6 per 1000 infants, while the risk is around 10-fold higher in low-income countries [41]. Therapeutic hypothermia (TH) initiated within 6 h of birth constitutes the standard of care for infants with moderate or severe HIE reducing mortality and improving neurodevelopmental outcome in survivors [42].

At present, no bedside test is available for an accurate and early diagnosis of HIE. In the delivery room, physicians rely on prenatal clinical information and serial Apgar scores with special emphasis on neurological assessment. In addition, cord blood gases, metabolic acidosis, and increased lactacidemia further reflect the severity of anaerobic metabolism [23]. The modified Sarnat staging system grades neonatal HIE according to the severity of the brain insult [43]. Later on, amplitude-integrated electroencephalography (aEEG) and/ or

multichannel EEG and cranial ultrasound will confirm the diagnosis [44]. Magnetic resonance imaging (MRI), including diffusion weighted imaging and spectroscopy, performed 5–7 days after birth, is the cornerstone for neurodevelopmental outcome prediction [45]. Particularly, time-dependent reductions in brain N-acetyl aspartate and creatinine concentrations at 18–96 h and 7–14 days are able to accurately predict adverse outcomes, whereas elevated cerebral lactate, glutamate, and glutamine concentrations have been found to be transient [46]. However, unstable neonates may not tolerate transport necessary for MRI or MRI scanning duration. Moreover, hypothermia may alter EEG recordings and limit its early predictive capacity [23].

HIE has been associated with damage to the integrity of the blood–brain barrier and, hence, brain injury could be reflected in peripheral blood samples [47]. In the search for blood biomarkers capable of determining the degree of brain injury and providing prognostic information, an array of different molecules has been proposed including neuronal tissue specific proteins, proteins involved in the pathogenesis of traumatic brain injury, excitatory amino acids, lipid peroxidation products, specific microRNAs, and inflammatory markers [23,44]. Despite the potential of these markers, few small pilot studies have validated their utility in the clinical practice [48] and none has been added to clinical guidelines [24].

Blood lactate, a hallmark of anaerobic metabolism, has been traditionally employed as surrogate marker for tissue hypoxia and/ or ischemia. Pyruvate dehydrogenase controls the metabolic flux between the tricarboxylic acid cycle and glycolysis. Under hypoxic conditions, glucose is metabolized into lactate and exported to the extracellular compartment [49] In infants with moderate/ severe brain injury, a very

strong correlation was found between serum and cerebral lactate concentrations at the basal ganglia, thalamus, and gray matter regions during TH [49]. It has been suggested that monitoring lactate could be useful for assessing the degree of HIE and even predict long-term neurodevelopmental outcomes [50]. However, these speculations were not based on adequately powered clinical studies.

Comprehensive metabolic phenotyping has been increasingly employed for identifying possible therapeutic targets, and the discovery of biomarkers to support treatment selection, patient stratification, and enhanced diagnosis [24]. However, metabolomics has only been scarcely used for progressing our understanding of the multilayer effects of HIE and TH on the newborn [51]. ^{1}H-nuclear magnetic resonance was used to characterize umbilical cord blood samples from infants with perinatal asphyxia or HIE compared to matched healthy controls, revealing significant changes in 18 metabolites [52]. A panel of four metabolites showed potential for predicting HIE severity according to Sarnat staging; however, it was not found to be superior to EEG or the Sarnat score for predicting neurodevelopmental outcome at three years of age [53]. Umbilical cord blood of a similar cohort of newborns with signs of perinatal asphyxia and HIE as well as matched healthy controls was studied employing direct infusion Fourier-transform ion cyclotron resonance mass spectrometry (MS) [54]. Eight putatively annotated metabolites were identified to be significantly altered in newborns with HIE and four metabolites differentiated across severity grades of HIE based on continuous multichannel EEG monitoring at 24 h of life. In a longitudinal study involving six infants with mild/ severe HIE, a specific metabolic profile was identified in urine samples as compared to healthy control subjects on Days 1 and 3 after birth [55].

The aim of this study was to elucidate dynamic metabolic changes in a cohort of newborn infants evolving to moderate/ severe HIE undergoing TH in which hypoxia–ischemia-induced brain injury was assessed employing MRI. This study describes for the first time the evolution of the neonatal plasma metabolome of HIE covering the time period between birth and completion of TH treatment. The objectives of the present study were focused on preselecting disease-specific pathways at the phenotypic level that might be suitable for enabling an identification of those infants at risk of developing brain injury within the infants that qualify for hypothermia treatment as well as for monitoring the individual response to treatment and elucidating new potential therapeutic targets.

1.3 Results

1.3.1 Patients Characteristics

Population characteristics are shown in **Table 1.1.** There were only minor, non-significant differences between the control and the pathologic group, i.e., a higher proportion of males in the control group (59% vs. 42%) and higher proportion of C-section in the pathologic group (64% vs. 41%). Regarding the Sarnat staging, in the normal group, 86% of infants were initially identified as Sarnat 2, whereas, in the pathologic group, the proportion was 58% (p-value = 0.05). Although the analysis of the effect of topiramate vs. placebo was out of the scope of this study, the inclusion of a similar proportion of individuals from both treatment groups (p-value = 0.7) allowed compensating for the impact (confounder) of potential effects of pharmacological treatment on the metabolome.

Table 1.1 Clinical and demographic data of newborns

Parameter	Normal (N=22)	Pathologic (N=33)	p-value
Inborn	3 (14%)	8 (24%)	0.5
Maternal age (years)	34 (5)	33 (6)	0.4
Gestational age (weeks)	38.4 (37.3, 40.6)	39.0 (38.0, 40.6)	0.3
Gender (male, %)	13 (59%)	14 (42%)	0.3
Birth weight (g)	3265 (552)	3295 (697)	0.4
Length (cm)	51 (3)	51 (3)	0.4
Head circumference (cm)	34 (2)	34 (2)	0.3
Delivery mode (C-section)	9 (41%)	21 (64%)	0.2
Apgar score 1 min	2 (1, 4)	1 (1, 3)	0.6
Apgar score 5 min	4 (2, 5)	3 (1, 5)	0.3
Apgar score 10 min	5 (4, 6)	5 (4, 6)	1.0
Sarnat 2 / Sarnat 3	19/3	19/14	0.05
pH UC	7.06 (0.27)	6.97 (0.17)	0.09
BE UC	-13 (10)	-16 (7)	0.2
pCO_2 (mmHg) UC	71 (33)	59 (33)	0.2
HCO_3 UC	15 (6)	13 (6)	0.2
Topiramate treatment (yes, %)	10 (45%)	17 (52%)	0.7
MR (days)	7 (5, 10)	7 (7, 10)	0.4

Note: values are mean (SD), median (interquartile range), or n (%); p-values have been calculated employing the Student's t-test for unequal variances, the Wilcoxon ranksum test (α=0.05) or the chi2-test (α=0.05); UC = umbilical cord; BE = base excess; MR = magnetic resonance; inborn refers to infants born at the hospital where hypothermia treatment was carried out

1.3.2 Plasma Lactate and Pyruvate Levels

The evolution of lactate and pyruvate plasma concentrations as well as lactate/pyruvate with time are shown in **Figure 1.1.** For lactate, as well as pyruvate median concentrations at all studied time points were higher in newborns with pathologic MRI outcomes. In order to assess the potential of lactate, pyruvate and lactate/pyruvate levels determined in blood before the initiation of TH and 24, 48 and 72 h after initiation

of TH for predicting pathologic MRI outcomes, groups were compared employing the Wilcoxon rank sum test. Newborns with pathologic MRIs had significantly higher levels of lactate at 24 and 48 h as well as pyruvate at 72 h. Lactate/pyruvate did not show a clear trend with time and was not useful for discriminating between normal and pathologic MRI outcomes at any studied time point.

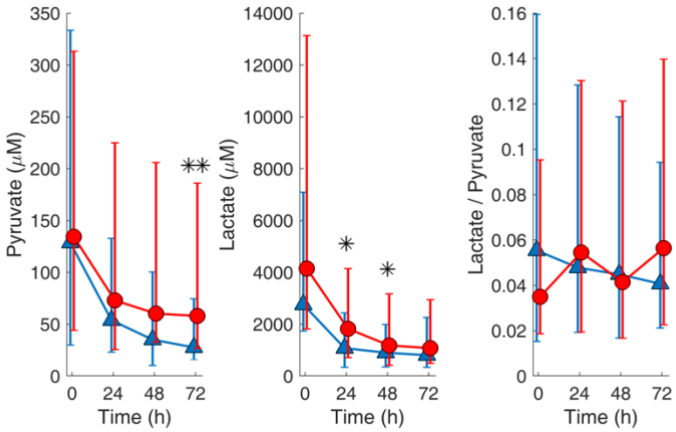

Figure 1.1 Evolution of pyruvate and lactate concentrations and lactate/pyruvate in plasma samples from newborns with normal (blue Δ and errorbars are median and percentile 25 and 75, respectively) and pathologic (red o and errorbars are median and percentile 25 and 75, respectively) MRI outcomes. Note: norm vs. pathologic at 0 h N=13 and 23; at 24 h N=20 and 30; at 48 h N=22 and 28; and at 72 h N=20 and 32, respectively; * and ** indicate p-vales below 0.05 and 0.01, respectively (Wilcoxon ranksum test) for comparing normal vs. pathologic MRI outcomes.

1.3.3 Untargeted Metabolomic Analysis

Figure 1.2 shows Principal Component Analysis (PCA) scores plot of plasma metabolomic analysis collected at the different time points. The strong impact of time on the plasma metabolome can be observed in direction of principal component (PC) 2 (9.5% of the total variance). Based on this observation, further data analysis was stratified by the sampling time point.

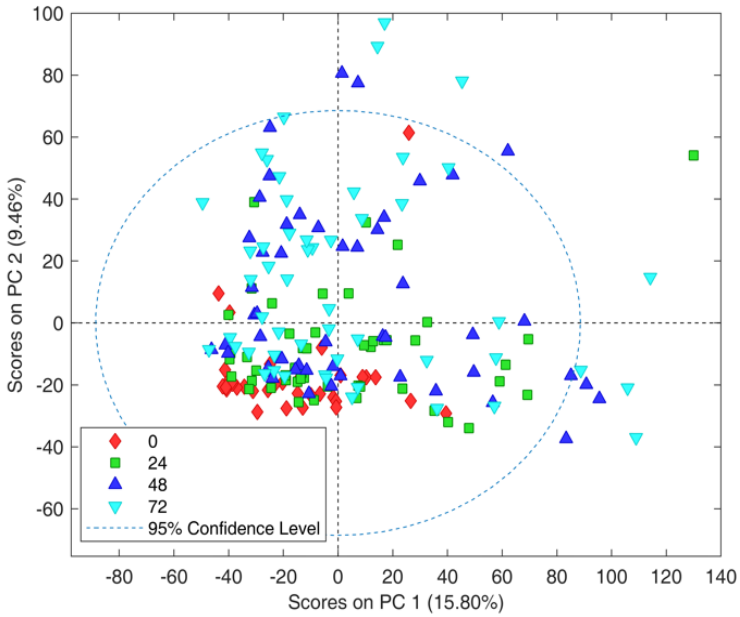

Figure 1.2. PCA scores plot of plasma metabolomic fingerprints.

Figure 1.3 shows the number of features with different mean values (t-test, $\alpha = 0.05$) comparing normal vs pathologic outcomes as determined by MRI. It can be observed that the number of altered features increases with time. Whereas 208 (2.6%) of the total of 8122 detected features showed different mean concentrations in blood before the initiation of TH, 24 h after the initiation of TH already 491 (6.0%) were altered; 48 h and 72 h after the initiation of TH this value further increased up to 1228 (15.1%) and 1330 (16.4%), respectively. Furthermore, the pattern of affected metabolites shifted over time with only 65 of altered features shared between blood before the initiation of TH and 24h samples, to 279 between 24 and 48 h samples and 776 between 48 and 72 h samples. This indicates, that the alteration of the metabolome in newborns with pathologic MRI outcomes rapidly changes at early time points and slowly stabilizes thereafter. In **Figure 1.4**, heatmaps of the intensities of 2071 metabolic features that showed different distributions between normal and pathologic groups in at least

one of the sampling times are depicted. Visual inspection of heatmaps confirms an increase of HIE specific plasma metabolite patterns with time: whereas no clear patterns are observed from metabolites detected in blood before the initiation of TH, differences are visible after 24 h and become more evident after 48 and 72 h.

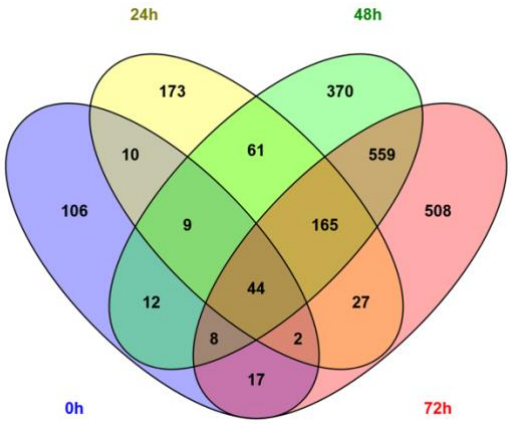

Figure 1.3. Venn-diagram showing the overlap among altered metabolic features in plasma samples collected 0, 24, 48 and 72 h.

Table 1.2 summarizes the metabolic pathways significantly altered in at least one of the studied time points and **Table A.1.1** shows the annotation of altered metabolites detected in plasma samples from newborns with HIE and normal vs. pathologic MRI outcomes. In line with previous observations, different pathways were affected in blood before the initiation of TH as compared to the remaining sampling times. Again, the number of altered pathways varies with time with 3, 2, 5 and 9 altered pathways in the first blood sample collected, and 24, 48, and 72 h after the initiation of TH, respectively. In blood collected before the initiation of TH, purine, seleno amino acid metabolism, and steroid hormone synthesis were affected in newborns with pathologic MRI outcomes. Later on, additional pathways mainly related to amino acid

metabolism were altered. Only one metabolic pathway, i.e. steroid hormone biosynthesis, remained altered during the whole study period. **Figure 1.5** shows the steroid hormone synthesis pathway and its intermediates highlighting metabolites detected and/or altered in this study at the four studied time points.

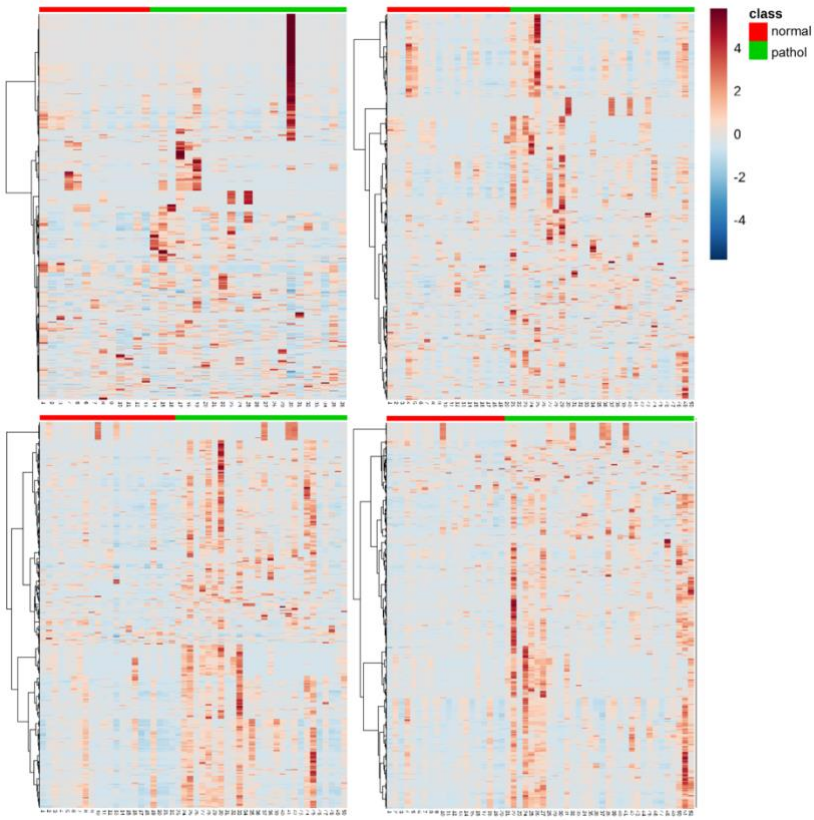

Figure 1.4. Heatmaps of altered plasma metabolic features (N=2071) in samples collected at 0 (top, left), 24 (top, right), 48 (bottom, left) and 72 h (bottom, right). Note: norm vs. pathologic at 0 h N=13 and 23; at 24 h N=20 and 30; at 48 h N=22 and 28; and at 72 h N=20 and 32, respectively.

Table 1.2. Altered pathways in newborns suffering from HIE with pathologic MR outcomes.

Pathway	Total # of metabolites	Hits (total)	Hits (sig)	Fisher's P	Hits (sig)	Fisher's P	Hits (sig)	Fisher's P	Hits (sig)	Fisher's P
			T0		T24		T48		T72	
Alanine, aspartate and glutamate metabolism	24	19	6	0.14	5	0.9	13	0.4	16	0.04
Arginine and proline metabolism	77	50	10	0.5	21	0.4	41	0.002	41	0.003
Caffeine metabolism	21	2	2	0.04	2	0.2	2	0.4	2	0.4
D-Glutamine and D-glutamate metabolism	11	7	1	0.8	3	0.6	7	0.03	7	0.04
Limonene and pinene degradation	59	7	2	0.4	1	1.0	4	0.7	7	0.04
Lysine biosynthesis	32	20	3	0.8	11	0.10	17	0.02	19	0.0013
Lysine degradation	47	32	7	0.4	17	0.07	21	0.4	28	0.002
Nitrogen metabolism	39	16	4	0.4	7	0.4	11	0.4	14	0.03
Phenylalanine metabolism	45	25	5	0.5	15	0.02	24	0.00009	21	0.02
Selenoamino acid metabolism	22	2	2	0.04	1	0.6	2	0.4	2	0.4
Steroid hormone biosynthesis	99	29	11	0.01	23	0.000009	25	0.004	25	0.006

Note: results with a Fisher's P-value < 0.05 are gray-shaded.

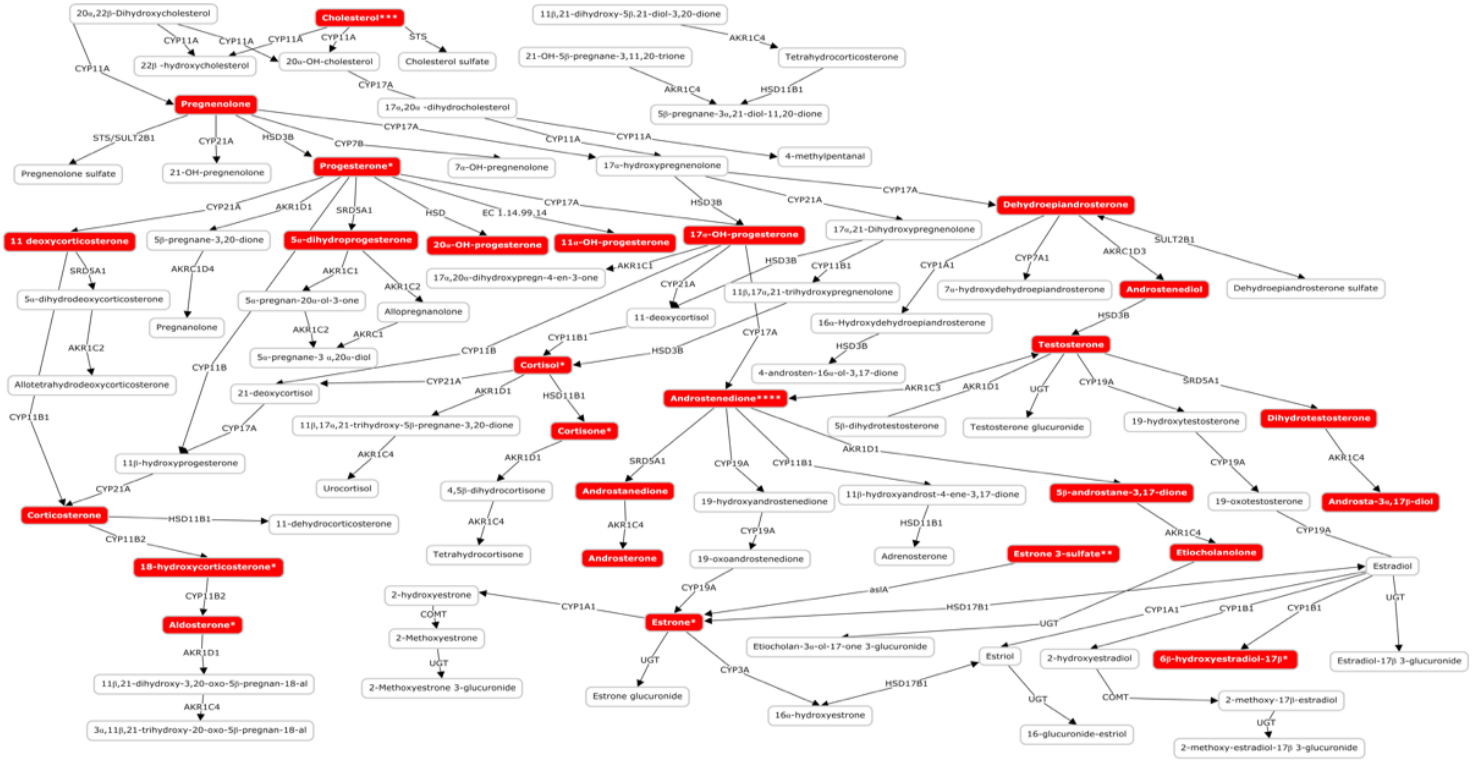

Figure 1.5. Altered metabolites of the steroid hormone biosynthesis pathway in plasma samples from newborns suffering from HIE at birth and 24, 48 and 72 h after the initiation of TH. Note: * = altered only at 24, 48 and 72 h after the initiation of TH; ** = altered only at 48 and 72 h after initiation of TH; *** altered only at 48 after the initiation of TH; **** = altered only at 72 h after the initiation of TH

1.4 Discussion and conclusions

The HYPOTOP trial was designed to minimize shortcomings of single center trials thus improving the generalizability of the observations. This is underpinned by the homogeneity of the clinical and demographic parameters between both study groups (normal vs. pathologic MR outcome) as shown in Table 1. For the quantitative determination of lactate and pyruvate, a targeted gas chromatography-mass spectrometry (GC-MS) method was used, whereas untargeted fingerprinting was carried out using LC-TOFMS. For lactate and pyruvate concentrations in plasma samples collected before the initiation of TH, poor predictive values were found, whereas during TH, lactate (24 and 48 h) and pyruvate (72 h) were able to discriminate between newborns with confirmed brain injury and normal outcomes as, shown in **Figure 1.1**. Optimum cut-off values from receiver operating characteristic (ROC) curves of 1.1 mM and 51.4 μM for lactate at 24 and 48 as well as pyruvate at 72 h, respectively, were obtained for the discrimination between both groups. The difference in concentration levels of lactate between newborns with normal and pathologic MRI outcomes decreased over time, whereas an increase was noted for pyruvate concentrations. Due to the high capacity for lactate transport into and out of the brain, blood lactate has been employed as surrogate marker for brain tissue hypoxia and/or ischemia. It has been demonstrated that serum lactate strongly correlates with cerebral lactate concentrations at the basal ganglia, thalamus, and gray matter regions measured during TH in newborns with moderate to severe brain injury [49]. In accordance with findings on blood lactate, the relative increase

in serum lactate dehydrogenase concentration between Days 1 and 3 was associated with central gray matter lesions [56]. Moreover, lactate and pyruvate concentrations were found to be elevated in plasma from newborns with HIE undergoing TH at 48 h as compared to a control group of healthy term infants [21] and serum lactate was significantly elevated at 72 h of life in newborns with poor neurodevelopmental outcomes [57]. Lactate levels acquired within the first hour of life in combination with serial measurements of lactate have been proposed as predictors of moderate/severe HIE [58] and prolonged time to normalization of serum lactate occurred in severe HIE with prolonged electrographic seizures [59]. In contrast, to date, no literature is available on blood pyruvate levels in newborn infants with HIE. In experimental studies, both concentrations of cerebral pyruvate and lactate were found to be elevated un hypoxia and hypoxia-ischemia [50].

A complementary analytical approach aimed at exploiting the potentials of untargeted metabolomic fingerprinting for enhancing the current understanding of the complex perturbations of hypoxia-ischemia on the individual, phenotypic level and its impact on the pathophysiology of HIE. The importance of repeated phenotypic monitoring should be highlighted as it is well known that HIE passes through different phases and TH induces a reduction in cerebral and whole-body metabolism [23]. Furthermore, the transition of the neonate from hypoxic in utero conditions to a relatively oxygen-rich environment induces changes in the metabolome. In an animal model, 23% of the detected metabolites showed a significant change in concentration when comparing umbilical cord blood to blood samples drawn until after birth [60]. In the present study, a clear effect of the time elapsed from birth until sample collection has been observed (see **Figure 1.2**), with the

pattern of injury becoming more visible as time evolves (see **Figure 1.3**; **Figure 1.4**). This was further corroborated by the results of pathway analysis shown in **Table 1.2** and **Table A.1.1**, where an upward trend in the number of altered pathways with time was observed while the pattern of injury emerges during secondary energy failure.

We demonstrated that the early evolving blood metabolome provides useful information for the discrimination of newborns who will show pathologic MRI patterns after TH. In the first blood sample analyzed in this study, collected before initiation of TH, levels of two metabolites of the purine metabolism, i.e., xanthine and its derived nucleoside xanthosine, were found to be altered. Purine metabolism has been described repeatedly to be affected in animal experiments on hypoxia/reoxygenation [61]. Furthermore, the steroids hormone biosynthesis pathway was affected over the whole study period in newborns with HIE and pathological MRI outcomes, but became especially relevant during TH. In agreement with our observations (see **Table A.1.1**), a significant increase of neonatal 17-hydroxyprogesterone levels has been reported in blood samples from infants suffering from birth asphyxia and neonatal seizures [62]. Although the influence of drugs administered for sedation, or antibiotics and vasopressor drugs cannot be ruled out, the observed effect might likely be linked to the response to stress and pain that inevitably triggers a hormonal response affecting epinephrine, norepinephrine, and cortisol levels. On the other hand, the use of hormones has been proposed as therapeutic drugs in the context of HIE. In experimental studies, the administration of glucocorticoids [63] and progesterone [64] ameliorated neonatal hypoxic-ischemic brain injury.

At later time points in sample collected during TH, a total of eight pathways involving amino acid metabolism, synthesis and degradation have been observed to be perturbed when comparing between normal vs. pathologic groups. In the literature, several reports on the perturbation of amino acids in hypoxia and hypoxia-ischemia in experimental models an neonates ca be found [51] and the accumulation of excitatory amino acids (glutamate and aspartate) in cerebral tissue during the acute phase as well as secondary energy failure have been extensively described [23]. In umbilical cord blood of newborns with HIE in comparison to a healthy control group, alanine aspartate, and glutamate metabolism, as well as phenylalanine metabolism, were found to be altered [54] and changes in metabolite levels involved arginine and proline metabolism (i.e., proline [65]), nitrogen metabolism (i.e., phenylalanine [65] and tryptophan [54]), and phenylalanine metabolism (i.e., phenylalanine [65] and succinate [52–54] were observed.

This study has some limitations. Although TH is a routine clinical practice, patients need to be transferred to level III NICUs to receive this treatment. Consequently, umbilical cord blood could not be collected from these patients. This is an intrinsic problem of studies on infants with HIE and the exclusion of outborn infants would dramatically increase the time needed for the recruitment of a representative number of subjects. In addition, this study does not include a healthy control group or newborns with asphyxia or classified as mild HIE (Sarnat 1), as only newborns subjected to hypothermia treatment were included. There is risk of adverse neurodevelopmental outcome of mild HIE newborns, but, up to now, there is no evidence to support cooling in these babies, and therefore we consider that the study of the metabolic fingerprint of those infants in correlation with the clinical outcomes would be of

interest [66]. Furthermore, metabolomic coverage could be increased by taking advantage of complementary methods and analytical platforms. The use of complementary methodological approaches might help to achieve a more comprehensive view of the global effects of HIE on the plasma metabolome. Before the findings described in this study can be translated to the clinic, an exhaustive validation of the results is necessary involving the identification and quantification with primary standards following guidelines of regulators such as the U.S. Food & Drug Administration and European Medicines Agency.

We report the first metabolomic study involving human subjects and serial sample collections in HIE for modeling brain injury as confirmed with MRI. Herein, the time-dependent evolution of lactate and pyruvate levels in newborns with HIE undergoing TH is shown. Our data underpin the usefulness of blood lactate with a cut-off value of 1.1 mM between 24 and 48 h and pyruvate with a cut-off value of 51.4 µM at 72 h for anticipating favorable/ unfavorable MRI outcomes. Although these findings need to be validated in independent cohorts, these biomarkers could be easily implemented within clinical routine care, as portable devices for point-of-care testing are commercially available. However, at very early sampling time points (before initiation of TH), the measurement of those parameters does not support outcome prediction. Metabolic pathway analysis revealed the time-dependent perturbation of several pathways. Purines (i.e., xanthine and xanthosine) were found to be altered in blood samples from newborns with pathologic MRI outcomes drawn before the initiation of TH and the steroid hormone biosynthesis pathway has been significantly altered during the whole study period comprising early samples collected shortly after birth and until completion of TH after 72 h. Hence, this

study provides evidence of the usefulness of metabolites from both pathways as candidate biomarkers to be evaluated in future clinical validation studies as they might allow an early prediction of central nervous system impairment reflected in an anatomic alteration detectable by MRI. In depth knowledge of metabolic alterations might furthermore support studies targeting the development of adjuvant therapies to be combined with TH, e.g., the administration of allopurinol and steroid hormones.

1.5 Materials and Methods

1.5.1 Study Approval

The study was approved by the Ethics Committee for Biomedical Research of the Health Research Institute La Fe (Valencia, Spain) and registered as EudraCT 2011-005696-17 under the acronym HYPOTOP. Informed consent was obtained from parents of all participants and all methods were performed in accordance with relevant guidelines and regulations.

1.5.2 Population

A cohort of 62 newborns enrolled in the HYPOTOP trial was included in this study according to pre-established inclusion and exclusion criteria. The HYPOTOP trial is a randomized, controlled, multicenter, double-blinded clinical trial aiming to assess the efficacy of topiramate *vs* placebo in patients with HIE undergoing TH. A detailed description of the HYPOTOP trial including the study design and sample-size estimation can be found elsewhere [39].

1.5.3 Magnetic Resonance Imaging

MRI was performed between days 4 and 8 after birth. It was carried out using a 3T magnet system (Signa Excite®, General Electric Healthcare, USA) and always included 3D Gradient Echo T1 weighted MR images, coronal and axial Fast Spin Echo T2 weighted MR images, diffusion weighted images (b0 and b1000 values), and susceptibility weighted imaging. In most of the cases, single voxel MR spectroscopy in thalamus, white, and grey matter was acquired using PROBE sequence, as well as diffusion tensor imaging (32 directions). The score used to differentiate mild from moderate and severe HIE was based on the MR score described by Barkovich [67]. Acute hypoxic ischemic insult in basal ganglia and thalami (BGT) was classified as mild if focal injury with normal posterior limb of the internal capsule (PLIC) was seen; as moderate if multifocal BGT pattern and equivocal or normal PLIC was identified, and as severe when diffuse BGT patterns and abnormal PLIC was detected. To evaluate white matter injury as well as cortical injury we defined mild injury when only periventricular white matter was involved and normal cortex was preserved, moderate when subcortical white matter and focal areas of cortical highlighting were identified and severe when widespread abnormalities with extensive cortical involvement were described. MRI results were interpreted by experienced, blinded radiologists. Based on the results of MRI, patients were classified as “normal” (N=22) or “pathologic” (N=33) neuronal outcomes following the criteria explained elsewhere [68]. Seven patients were excluded from further analysis as no MRI results were available. Patient characteristics of the remaining 55 infants are shown in **Table 1**.

1.5.4 Blood sampling, Processing and Storing

0.5 mL of whole blood were extracted at birth (umbilical cord blood, when available, or extracted as early as possible before the initiation of TH; N=36) and at 24 (N=50), 48 (N=50) and 72 h (N=52) after the administration of the first dose of medication or placebo from a peripheral vein using heparinized syringes (1% sodium heparin). Blood samples were centrifuged immediately at 1800 x *g* and 20 ºC during 10 min. Plasma was collected and stored at -80 ºC until analysis.

A total of 188 samples was collected from 62 newborns with moderate or severe HIE. Patients were recruited at 13 sites following a stringent study protocol and written standard operating procedures to limit the probability of chance correlations due to bias, systematic errors, or flaws in the experimental design.

1.5.5 Analytical Methods

1.5.5.1 Determination of Lactate and Pyruvate

The determination of lactate and pyruvate was carried out in plasma samples employing a two-step oximation-silylation procedure and a validated GC-MS method, employing a 6890GC-5973N GC electron impact quadrupole MS system as described elsewhere [21].

1.5.5.2 Untargeted Metabolomic Analysis

Plasma samples were thawed on ice and homogenized on a Vortex® S0200 mixer (LabNet, Edison, NJ, USA) during 10 s at maximum speed. 75 µL of cold (4 ºC) CH_3OH were added to 25 µL of plasma and samples were centrifuged at 16000 g during 15 min at 4 ºC.

80 µL of supernatant were collected and evaporated to dryness on a miVac centrifugal vacuum concentrator at room temperature and re-dissolved in 60 µL de H_2O:CH_3CN (0.1% v/v HCOOH) 95:5 containing phenylalanine-D_5, caffeine-D_9, leucine enkephalin, and reserpine, each at a concentration of 2 µM. Blank extracts were prepared by replacing whole blood with 500 µL of H_2O. A quality control (QC) sample was prepared by mixing 5 µL of each plasma sample and a total of 10 QC sample aliquots were processed as described for plasma samples.

Chromatographic separations were performed on an Agilent 1290 Infinity UHPLC chromatograph using a UPLC ACQUITY BEH C18 column (2.1 mm × 100 mm, 1.7 µm, Waters, Wexford, Ireland) and a flow rate of 400 µL min^{-1}. Autosampler and column temperatures were set to 4 and 40 °C, respectively, and an injection volume of 4 µL was used. Initial conditions of 98% of mobile phase A (H_2O (0.1% v/v HCOOH)) were kept for 0.5 min, followed by a linear gradient from 2 to 20% of mobile phase B (CH_3CN (0.1% v/v HCOOH)) in 3.5 min and from 20 to 95% B in 4 min. Conditions of 95% B were held for 1 min and a 0.25 min gradient was used to return to the initial conditions, which were held for 2.75 min.

Full-scan MS data between 100 and 1700 m/z with a scan frequency of 6 Hz (1274 transients/spectrum) were collected on an iFunnel quadrupole time-of-flight Agilent 6550 spectrometer operating in ESI^+ and TOF MS mode. The electrospray ionization parameters were set as follows: gas T, 200 °C; drying gas, 14 L min^{-1}; nebulizer, 37 psig; sheath gas T, 350 °C; sheath gas flow, 11 L min^{-1}. For automatic MS spectra re-calibration during analysis, a mass reference standard was introduced into the source via a reference sprayer valve using 149.02332

(background contaminant), 121.050873 (purine), and 922.009798 (HP-0921) *m/z* as references.

System suitability was checked employing a standard mixture containing internal standards. The analytical system was conditioned by injecting the QC extract 9 times at the beginning of the batch. Data acquired during system conditioning were discarded from data analysis. A total of 188 plasma sample extracts were analyzed in random order in a single analytical batch. QC samples were analyzed every 5^{th} sample and twice at the beginning and end of the batch for assessment and correction of instrumental performance [69]. Furthermore, automated UHPLC-ESI(+)-QqTOF (MS/MS) analysis of the QC sample was performed using two collision energies (20 and 40 V) to support metabolite annotation. The blank extract was injected a total of 4 times and used for data clean-up with the aim of identifying signals from other than biological origin.

1.5.5.3 Statistics

Raw UHPLC-TOFMS data was converted into centroid mzXML format using ProteoWizard [70]. Metabolomics data have been deposited to the EMBL-EBI MetaboLights database with the identifier MTBLS1041 and the complete dataset can be accessed here [71]. A peak table was extracted using XCMS (version 3.4.2) [72] running in R (version 3.5). A total of 38014 features were initially detected after peak detection, integration, chromatographic deconvolution, and alignment. The CAMERA [73] package was used for identifying peak groups and annotation of isotopes and adducts.

The obtained peak table was imported into MATLAB R2017b (Mathworks Inc., Natick, MA, USA) for further data processing and

analysis. To reduce intra-batch variation, the Quality Control-Support Vector Regression algorithm [74] and the LIBSVM library [75] were applied using an ε–range of 2.5 to 7.5, a γ-range of 1 to 10^5. C was defined for each feature as the median value in QCs. Then, features detected in blanks (i.e., median peak area in QCs < 5 times the maximum value detected in blanks) and those with a RSD% in QC samples ≥20% were excluded. The final peak table contained 8122 features. Systematic identification of detected features was carried out by matching *m/z* values against the Human Metabolome Database (version 4.0) [76] with 5 ppm accuracy. To increase confidence in the identification, MS/MS fragmentation spectra were matched against reference spectra from HMDB and METLIN databases. Peak intensities of internal standards and QC samples were used for monitoring the instrumental response during data acquisition throughout the batch as described elsewhere [74,77].

MATLAB 2017b inbuilt functions as well as in-house written scripts (available from the authors upon reasonable request) and the PLS Toolbox 8.0 from Eigenvector Research Inc. (Wenatchee, USA) were used for PCA, non-parametric Wilcoxon ranksum test, and *t*-test (α = 0.05, unequal variances). MetaboAnalyst (version 4.0) [78] was used for hierarchical clustering and the generation of heatmaps from auto scaled data employing Euclidean distance and Ward's method. As an input for pathway analysis, *t*-test *p*-values (α = 0.05, unequal variances) and fold changes were computed for each metabolic feature comparing normal and pathologic outcomes for each sampling time point separately. Pathway analysis was carried out using MetaboAnalyst with the 'MS peaks to pathways' tool (mass accuracy = 5 ppm; *mummichog* algorithm with *p*-value cutoff set to the top 10% of peaks) and the Kyoto

Encyclopedia of Genes and Genomes (KEGG) pathway library (*Homo sapiens*). Pathways with *p*-values from Fisher's exact *t*-test < 0.05 were considered as altered. Putative identifications based on *m/z* from pathway analysis were corroborated by manual inspection of raw data and MS/MS data when available ('level 2' identification as defined by The Metabolomics Standards Initiative [79]).

Chapter 2. Non-invasive monitoring of evolving urinary metabolic patterns in Hypoxic-ischemic encephalopathy

2.1 Abstract

Background: Infants with moderate and severe neonatal encephalopathy (NE) frequently suffer from long-term adverse outcomes. We hypothesize that the urinary metabolome of newborns with NE reflects the evolution of injury patterns observed with magnetic resonance imaging (MRI).

Methods: eligible patients were newborn infants with perinatal asphyxia evolving to NE and qualifying for therapeutic hypothermia (TH) included in the HYPOTOP trial. MRI was employed for characterizing brain injury. Urine samples of 55 infants were collected before, during, and after TH. Metabolic profiles of samples were recorded employing three complementary mass spectrometry-based assays, and the alteration of detected metabolic features between groups was assessed.

Results: The longitudinal assessment revealed significant perturbations of the urinary metabolome. After 24 h of TH, a stable disease pattern evolved characterized by the alterations of 4-8% of metabolic features related to lipid metabolism, metabolism of cofactors and vitamins, glycan biosynthesis and metabolism, amino acid metabolism, and

nucleotide metabolism. Characteristic metabolomic fingerprints were observed for different MRI injury patterns.

Conclusions: This study shows the potential of urinary metabolic profiles for the noninvasive monitoring of brain injury of infants with NE during TH.

Impact:

- A comprehensive approach for the study of the urinary metabolome was employed involving a semi-targeted capillary electrophoresis-time-of-flight mass spectrometry (TOFMS) assay, an untargeted ultra-performance liquid chromatography (UPLC)-quadrupole TOFMS assay, and a targeted UPLC-tandem MS-based method for the quantification of amino acids.
- The longitudinal study of the urinary metabolome identified dynamic metabolic changes between birth and until 96 h after the initiation of TH.
- The identification of altered metabolic pathways in newborns with pathologic MRI outcomes might offer the possibility of developing noninvasive monitoring approaches for personalized adjustment of the treatment and for supporting early outcome prediction.

2.2 Introduction

Perinatal asphyxia is defined as the interruption of blood flow and gas exchange to the fetus in the perinatal period. Prolonged hypoxia-ischemia can trigger a cascade of events leading to injury to vital organs, especially the brain (i.e., neonatal encephalopathy, NE). NE following birth asphyxia is a major cause of early neonatal death, cerebral palsy,

or neurodevelopmental disability in term neonates, affecting ~0.5-1.5 per 1000 live births in high-income countries and ~ 1 million infants every year worldwide [80–82]. Magnetic resonance imaging (MRI), including diffusion-weighted imaging and spectroscopy performed between the fifth and seventh day after birth, has become the cornerstone for establishing the degree of brain injyry and predicting neurodevelopmental outcome [83]. There is compelling evidence suggesting that perinatal asphyxia and the administration of supplemental oxygen may influence the brain at the molecular level by stimulating epigenetic modifications, including DNA methylation/demethylation, histone modifications, and miRNAs and epigenetic mechanism, that may be involved in the development of a hypoxic/ischemic-sensitive phenotype [84,85].

It has been observed that the combination of decreased cerebral perfusion and subsequent hypoxia triggers an evolving sequence of biochemical alterations that, lasting days, weeks, or even months, lead to anatomical and physiological injuries characterizing NE [22,23]. Therefore, a longitudinal biochemical assessment of NE is needed from birth until beyond the duration of therapeutic hypothermia (TH). NE has been associated with damage to the integrity of the blood–brain barrier, and therefore brain injury could be reflected in peripheral blood samples or other biofluids [47] theoretically enabling the implementation of noninvasive monitoring approaches. Metabolomics is a systems biology approach aiming at the holistic study of the complete pool of small molecules forming the metabolome of a biological sample. While metabolites are downstream products of the genome, transcriptome, and proteome, they reflect their interactions and the interaction with the environment, thereby providing a direct, dynamic, and meaningful read

out of the biochemical status of a system closely related to its actual phenotype [86]. Literature reports on the use of metabolomics for the study of perinatal asphyxia in newborns with NE are highly encouraging, although the main scope has been the early diagnosis of NE based on the comparison of asphyxiated/NE infants to healthy control infants [51–54,65,87], and metabolomics has only been scarcely used for progressing our understanding of the multilayer effects of NE and TH on the newborn [51,88]. Recently, the analysis of metabolic profiles of plasma samples collected between birth and until completion of TH enabled the identification of a dynamic perturbation of 11 metabolic pathways, including amino acid and purine metabolism, and the steroid hormone biosynthesis, in addition to pyruvate and lactate, in newborns with pathologic MRI outcomes [89]. In this study, we hypothesized that the urinary metabolome of newborns with NE recorded during the first 96 h of life encompasses the evolution of the injury pattern of the brain that is evidenced by MRI outcomes. Hence, the goal of this study is to provide insight into metabolic alterations secondary to brain injury in a clinical cohort of newborn infants with NE undergoing TH, with the aim of generating a knowledge base for the future development of a noninvasive monitoring approach, supporting the prediction of long-term clinical outcomes.

2.3 Materials and methods

2.3.1 Study approval and population

The study was approved by the Ethics Committee for Biomedical Research of the Health Research Institute La Fe (Valencia, Spain) and registered under the acronym HYPOTOP (EudraCT2011-005696-17).

The HYPOTOP trial is a randomized, controlled, multicenter, double-blinded clinical trial for assessing the efficacy of topiramate vs. placebo in newborns, with NE undergoing TH. All methods were performed in accordance with relevant guidelines and regulations, and informed consent was obtained from legal representatives of enrolled infants. For a detailed description of the HYPOTOP trial, including the study design and the established inclusion and exclusion criteria, the reader is referred to the literature [39]. In this study, a sub-cohort of 55 newborns enrolled in the HYPOTOP trial was included.

Samples were collected from urinary catheters or using sterile cotton pads placed in the diaper following a standard operating procedure to avoid bias and systematic errors. Urine samples were collected before initiation of TH at 6 h, as well as 12, 24, 48, 72, and 96 h after the initiation of TH. Samples were aliquoted into three dry microcentrifuge tubes and stored immediately at −80 °C until analysis.

2.3.2 Magnetic Resonance Imaging

MRI was carried out using different high-field magnet systems between days 4 and 8 after birth. In all cases, 3D Gradient Echo T1-weighted MR images, axial Fast Spin Echo T2-weighted MR images, and diffusion-weighted images were acquired. The interpretation of MRI results was carried out by an experienced, blinded pediatric neuroradiologist, rating the extent of the injury in posterior limb internal capsule, basal ganglia, thalami, white matter, and cortex [68] and using a standardized score according to the National Institute of Child Health and Human Development (NICHD) Neonatal Research Network (NRN), discerning between injury patterns as described by Shankaran et al. [90].

2.3.3 Metabolomic fingerprinting of urine samples

Three complementary analytical approaches were employed for the analysis of metabolic fingerprints of urine samples to enhance metabolome coverage, i.e., (i) a semi-targeted capillary electrophoresis–time-of-flight mass spectrometry (CE–TOFMS) assay, (ii) an untargeted ultra-performance liquid chromatography–quadrupole time-of-flight mass spectrometry (UPLC–QTOFMS) assay, and (iii) a targeted UPLC-tandem MS (MS/MS)-based method for the quantification of amino acids. Results were normalized to creatinine concentrations and are made available as **Table A.2.1**.

2.3.4 Semi-targeted CE-TOFMS analysis

A total of 279 urine samples were thawed on ice and homogenized on a Vortex® mixer for 1 min. A total of 50 µL of the sample were mixed with 50 µL of 0.2M formic acid containing 0.4mM methionine sulfone (internal standard, IS). After homogenization on a Vortex® mixer for 5 min and centrifugation at 13,200 × *g* for 10 min at 4 °C, 60 µL of the supernatant were collected and mixed with 180 µL of cold methanol for 5 min. Samples were centrifuged at 13,200 × *g* for 15 min at 4 °C, and 200 µL of supernatant were transferred into microcentrifuge tubes and evaporated to dryness using a Speedvac concentrator. Finally, sample extracts were redissolved in 60 µL of 0.2M formic acid, shaken for 5 min on a Vortex® mixer,
and centrifuged at 2000 × *g* at 4 °C for 5 min. A total of 50 µL of supernatant were transferred to CE vials for analysis. Quality control

(QC) samples were prepared by pooling 5 µL from each sample and processed applying the same procedure, as described for samples.

The analysis of urine samples was carried out by capillary electrophoresis–electrospray–time-of-flight MS (CE-ESI TOFMS), using instrumental conditions described elsewhere [91]. Briefly, CE–ESI–TOFMS analysis was performed on an Agilent 7100 Capillary Electrophoresis system (Agilent Technologies, CA) coupled to an Agilent 6224 TOFMS instrument. The separation was performed on a fused silica capillary (Agilent; total length, 100 cm; i.d., 50 µm) in normal polarity with a background electrolyte composed of 1.0M HCOOH solution in 10% CH_3OH (v/v). Samples were hydrodynamically injected at 50 mbar for 17 s followed by the injection of background electrolyte at 100 mbar for 10 s. The separation voltage applied was 30 kV with 25 mbar of internal pressure and the run time was 40 min. The sheath liquid (6 µL min^{-1}) composition was CH_3OH:H_2O (1:1, v/v) containing two reference masses (purine and HP-0921). The MS parameters used were: fragmentor 125 V, skimmer 65 V, octopole 750 V, nebulizer pressure 10 p.s.i., drying gas temperature at 200 °C, and flow rate 10 mL min^{-1}. The capillary voltage was 3500 V. Full-scan MS spectra from *m/z* 70 to 1000 were acquired in positive dual-ESI mode at a scan rate of 1.02 scan s^{-1}. MassHunter Workstation version B.06.01 controlled the CE–TOFMS system. The analysis of the samples was carried out in four batches of randomized samples. At the beginning of each batch, six QCs were injected for pre-sequence system conditioning, and a QC was injected every ninth sample to monitor the system performance. CE–TOFMS data processing using the Profinder software (B.06.00, Agilent) enabled the identification of 102 metabolites (**Table A.2.2**) in the urine sample set.

2.3.5 Untargeted UPLC-QTOFMS analysis

A total of total of 293 urine samples were prepared and analyzed by UPLC–QTOFMS assay, as described elsewhere [92]. Urine samples were randomly split into three analytical batches. Briefly, urine samples were thawed on ice, homogenized on a Vortex® mixer during 30 s, and centrifuged (16,000 × *g* during 15 min at 4 °C). A total of 50 µL of supernatant were withdrawn and spiked with 50 µL of IS solution in 96-well plates containing phenylalanine-D_5 (Cambridge Isotopes Laboratory Inc., Andover, MA), caffeine-D_9 (Toronto Research Chemicals, Toronto, Ontario, Canada), leukine enkephalin (Sigma-Aldrich Química SA, Madrid, Spain), and reserpine (Sigma-Aldrich Química SA) in H_2O:CH_3OH (1:1, 0.1% v/v HCOOH) at concentrations ranging between 2 and 4 µM. Blanks were prepared by replacing urine with H2O and a QC was prepared by mixing 5 µL of each final sample extract. The QC was split into three aliquots, each being measured in a single analytical batch to avoid additional freeze–thaw cycles. Sample extracts, blanks, and QCs were stored at −80 °C until analysis. Before analysis of each batch, sample extracts, blanks, and a QC aliquot were thawed on ice.

UPLC–QTOFMS analysis was performed on an Agilent 1290 Infinity UPLC chromatograph equipped with a UPLC BEH C_{18} (100 × 2.1 mm, 1.7 µm, Waters, Wexford, Ireland) column running a binary mobile phase gradient (mobile phase A: H_2O, 0.1% v/v HCOOH and mobile phase B: CH_3CN, 0.1% v/v HCOOH), and acquiring full-scan MS data from 100 to 1700 m/z with a scan frequency of 6 Hz on an iFunnel QTOF Agilent 6550 spectrometer in the positive electrospray

(ESI^+) mode. The QC sample was injected ten times at the beginning of each batch for system conditioning, as well as after every five urine samples for the monitoring and control of the instrumental performance. The blank extract was injected twice, at the beginning and end of each batch.

The peak table was generated for each batch separately usin XCMS (version3.4.2) (https://bioconductor.org/ packages/release/bioc/html/xcms.html) running in R (version 3.6.1), using the centWave method [93]. Intensity weighted *m/z* values of each feature were calculated using the wMean function and peak limits used for integration were found through descent on the Mexican hat filtered data. Peak grouping was carried out using the rearrest method, and the fillPeaks method was applied to fill missing peak data.

All further calculations were carried out in MATLAB R2019b (Mathworks Inc., Natick, MA) using in-built, as well as in-house written scripts and functions and the PLS Toolbox 8.7 (Eigenvector Research Inc., Wenatchee). Blank samples were used to identify and remove features arising from contaminants and carryover with a ratio of median intensities in QCs and blanks <9 [94]. The three data sets were aligned using m/z and RT tolerances of 50 mDa and 0.1 min, and a mzVsRT = 1. Within-batch effects were corrected for each batch separately employing the Quality Control-Support Vector Regression algorithm [92] and the LIBSVM library [75] method with and ε-range from 2.5 to 5, a γ-range from 1 to 105, and a C-interval of 50 [95,96]. Between-batch effects were linearly corrected using the median values in QCs as reference [92]. UPLC-MS features with a relative intensity change across batches >5, and those with a D-ratio ≥ 20% in QCs after within

and between-batch effect correction were classified as unreliable [69] and removed.

2.3.6 Quantitative amino acid profiling

A total of 237 urine samples were thawed on ice and homogenized on a Vortex® S0200 mixer (LabNet, Edison, NJ) during 10 s. A total of 70 µL of water (Optima LC/MS grade, Fisher Scientific) were added to 5 µL of urine. Amino acid levels were quantified using a ultraderivation kit (AccQ TagTM Ultra Derivatization Kit, Waters), following the manufacturer's protocol. Blanks were prepared by replacing the urine sample with water (Optima LC/MS grade). A QC was prepared by mixing 5 µL of each sample. Quantitative analysis of amino acids was performed employing a 1290 Infinity UPLC system from Agilent equipped with a UPLC CORTECS C_{18} column (150 × 2.1 mm, 1.6 µm) from Waters coupled to an Agilent 6460 triple quadrupole MS system operating in ESI^+ mode. The flow rate was set to 500 µL min^{-1} running a binary gradient with 0.1% v/v HCOOH in H_2O and 0.1% v/v HCOOH in CH_3CN as mobile phase components. Column and autosampler were kept at 55 and 4 °C, respectively and the injection volume was 3 µL. Raw data were acquired and processed employing MassHunter Workstation (version B.07.00, Agilent). Missing values were imputed as 0.5 × LOQ of each compound. In **Table A.2.3** a list of the parameters employed for amino acid quantification can be found.

2.3.7 Creatinine determination

Creatinine was quantified following the protocol of the Urinary Creatinine Detection Kit (Arbor Assays™, Ann Arbor, MI), employing a dilution factor of 1:4 and measuring the absorbance at 490 nm.

2.3.8 Data processing and statistics

Metabolic fingerprints were normalized to creatinine, $\log_{10}$ transformed, and pareto scaled. Between group comparisons of clinical and demographic variables were carried out employing the Student's *t* test for unequal variances (α=0.05), Wilcoxon ranksum test (α=0.05), or χ^2-test (α=0.05), according to the underlying distribution. For determining differentially regulated metabolites or UPLC–QTOFMS features, as well as for comparing MRI outcomes at each time point, Student's *t* tests for unequal variances (α=0.05) were applied and fold change (FC) was calculated as the ratio of means between groups.

The standardized mean difference using the simplified Cohen equation to determine the pooled standard deviation [97] was calculated for each metabolite/metabolic feature at each of the six sample collection time points. Then, the Pearson correlation coefficient was calculated between the standardized mean difference and time and obtained FDR-adjusted *P* values were calculated [98].

MetaboAnalyst (version 5.0) [78] was used for the generation of heatmaps from autoscaled data employing Euclidean distance and Ward's method. Pathway analysis was carried out using the *mummichog* algorithm (*P* value cutoff set to 0.05) with a *m/z* accuracy = 10 p.p.m. and the Kyoto Encyclopedia of Genes and Genomes (KEGG) pathway library (*Homo sapiens*). As an input, *t* test *P* values estimated assuming

unequal variances between distributions, and FCs were computed for each metabolic feature comparing normal and pathologic outcomes. Pathways with gamma *P* values <0.05 were considered as significantly altered. The PLS Toolbox 8.7 (Eigenvector Research Inc., Wenatchee) was used for partial least squares (PLS) and PLS discriminant analysis (PLSDA) of autoscaled data. For *k*-fold cross validation, samples were distributed into folds by subject to prevent person-specific information crossover between the training folds and the test fold. Receiver operating characteristic (ROC) curves were constructed based on PLSDA predictions and cross validation results.

2.4 Results

2.4.1 Patient characteristics

A total of 55 infants from the HYPOTOP cohort were included in this study. The characteristics of the studied population, including 55 newborns with NE undergoing TH are shown in **Table 2.1**. No significant differences between the control (i.e., normal neurological outcome) and pathologic groups were found in any of the collected anthropometric, clinical, or biochemical parameters. Furthermore, both groups were balanced in the proportion of infants receiving topiramate as adjuvant therapy.

Table 2.1 Patients characteristics of study population.

Parameter	Normal (N=22)	Pathologic (N=33)	*p-value*
Inborn [%]	5 (23%)	6 (18%)	0.7
Maternal age (years) [mean±s]	34 (4)	33 (6)	0.3
Gestational age (weeks) [median, IQR]	38.4 (37.4, 40.5)	39.0 (38.0, 40.6)	0.7
Gender (male/female)	11/11	17/16	0.9
Birth weight (g) [mean±s]	3321 (566)	3258 (689)	0.7
Length (cm) [mean±s]	52 (4)	50 (3)	0.3
Head circumference (cm) [mean±s]	35 (1)	34 (2)	0.3
Delivery mode (C-section) [%]	9 (41%)	21 (64%)	0.1
Apgar Score 1 min [median, IQR]	2 (1, 4)	1 (1, 3)	0.5
Apgar score 5 min [median, IQR]	4 (3, 5)	3 (1, 5)	0.1
Apgar score 10 min [median, IQR]	5 (5, 8)	5 (3, 6)	0.2
Sarnat 2 / Sarnat 3	17/5	21/11	0.3
MRI[a] [%]			
Score-0	22 (100%)	0 (0%)	
Score-1	0 (0%)	11 (33%)	
Score-2	0 (0%)	15 (45%)	
Score-3	0 (0%)	2 (6%)	
pH UC [mean±s]	7.0 (0.3)	7.0 (0.2)	0.8
BE UC (mEq L^{-1}) [mean±s]	-15 (10)	-15 (8)	0.8
pCO_2 UC (mmHg) [mean±s]	67 (27)	63 (38)	0.7
HCO_3 UC (mEq L^{-1}) [mean±s]	13 (4)	15 (8)	0.3
MR (days) [median, IQR]	8 (6, 10)	7 (7,9)	1.0
Initiation of TH (h) [mean±s]	34 (1.2)	34 (1)	0.7
Topiramate treatment (yes) [%]	10 (45%)	17 (52%)	0.7

[a]MIR scores assigned according to the National Institute of Child Health and Human Development (NICHD) Neonatal Research Network (NRN), as described by Shankaran et al [90] for five newborns from the pathologic group no information on the degree of injury was available.

2.4.2 Dynamics of the urinary metabolome

The urinary metabolome of newborns with NE was studied employing three complementary analytical methods, i.e., untargeted UPLC–QTOFMS, semi-targeted CE–TOFMS, and a targeted method for the determination of amino acids. Using UPLC–QTOFMS, a total of

293 urine samples were analyzed with N = 37 collected before the initiation of TH and N = 45, N = 54, N = 54, N = 54, and N = 49 collected 12, 24, 48, 72, and 96 h, respectively, after the initiation of TH. After initial data preprocessing and filtering, 11,561 features were retained and used for further analysis. In case of CE–TOFMS, a total of 279 urine samples were analyzed with N = 35 collected before the initiation of TH and N = 44, N = 52, N = 53, N = 53, and N = 42 collected 12, 24, 48, 72, and 96 h, respectively, after the initiation of TH. A list of metabolites that were consistently detected in urine samples with the CE–TOFMS target assay can be found in **Table A.2.2.** Amino acids were quantified in 237 samples, N = 27 collected before the initiation of TH and N = 40, N = 41, N = 47, N = 43, and N = 39 collected 12, 24, 48, 72, and 96 h, respectively, after the initiation of TH (see **Table A.2.3**). The longitudinal analysis of the metabolic fingerprint of infants with NE showed a dynamic behavior. **Figure 2.1** (left) depicts the percentage of differentially expressed features and metabolites (*t* test *P* value < 0.05) after the initiation of TH, using the first urine samples collected as reference. The majority of detected signals showed a decreasing trend with time ranging between 16 and 59% at 12 and 96 h after the initiation of TH, respectively. Simultaneously, only between 0.08 and 1% were upregulated. Changes are most pronounced during the first 48 h after the initiation of TH, whereas rewarming (96 h) did not seem to have a strong impact.

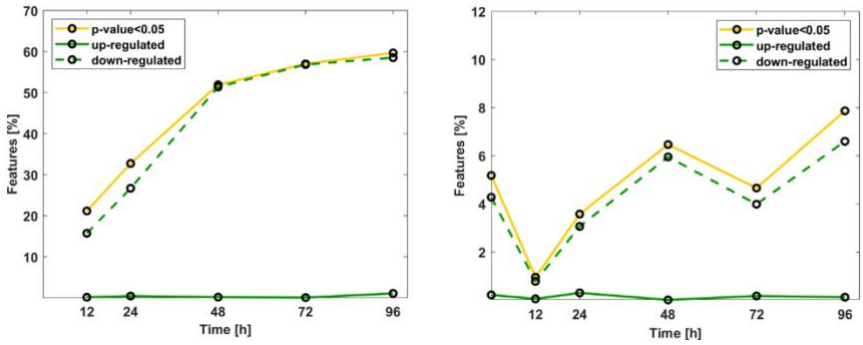

Fig. 2.1 Metabolic changes in urine samples from newborns with NE detected by multi-platform metabolomics. Left: % of significantly changing features (P value < 0.05) and % of upregulated and downregulated features at each time point during 96 h after initiating TH with respect to the first urine sample collected before the initiation of TH. Right: % of significantly changing features (P value < 0.05) and % of upregulated and downregulated features in urine samples from infants with vs. without brain injury, as detected by MRI.

The effect of time is further represented in **Fig. 2.2**, where metabolite concentrations with a significant correlation with time are represented. In total, 43% of the features of the urinary metabolic fingerprint showed a significant correlation with time, and out of the correlated features, 53% tended to increase with time.

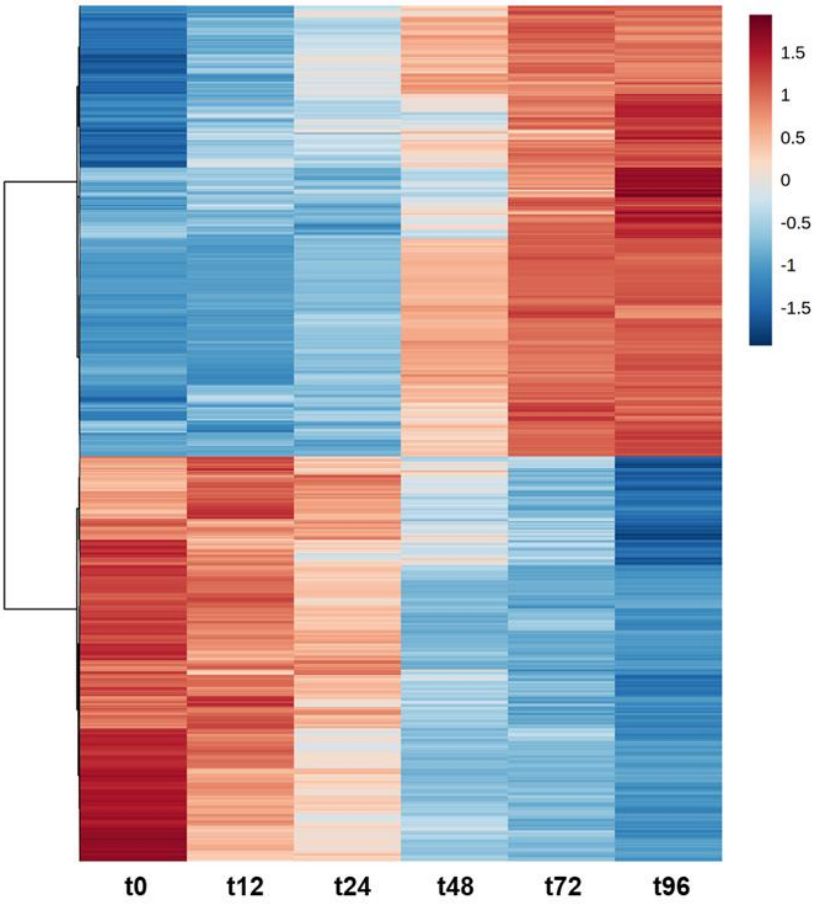

Fig. 2.2 Metabolic changes associated to time. Note: color represents standardized mean difference between time points; blue—metabolite levels lower than average, and red—metabolite levels higher than average. P values from Pearson correlation with time were computed, and significant metabolites after multiple testing correction are shown; heatmap calculated using Euclidean distance and Ward algorithm representing autoscaled features.

2.4.3 Perturbation of the urinary metabolome in infants with pathologic MRI outcome

Differences in the urinary metabolic fingerprints of infants with normal and pathologic MRI outcome were assessed throughout the first 96 h of life. As shown in **Figure 2.1** (right), the number of significantly altered metabolic features reaches a minimum at 12 h and ranges

between 4 and 8% at the remaining time points (6 ± 2%). The proportion of upregulated features ranges between 0 and 0.2%, whereas the proportion of downregulated features was rising from 0.8% at 12 h to 7% at 96 h. **Figure 2.3** illustrates the metabolic pathways altered between newborn infants with pathologic and normal MRI outcomes. Significant alterations on the pathway level were found in urine samples collected at all studied time points. Pathways related the amino acid and lipid metabolism were consistently identified to be affected in infants with pathologic MRI. Pathways related to the metabolism of cofactors and vitamins were altered during TH. Differences in pathways associated to xenobiotics biodegradation and metabolism were found repeatedly before, during and after TH. Carbohydrate metabolism and glycan synthesis and metabolism were altered during the first 24 h. Other pathways related to the metabolism of terpenoids and polyketides, and nucleotide and energy metabolism were affected transiently. Accordingly, **Figure 2.3** also shows the classes of changing metabolites, with "carboxylic acids and derivatives", "organooxygen compounds", "fatty acyls", "steroids and steroid derivatives", "indoles and derivatives", and "tetrapyrroles and derivatives" being the prominent metabolite classes affected. A detailed list of identified altered metabolites is provided in **Table A.2.4**.

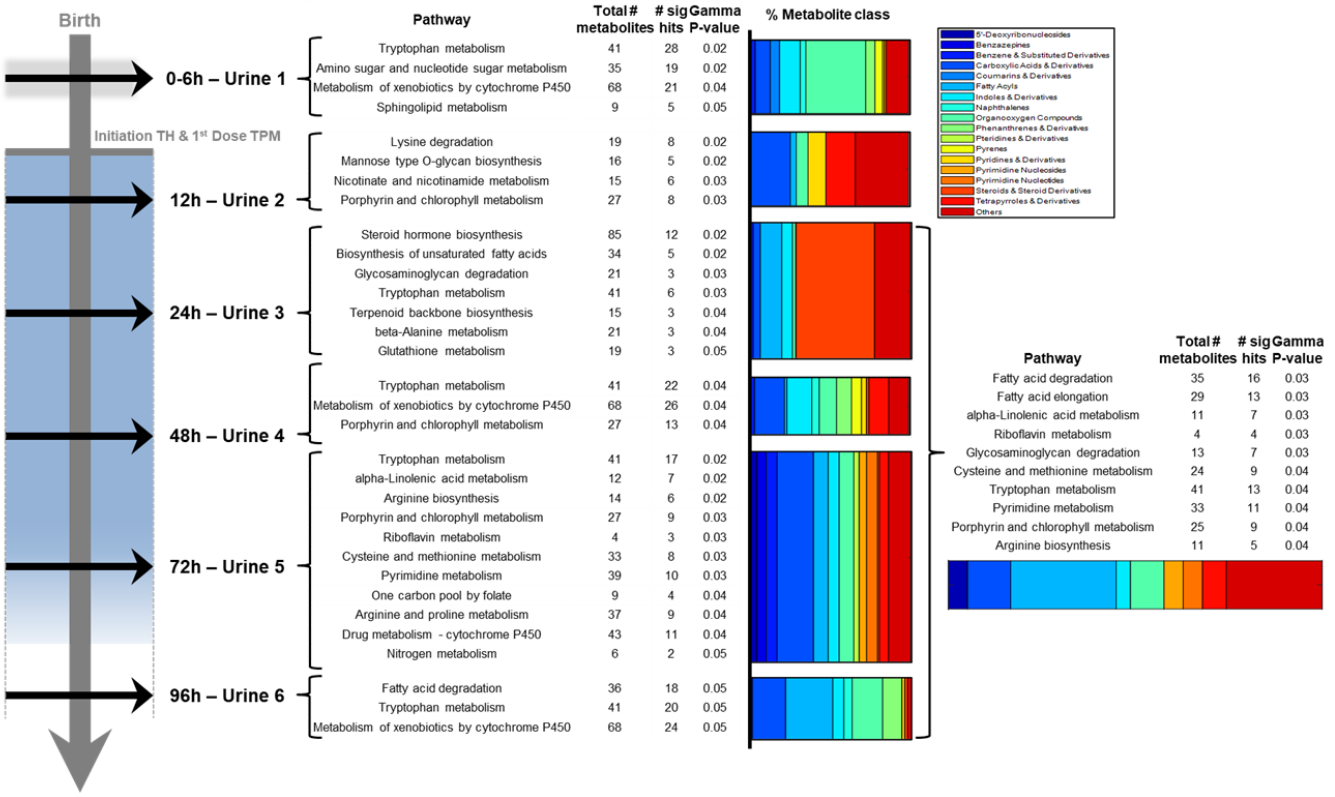

Figure 2.3 Dynamic metabolic alterations detected in urine samples from infants with brain injury in comparison to infants without brain injury detected by MRI. Altered pathways and associated metabolites are shown for urine samples collected between birth and 96 h after the initiation of TH.

With the aim of defining a disease pattern in urine metabolic fingerprints, pathway analysis was repeated for all samples collected between 24 and 96 h after the initiation of TH together, as the differences between newborns with NE and pathologic vs. normal MRI outcomes in the metabolome became more stable (see **Figure 2.1**). Pathway analysis confirmed the consistent alteration of ten pathways associated to amino acid and lipid metabolism, metabolism of cofactors and vitamins, glycan biosynthesis and metabolism, and nucleotide metabolism, as shown in **Figure 2.3**. Using the metabolic features corresponding to metabolites included in those pathways as annotated by the mummichog algorithm (i.e., 398 features), a PLSDA model with four latent variables was computed for discerning between metabolic fingerprints of newborns with pathologic (Scores 1, 2, or 3) and normal MRI outcomes (Score-0) retrieved between 24 and 96 h after the initiation of TH. The significance of the model was confirmed by a permutation test (500 permutations) and ROC curves are shown in **Figure 2.4.**

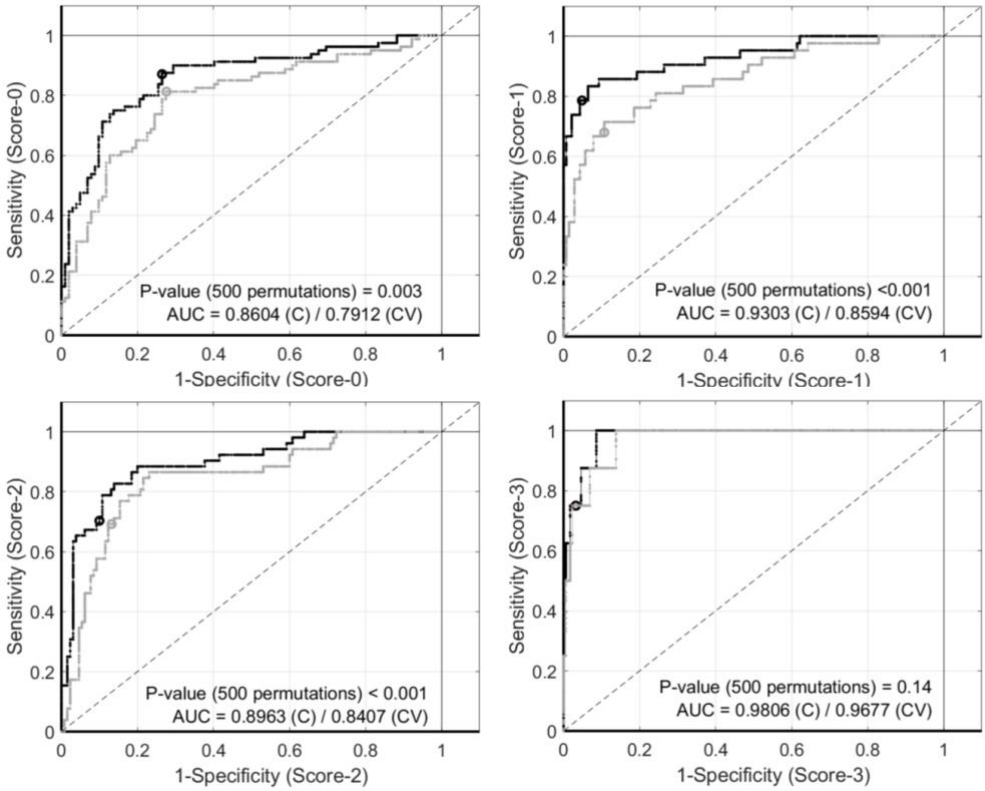

Figure 2.4 Disease pattern of NE as reflected in the urinary metabolome between 24 and 96 h. ROC curves from a PLSDA model (four latent variables) for Score-0 (top, left), Score-1 (top, right), Score-2 (bottom, left), and Score-3 (bottom, right) calculated, using relative intensities of 398 metabolic features from altered metabolic pathways shown in **Figure 2.3**. Note: black lines represent estimated PLSDA ROC curves (calibration set); gray lines represent estimated PLSDA ROC curves (cross validation); dashed lines represent 50% lines; and circles indicate model thresholds. Noninvasive monitoring of evolving urinary metabolic patterns in neonatal.

2.5 Discussion

A severe hypoxic insult suffered in the perinatal period causes an imbalance of the homeostasis manifesting at a systemic level in the newborn. This perturbation can be readily monitored employing urinary metabolomics allowing to study dynamic changes of the phenotype over

time. In this study, a continuously increasing proportion of altered metabolic features with time was detected affecting up to 59% of features (**Figure 2.1**, left) and 43% of features showed a significant correlation with time (**Figure 2.2**). The number of downregulated features was steadily increasing and higher than the number of upregulated features at all studied time points (**Figure 2.1**, left). This observation is in good agreement with earlier literature reports on metabolomics studies involving the analysis of the urinary metabolome of NE infants over time [55,87,88], reporting continuous changes during the neonatal period with some metabolites showing a relative increase in concentration, while others tended to decrease.

The main aim of this study was to search for a metabolic fingerprint able to discern urine samples from infants, which showed pathologic patterns during a subsequent MRI analysis from those with normal MRI results. This is the first Study reporting distinct patterns in urinary metabolic fingerprints of newborns with NE and pathologic vs. normal MRI outcomes. The injury pattern showed a dynamic behavior. Initially detected differences between groups almost disappeared 12 h after the initiation of TH, which might reflect a partial recovery during the latent injury phase, and then became more evident again after 24 h of TH (**Figure 2.1**, right).

To further elucidate the effect of brain injury on the metabolome, pathway analysis was employed. Pathway analysis aims to place the seemingly disjointed list of altered metabolites into a broader biological context by jointly assigning metabolites to relevant metabolic pathways, providing an interaction network that may identify centralized hubs, where metabolic pathways coincide or where bottlenecks may occur. Pathway alterations affecting between 3 and 11 pathways (**Figure 2.3**)

were detected across all studied time points, covering before and during TH, as well as after rewarming with some alterations being transient and others being detected consistently (e.g., tryptophan metabolism).

From the clinical perspective and with the aim of developing a monitoring approach the discovery of stable disease patterns is valuable. We found that a total of ten pathways were consistently altered in urine samples of infants with NE and pathologic MRI outcomes, when urine samples collected between 24 and 96 h after the initiation of TH were analyzed (**Figure 2.3**). Seemingly, after a period of 24 h after the initiation of TH, biochemical alterations that evolve to anatomical lesions in the brain that are later detectable by MRI are mirrored in the urinary metabolome. Metabolites associated to the ten altered metabolic pathways were successfully employed to discern between newborns with different injury patterns (i.e., Scores 0, 1, 2, and 3) as shown by ROC curves in **Figure 2.4**. Statistically highly significant models could be obtained for all comparisons, with exception of the model for the discrimination of Score-3, probably due to the limited number of samples, as only two infants showed the highest degree of brain injury. Hence, our data provides evidence of gradual changes detectable in urine samples, providing a knowledge base for the development of biomarkers that might support clinical monitoring compatible with TH in the future.

To the best of our knowledge, this study has analyzed and compared for the first time the evolution of the metabolome of newborns with NE and pathologic vs. normal MRI outcomes over time. The use of a representative control group of newborns with NE instead of healthy control newborns has facilitated the interpretation of the outcomes. Due to substantial differences in the experimental design between this study and previous results [55,87,88] a detailed comparison of the outcomes

was not possible. However, alterations of amino acids and associated pathways, including tryptophan metabolism and aminoacyl-tRNA biosynthesis [55,88] had been reported. In umbilical cord blood samples from infants with NE vs. healthy control newborns, the terpenoids backbone biosynthesis pathway and, also a significant alteration of kynurenine, a metabolite from the tryptophan metabolism pathway, were identified [54] Interestingly, in a mouse model with induced excitotoxic lesion, changes in amino acid metabolism in brain tissue were sustaining acute and delayed responses to injury [99].

In a previous study, we analyzed the plasma metabolic fingerprints of the newborns included in this study [89]. Several metabolic pathways altered in urine (Fig. 3) were also found to be affected in plasma, i.e., arginine and proline metabolism (48 and 72 h in plasma vs. 72 h in urine), lysine degradation (72 h in plasma vs. 12 in urine), nitrogen metabolism (72 h in plasma and urine), and steroid hormone biosynthesis (0, 24, 48, and 72 h in plasma vs. 24 h in urine). Hence, the results from metabolic fingerprinting in plasma and urine samples are in good agreement, indicating that the development of brain injury secondary to asphyxia is broadly affecting metabolism.

This study has limitations. No newborns with asphyxia or classified as mild NE (Sarnat 1) were included. There is risk of adverse neurodevelopmental outcome of newborns with mild NE, but to date, there is no evidence to support cooling in these babies. Furthermore, as NE is frequently associated to a transient renal insufficiency secondary to proximal tubular necrosis with decreased urine output and creatinine clearance, hematuria, and proteinuria, analytical determinations might have been influenced by renal insufficiency especially in babies with severe NE [100].

In summary, this is the first time that a dynamic perturbation of the urinary metabolome of newborns with NE undergoing TH, and showing pathologic and normal MRI outcomes is reported. Undoubtedly, TH significantly influences patient's metabolism. However, since TH has become a standard of care, our results truly reflect the clinical situation undergone by patients with moderate to severe NE. From birth and until completing 24 h of TH, the metabolic fingerprint experienced a gradual shift and a distinct disease pattern evolved. This disease pattern is characterized by the alteration of amino acid and lipid metabolism, metabolism of cofactors and vitamins, glycan biosynthesis and metabolism, and nucleotide metabolism. Although follow-up studies are required for further confirming the observations from this study, this new insight might be meaningful for patient monitoring in the NICU and for supporting early outcome prediction.

Chapter 3. Targeted Metabolomics data and miRNA-seq assessment from HIE newborns during hypothermia treatment

3.1 Introduction

Hypoxic-ischemic encephalopathy (HIE) is an injurious event that precipitates a cellular bioenergetics failure followed by excitotoxicity, oxidative stress, blood-brain barrier (BBB) dysfunction, and post-ischemic inflammation, which contribute to neuronal cell lesion or death through apoptotic mechanisms or directly necrosis [23]. Pathogenic events in HIE trigger a massive release of glutamate from neuronal cells that binds to the postsynaptic NMDA receptors. These events produce excitotoxicity and subsequently a burst of reactive oxygen species (ROS) [101]. The deprivation of blood flow and the production of ROS, damages the architecture of the blood brain barrier (BBB), allowing the translocation of leukocytes into the cerebral parenchyma. Resident cells, especially microglia, astrocytes and translocated cells, release pro-inflammatory cytokines causing neuroinflammation exacerbating brain damage [102].

Tryptophan is an essential amino acid that, under physiological conditions, is catabolized through the kynurenine pathway (KP) to synthesize the vital energy cofactor, nicotinamide adenine dinucleotide (NAD+). Several downstream metabolites of the KP are biologically active in various physiological and pathological processes, including kynurenine, kynurenine acid, 3-hydroxykynurenine, anthranilic acid, 3-

hydroxyanthranilic acid, picolinic acid, and quinolinic acid [103]. Two tryptophan-metabolizing enzymes, indoleamine-2,3-dioxygenase (IDO1 and IDO2), keep track of the tryptophan catabolism-signaling pathway. The generation of kynurenine and other tryptophan metabolites can modulate T-cell immunity via activation of suppressive regulatory T-cells and regulate immunity, stem cell maintenance, and cellular differentiation through activation of aryl hydrocarbon receptors, thus promoting cancer cell survival [104]. In brain, tryptophan metabolites have the ability to modulate glutamatergic and nicotinic receptors to regulate the response of the immune system after inflammation and/or infection and even to modify the generation of ROS [105–107].

In addition, non-targeted metabolomic studies in a multicenter randomized double blind controlled clinical trial cohort (HYPOTOP) [39] have shown alterations of the steroid hormone biosynthesis pathway [89,108]. This pathway was affected throughout the study period in newborns with HIE and pathological vs normal MRI outcomes. Under this premise, some of the most important components of the steroid hormone biosynthesis pathway were measured.

Moreover, metabolomic studies in animal models revealed the potential of choline, cytidine, uridine, and betaine in plasma for tracking back the duration of asphyxia and hence, severity of HIE [61]. Supported by these observations, a metabolite score was proposed to provide an estimate of the duration and intensity of hypoxia based on LC-MS. Besides, the evolution of several energy-related key metabolites in newborns with HIE undergoing TH, i.e., lactate, pyruvate, ketone bodies, and several Krebs cycle intermediates may be associated with the

aerobic metabolism of newborns with neuronal disease within the physiopathology of HIE [21].

MicroRNAs are a family of small non-coding RNAs between 19 and 25 nucleotides in length that play an important role in the regulation of post-transcriptional gene expression. Its functioning appears to be associated with the ability to bind to the 3' untranslated region of the mRNA of protein-coding target genes, leading to its silencing by excision, translational repression, and de-adenylation [109]. MicroRNAs appear to influence various stages of neurogenesis including cell differentiation, proliferation, and synaptogenesis in both *in vivo* and *in vitro* studies. Studies in mice and humans have shown that approximately 70% of the identified microRNAs are expressed in brain tissue in relation to the complexity of the CNS and its connection [110]. Thus, both miR-126, miR-132 play a relevant role in neuroinflammation in Alzheimer pathogenesis [111]. It has recently been shown that miR-29b, a microRNA that is activated during neuronal maturation, plays a relevant role in the inhibition of neuronal apoptosis [112]. Finally, microRNA-155 is involved in the immune response mediated microglia [111]. However, this information has not yet comprehensively revealed the physiological and pathophysiological role of microRNAs in the newborn period, and knowledge gaps need still to be filled in. Given the situation of rapid brain development in the postnatal period, the expression of microRNAs during this specific period of human development, should be characterized and the correlation with the regulatory capacity in adults established.

Therewith, four metabolomic methods were used for the determination of relevant metabolites and RNA sequencing was used for the analysis of microRNAs. The methods were applied to 359 plasma samples from HYPOTOP patients [39] collected from the umbilical cord and 24, 48, and 72 hours after initiation of TH.

3.2 Material and methods

In this study, altogether 34 compounds were determined using fours methods. First, eight compounds of the steroids hormone biosynthesis pathway, seven compounds of the Metabolite Score, and eleven compounds of the tryptophan pathway with LC-MS analysis; in addition, eight energy-related metabolites were assessed employing GC-MS analysis. Secondly, the analysis of microRNA, was carried out on an Illumina platform by the Novogene Company (Beijing, China).

3.2.1 Steroids metabolites

For the quantification of 8 steroid metabolites a CHS^{TM} MSMS Steroids Kit of PerkinElmer (Waltham, MA USA) was using. Briefly, 200 µL of Daily Precipitation Solution (DPS) solution were mixed with 100 µL of plasma sample. Then, samples were vortexed during 15 min and centrifuged at 4210 *x g* for 30 min at 4 °C. The supernatant was transferred to a V plate and evaporated with Thermo SPD121P SpeedVac concentrator (Waltham, MA USA). The samples were reconstituted in 125 of reconstitution solution. Finally, the plate was vortexed during 15 min and UPLC-MS/MS analysis was carried out on an Acquity-Xevo TQS system using an UPLC ACQUITY BEH C8 (2.1

× 10 mm, 1.7 µm, Waters, Wexford, Ireland). Flow rate and column temperature were 300 µL min^{-1} and 50 °C, respectively. Injection volume was 5 µL and autosampler temperature was set at 6 °C during sample analysis. Mobile phase H_2O:CH_3CN 90:10 v/v were, and the gradient elution was as follows: in initial conditions phase B was held 35% from 0 to 0.1 min. Then phase B was increased to 70% from 0.1. to 4.5 min. Phase B was held 100% from 4.6 to 5.9 min followed to a return to initial conditions between 6.00 to 7.00. Electrospray ionization was carried out using the following conditions: capillary 2.9 kV, cone 25 V, source temperature 120 °C, desolvation temperature 395°C, N_2 cone and desolvation gas flow rates were 150 and 800 L h^{-1}, respectively.

3.2.2 Metabolite Score

In Eppendorf tubes, 10 µL of plasma were added in 7 µL of internal standards of betaine-d_{11} phe-d_5, hypoxanthine-d_4, Cytidine $^{13}C_9$, $^{15}N_3$ and Uridine $^{13}C_9$, $^{15}N_2$. Then, 39 µL of cold CH_3CN were added for protein precipitation. Next, samples were vortexed and centrifuged at 13000 *x g* for 10 min at 4 °C. The supernatants were evaporated in a Thermo SPD121P SpeedVac concentrator and the residues were reconstituted in 150 µL of mobile phase (H_2O:CH_3CN 97:3 with 0.1% HCOOH. Finally, quantitative analysis was performed employing an Acquity UPLC-MS/MS system coupled to a Xevo-TQ triple quadrupole MS detector operating in the positive electrospray ionization mode (ESI^+) (Waters, Manchester, UK). A Acquity UPLC BEH C8 column (100 × 2.1 mm, 1.7 µm) and a 30:70 v/v H_2O:CH_3CN mobile phase at pH 7 containing 5 mM ammonium formate. Flow rate, column temperature and injection volume were set at 0.4 ml min^{-1}, 40 °C and 3

µl, respectively. Detection conditions were set as follows: capillary voltage to 3.5 kV, source temperature to 120 °C and the cone, desolvation and collision gas flows were 50 L h^{-1}, 700 L h^{-1} and 0.2 mL min^{-1}, respectively.

3.2.3 Tryptophan metabolites

For the quantification of 23 tryptophan metabolites, aliquots of 50 µL of plasma samples were placed into 1.5 mL Eppendorf tubes and 150 µL of cold MeOH were added for protein precipitation. Then, samples were vortexed for 15 s and subsequently centrifuged at 13000 *x g* for 10 min at 4 °C. The supernatants (150 µL) were transferred to clean tubes and centrifuged again at 13000 *x g* for 10 min at 4 °C. The supernatants (125 µL) were evaporated in a Thermo SPD121P SpeedVac concentrator (Waltham, MA USA). The residues were reconstituted in 25 µL of internal standards solution of hydroxytryptophan-D_4, L-kynurenine-D_4, indole-D_5-3-acetamide, 4-chloro-kynurenine-$^{13}C_2$,^{15}N, 6-hydroxymelatonin-D_4, kynurenic acid-D_5, PAGN-D_5, phenylalanine-D_5, serotonin-D_4, tryptamine-D_4, tryptophan-D_5, xanthurenic acid-D_4 and phenylalanine-D_5 (900 nM each). Finally, the supernatants were transferred to a 96-well plate for analysis. A diluted sample (dilution factor: 50) was prepared to ensure that metabolites typically present at higher concentrations in samples (e.g., tryptophan) fall within the linear range. UPLC-MS/MS analysis was carried out on an Acquity-Xevo TQS system using using an Acquity HSS T3 C18 (100 x 2.1 mm, 1.8 µm) column. Mobile phases were H_2O (0.1% v/v HCOOH) (A) and (0.1% v/v HCOOH) CH_3CN (B). The gradient elution was as follows: phase B was held 2% from 0 to 0.5 min, then increased linearly to 45% over the

following 5 min. Then phase B was increased to 90% in 0.2 min followed by a fast return to initial conditions between 5.7 and 6 min, which were held for 1.5 min for column re-equilibration. Injection volume, flow rate and column temperature were set at 3 µL, 550 µL/min and 55 °C, respectively. Autosampler temperature was set at 6 °C during sample analysis. Electrospray ionization was carried out using the following conditions: capillary 2.9 kV, cone 25 V, source temperature 120 °C, desolvation temperature 395°C, N2 cone and desolvation gas flow rates were 150 and 800 L/h, respectively.

3.2.4 Energy related metabolites

Aliquots of plasma samples were thawed and homogenized during 30 s. 50 µL of plasma samples were added to 250 µL of cold CH_3CN. The solution was centrifuged at 11000 g during 10 min at 4 °C. Thereafter, 200 µL of supernatant were transferred to Eppendorf tubes with internal standard solution with a concentration of 1 mM. Subsequently, samples were evaporated on a SpeedVac concentrator from Genevac Ltd (Ipswich, UK) at 40 °C and dry residues were suspended in 20 µL of a freshly prepared 4% (w/w) methoxyamine solution in pyridine. Samples and standards were incubated during 90 min at 30 °C on a thermomixer (MKR 13, Ditabis) under agitation. After, a solution of 20 µL MSTFA + 1% TMCS were added. 30 min of reaction time at 37 °C under agitation later, samples were diluted with 40 µL of hexane and placed in capped glass vials for GC-MS analysis. All samples were carried out with a 6890GC-5973N gas chromatography electron impact quadrupole mass spectrometric system equipped with a HP-5MS column from Agilent Technologies (Santa Clara, CA, USA). The GC

was operated at a constant He carrier gas flow at a flow rate of 1.2 mL min^{-1}. The injector temperature was set to 260 °C and 1 μL of sample was injected at a split ratio of 5:1. The oven temperature was maintained at 60 °C during 1 min followed by a linear gradient of 10 °C min^{-1} until reaching 310 °C which were held during 10 min.

3.2.5 microRNAs

DNA extraction was carried out using a commercial kit (miRNeasu Serum/Plasma kit) of Qiagen (Hilden, Germany). Briefly, 100 μL were added to 250 μM QIAzol Lysis Reagent. Then, 3.5 μM of miRNeasy Serum/Plasma Spike-In Control and 50 μM chloroform were added to the solution. Next, the samples were vortex vigorously for 15 s and centrifuged for 15 min at 13000 *x g* for 10 min at 4 °C. After centrifugation, 150 μL of CH_3OH were added. 700 μL of the solution were centrifuged at 8000 *x g* for seg at room temperature. After, 700 μL, 500 and 500 of buffer and CH3OH were added respectively on MinElute spin column and, finally, 14 μL of RNase-free water were added and centrifugated for 1 min at full speed to elute the RNA. Subsequently, all RNA samples were sequencing by Illumina through the company Novogene (Beijing, China). The first step was libraru preparation and sequencing. To guarantee the reliability of the data, quality control was performed on each step of the procedure. Three methods of quality control (QC) for RNA samples were used: (i) quantification with Nanodrop, (ii) agarose gel electrophoresis to test RNA degradation and contamination and (iii) Agilent 2100 to check RNA integrity and quantification. After QC, library was constructed by Small RNA samples Pre Kit. The final cDNA library was ready after a round of sequencing

adaptor ligation, reverse transcription, PCR enrichment, purification, and size selection. Libraries were fed into Illumina machine after pooling according to activity and expected data volume.

3.3 Results

359 plasma samples were analyzed employing four validated, quantitative LC-MS-based methods. Out of the 34 measured metabolites, 34 were detected in 90% samples and 1788 microRNAs were sequenced. Regarding the characteristics of the studied population, we found significant differences between study groups. The following table (**Table 3.1**) shows the result of comparations of detected metabolites (Mann Whitney U test, $\alpha = 0.05$) between different study populations.

Table 3.1. Mann Whitney U test of detected metabolites in different study groups.

Compound	normal vs pathologic MRI	HYPOTOP group vs control group
4-androstene-3,17-dione	$8 \cdot 10^{-2}$	0.4
corticosterone	1	**$2 \cdot 10^{-3}$**
cortisol	0.8	**$2 \cdot 10^{-2}$**
11-deoxycortisol	0.3	**$1 \cdot 10^{-11}$**
Dehydroepiandrosterone sulfate	1	**$3 \cdot 10^{-2}$**
progesterone	0.1	**$1 \cdot 10^{-16}$**
17alfa-hydroxyprogesterone	0.1	**$5 \cdot 10^{-16}$**
testosterone	$5 \cdot 10^{-2}$	**$9 \cdot 10^{-4}$**
choline	0.4	**$1 \cdot 10^{-7}$**
betaine	$6 \cdot 10^{-2}$	**$3 \cdot 10^{-7}$**
cytidine	0.7	0.5
Uridine	0.9	**$1 \cdot 10^{-8}$**
Hypoxanthine	0.6	**$3 \cdot 10^{-5}$**
Xanthine	0.2	0.9
Lactic acid	**$2 \cdot 10^{-3}$**	**$1 \cdot 10^{-8}$**
Anthranilic acid	0.5	**$1 \cdot 10^{-3}$**
Hydroxy-anthranilic acid	0.5	0.3
Kynurenic acid	0.9	**$5 \cdot 10^{-3}$**
Tryptophan	0.9	**$2 \cdot 10^{-4}$**
Xanthurenic acid	0.8	0.7
Kynurenine	0.9	**$3 \cdot 10^{-3}$**
N-Formyl kynurenine	0.8	**$3 \cdot 10^{-3}$**
PAGN	**$1 \cdot 10^{-2}$**	$5 \cdot 10^{-2}$
Indole-lactic acid	0.4	**$4 \cdot 10^{-4}$**
Indole-acetic acid	0.7	$8 \cdot 10^{-2}$
4-chloro kynurenine	0.9	**$9 \cdot 10^{-3}$**
Pyruvate	**$4 \cdot 10^{-2}$**	**$3 \cdot 10^{-7}$**
Lactic acid	**$4 \cdot 10^{-2}$**	**$2 \cdot 10^{-5}$**
Acetoacetate	0.4	**$2 \cdot 10^{-10}$**
Beta hydroxybutyrate	**$9 \cdot 10^{-2}$**	**$6 \cdot 10^{-9}$**
Succinate	**$1 \cdot 10^{-3}$**	0.4
Fumarate	0.8	0.4
Malate	0.8	0.9
Ketoglutarate	**$4 \cdot 10^{-2}$**	0.8

Significant differences (t-test, p-value <0.05) in concentration levels of several metabolites in newborns with pathological MRI outcomes compared with normal MRI outcome were found for lactic acid, phenylacetylglutamine, pyruvate, succinate, and ketoglutarate. Secondly, the comparison between the group with pathologic MRI outcomes and the control group, showed that compounds of all metabolic pathways had significantly different concentrations (t-test, p-value <0.05). Remarkably, corticosterone, cortisol, 11-deoxycortisol, dehydro-epiandrosterone, progesterone, and 17-hydroxyprogesterone were altered along the steroid hormone biosynthesis pathway; choline, betaine, uridine, hypoxanthine, and lactic acid were altered in the metabolite score; anthranilic acid, kynurenic acid, tryptophan, kynurenine, N-formyl kynurenine, indole-lactic acid and 4-chloro kynurenine were altered in the tryptophan pathway, and pyruvate, lactate, acetoacetate, beta hydroxybutyrate, and succinate were altered in the energy-related metabolic pathway. These results confirm the alteration of the metabolomic pathway in newborns with HIE.

Regarding the analysis of the sequencing data of microRNAs, the intensities of 1788 microRNAs was detected and annotated in plasma samples. Fold Change (FC) > 1 and t-test (p-value < 0.05) were used with the intention of finding intensities that could discriminate between newborns with pathological and normal MRI. These results were represented in a volcano plot (**Figure 3.1**). A set of 29 discriminant variables with t-test < 0.05 and FC > 1 were identified.

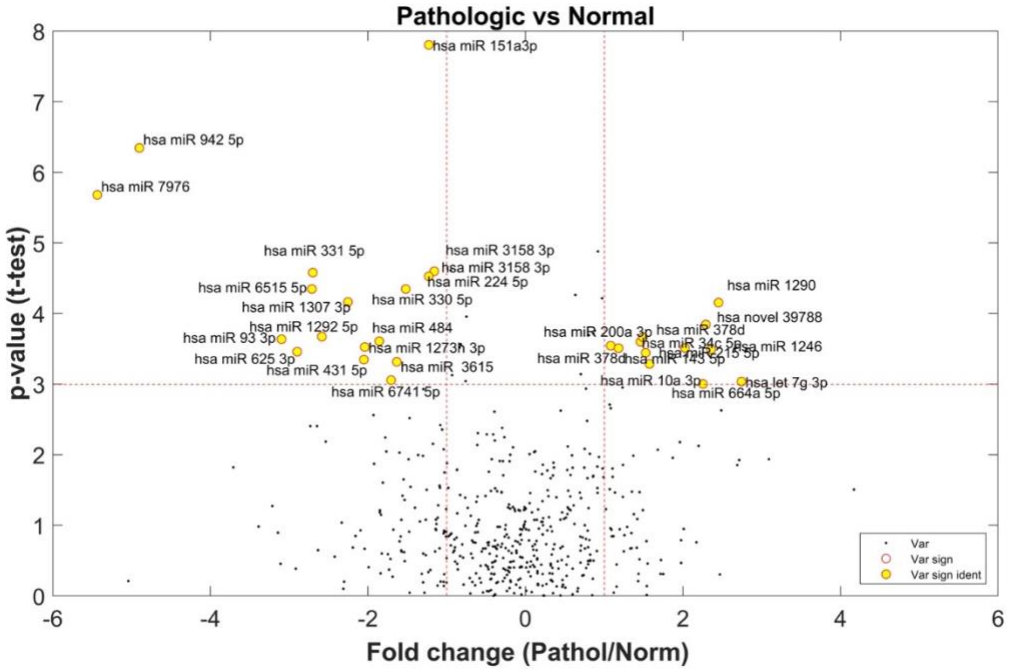

Figure 3.1. Volcano plot. Black point corresponds to microRNA intensity, yellow point corresponds to microRNA intensity with t-test p-value < 0.05 and FC >1.

3.4 Discussions and conclusions

The analysis of metabolites and miRNAs in the HYPOTOP cohort [39] aimed to identify novel biomarkers allowing to assess hypoxia-induced brain damage at early-stages. Results show that intermediates of lactate, phenylacetylglutamine, pyruvate, succinate, and ketoglutarate were altered in plasma of newborns with pathologic vs. normal MRI. Thus, the intermediates of the steroid hormone biosynthesis pathway, metabolite score metabolites, tryptophan pathway, and energy related metabolism were altered in plasma of newborn

infants with pathologic when compared to the control group with normal MRI.

In case of steroid hormone biosynthesis pathway, the results showed alterations in corticosterone, cortisol, 11-deoxycortisol, dehydroepiandrosterone, progesterone, and 17-hydroxyprogesterone in newborns with pathologic MRI compared to normal controls. Preliminary studies have described the neuroprotective effects achieved by the administration of glucocorticoids to ameliorated brain damage in neonatal HIE injury [63]. Furthermore, our previous studies employing nontargeted metabolomics indicated that the steroid hormone biosynthesis was affected over time (0h, 24h, 48h and 72h) in newborns with HIE and pathological MRI outcomes but became especially relevant during therapeutic hypothermia (TH) [89]. Alteration of these compounds confirm our previous results and opens the possibility to obtain new therapeutic targets and novel biomarkers.

Regarding tryptophan pathway alterations, our results suggest the alteration of anthranilic acid, kynurenic acid, tryptophan, kynurenine, N-formyl kynurenine, indole-lactic acid, and 4-chloro kynurenine. The alteration of this pathway can be indicative of apoptosis and cell necrosis. The initial step of this pathway is carried out by two key enzymes, IDO-1 and IDO-2 and tryptopah-2,3-dioxygenase. These two enzymes catalyze the conversion of tryptophan to kynurenine and can be activated during brain injury and are directly related with inflammatory processes and the immune system [113–115] In addition, kynurenic acid is an endogenous neuroprotector and is mainly known to be an antagonist of glutamate receptors inhibiting all three ionotropic glutamatergic

receptors: a-amino-3-hydroxy-5-methyl-4-isozazolepropionic acid (AMPA), n-methyl-D-aspartate (NMDA) and 77 -kainate receptors (KAR) [116–118]. Kynurenic acid is also antagonist of the α7acetylcholine receptor [119] and ligand of G-protein coupled receptor (GPR35) [120]. The strongest inhibitory effects of kynurenic acid in glutamatergic transmission are mainly mediated by acting as an inhibitor of glycine-binding site of the NMDA receptor [121]. Several studies conclude that the excitotoxicity caused by high levels of glutamate is mediated by NMDA receptor that can be found in dopaminergic neurons. Glutamate activates microglia and neuronal damage occurs. Therefore, the powerful inhibitory characteristics increase the possibility of neuroprotective efficacy against NMDA-mediated excitotoxicity. KNYA could also modulate the expression and/or the release of different growth factors such as nerve growth factor (NGF) or fibroblast growth factor-1 (FGF-1). In the case of neuronal ischemia, deficiency of oxygen and production of ROS cause alteration of the BBB which allows the extravasation of leukocytes into the CNS [122]. Of note, the phagosomes of neutrophils' myeloperoxidase enzyme (MPO) are present. MPO produces hypochlorous acid from hydrogen peroxide and chloride anion during the neutrophil's respiratory burst leading to the formation of hypochlorite and subsequently to microbicidal byproducts such as chlorine, chloramines, hydroxyl radical and singlet oxygen. Hence, compounds such as 4-chloro kynurenine can be formed by oxidations without the need for any enzymatic catalysis.

Conversely, our results suggest the alteration of pyruvate, lactate, acetoacetate, beta hydroxybutyrate, ketoglutarate, and succinate in newborns with pathologic MRI as compared with normal controls. All

of these compounds participate in the mitochondrial energy production linking the Krebs cycle with the Electron Transport Chain. However, under pathologic circumstances (i.e. hypoxia/reoxygenation), these compounds trigger mitochondrial ROS production especially by reversing electron flow through the succinate voltage-gate [123]. Hence, levels of succinate are intrinsically related to inflammatory processes and regulate ROS production in ischemia/reperfusion [124,125].

At last, microRNA analysis significantly suggests alterations between 29 microRNAs. It is noted that annotated microRNAs were described in pathological aspects related to hypoxia. microRNAs such as miR-10a are implicated in alteration of immune system [126,127] or miR-93 are involved in regulation of angiogenesis [128]. In any case, the mechanism of action of these altered microRNAs has not been yet described in the physiopathology of HIE, therefore more studies are required.

Our findings have unraveled interesting aspects of the pathophysiology of Hypoxic-Ischemic encephalopathy. The new information gathered could be used in the next future to enhance our ability to early diagnose and selectively treat newborn infants suffering from this extremely severe condition.

Section II. Assessment of the impact of diet on the growth and development of preterm infants

Chapter 4. Effect of donor human milk on host-gut microbiota and metabolic interactions in preterm infants

4.1 Abstract

Background & aims: Human milk is the gold standard for infant nutrition. Preterm infants whose mothers are unable to provide sufficient own mother's milk (OMM), receive pasteurized donor human milk (DHM). We studied metabolic signatures of OMM and DHM and their effect on the interplay of the developing microbiota and infant's metabolism.

Methods: Metabolic fingerprinting of OMM and DHM as well as infant's urine was performed using liquid chromatography-mass spectrometry and the infant's stool microbiota was analyzed by 16S rRNA sequencing.

Results: Significant differences in the galactose and starch and sucrose metabolism pathways when comparing OMM and DHM, and alterations of the steroid hormone synthesis and pyrimidine metabolism pathways in urine were observed depending on the type of feeding. Differences in the gut-microbiota composition were also identified.

Conclusion: The composition of DHM differs from OMM and feeding of DHM has a significant impact on the metabolic phenotype and microbiota of preterm infants. Our data help to understand the origin of the observed changes generating new hypothesis: i) steroid hormones present in HM have a significant influence in the activity of the steroid hormone biosynthesis pathway in preterm infants; ii) the pyrimidine metabolism is modulated in preterm infants by the activity of gut-

microbiota. Short- and long-term implications of the observed changes for preterm infants need to be assessed in further studies.

4.2 Introduction

Breastfeeding is regarded as the best nutrition in the first six months of life. Apart from providing nutritional elements needed for growth, known short and long-term benefits for the infant-mother dyad are numerous [129,130]. Progress in medical interventions has allowed to increase the survival of extremely low gestational age newborns and early infant nutrition has become a major player in improving clinical outcomes of survivors [131]. Human Milk (HM) is recommended for preterm infants based on an array of benefits provided to this highly vulnerable population [29,132–137].

Currently, pasteurized donor human milk (DHM) is preferred over premature infant formula for premature infants whose mothers are unable to provide an adequate supply of milk [138]. Most DHM is provided by women who have delivered at term and donate their milk in later stages of lactation from weeks to several months after delivery. In comparison to milk produced during the first weeks after delivery, milk donated in later stages of lactation is typically low in protein, fat, and other bioactive molecules [139]. The composition is further affected by the processing of expressed milk following stringent protocols applied in HM banks involving pasteurization, necessary for minimizing the potential to transmit infectious agent as well as freezing and long-term storage [140–142]. While the macronutrient composition remains relatively intact, several bioactive components, such as enzymes and immune cells are compromised or destroyed [143,144].

The use of DHM in comparison to the use of formula milk results in lower rates of weight gain, lineal growth, and head growth, but it was shown that DHM might reduce the incidence of necrotizing enterocolitis (NEC) [25,145]. Beyond the assessment of clinical parameters, scientific evidence for the effects of DHM on preterm infants is scarce. Recently it was shown that despite pasteurization, DHM does not compromise the protection against oxidative stress in comparison to the use of own mother's milk (OMM) [146]. Furthermore, the study of the composition of the developing gut-microbiome of preterm infants depending on the type of nutrition was in the spotlight of clinical studies [147,148], as diseases such as NEC and neonatal sepsis have been linked to shifts in microbial dynamics and early gut-microbiota [149,150]. It was observed that DHM fed preterm infants showed differences in the microbial patterns as compared to OMM fed infants. However, changes in the bacterial composition between DHM and OMM fed infants were smaller than in comparison to formula fed infants [148].

The metabolome represents a complex milieu of compounds of different origins, including human metabolism, the diet, xenobiotics, as well as metabolites produced by bacteria residing in the human gut that may cross the intestinal barrier and hence, it allows to untangle the relationships between diet, metabolome and health status [151]. The usefulness of metabolomics for characterizing the functional status of host-gut microbiota interactions has been repeatedly described [12,152] and comprehensive approaches seek to monitor alterations in the microbiota and host co-metabolites to identify metabolic patterns associated to changes in the microbiota functionality [153].

We hypothesize that differences in the composition of pasteurized DHM in comparison to OMM have an impact on the

physiological response of preterm infants at the phenotypic level, and more specifically on the host-gut microbiota metabolic interactions. The study of the composition of the gut-microbiota as well as the urinary metabolome of preterm infants exclusively consuming either DHM or OMM (i.e. ≥80% v/v of the total intake) aided by state-of-the art bioinformatics tools based on metabolic networks allowed to gain insight into their response to nutrition as well as the interaction between diet, microbiome and infant's metabolism.

4.3 Material and methods

4.3.1 Study population

A prospective, observational cohort study was conducted including consecutively admitted preterm infants born ≤32 weeks of gestation and/or birth weight ≤1500 g in the Division of Neonatology of the University and Polytechnic Hospital La Fe (Valencia, Spain) during a 12-month period. Two groups were recruited according to the main feeding type accounting for ≥80% v/v of the nutritional intake with either OMM or DHM after achieving full enteral nutrition (150 mL/kg/day). Inclusion and exclusion criteria are listed in **Supplemental Table A.4.1**. The study protocol was approved by the Ethics Committee for Biomedical Research of the Health Research Institute La Fe (Valencia, Spain) with approval number 2014/0247. All methods were performed in accordance with the relevant guidelines and regulations and written permission was obtained from legal representatives by signing an informed consent form.

The protocols of the Division of Neonatology strongly support breastfeeding. If necessary, DHM is administered under medical

prescription as a supplement to preterm infants born below ≤32 weeks or ≤1500 g of birth weight. Also, in case mothers refuse to breastfeed, DHM is offered. DHM is collected, processed, and stored in milk banks. Milk bank guidelines recommend Holder pasteurization (62.5 °C, 30 min) to inactivate viral and bacterial agents [141]. Both, DHM and OMM are routinely fortified with HM fortifier (PreNAN FM 85, Nestle "R", Vevey, Switzerland), adding one gram per 25 mL of milk. The nutritional intake was prospectively monitored, but not modified for this observational study.

4.3.1.1 Maternal and infant biological samples

OMM (n = 15) was collected one month after preterm birth. DHM (n = 12) was provided by volunteers admitted after the routine screening and interview at the HM bank (Banco de Leche Materna at the Hospital Universitario y Politécnico La Fe).

Mothers expressed milk using breast milk pumps following a standard operating procedure employed routinely in the hospital and the HM bank. Before extraction, hands must be washed with soap and water and nipples are cleaned with water. The removable parts of the breast milk pump as well as the collection bottles are sterilized. Aliquots of DHM were collected after Holder pasteurization. OMM and DHM samples were agitated and 1 mL aliquots were collected in dry, 1.5 mL microcentrifuge tubes.

Urine samples were collected from infants exclusively receiving DHM (n = 20) or OMM (n = 20) one month after birth using sterile cotton pads placed in the diaper. Cotton pads were retrieved after one hour and squeezed with a syringe. The process was repeated until a minimum volume of 1 mL was collected. Stool samples from preterm

infants exclusively receiving OMM (n = 18) or DHM (n = 18) were collected directly from the diaper when full enteral nutrition was achieved. All samples (urine, HM and stool) were stored at -80 °C until analysis.

4.3.2 Liquid Chromatography-quadrupole time-of-flight mass spectrometry (LC-QTOFMS) metabolomic screening of urine and HM samples

4.3.2.1 Standards and reagents

Acetonitrile (CH_3CN), methanol (CH_3OH), and isopropanol (IPA), all LCMS grade, methyl tert-butyl ether (MTBE, reagent grade), ammonium acetate (≥98%), formic acid (HCOOH, >98%), reserpine (>99%), and leucine-enkephalin (97%) were obtained from Sigma Aldrich Quimica S.A (Madrid, Spain). Ultra-pure water (>18.2 MΩ) was generated using a Mili-Q Water Purification System (Merck Millipore, Darmstadt, Germany). Phenylalanine-D_5 (98%) and methionine-D_3 (98%) were purchased from Cambridge Isotopes Laboratory Inc. (Andover, MA, USA); caffeine-D_9 (98%) was from Toronto Research Chemicals (Toronto, Ontario, Canada); (15,15,15,16,16,17,17,18,18,18-D_9) oleic acid-D_9 (>99%) was purchased from Avanti Polar Lipids (Alabaster, AL, USA) and prostaglandin F_{2a}-D_4 (≥98%, deuterated incorporation ≥99%) was purchased from Cayman Chemical Company (Ann Arbor, MI, USA).

4.3.2.2 HM preparation and analysis

Parameters employed for HM fingerprinting have been described elsewhere [154]. In summary, OMM and DHM samples were subjected

to a single-phase extraction procedure by adding 175 µL of CH3OH followed by 175 µL of MTBE [31] and 20 mL of supernatant were added to 80 µL of a CH3OH:MTBE (1:1, v/v) solution.

Untargeted metabolomics analysis was carried out employing a 1290 Infinity UPLC system from Agilent Technologies (Santa Clara, CA, USA) equipped with a Kinetex C18 column (50×2.1 mm, 1.7 mm) from Phenomenex (Torrance, CA, USA) running a binary gradient with (5:1:4 IPA: CH_3OH:H_2O 5 mM ammonium acetate, 0.1% v/v HCOOH) and (99:1 IPA:H_2O 5mM ammonium acetate, 0.1% v/v formic acid) as mobile phase components. Column and autosampler were kept at 55 and 4 °C, respectively and the injection volume was 4 mL. For detection, an Agilent 6550 iFunnel QTOF-MS system working in the ESI^+ mode was used in the range between 70 and 1700 *m/z* with automatic MS spectra recalibration during analysis. LC-QTOFMS data acquisition was carried out employing MassHunter Workstation (version B.07.00) from Agilent.

4.3.2.3 Urine preparation and analysis

Urine samples were thawed on ice and thoroughly shaken on a Vortex® mixer during 10 s followed by centrifugation at 16 000 × g and 4 °C during 10 min. 50 µL of supernatant were added to 50 µL of an internal standard (IS) solution containing reserpine, phenylalanine-D_5, leucine-enkephalin, caffeine-D_9, and methionine-D_3 at 2 µM each in H_2O:CH_3CN (96:4, 0.1% HCOOH v/v) and transferred to a 96-well plate. A blank extract was prepared using water instead of urine and following the same procedure as described for urine samples. A pooled quality control (QC) sample was prepared by mixing 5 µL of each study sample. Metabolomic analysis was carried out employing a 1290 Infinity UPLC system from Agilent Technologies equipped with a UPLC BEH C_{18}

column (100 × 2.1 mm, 1.7 μm) from Waters (Wexford, Ireland). The flow rate was set to 400 μL min^{-1} running a binary gradient with 0.1% v/v HCOOH in H_2O and 0.1% v/v HCOOH in CH_3CN as mobile phase components. All remaining analysis parameters were set as described for HM analysis.

4.3.2.4 QC procedures

Before LC-QTOFMS experiments, a system suitability check was carried out by analyzing a 2 mM IS solution to ensure that the retention times, peak area and shape values and mass accuracies were within laboratory defined limits. Eight QCs were injected prior to the study samples at the beginning of the analysis batch for conditioning of the LC-QTOFMS system. Data acquired during the analysis of those samples were discarded. The blank extract was injected twice, once during system conditioning and at the end of the measurement sequence to identify signals from other tan biological origin and data clean-up [94]. The injection order of samples and twice at the beginning and end of the batch for assessment and correction of instrumental performance [69].

4.3.3 Microbiota analysis

The analysis of the fecal microbiota composition has been described elsewhere [148]. Briefly, total fecal DNA was isolated using the MasterPure Complete DNA & RNA Purification Kit (Epicentre, Madison, WI United States) and V3—V4 region 16S rRNA libraries were sequenced using a 2 ×300 bp paired-end run (MiSeq Reagent kit v3) on a MiSeq-Illumina (Illumina, San Diego, USA) platform.

4.3.4 Data processing and statistics

4.3.4.1 Metabolomics data pre-processing

The pre-processing pipeline for data acquired during the analysis of HM samples has been described elsewhere [154]. For urine, centroid LC-QTOFMS raw data were converted to mzXML format employing ProteoWizard [155] (http://proteowizard.sourceforge.net/). The selection of parameters for peak table extraction and alignment was based on the observed variation of retention times and m/z values of ISs. XCMS software (http://metlin.scripps.edu/xcms/) [93,125,156] and CAMERA [73] in R 3.6.1 were employed for the generation of peak tables. For data acquired from urine samples, the centWave method with the following settings was used for peak detection: *m/z* range = 70-1200, ppm = 15, peakwidth = (3 and 20), snthr = 6. A minimum difference in *m/z* of 0.01 Da was selected for overlapping peaks. Intensity-weighted *m/z* values of each featurewere calculated using the wMean function. Peak limits used for integration were found through descent on the Mexican hat filtered data. Peak grouping was carried out using the "density" method using mzwid = 0.015 and bw = 6. Retention time correction was carried out using the "obiwarp" method. After peak grouping, the fillPeaks method with the default parameters was applied to fill missing peak data. Automatic integration was assessed by comparison to manual integration using IS signals. A total of 40,513 features were initially detected after peak detection, integration, chromatographic deconvolution, and alignment in urine samples.

Further data processing and statistical analysis were carried out in MATLAB 2017b (Mathworks Inc., Natick, MA, USA) using inhouse written scripts (available from the authors) and the PLS Toolbox 8.7

(Eigenvector Research Inc., Manson, WA, USA). During data pre-processing and filtering of data from urine analysis, features with an intensity <800 AU and those with a mean peak area <9 × mean peak area in blank samples, were removed [69]. Intrabatch effect correction was performed using Quality Control- Support Vector Regression algorithm [92,95,96] and the LIBSVM library [75] with the following parameters: ε -range = 2-5%; γ range = 1-10^5; C interval = 50%. Finally, features with a %RSD in QC samples >20% after QC-SVRC were removed from the peak table. Urinary metabolic data were normalized to the creatinine concentration in each urine sample quantified by the modified Jaffe method (DetectX® urinary creatinine detection kit, Arbor Assays, Ann Arbor, MI, USA) following the manufacturer's protocol and employing a dilution factor of 1:4 during sample preparation.

4.3.4.2 Microbiota data

Sequencing data were processed using a QIIME pipeline (version 1.9.0) [157] running in R. Operational taxonomic units (OTUs) tables with 97% identity were constructed and representative sequences were taxonomically classified based on the Greengenes 16S rRNA gene database (version 13.8). OTUs with detection frequency <20% across all samples were removed and predictive inferred functional analysis was performed using the Phylogenetic Investigation of Communities by Reconstruction of Unobserved States (PICRUSt) approach, as described elsewhere [158]. Alpha-diversity indices (Chao1 and Shannon, richness and diversity index, respectively), Principal Coordinate Analysis

(PCoA) of beta diversity based on UNOFRAC distance (phylogenetic) and permutational multivariate analysis of variance (PERMANOVA) test with 999 permutations were obtained to show the significance between-groups.

4.3.4.3 Pathway analysis

Differences between OMM and DHM groups were studied on the pathway level employing the "MS Peaks to Pathways" tool (version 2.0) available in MetaboAnalyst 4.0 [78] using a mass accuracy of 5 ppm, the mummichog algorithm with a p-value cut-off of 0.05, and the Kyoto Encyclopedia of Genes and Genomes (KEGG) *Homo sapiens* pathway library [159,160]. As an input, a four column table was generated including *m/z*, RT, the *p*-values from a t-test comparing mean values between each group and accounting for unequal variances, and fold changes (FC) calculated as the ratio of medians between groups. Metabolites included within significantly altered pathways were annotated in LC-QTOFMS data from HM samples using the output retrieved from the *mummichog* algorithm ('level 3' identification as defined by The Metabolomics Standards Initiative [161]).

AMON (Annotation of Metabolite Origins via Networks) was used to integrate microbiome and metabolome data [162]. This tool produces a table indicating which compounds could be produced by the microbiome, the host, or both based on the provided lists of gut-microbiome and human KEGG Orthology identifiers (KOs). AMON was used to compute enrichment of KEGG pathways in the compounds that were detected via LC-QTOFMS based on the list of annotated KEGG compound IDs provided by *mummichog* and were predicted to be generated either by the fecal microbiome or the host metabolism. This

calculation is performed for all KEGG pathways with at least one metabolite predicted to be produced by the input gene sets.

4.3.4.4 Statistical tests

Categorical variables were compared using Pearson's chi-squared test ($\alpha = 5\%$). KolmogoroveSmirnov analysis was performed to test the normal distribution of the data. Continuous variables were expressed as mean ± standard deviation or medians with interquartile range (IQR) depending on underlying distributions and comparisons were carried out using the Student's t-test ($\alpha = 5\%$) for data following a normal distribution or alternatively the Wilcoxon rank-sum test ($\alpha = 5\%$). values were false Discovery rate (FDR)-adjusted where indicated. Pearson correlation was used to assess correlations between variables. Venny 2.1.0 was used for generating the Venn diagram [163].

4.3.4.5 Data availability

Peak tables extracted from urine and HM LC-QTOFMS data are accessible via the Mendeley Data repository (https://data. mendeley.com/) under https://doi.org/10.17632/7tb4d66z7c.1 and https://doi.org/10.17632/fnzbxmkv83.1, respectively. Sequencing data from the preterm gut microbiota of the infants matching the individuals included in this study can be retrieved from GenBank Sequence Read Archive Database under project accession number PRJEB25948 [148].

4.4 Results

4.4.1 Clinical data

In this observational study, OMM samples from mothers of preterm infants (n = 15) as well as DHM samples (n = 12) provided by volunteers at the HM bank were analyzed. OMM samples were collected at 1 month of age. The time of sample collection of DHM samples was heterogeneous, since for each mother several aliquots were collected over time and pooled prior to pasteurization. In this study, the elapsed time between the first and last expression of a pooled DHM sample ranged between 9 and 72 days. The median value of this elapsed time was used to represent the time of collection with respect to the infants' age. As a result, time of collection of DHM samples ranged between 21 and 164 days after delivery with a median value of 87 days (83 IQR). With respect to GA the median (5^{th}-95^{th} percentile) in the OMM group was 29 (25-32) in comparison to 40 (27-41) for milk donors (DHM group). 20 preterm infants exclusively receiving OMM and 20 exclusively fed with DHM were enrolled. **Table 4.1** displays the demographic, perinatal, clinical, and analytical data of the recruited infants grouped according to the type of feeding. No statistically significant differences (p-values >0.05) were observed between the study groups.

Table 4.1. Characteristics of the study population (infants).

Parameter	OMM (N=20)	DHM (N=20)	*p*-value
Gender, N (%)			
- Male	14 (70)	12 (60)	0.06
- Female	6 (30)	8 (40)	
GA median (5-95% CI)	28 (27-29)	29 (28-30)	0.06
Antenatal steroids, N (%)	17 (85)	17 (85)	0.6

Parameter	OMM (N=20)	DHM (N=20)	*p*-value
Birth Weight (g), mean (SD)	1300 (300)	1400 (200)	0.9
Preeclampsia, N (%)	2 (10)	5 (25)	0.2
Chorioamnionitis, N (%)	5 (25)	2 (20)	0.2
Mode of birth, N (%)			
- Vaginal	9 (45)	9 (45)	0.6
- C-section	11 (55)	11 (55)	
Apgar 1 min, median (IQR)	8 (5-9)	8 (6-9)	0.5
Apgar 5 min, median (IQR)	10 (8-10)	9 (8-10)	0.4
Umbilical artery blood gases, mean (SD)	7.2 (0.3)	7.28 (0.07)	0.9
Days of oxygen supplementation, median (IQR)	0 (1.3)	0 (0)	0.2
Respiratory distress syndrome, N (%)	8 (40)	5 (25)	0.13
Apneic syndrome, N (%)	17 (85)	15 (75)	0.2
Mechanical ventilation, N (%)	5 (25)	4 (20)	0.7
Non-invasive ventilation, N (%)	18 (90)	18 (90)	0.06
Postnatal steroids, N (%)	1 (5)	0 (0)	n.a.
Antibiotic therapy, N (%)	8 (40)	7 (35)	0.6
- Pre/intra-partum	20 (100)	20 (100)	1.0
- Post-partum	8 (40)	7 (35)	0.6
Necrotizing enterocolitis, N (%)	0 (0)	1 (5)	n.a.
Bronchopulmonary dysplasia, N (%)	1 (5)	1 (5)	0.6
Persistent ductus arteriosus, N (%)	9 (45)	3 (15)	0.10
Intra-periventricular hemorrhage ≥grade 2 (Papile's classification [164], N (%)	6 (30)	0 (0)	n.a.

Note: CI = confidence interval; SD = standard deviation; IQR = interquartile range; categorical variables were compared using Pearson's chi-squared test (α=0.05). Kolmogorov-Smirnov analysis was performed to test the normal distribution of the data. Continuous variables were expressed as mean ± standard deviation or medians with interquartile range depending on underlying distributions and comparisons were carried out using the Student's t-test (α = 5%) for data following a normal distribution or alternatively the Wilcoxon rank-sum test (α = 5%).

4.4.2 Metabolomic analysis of HM samples

Metabolic fingerprint of OMM and DHM consumed by the preterm infants included in this study were acquired employing an LC-QTOFMS platform retrieving a total of 7109 metabolic features after peak

detection, deconvolution, integration, alignment, within-batch effect correction, and clean-up. For 1034 features (14.6%), significant differences in mean values of OMM and DHM groups (t-test, *p*-value <0.05) were found and for 21 and 199 features $\log_2$(FC) <-1 and >1, respectively, were detected. Metabolic network analysis was employed for a functional interpretation of the acquired metabolic profiles within relevant networks using the mummichog algorithm [165]. Pathway analysis detected 13 pathways with more than two significantly changing metabolites (see **Table 4.2**). Significant differences between DHM and OMM groups were found for galactose and starch and sucrose metabolism (*gamma p*-value < 0.05).

Table 4.2. Altered pathways in DHM vs. OMM.

Pathway name	Hits (all)	Hits (sig)	*p*-value	*gamma p*-value
Galactose metabolism	5	5	0.0004	0.007
Starch and sucrose metabolism	4	4	0.002	0.03
Fructose and mannose metabolism	7	4	0.04	0.2
Tyrosine metabolism	4	3	0.03	0.2
Amino sugar and nucleotide sugar metabolism	5	3	0.07	0.3
Linoleic acid metabolism	6	3	0.12	0.4
Glycolysis / Gluconeogenesis	2	2	0.05	0.4
Ascorbate and aldarate metabolism	2	2	0.05	0.4
Neomycin, kanamycin and gentamicin biosynthesis	2	2	0.05	0.4
Inositol phosphate metabolism	2	2	0.05	0.4
Phosphatidylinositol signaling system	2	2	0.05	0.4
Lysine degradation	3	2	0.12	0.5
Biosynthesis of unsaturated fatty acids	14	4	0.4	0.6

Note: *P*-values from Fisher's exact t-test (*p*-value) and adjusted for permutations (*gamma p*-value); all detected pathways with at least 2 significantly altered features are reported.

4.4.3 Preterm gut-microbiota

Gut-microbiota profiles differed between DHM and OMM groups as shown in **Figure 4.1**. Significant differences in beta diversity were detected (PCoA, PERMANOVA *p*-value = 0.04), although alpha diversity indexes were not different between groups. Significantly higher abundances of Staphylococcaceae (*Staphylococcus genus*) and Pasteurellaceae members (Wilcoxon rank-sum test, p-value <0.05) were observed in the DHM group, but differences did not remain significant after FDR correction. Likewise, functional prediction of KEGG pathways identified changes in ten metabolic pathways (*p*-value < 0.05) that were non-significant after FDR correction.

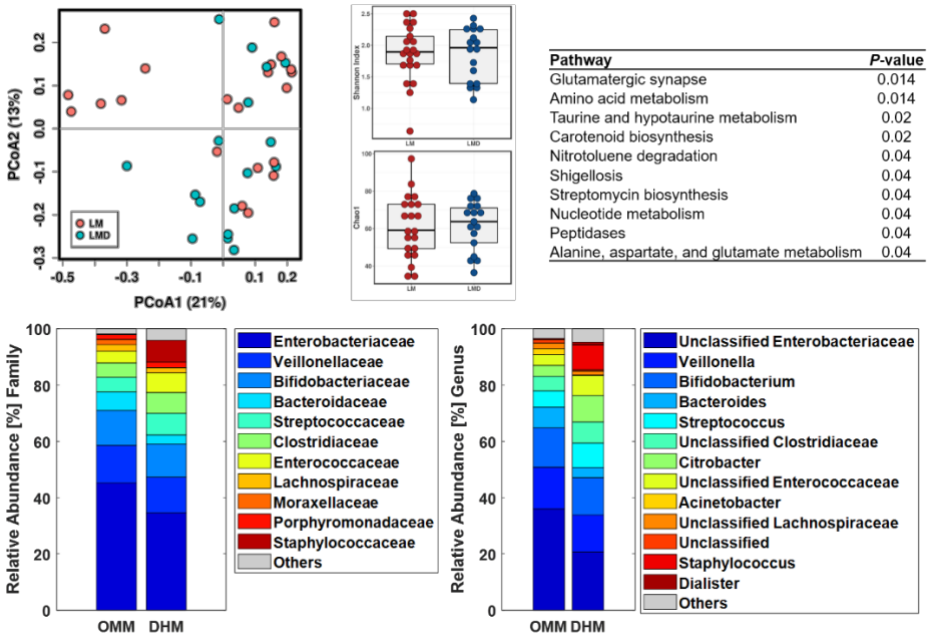

Figure 4.1. Gut-microbiota profile of preterm infants exclusively receiving OMM and DHM. PCoA scores plot representing beta diversity relationships (top, left), alpha diversity (Shannon index) and richness (Chao1 index) (top, middle), functional predictions of KEGG pathways with significant differences between groups (top, right), and relative abundances at the family (bottom, left) and genus levels (bottom, right). OMM = light blue and DHM = orange (For interpretation of the references to colour in this figure legend, the reader is referred to the Web version of this article).

4.4.4 Metabolomic analysis of urine samples

Urinary metabolic fingerprints of preterm infants exclusively receiving DHM vs. OMM were recorded employing an LC QTOFMS platform. Initial pre-processing of data identified 10,450 metabolic features after feature extraction and pre-processing. In this study, 849 features (8.1% of the total) showed significantly different mean values between both groups (t-test, *p*-value <0.05) with 21 and 343 features showing $\log_2$(FC) of <-1 and >1, respectively, when comparing DHM and OMM groups. A list of the detected metabolic pathways with at least two significantly altered metabolic features is shown in **Table 4.3**. From the 32 detected pathways, only the steroid hormone biosynthesis pathway and pyrimidine metabolism were found to be significantly altered in urine samples from preterm infants consuming DHM as compared to OMM (*gamma p-value* < 0.05).

Using the results of the *mummichog* algorithm, 331 features were tentatively assigned to steroid hormones belonging to the steroid hormone synthesis pathway (KEGG map00140). Between group comparison of their intensities (i.e. OMM vs DHM) showed that 19 features (see **Table A.4.2**) had significantly different mean values (FDR-adjusted p-value <0.05) and |log2(FC)| >1 (see **Figure 4.2**, left). Remarkably, for all 19 features, higher intensities were detected in the OMM group as compared to the DHM group (**see Figure 4.2**, right). This result confirms the alteration of the steroid hormone synthesis pathway detected by pathway analysis in newborns receiving DHM vs. OMM.

Table 4.3 Altered pathways in urine samples from preterm infants consuming DHM vs. OMM.

Pathway name	Hits (all)	Hits (sig)	*p*-value	*gamma p*-value
Steroid hormone biosynthesis	96	43	4E-09	1.1E-08
Pyrimidine metabolism	24	10	0.013	0.04
Alanine, aspartate and glutamate metabolism	22	9	0.02	0.06
Glyoxylate and dicarboxylate metabolism	8	5	0.011	0.06
Nitrogen metabolism	7	4	0.04	0.2
Metabolism of xenobiotics by cytochrome P450	36	11	0.10	0.2
Linoleic acid metabolism	4	3	0.03	0.2
D-Glutamine and D-glutamate metabolism	10	4	0.13	0.3
Retinol metabolism	8	3	0.2	0.5
Arginine biosynthesis	13	4	0.3	0.5
Arachidonic acid metabolism	13	4	0.3	0.5
Drug metabolism - other enzymes	9	3	0.3	0.6
Biosynthesis of unsaturated fatty acids	4	2	0.2	0.6
Cysteine and methionine metabolism	22	5	0.5	0.7
Phenylalanine metabolism	34	7	0.6	0.7
Aminoacyl-tRNA biosynthesis	40	8	0.6	0.7
Phenylalanine, tyrosine and tryptophan biosynthesis	18	4	0.5	0.7
Butanoate metabolism	6	2	0.4	0.7
Valine, leucine and isoleucine degradation	14	3	0.6	0.8
Drug metabolism - cytochrome P450	29	5	0.7	0.9
Ubiquinone and other terpenoid-quinone biosynthesis	10	2	0.6	0.9
Tryptophan metabolism	66	11	0.8	0.9
Vitamin B6 metabolism	11	2	0.7	0.9
Pantothenate and CoA biosynthesis	11	2	0.7	0.9
Glycine, serine and threonine metabolism	12	2	0.7	0.9
Histidine metabolism	20	3	0.8	0.9
Purine metabolism	49	7	0.9	1.0
Folate biosynthesis	15	2	0.8	1.0
Tyrosine metabolism	64	9	0.9	1.0
Porphyrin and chlorophyll metabolism	16	2	0.9	1.0
Lysine degradation	18	2	0.9	1.0
Arginine and proline metabolism	38	2	1.0	1.0

Note: *P*-values from Fisher's exact t-test (*p*-value) and adjusted for permutations (*gamma p*-value); all detected pathways with at least 2 significantly altered features are reported.

Likewise, 101 (1.0%) features were tentatively annotated as metabolites included in the pyrimidine metabolism pathway. However, none of these features showed significant differences in their mean intensities (FDR-adjusted p-value<0.05) and $|\log_2(FC)| > 1$. This indicates that alteration of pyrimidine metabolism is less evident than observed for the steroid hormone biosynthesis pathway, which agrees with the *gamma* p-values reported in **Table 3.3** of 1.1E-08 vs. 0.04, respectively.

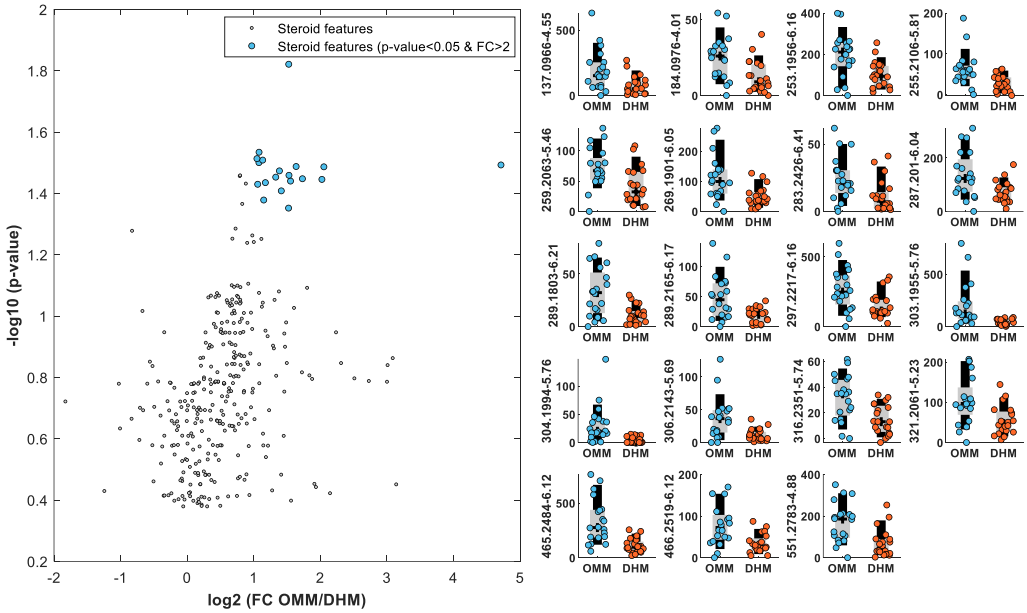

Figure 4.2 Steroid hormone signals with different relative signal intensities found in urine samples from preterm infants exclusively receiving OMM or DHM.

4.4.5 Integrative analysis of data from metabolomics and microbiota profiling

Integrative analysis of omics data was performed to elucidate the origin of observed pathway alterations in urine samples. The HM peak table was searched for metabolites of the steroid hormone biosynthesis

pathway using tentative mummichog annotations. 73 unique features were assigned and out of those, 10 features (see **Table A.4.3**) showed significant differences in mean values and $|\log_2(FC)| > 1$ (see **Figure 4.3**, left). Again, consistently higher intensities were detected in the OMM group as compared to the DHM group (see **Figure 4.3**, right).

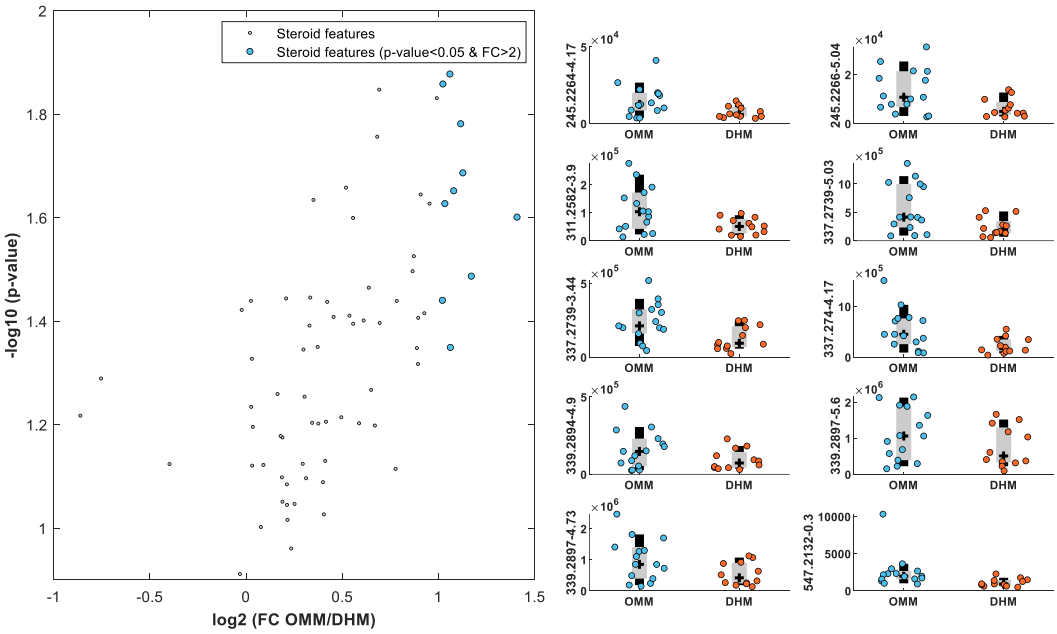

Figure 4.3 Steroid hormone signals with different relative signal intensities found in OMM and DHM samples consumed by preterm infants.

Figure 4.4 represents Pearson correlation coefficients (R) calculated between metabolic features annotated as steroid hormones in HM and urine. In HM samples, steroid hormone levels typically showed strong correlations with a median R=0.9 (0.6-1.0 5th-95th percentile), whereas moderate correlation were found within urine samples (R=0.5, 0.2-1.0 5th-95th percentile) as well as between urine and HM steroid levels (R=0.38, 0.06-0.6 5th-95th percentile). Conversely, microbiota relative

abundances overall did show weak correlations among them (R=-0.1, -0.2-0.7 5^{th}-95^{th} percentile) as well as with HM and urine steroid levels (R=0.0, -0.3-0.6 5^{th}-95^{th} percentile and R=0.0, -0.3-0.4 5^{th}-95^{th} percentile, respectively). However, some specific microbiota (i.e. *Blautia*, *Unclassified Lachnospiraceae*, and *Enterobacter*) were consistently correlated with steroid hormones in HM (R=0.6, 0.6-0.6 5^{th}-95^{th} percentile).

Figure 4.5 depicts the steroid hormone biosynthesis pathway in which the altered metabolites annotated in urine and HM were highlighted for better visualization. It can be observed that metabolites found in HM and in urine were at close pathway distances. For example, pregnenolone was altered in HM samples, while direct downstream metabolites (i.e. 21-hydroxy-pregnenolone, 7α-hydroxy-pregnenolone, progesterone, 17α-hydroxy-pregnenolone) were altered in urine samples between DHM and OMM groups.

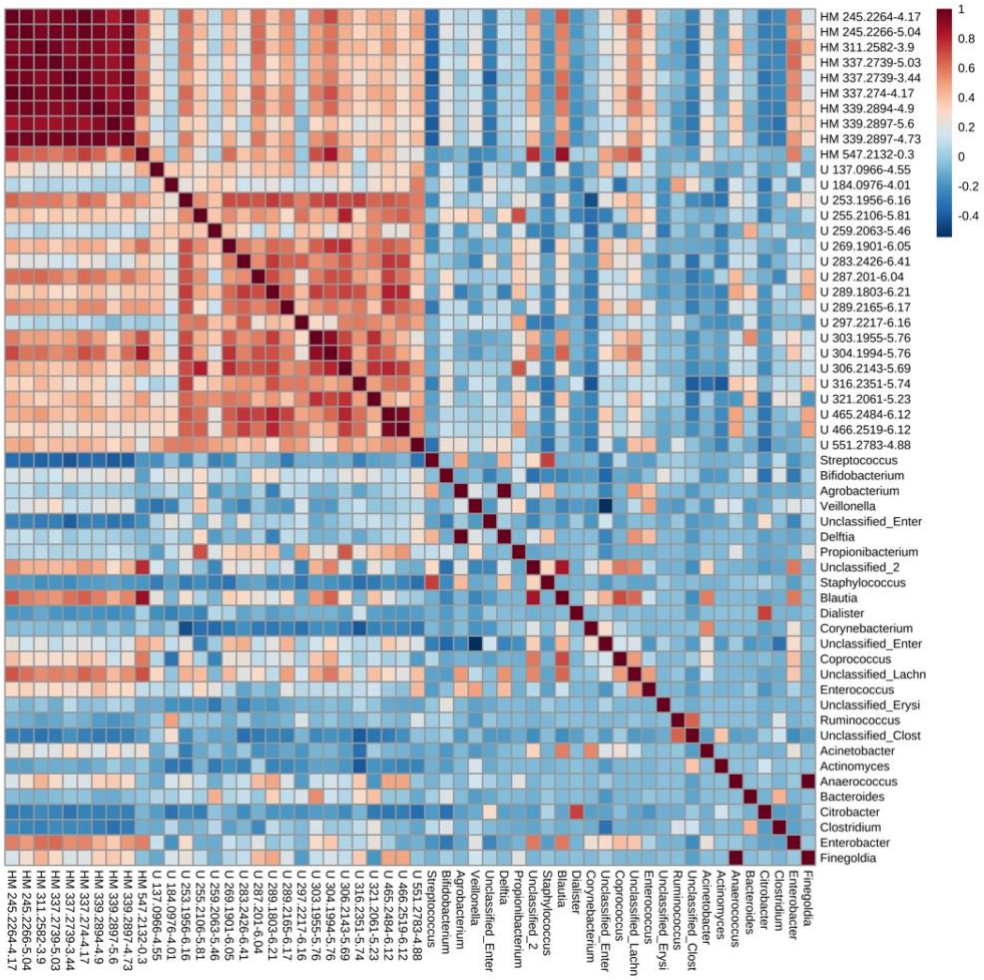

Figure 4.4. Correlation coefficients of steroid hormones in urine and HM samples as well as microbiota profiles (genus level).

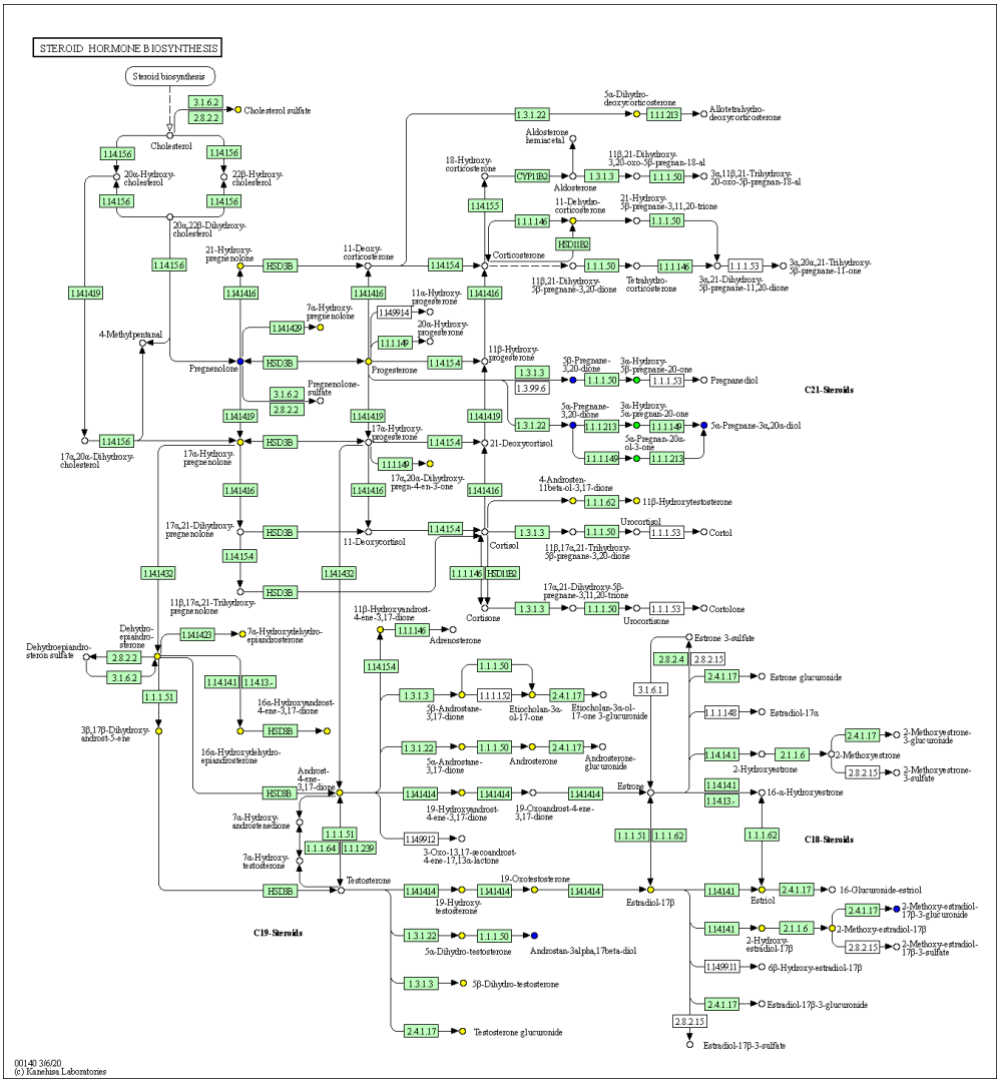

Figure 4.5. Altered metabolites of the steroid hormone biosynthesis pathway detected in HM (blue), urine (yellow), or both (green).

To explore whether the pathway alteration detected in urine samples could be caused by the activity of the gut-microbiome, an integrative approach (AMON) for the analysis of the gut-microbiome and metabolome data via networks was employed. This tool allows to gain insight on the metabolite origins, i.e. to determine the degree to which annotated compounds in the urinary metabolome of preterm

infants may have been produced by bacteria present in fecal samples, the host, either, or neither. From 80 OTUs detected in fecal samples, PICRUSt predicted 6909 unique KOs. For representing the human gene content, the KEGG list of KOs in the human (*Homo sapiens*) genome was used. Altogether, from the 13019 predicted KOs to be present in the gut microbiome and the human host, and with the information available in KEGG, it was predicted that these KOs produce 3746 compounds via 5463 reactions.

The employed metabolomics assay detected 10450 metabolic features in urine samples from preterm infants. In total, 869 unique metabolites could be annotated by using the *mummichog* algorithm in the data set. Of these, 765 were predicted to be produced by enzymes in either human only or human and stool bacterial genomes while none of the detected metabolites was exclusively attributed to the gene products of intestinal microbiota (see **Figure 4.6a**). The remaining 104 metabolites were not predicted to be from the human or the gut-microbiome either.

The enrichment of pathways that can be produced by each input KO is tested relative to the full set of all compounds in that pathway for the detected human and bacterial metabolites. In total, the calculation was performed for 217 KEGG pathways that had at least one metabolite predicted to be produced by the provided gene sets. For 127 and 98 pathways, FDR adjusted p-values <0.05 and <0.01, respectively, were found in human and/or microbial metabolism (**Figure 4.6b**). Clearly, the impact on the steroid hormone biosynthesis pathway can be ascribed to human metabolism rather than the microbiome with adjusted p-values of 0.0005 and 1.0, respectively. In case of pyrimidine metabolism, adjusted p-values of 0.0005 and 7×10^{-8} were obtained for host and microbiota,

respectively. Hence, metabolites from the pyrimidine metabolism pathway are influenced by both, host and microbiome, although the impact was much more pronounced in case of bacterial metabolism. The metabolite origin within the pyrimidine metabolism pathway was further visualized in **Figure 4.7.**

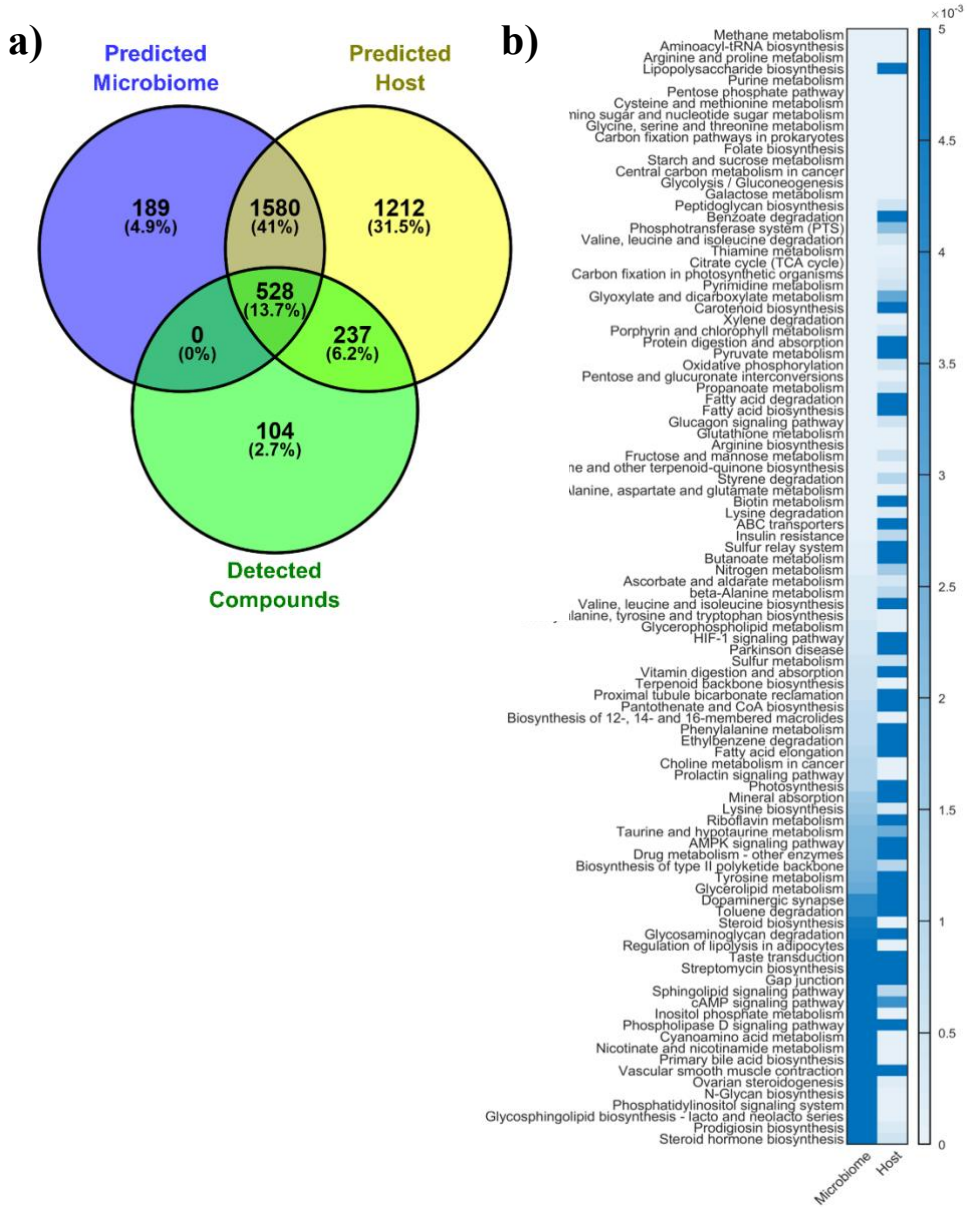

Figure 4.6. Metabolic interactions of host-gut microbiota in preterm infants. Metabolites predicted to be produced by the gut-microbiome and the host as well as measured compounds (LC-QTOFMS) (a) and heatmap showing the adjusted *p*-values associated with a pathway enrichment analysis of KEGG pathways in compounds that were detected via untargeted LC-QTOFMS analysis of urine samples and were predicted to be generated by members of the fecal microbiota or the human host (b) Note: only pathways with adjusted *p*-values<0.01 in host and/or microbiome are shown to enhance visibility.

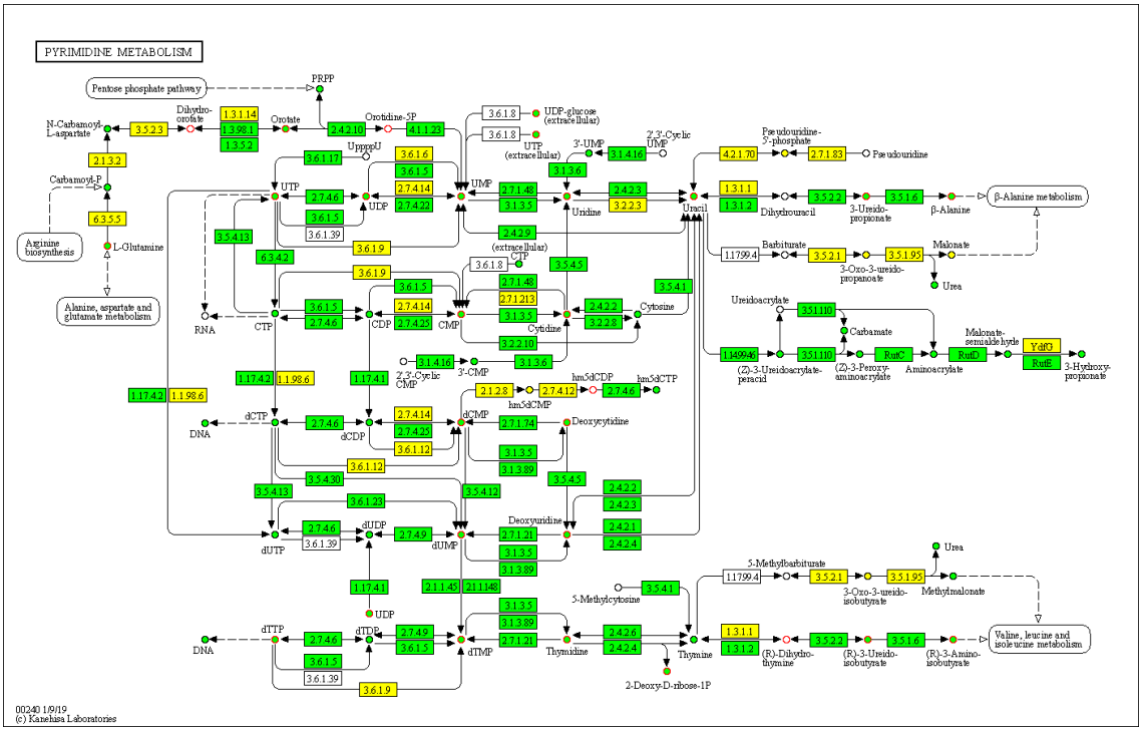

Figure 4.7. Pyrimidine metabolism map (KEGG map00240) colored by putative origin of compounds (circles), and presence of the reaction (rectangles). Note: yellow indicates human origin, green indicates human or bacteria origin, and red outlined compounds that were detected by LC-QTOFMS.

4.5 Discussion and conclusions

This study assesses the impact of the administration of DHM in comparison to OMM on the microbiome profiles and metabolic fingerprints of preterm infants during the NICU stay. The comparison of the HM metabolome from DHM and OMM revealed differences in two pathways related to carbohydrate metabolism (see **Table 4.2**). The total carbohydrate concentration is higher in milk from mothers of preterm infants in comparison to full-term milk [166] and specifically lactose and human milk oligosaccharides (HMOs) have been found at significantly

higher concentrations in preterm milk. In this study, DHM was mainly provided by mothers of term infants and therefore the observed alterations of metabolic pathways related to carbohydrates are consistent with results reported in the literature [166]. Furthermore, although HM carbohydrate contents, including the most abundant carbohydrate lactose and HMOs and glycosaminoglycans, are not significantly reduced by Holder pasteurization [167–169], a significant decrease of lactose contents was reported under conditions of frozen storage of pasteurized milk at -20°C [167]. Observed differences in carbohydrate metabolism might be especially relevant, as it has been reported that bioactive factors contained in HM, such as non-digestible HMOs, could possibly modulate the composition of microbial communities in the gut, selecting for beneficial bacteria, and are emerging as early mediators in the relationship between the development of the gut-microbiome in early life and clinical outcomes [147]. When assessing the composition of the gut-microbiome of preterm infants exclusively fed DHM in comparison to OMM (see **Figure 4.1**), we observed subtle differences.

The impact of the changing milk composition and microbiome on the preterm infant was measured through the study of the urinary metabolome. Our results have unraveled the presence of significant differences in the metabolome (see **Table 4.3**) that may exert an influence upon specific aspects of preterm physiology of yet unknown short-and-long-term consequences. Specifically, we detected the alteration of the steroid hormone biosynthesis pathway and the pyrimidine metabolism in preterm infants exclusively receiving DHM in comparison to OMM.

Milk-borne hormones including glucocorticoids are postulated to play a role in the proliferation and differentiation of the intestinal epithelium and vertical transmission of glucocorticoids via HM has been described [170]. Hence, the possibility of attributing the changes in the preterm infant's metabolism to differences in the composition of DHM and OMM was explored. Metabolites of the steroid hormone biosynthesis pathway were found to decrease in infants consuming DHM (**Figure 4.2**) and the same trend was observed in DHM as compared to OMM (**Figure 4.3**) while no differences in antenatal or postnatal steroid administration were found between infants receiving DHM or OMM. Of note, changes in the hormonal environment in the mother giving birth preterm or term could explain the differences found [170,171]. However, further studies addressing this specific issue are needed. Interestingly, in our study, some of the metabolites that showed significantly different concentrations between DHM and OMM were direct precursors of metabolites altered in urine samples (see **Figure 4.5**). It has been observed that HM glucocorticoid hormone levels follow the diurnal rhythm of maternal hypothalamus-pituitary-adrenal axis activity reflected in diurnal changes [171]. DHM is processed in batches as a pool from HM aliquots collected on different days and the collection time may vary between HM aliquots. Furthermore, administered DHM was subjected to Holder pasteurization. There is controversy about the stability of hormones during heat treatment [171–174] and comprehensive studies covering metabolites from the steroid hormone biosynthesis pathway are lacking.

We also explored the possibility of gut-microbiota to contribute to the observed changes in steroid hormone biosynthesis pathway in preterm infants fed with DHM vs. OMM. HM glucocorticoids might

modify the intestinal microbiome and intestinal bacteria can metabolize steroid hormones and are possibly involved in metabolizing endogenous glucocorticoids [170,175]. In this study overall, weak correlations were observed within microbiota as well as between microbiota and HM and urine steroids. However, some specific microbiota, i.e. *Blautia*, Unclassified *Lachnospiraceae*, and *Enterobacter*, showed moderate, but consistent correlations (R=0.6) across altered HM steroids between DHM and OMM groups (**Figure 4.4**). Yet, relative abundances of these microbiota did not correlate with urine steroids.

The urinary metabolome gives a snapshot of the metabolic state of the preterm infant at one month of age. In addition, through the detection of bacterial (co-)metabolites it might mirror the activity of the gut-microbiota. To decipher the origin of observed metabolites, we applied a network-based approach. In our study, the majority of detected metabolites could be produced by both, host and gut-microbiota and none of the detected metabolites was exclusively assigned to bacteria. Pathway enrichment analysis of KEGG pathways in detected compounds indicates that alterations in the steroid hormone biosynthesis pathway are not related to bacterial metabolism (adjusted *p*-value = 1), but significantly affected by human metabolism (adjusted *p*-value = 5 x 10^{-4}). This supports the hypothesis that changes between steroid levels in DHM and OMM might cause these changes observed in preterm infants. However, pyrimidine metabolism, the second pathway altered in the urinary metabolome of preterm infants, is significantly affected by both, bacterial and host metabolism (adjusted *p*-values of 7 x 10^{-8} and 5 x 10^{-4}, respectively) and hence, the metabolites of this pathway seem to be strongly influenced by the activity of the gut-microbiome. Pyrimidine metabolism could be the link between ingestion of OMM and improved

neurodevelopmental outcome at later stages, as it is tightly related to brain growth and metabolism. Cytidine and uridine act as precursors of the cytidine triphosphate used in the biosynthetic pathway of phosphatidylcholine and phosphatidylethanolamine via the Kennedy cycle [176] Brain growth and exponential establishment of synaptic connections are essential in the neonatal period.

The study has some limitations. This is a pilot study and hence, the number of subjects included is limited requiring the validation of the reported findings in follow-up studies. However, the aim here was to test the feasibility of the study design and to provide a knowledge base for future studies. DHM samples were different from OMM in terms of GA as well as collection time. However, this resembles the characteristics of HM provided by HM banks. Furthermore, the metabolism of HM-specific compounds is not well-covered in KEGG pathways. Finally, AMON does not account for co-metabolism between the host and microbes which might be a limitation when combined with metabolomics data from urine samples, as many metabolites need to be transformed by human metabolism prior to their excretion.

In summary, this is, to the best of our knowledge, the first time that the interplay between DHM, preterm infant and the gut-microbiome has been comprehensively assessed. The results obtained indicated differences between DHM from a HM bank and OMM samples from mothers of preterm infants related to carbohydrate metabolism. Preterm infants exclusively receiving either DHM or OMM showed a clear alteration in urinary steroid hormone levels and the alteration of the pyrimidine metabolism between groups was detected. Our data help to understand the origin of the observed changes generating new hypothesis: i) steroid hormones present in HM have a significant

influence in the activity of the steroid hormone biosynthesis pathway in preterm infants, either directly or through the modification of gut-microbiota; ii) the pyrimidine metabolism is modulated in preterm infants by the activity of gut-microbiota. Future studies making use of targeted approaches for the validation of the changes highlighted by pathway analysis are required, specifically focusing on the quantification of metabolites from the steroid hormone biosynthesis pathway in urine and HM and assessment of carbohydrate metabolism in HM. In addition, short- and long-term consequences of the observed changes in the neonatal period need to be evaluated. Finally, the findings of this study are of practical relevance as they might trigger alternative strategies for improving neonatal nutrition based on modifying the properties of DHM through the changes of guideline for DHM collection, targeted fortification and HM processing and storage.

Section III. Monitoring of metabolic switch in neonates with congenital heart disease after surgery

Chapter 5. A reductive metabolic switch protects infants with congenital heart defect undergoing atrial septostomy against oxidative stress.

5.1 Abstract

Transposition of the great arteries (TGA) is one of the most common cyanotic congenital heart diseases requiring neonatal surgical intervention. Parallel circulations that result in impaired cerebral oxygen delivery already in utero may lead to brain damage and long-term neurodevelopmental delay. Balloon atrial septostomy (BAS) is often employed to mix deoxygenated and oxygenated blood and the atrial level. However, BAS causes a sudden increase in arterial blood oxygenation and oxidative stress. We studied changes in oxygen saturation as well as metabolic profiles of plasma samples from nine newborns infants suffering from TGA before and until 48 h after undergoing BAS. The plasma metabolome clearly changed over time and alterations of four metabolic pathways, including the pentose phosphate pathway, were linked to changes in the cerebral tissue oxygen extraction. In contrast, no changes in levels of lipid peroxidation biomarkers over time were observed. These observations suggest that metabolic adaptations buffer the free radical burst triggered by re-oxygenation, thereby voiding structural damage at the macromolecular level. This study enhances our understanding of the complex response of infants with TGA to changes in oxygenation induced by BAS.

5.2 Introduction

Transposition of the great arteries (TGA) is one of the most common cyanotic congenital heart diseases with an incidence of 0.3 per 1000 live births that requires surgical intervention in the neonatal period [177]. In hearts with TGA, systemic and pulmonary circulations run in parallel rather than in serial. This results in significant hypoxemia clinically reflected as central cyanosis. Survival after birth is only possible if there is an adequate blood mixing between the two circulations. Most hypoxemic neonates with TGA benefit from early institution of prostaglandin E1 (PGE) for ductal patency. If hypoxemia persist despite prostaglandin E1 (PGE1) infusion, balloon atrial septostomy (BAS) is needed to increase systemic oxygenation by improving the mixing to deoxygenated and oxygenated blood at the atrial level. After stabilization, arterial switch operation (ASO) is low in the current era, however, morbidity is high nd neonates with TGA are at risk of impaired neurodevelopmental outcome. Thus, long-term follow-up demonstrates that 30-50% of school-aged children with TGA show some form of developmental delay [178].

The underlying mechanism of developmental delay is thought to be multifactorial and include prenatal and postanal factors. Hence, fetal hypoxia due to decreased oxygen delivery has been implicated in the abnormal brain development seen in newborns with TGA [179]. Moreover, reduced fetal cerebral oxygen consumption in TGA neonates has been associated with smaller head circumference and brain volume than those of normal neonates [180]. In addition, postnatal factors such as postnatal chronic hypoxemia, open-heart surgery with deep hypothermic circulatory arrest, and balloon atrial septostomy (BAS)

gave also been considered responsible for brain injury [181]. BAS improves mixing of systemic and pulmonary circulation and leads to an immediate increase in arterial oxygen content. However, BAS does not allow for full normalization of systemic oxygenation preoperatively. Very little is known about the direct effect of BAS in the neonatal brain, on cerebral oxygenation and oxygen metabolism [182], and whether the rapid increase of oxygen delivery results in brain reperfusion injury in neonates with TGA [183,184].

In mammals, aerobic metabolism with the concourse of oxygen is the most efficient biological means to supply energy required to sustain life. Under anaerobic conditions, pyruvate is converted into L-lactate. Anaerobic metabolism is by far less energy efficient than aerobic metabolism. Hence, in the absence of oxygen, the energy consumed by neurons rapidly leads to an exhaustion of the ATP reserves [23]. Due to the high metabolic rate of the brain, survival is almost exclusively dependent on the energy generated by aerobic glycolysis. The lack of oxygen stores and the reduced glycolytic capacity compel brain tissue to rely entirely on an continuous supply of oxygen and glucose provided by cerebral perfusion. Under these circumstances, acutely or chronically reduced oxygen availability due to environmental or pathophysiological cause inevitably leads to alterations of the brain structure and function [185].

Incomplete reduction of oxygen leads to the formation of reactive oxygen species (ROS), some of which are free radicals (e.g., anion superoxide and hydroxyl radicals). These extremely short half-life metabolites are capable of damaging nearby cellular components such as proteins, lipids, carbohydrates or DNA [186]. Both, acute and chronic hypoxia, enhance the formation of ROS through mitochondrial

uncoupling provoking oxidative stress (OS) [187]. In addition, during reoxygenation, the increased availability of oxygen causes the activation of oxidases such as nicotinamide adenine dinucleotide phosphate (NADPH) oxidase or xanthine oxidase, further increasing the formation of anion superoxide and nitric oxide [186]. Neurons are highly vulnerable to the deleterious effects of ROS generated during acute hypoxia and/or hyperoxia. ROS trigger specific pathways that lead to apoptosis, necrosis, and inflammation of vulnerable areas of the brain causing long term neurodevelopmental, motor, and cognitive impairment [185].

Blood lactate has been largely employed as a surrogate for tissue hypoxia and/or ischemia. However, exclusive monitoring of serum lactate has neither provided sufficient insight into the magnitude of brain hypoxia nor conferred reliable prognostic information regarding long-term neurodevelopmental impairment [49,89]. More recently, comprehensible metabolic fingerprinting characterized by the simultaneous measurement of hundreds of metabolites from biological matrices has been increasingly employed for identifying predictive biomarkers or patient stratification [188].

In the present study we focused on the metabolic switch in infants with TGA after BAS. We performed serial analysis of lipid peroxidation byproducts as well as the plasma metabolome before and after BAS. This allowed us to study the impact of the rapid change in arterial blood oxygen content switching from a chronic hypoxic environment to an almost normoxic one, thus giving an insight into the dynamic hypoxia-related changes on the phenotypic level.

5.3 Material and methods

5.3.1 Study population

We performed a prospective single center study to evaluate changes in cerebral oxygenation and metabolism before and for a period of 96 h following BAS in neonates with TGA. All patients with TGA admitted to Children´s Hospital, Helsinki University Hospital, between 1 January 2015, and 1 June 2017, were considered for inclusion in the present study. Inclusion criteria included term gestational age and simple TGA without any significant associated heart defects (i.e., patients with ventricular septal defect were excluded). Reasons for failure to enroll included unavailability of parents for the consent process or parental refusal.

The study protocol was approved by the Ethics Committee of Helsinki University Hospital. All procedures were performed in accordance with relevant guidelines and regulations and written permission by signing an informed consent form or phone permission in urgent cases was obtained from legal representatives.

Data collected included peripheral oxygen saturation (SpO_2), mixed venous saturation, regional cerebral tissue oxygen saturation ($rcSO_2$) measured by near infrared spectroscopy (NIRS), heart rate, blood pressure, blood lactate levels, pH, base excess, and hemoglobin prior to and following BAS. Blood samples for metabolic analysis were collected from arterial cannula 5 min prior to and 5 min, 6 h, 24 h, 48 h, 72 h, and 96 h following BAS. At each timepoint, 1 mL of blood was collected into lithium heparin tubes, centrifuged, aliquoted, and store at -70 °C. Differences during $rcSO_2$, preductal peripheral oxygen saturation, fractional tissue oxygen extraction (FTOE), and cerebral oxygen

extraction (CEO_2) were analyzed prior to and following BAS. Cerebral oxygen extraction was estimated from the difference of SaO_2 and ScO_2 as ScO_2 is close to venous SO_2. FTOE was calculated as CEO_2/SaO_2. Information regarding medications used prior to and following BAS was collected from electronic patient records.

5.3.2 Analytical procedures

5.3.2.1 Lipid peroxidation biomarkers

Biomarkers of lipid peroxidation were analyzed in 63 plasma samples following previously published procedures [20,189]. Deuterated internal standards (IS) ($PGF_{2\alpha}$-d4 and 15-F_{2t}-Isoprostane-d4) were purchased from Cayman Chemical Company (Ann Arbor, MI, USA). Form sample processing, 100 µL of plasma were thawed on ice and 100 µL of KOH solution at 15% (*w/v*) were added. The mixture was incubated at 40 °C for 30 min. A volume of 3µL of aqueous IS solution (20 µM) was added to hydrolyzed samples and diluted to 900 µL with H_2O:MeOH (85:15, 2.8% *v/v* HCOOH, pH 3) and 500 mL heptane. Finally, cartridges were dried with room air and the compounds of interest were eluted with 4 x 100 µL ethyl acetate. The eluate was evaporated using a miVac centrifugal vacuum concentrator (Genevac LTD, Ipswich, UK) and dissolved in 60 µL H_2O (0.1% *v/v* HCOOH, pH 3): CH_3OH (85:15 *v/v*).

An Acquity-Xevo TQS system from Waters (Milford, MA, USA) operating in negative electrospray ionization (ESI^-) mode was employed for UPLC-MS/MS analysis. A waters BEH C_{18} column (2.1 mm × 100 mm, 1.7 µm, Waters, Wexford, Ireland) was used. Flow rate, column temperature, and injection volume were set at 450 µL min^{-1}, 45 °C, and

9 μL, respectively. A binary mobile phase H_2O (0.1% *v/v* HCOOH):CH_3CN (0.1% *v/v* HCOOH) gradient with a total runtime of 7.0 min was run as follows: from 0.0 to 0.1 min 15% *v/v* CH_3CN (0.1% *v/v* HCOOH) (mobile phase channel B); from 0.1 to 5. Min % B increased up to 40%; from 5.0 to 6.0 min %B followed by the return to initial conditions (i.e., 15%B) between 6.15 and 6.25 min; conditions were maintained for 0.75 min for system re-equilibration. ESI interface conditions were selected as follows: capillary voltage was set to 2.9 kW; source and desolvation temperatures were 150 °C and 395 °C, respectively: and nitrogen cone and desolvation gas flows were 150 and 800 L h^{-1}, respectively. Parameters selected for determination of lipid peroxidation biomarkers are shown in **Table 5.1**.

Table 5.1. Mass spectrometric parameters and chromatographic windows employed for the lipid peroxidation biomarkers.

Analyte	RT [min]	Parent ion (*m/z*)	Daughter ion (*m/z*)	CE (eV)	Cone Voltage (V)
Total IsoPs [p.d.u.]	4.3-6.6	353.20	115.00	30	35
Total Dihomo-IsoPs [p.d.u.]	5.0-6.8	381.00	143.00	20	20
Total Diohomo-IsoFs [p.d.u.]	3.5-6.5	397.00	155.00	24	35
Total NeuroFs [p.d.u.]	2.70-6.50	393.00	193.00	20	35
Total IsoFs [p.d.u.]	2.1-6.60	369.20	115.00	20	45
Total NeuroPs [p.d.u.]	2.30-6.50	377.00	101.00	20	35

Note: IsoPs Isoprostans. IsoFs Isofurans. NeuroFs Neurofurans. NeuroPs Neuroprostanes. RT stands of Retention times. CE stands of collision energy.

5.3.2.2 Untargeted Ultra-Performance Liquid Chromatography coupled to time-of-flight Mass Spectrometry (UPLC-TOFMS) metabolomics analysis

Plasma samples were thawed on ice and homogenized on a Vortex mixer. 75 µL of cold acetonitrile were added to 25 µL of plasma, homogenized and kept on ice during 15 min followed by centrifugation at 16000 × *g* during 15 min at 4 °C. 80 µL of supernatant were collected and transferred to dryness on a miVac centrifugal vaccum concentrator (Genevac LTD, Ipswich, UK) at room temperature and dissolved in 60 µL of an internal standard (IS) solution containing betaine-D_{11}, methionine-D_3, hypoxanthine-D_3, cytine-D_4, tyrosine-D_2,

prostaglandin$F_{2\alpha}$-D_4, uridine-$C^{13}N^{15}$, reserpine, phenylalanine-D_5, leucine enkephalin, caffeine-D_9, and tryptophane-D_5 with purities ≥99% at a concentration of 1.5 µM in H_2O:CH_3CN (0.1% HCOOH) (95:% *v/v*).

A QC sample was prepared by mixing 5 µL of each plasma sample and a total of three aliquots were processed alongside with the plasma samples applying the same procedures. A blank extract was prepared by using a heparinized syringe and 0.5 mL of ultrapure H_2O and processed as described for plasma samples.

For chromatographic separations, an Agilent Technologies (Santa Clara, CA, USA) 1290 Infinity UPLC chromatograph equipped with a UPLC ACQUITY BEH C18 column (2.1 mm × 100 mm, 1.7 µm, Waters, Wexford, Ireland) was employed. Autosampler and column temperatures were set to 4 and 40 °C, respectively. A flow rate of 400 µL min^{-1} and an injection volume of 4µL were used. Separations were carried out keeping 98% of mobile phase A (H_2O, 0.1% *v/v* HCOOH) for 0.5 min, followed a lineal linear gradient from 2 to 20% of mobile phase B (CH_3CN, 0.1% v/v HCOOH) in 3.5 min and from 20 to 95% B in 4 min. Conditions of 95% B were maintained for 1 min and a 0.25 min gradient was used to return to the initial conditions, which were held until reaching 8.5 min.

Full-scan MS data were acquired between 100 and 1700 m/z with a scan frequency of 6 Hz (1274 transients/spectrum) on an iFunnel quadrupole time-of-flight (QTOF) Agilent 6550 spectrometer operating in the TOF MS mode. The following electrospray ionization settings were used: gas T, 200 °C; drying gas, 14 L min^{-1}; nebulizer, 37 psig; sheath gas T, 350 °C; sheath gas flow, 11 L min^{-1}. A mass reference standard used for automatic MS spectra re-calibration during analysis was introduced into the source via a reference sprayer valve using the

149.02332 (background contaminant), 121.050873 (purine), and 922.009798 (HP-0921) *m/z*. MassHunter workstation from Agilent was employed for data acquisition and manual integration of ISs.

Before launching the analytical sequence, system suitability was checked employing a standard mixture containing ISs. The analytical system was conditioned by eight repeated injections of the QC at the beginning of the batch. Data acquired during system conditioning were discarded from data analysis. A total of 63 plasma sample extracts were analyzed in randomized order in a single analytical batch using the positive electrospray (ESI^+) mode. QC samples were analyzed every 6^{th} sample and at the beginning and end of the batch for assessment and correction of instrumental performance [69] The blank extract was injected a total of two times (once during system conditioning and once at the end of the batch) and used for data clean-up with the aim of identifying signals from other than biological origin. Subsequently, sample analysis was carried out in ESI^- mode repeating the same protocol described for the ESI^+ mode.

ProteoWizard [155] (http://proteowizard.sourceforge.net) software was used for conversion of raw UPLC-TOFMS data into centroid mzXML format. A peak table was extracted using XCMS (version 3.4.2) [93,125,156] (https://bioconductor.org/packages/release/bioc/html/xcms.html) running in R (version 3.5). For peak detection, the centWave method was used as follows: ppm = 20, peakwidth = (4 and 25), snthresh = 10. For the resolution of overlapping peaks, a minimum m/z difference of 7.5 mDa was selected. For each extracted feature, the 'wMean' function was used for calculating intensity-weighted *m/z* values and peak limits used for integration were found through descent on the Mexican hat filtered

data. For peak grouping the "nearest" method with mzVsRT = 1 and retention time (RT) and *m/z* tolerances of 6 s and 10 mDa, respectively, was used. Missing peak data was filled applying the fillPeaks method with the default parameters. A total of 18582 and 13479 features were initially detected after peak detection, integration, chromatographic deconvolution, and alignment in ESI^+ and ESI^- modes, respectively. The CAMERA [73] package was used for identifying peak groups and annotation of isotopes and adducts using the following settings: sigma=6, perfwhm=0.5, ppm = 20.

Peak integration accuracy was checked by comparing the generated peak table with areas obtained from manual integration of ISs. Peak intensities of ISs and QC samples were used for assessing the instrumental response during data acquisition throughout the batch as described elsewhere [92,190]. The Quality Control-Support Vector Regression (QC-SVR) algorithm [96] and the LIBSVM library [75] were used for correcting intra-batch variation using an ε–range of 2.5 to 7.5 and a γ-range of 1 to 10^5. C was defined for each feature as the median value in QCs. Then, features detected in blanks (< 5 x signal of the blank) and those with an RSD% in QC samples ≥20% were excluded. The final peak tables contained 3886 and 5600 features for ESI^+ and ESI^-, respectively, and were searched for molecular ion peaks of drugs and known drug metabolites that have been administered to infants, their isotope as well as Na and K adducts (m/z tolerance: 10 mDa). Metabolic features that were identified as drugs or their metabolites, isotopes and adducts were excluded from further data analysis.

MATLAB 2019b inbuilt functions as well as in-house written scripts (available from the authors upon reasonable request) and the PLS Toolbox 8.0 from Eigenvector Research Inc. (Wenatchee, USA) were

used for Principal Component Analysis (PCA) and the computation of Pearson correlations. For PCA, data sets generated in ESI^+ and ESI^- were concatenated. MetaboAnalyst (version 4.0) [78] was used for hierarchical clustering and the generation of heatmaps employing Euclidean distance and Ward's method (statistical analysis tool). Pathway analysis was carried out using MetaboAnalyst with the MS peaks to pathways tool (mass accuracy = 10 ppm, mummichog algorithm with top 10% peaks p-value cut-off) in the 4-column format (*m/z*, RT, ionization mode, p-value of Pearson correlation between metabolic features and FTOE) and the Kyoto Encyclopedia of Genes and Genomes (KEGG) pathway library (*Homo sapiens*). Metabolomics data are available on Zenodo (https://zenodo.org/record/4495124#.YBpwoC1DkWp).

The non-parametric Wilcoxon rank-sum test was used for assessing changes in levels of biomarkers of lipid peroxidation over time. *p*-values from Spearman correlations were used for clinical data, where appropriate.

5.4 Results

5.4.1 Clinical results

A total of 12 newborn infants fulfilled the study requirements. Out of these, one patient died, and two patients did not require BAS. The remaining 9 patients who underwent BAS, completed all analysis. Demographics and perinatal characteristics are detailed in **table 5.2.** Six patients (50%) had prenatal diagnosis and nine patients (75%) underwent BAS due to low preductal saturation at the age 4.6 (±2.7) hours. There was one early death prior to BAS. The patient was transferred from

another central hospital with prostaglandin infusion but had extremely low preductal saturations (<30%), severe lactate acidosis, and was in pulseless electrical activity at the time of admission and care was withdrawn. **Figure 5.1** describes evolving SpO_2, $rcSO_2$, FTOE, and CEO_2 before and after BAS. In the nine patients included in the study, the lowest preductal peripheral oxygen saturation (SpO_2) at admission had a median of 64.5% (range 39.0 – 92.0). Preductal SpO_2 increased from a median of 85.6% (range 62.0 – 90.6) before BAS to 89.1% (range 81.8 – 93-5) 6 h following BAS and 90.0% (range 85.2 – 93.6) 24 h following BAS. $rcSO_2$ at the same time points were 50.0% (range 35.0 – 70.0), 52.8% (range 36.4 – 72.5), 63% (range 48.2 – 74.1), and 69.2 (range 58.8 – 80.8), respectively. $rcSO_2$ correlated strongly with simultaneously measured SpO_2 (Spearman´s r = 0.89, *p*-value < 0.001). CEO_2 increased after BAS (27.2 – 28.1) but both, CEO_2 and FTOE, decreased 24 h following BAS (See **Figure 5.1**). Complete recovery of cerebral oxygen saturation did not occur until 24 h after BAS.

Table 5.2. Patients' demographics and timing of postnatal clinical and analytical interventions

Patients' demographics	**All patients**	**BAS patients**
Patients recruited, N (%)	12 (100)	9 (100)
Gender, N (%)		
- Male	10 (83)	8 (89)
- Female	2 (17)	1 (11)
Balloon atrial septostomy, N (%)	9 (75)	9 (100)
Expired, N (%)	1 (8.3)	0 (0)
Prenatal diagnosis, N (%)	6 (50)	4 (44)
Gestational age, weeks (median, range)	39.5 (37.0-41.3)	39.9 (38.4-41.3)
Birth weight, kg (median, range)	3.4 (2.0-4.0)	3.5 (3.1-4.0)
Postnatal age, hours (median, range)		
- At the time of the first measured peripheral saturation (h)	1.7 (0.5-13.2)	2.3 (0.5-6.7)
- At time of BAS (h)		3.2 (2.0-9.1)
Saturation % (median, range)		
- First peripheral saturation (SpO_2)	79 (51-91)	77 (56-88)
- Lowest peripheral saturation (SpO_2)	65 (39-86)	65 (39-86)
- First regional cerebral oxygen saturation ($rcSO_2$)	58 (37-79)	53 (37-79)
- 5-min post septostomy peripheral saturation (SpO_2)	86 (62-91)	86 (62-91)
Blood lactate mmol/L (median, range)		
- Before BAS	3.2 (1.3-4.9)	3.6 (1.3-4.9)
- 5-min after BAS	2.7 (1.4-5.0)	3.3 (1.4-5.0)

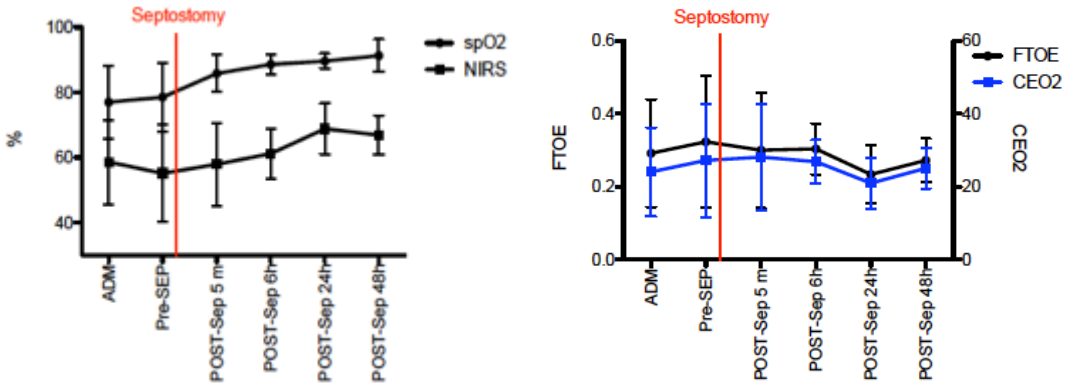

Figure 5.1. Evolution of SpO_2, $rcSO_2$ (left), FTOE and CEO_2 levels (right) before and after BAS. Black and blue lines and error bars are median and 25th and 75th percentile, respectively.

5.4.2 Lipid Peroxidation Biomarkers

Total di-homo-isoprostanes, di-homo-isofurans, and isoprostanes were excluded as these parameters were found <LOQ in all study samples. **Figure 5.2** depicts relative responses of total neurofurans, isofurans, and neuroprostanes obtained over time. No significative changes over time were detectable (Wilcoxon rank sum test, *p*-values >0.05). Furthermore, no strong (Pearson correlation coefficients > |0.5|) and significant correlations were found between isoprostanoid levels and FTOE.

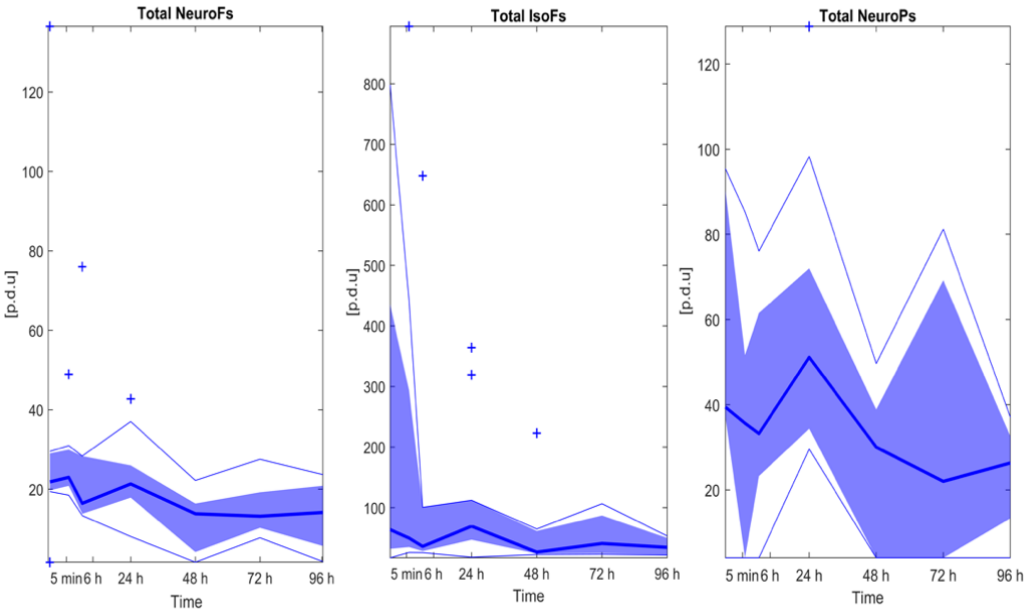

Figure 5.2. Isoprostanoid levels over time. Note: Bold blue lines correspond to median values, blue areas correspond to the interquartile range (1st and 3rd quartile), thin blue lines correspond to minimum and maximum values and + correspond to outliers. Note: NeuroFs = neurofurans; IsoFs = isofurans; NeuroPs =neuroprostanes.

5.4.3 Effect of time on the plasma metabolome

Figure 5.3 shows a PCA score plot of the plasma metabolic fingerprint of infants before BAS and at different time points after BAS. The scores plot from PC1 vs. PC2 illustrates the impact of the sampling time point on the plasma metabolome. For most patients, a time-dependent shift towards lower scores on PC1 with increasing time after septostomy was observed. Even though the applied data analysis workflow included the removal of drug metabolites, this effect might, at least partially, be related to the employed medication and the procedure itself. Also, a high inter-individual variation can be noted.

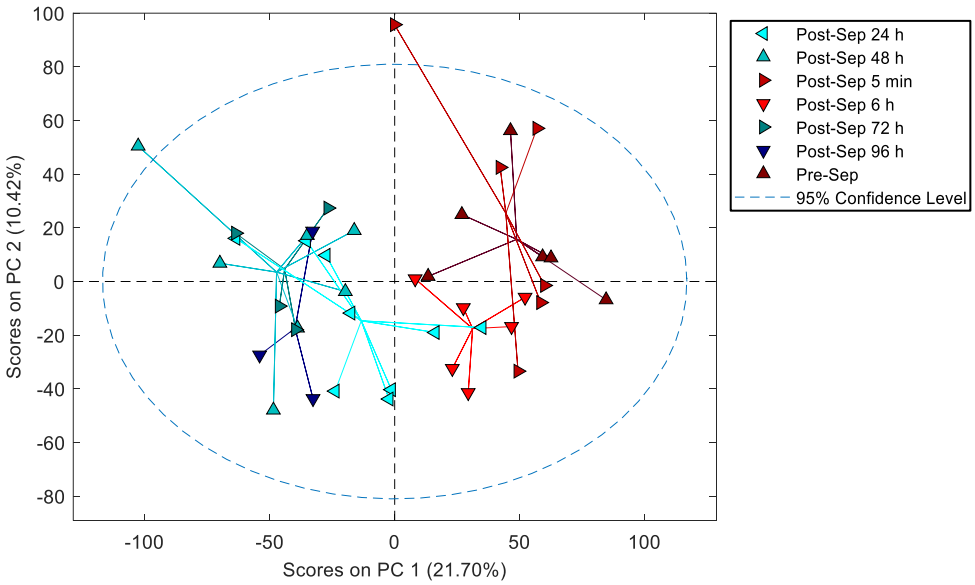

Figure 5.3. PCA results of samples collected before and at different time points after BAS. Note: sep stands for septostomy.

5.4.4 Correlation of metabolic features with FTOE

FTOE reflects the balance between oxygen supply and consumption in tissue and can, therefore, be used as an indicator of inadequate tissue perfusion and oxygenation. We specifically focused on

modelling the effects of metabolic changes in the plasma metabolome associated with FTOE. Pearson correlations for each metabolic feature with FTOE before and at different time points post-septostomy were calculated as shown in **figure 5.4.** A panel of features with a significant association with FTOE (i.e., *p*-values from Pearson correlation < 0.05) was identified including both, positively (red dots, correlation coefficient > 0.5) and negatively (blue dots, correlation coefficient < -0.5) correlated features. Two distinct cluster can be observed, with plasma fingerprints from samples collected before and 4 min as well as 6 h after BAS belonging to one cluster, and samples collected 24-96 h after BAS belonging to a second cluster. Most metabolic features in **Figure 5.5** showed a decreasing trend in relative intensities when comparing cluster one to cluster two. Pathway analysis detected four significantly altered pathways associated with changing FTOE in infants with TGA undergoing BAS (See **Table 5.3**).

Table 5.3. Pathway alterations associated with changing FTOE in infants with TGA undergoing atrial septostomy.

Pathway name	**Compound code (KEGG)**	**Pathway ID**	**# hits**	**# hits**	**sigP-value**
Pentose phosphate pathway	C01801; C00672; C00121; C00121; C00257; C00257; C00258	map00030	7	7	0.00002
Pentose and glucuronate interconversions	C01068; C00181; C00259; C00310; C00312; C00379; C00532; C00379; C00532; C00379; C00379; C00532; C00257; C00257; C00029; C00052; C00191; C00618; C02266	map00040	11	7	0.003
Ascorbate and aldarate metabolism	C00137; C00029; C02670; C00191; C00800	map00053	8	5	0.013
Inositol phosphate metabolism	C00137; C00222; C00191	map00562	4	3	0.03

Note: Mummichog input: 10 ppm; p-value cut-off: 10%; KEGG database.

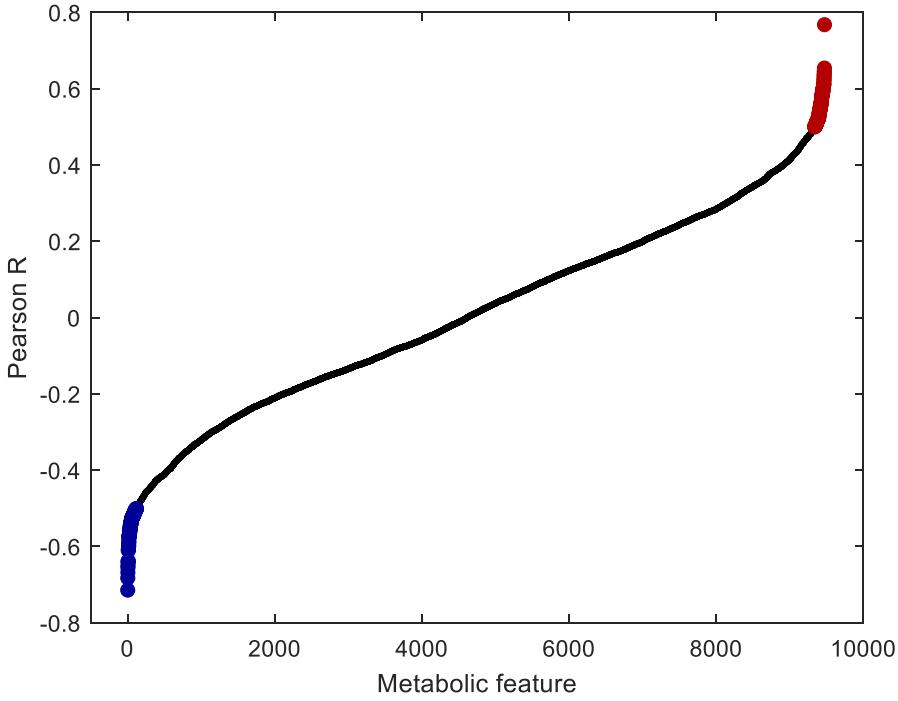

Figure 5.4. Pearson correlation coefficients between metabolic features and FTOE. Blue: features with p-values <0.05 and correlation coefficients < -0.5; red: features with p-values < 0.05 and correlation coefficients > 0.5; black: all remaining features.

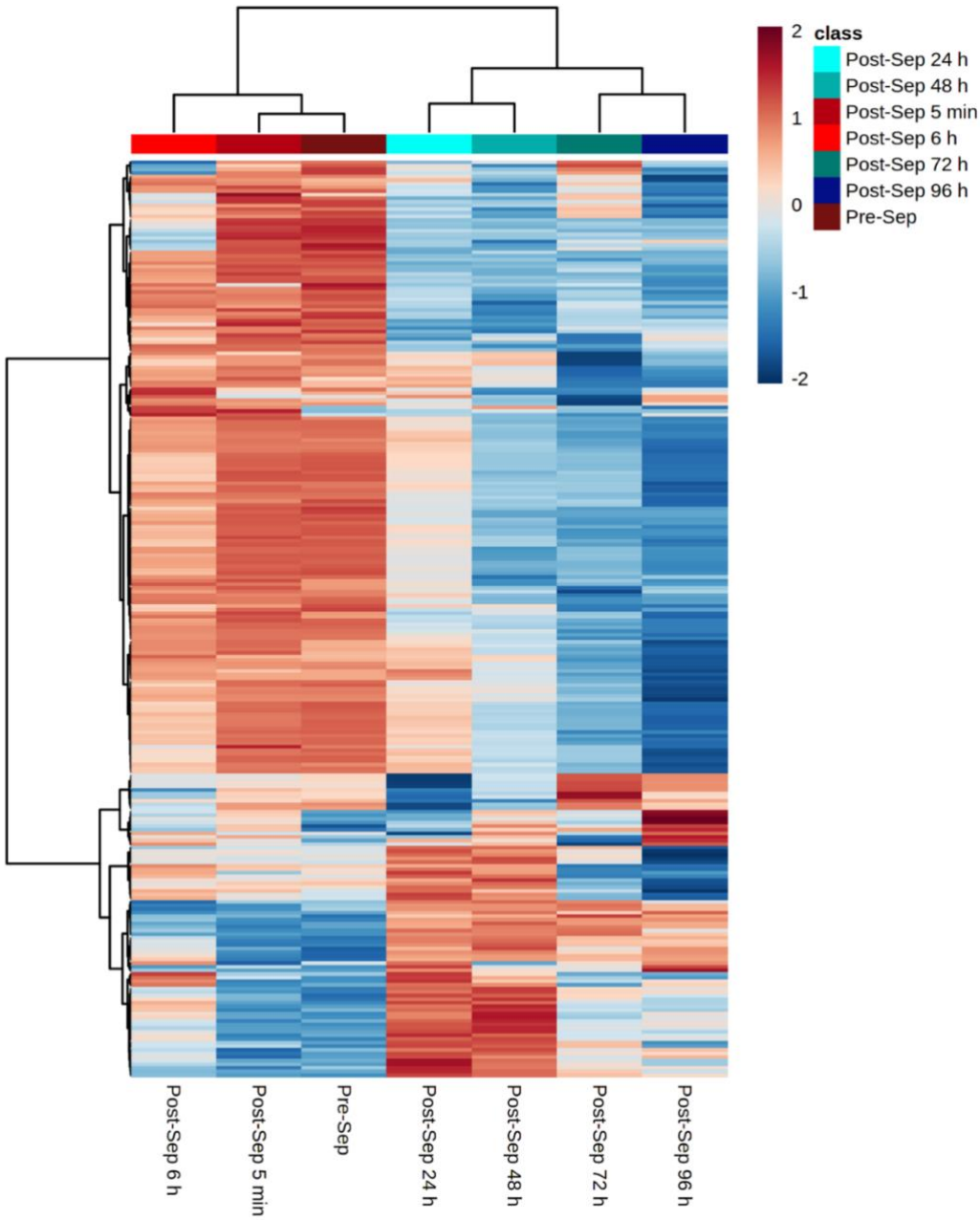

Figure 5.5. Relative intensities of metabolic features that correlate (i.e.: p-value < 0.05 and |correlation coefficients| > 0.5) with FTOE. Note: color represents autoscaled relative intensities; blue – metabolite levels lower than average, and red – metabolite levels higher than average. *P*-values from Pearson correlation were computed and significantly correlating metabolites are shown; heatmap calculated using Euclidean distance and Ward algorithm.

5.5 Discussion

TGA is a severe congenital cardiac malformation that causes hypoxemia during fetal life and in the newborn period [177]. TGA has deleterious consequences on growth and development due to a deficient tissue oxygenation that especially affects the Central Nervous System [178,180]. We report the first metabolomic study involving neonates with TGA who underwent BAS. We performed a study on oxidative stress biomarkers as well as a comprehensive qualitative characterization of plasma metabolites before and after BAS.

BAS in TGA patients caused a rapid switch from hypoxia to normoxia. Preductal peripheral pulse oximetry saturation as $rcSCO_2$ increased rapidly after BAS while simultaneously FTOE decreased. As a result, brain oxygenation substantially improved (See **Figure 5.1**). Thereafter, changes in oxygenation plateaued. Complete recovery of cerebral oxygen saturation occurred only 24 h after BAS. A gradual change was observed in the metabolome, accordingly (See **Figure 5.3**). The provision of energy to satisfy metabolic demands of the brain exclusively dependent on aerobic metabolism and oxygen deprivation caused by hypoxia and/or ischemia for just a few minutes may cause severe brain damage. Mitochondrial ROS production is regulated through tissue succinate levels and the activity of oxidases (NADPH oxidase, xanthine oxidase) [123]. During hypoxia and ulterior reoxygenation both, succinate levels and oxidase activation, generate a burst of ROS that directly damage tissue structure and function [123]. Moreover, the pro-oxidant imbalance provokes the activation of the caspase pathway and of transcription factor NF*k*B. Subsequently, programmed cell death and inflammation are triggered for hours, days,

or even weeks. Consequently, there is an amplification of the initial area of brain injury that contributes to aggravate long-term neurological prognosis [191–193].

Isoprostanes and isofurans, but especially neuroprostanes and neurofurans are highly sensitive to oxidative stress related brain damage [194]. However, we did not observe change in those compounds after BAS (see **Figure 5.2**). The attenuation of the expected pro-oxidant status after BAS suggest a pattern of metabolomic changes with a reducing profile. In this regard, post-Bas untargeted metabolomics evidenced a significant enhancement in the activity of the pentose phosphate pathway (PPP). The central role of the PPP has attracted more attention in recent years. Emerging evidence suggests that the PPP is tightly and meticulously controlled in cells and that its abnormal regulation leads to uncontrolled redox homeostasis [195]. The PPP has shown great versatility for *de novo* nucleotide biosynthesis via ribose-5-phosphate and adopts a simultaneous organization with glycolysis to produce NADPH. Nucleotide biosynthesis possibly participates in DNA damage repair. Our pathway analysis data revealed changes in the relative concentration of 2-deoxy-Dribose 1-phosphate (C00672), a precursor of ribose-4-phosphate, and substrate of phosphoribosyl pyrophosphate (PRPP). This substrate is an essential compound of purine, pyridine, and histidine synthesis. NADPH is a cofactor of glutathione reductase, an essential enzyme in the glutathione redox cycle that contributes to the reconversion of GSSG into GSH thus contributing to the normalization of the GSH/GSSG pair and the removal of ROS [196,197]. In this context, the pathway analysis data suggest an alteration of gluconic acid (C00257). The phosphorylation of this compounds generates 6-phosphogluconate, an essential substrate in the oxidative branch of the

PPP. Furthermore, alterations of other compounds such as ribitol-5-phosphate (C01068) and 2-deoxy-D-ribose (C00672) contribute as substrates for key PPP compounds. Indeed, the activity of the PPP is rapidly re-routed when cells are exposed to an oxidative burst. This response is exquisitely adjusted by cooperating of metabolic and gene regulatory mechanisms. Metabolic changes imply the inactivation of glycolytic enzymes which occurs immediately after the oxidant aggression thus blocking glycolysis [198]. Thereafter, the transcriptional response takes over and maintains higher PPP activity through up-regulation of enzymes and post-translational modifications including those which increase the activity of G6PDH [199]. Furthermore, to counteract mitochondrial ROS production under normal metabolic circumstances, but also during hypoxia or hypoxia-reoxygenation, steady NADPH production becomes essential as it represents the main electron donor for the generation of GSH that will provide electrons for the reduction of detrimental peroxides by glutathione peroxidase [195].

In addition, our results reveal the alteration of the pentose and glucuronate interconversion pathway, another key pathway in the homeostasis of metabolic pathways. The glucuronate pathway is an alternative pathway for the oxidative degradation of glucose without the production of ATP. Substrate compounds such as xylose (C00181), glucuronic acid (C00191), dehydrogulonate (C00618), xylonolactone (C002266), and ribitol-5-phosphate (C01068) were altered according to the reported pathway analysis data. Interestingly, in humans the synthesis of ascorbic acid is not feasible, therefore a substantial proportion of uridine diphosphate glucoronate (UDP-glucoronate) is converted into xylulose-5-phosphate which is further metabolized

through the PPP to fuel NADPH production and promote the preservation of a reduced environment [200].

Finally, pathway analysis also showed an alteration of ascorbate and aldarate and inositol phosphate metabolism. The ability of ascorbate to donate electrons enables it to act as a free radical scavenger and to reduce higher oxidation states of iron to Fe^{2+}. Ascorbic acid is an important antioxidant in plasma, where it consumes oxygen free oxidized form, dehydroascorbic acid. Intracellular dehydroascorbic acid is rapidly reduce to ascorbate by GAS in a direct chemical reaction, or indirectly with the concurrent action of glutaredoxin and thioredoxin reductases. Intracellular ascorbate can spare and possibly recycle, alpha distocopherol in the erythrocyte membrane. In turn, alpha tocopherol protects the cell membrane from lipid peroxidation. The ability of erythrocytes to recycle ascorbate, coupled with the ability of ascorbate to protect alpha tocopherol in the cell membrane and in lipoproteins, provides a potentially important mechanism for preventing lipid peroxidative damage secondary to hypoxia or hypoxia-reoxygenation events [201]

We acknowledge limitations of our study. First, the number of subjects included is limited and some of the blood samples during BAS were not collected. We would like to stress the stringent including criteria applied during patient recruitment and the low incidence of the condition. The present data provides evidence to justify large multi-center efforts for validating the current findings. Finally, we lack a control group of healthy infants for obvious ethical reasons.

5.6 Conclusion

In summary, this is a comprehensive metabolomic assessment of neonates with TGA. The results obtained suggest differences in oxygen supply and consumption in cerebral tissue during hypoxia and near-normoxia. The number of patients is limited, but the combined assessment of lipid peroxidation biomarkers and untargeted metabolomic screening of a cohort of infants with TGA undergoing BAS provides insightful information to understand the physiopathology of this complex disease. The metabolic switch after BAS causes oxidative stress. However, oxidative stress may at least be partially neutralized by the induction of different metabolic pathways but especially the PPP that supplies with reductive electrons. From a clinical point of view, although supplemental arterial oxygenation has limited effects on oxygenation in parallel circulation, our results suggest potential benefits of avoiding hyperoxia in patients undergoing BAS to prevent form attenuating the antioxidant effect inherent to the metabolic switch after septostomy.

6. Conclusions and Outlook

From the results obtained in the different metabolomic studies in the neonatal field, included in this Doctoral Thesis, it is possible to extract the following conclusions:

- The analysis of the alterations in the plasmatic metabolome of newborns with HIE undergoing TH allows to discriminate newborns with pathological MRI.
- The results suggest an association between HIE damage, established from MRI results, and longitudinal changes in the urinary metabolome of newborns. TH influence significantly in the newborn and the metabolomic patterns were monitored with moderate and severe HIE. These results open a new perspective for possible monitoring of patient in the NICU, as well as supporting early prediction of results.
- The quantitative determination of steroid biosynthesis compounds, tryptophan metabolic pathway, metabolite score, and energy related intermediates, with microRNA sequencing have revelated interesting physiological aspects and can help to delve into pathophysiology of the EHI.
- The composition of DHM differs to HM. The feeding of the DHM has a significant impact on the metabolomic phenotype and the microbiota of preterm infants. The results obtained can help to understand the origin of the changes observed depending on the metabolic pathway affected, although the short-and long-term implications must be evaluated with additional studies.

- The analysis of the metabolome of newborns with TGA allows to discriminate between the supply and consumption of oxygen at the cerebral level during hypoxia and normoxia. The combined evaluation of lipid peroxidation biomarkers and non-targeted metabolomics analysis provides valuable information to understand the pathophysiology of this complex disease.

Thus, the results and conclusions allow generating new line of research in neonatal field, including:

- The new information obtained through the results of the panel compounds, the identification of new altered metabolic pathways, as well as the sequencing of microRNAs in newborns with HIE, could be used in the future to improve early diagnostic capacity and selectively treat newborns according to their severity condition.
- The identification of new strategies for the optimization and personalization of neonatal nutrient through the modification of the composition of DHM, as well as possible changes in the guidelines for the collection, processing, and conservation of the DHM.
- The realization of a prospective observational study comparing possible situations of ductus arteriosus-dependent postnatal hypoxia together with comparison of the untargeted metabolomic profile before and after the establishment of prostaglandins for ductus arteriosus dilation. The information obtained might be valid for the evaluation of mechanism.

7. References

[1] C.W. Schmidt, Metabolomics: what's happening downstream of DNA, Environ Health Perspect. 112 (2004) A410-415. https://doi.org/10.1289/ehp.112-a410.

[2] S.G. Oliver, M.K. Winson, D.B. Kell, F. Baganz, Systematic functional analysis of the yeast genome, Trends Biotechnol. 16 (1998) 373–378. https://doi.org/10.1016/s0167-7799(98)01214-1.

[3] S.Y. Um, J.H. Park, M.W. Chung, K.H. Choi, H.J. Lee, 1H-Nuclear magnetic resonance-based metabolic profiling of nonsteroidal anti-inflammatory drug-induced adverse effects in rats, Journal of Pharmaceutical and Biomedical Analysis. 129 (2016) 492–501. https://doi.org/10.1016/j.jpba.2016.07.045.

[4] L. Lumata, C. Yang, M. Ragavan, N. Carpenter, R.J. DeBerardinis, M.E. Merritt, Chapter Two - Hyperpolarized 13C Magnetic Resonance and Its Use in Metabolic Assessment of Cultured Cells and Perfused Organs, in: C.M. Metallo (Ed.), Methods in Enzymology, Academic Press, 2015: pp. 73–106. https://doi.org/10.1016/bs.mie.2015.04.006.

[5] J.A. Kirwan, R.J.M. Weber, D.I. Broadhurst, M.R. Viant, Direct infusion mass spectrometry metabolomics dataset: a benchmark for data processing and quality control, Sci Data. 1 (2014) 140012. https://doi.org/10.1038/sdata.2014.12.

[6] M.R. Jacobs, E.F. Hilder, R.A. Shellie, Applications of resistive

heating in gas chromatography: A review, Analytica Chimica Acta. 803 (2013) 2–14. https://doi.org/10.1016/j.aca.2013.04.063.

[7] A. Albalat, H. Husi, J. Siwy, J.E. Nally, M. McLauglin, P.D. Eckersall, W. Mullen, Capillary electrophoresis interfaced with a mass spectrometer (CE-MS): technical considerations and applicability for biomarker studies in animals, Curr Protein Pept Sci. 15 (2014) 23–35. https://doi.org/10.2174/1389203715666140221123920.

[8] J.E. Adaway, B.G. Keevil, L.J. Owen, Liquid chromatography tandem mass spectrometry in the clinical laboratory, Ann Clin Biochem. 52 (2015) 18–38. https://doi.org/10.1177/0004563214557678.

[9] N. Glassbrook, C. Beecher, J. Ryals, Metabolic profiling on the right path, Nat Biotechnol. 18 (2000) 1142–1143. https://doi.org/10.1038/81116.

[10] N. Zamboni, A. Saghatelian, G.J. Patti, Defining the Metabolome: Size, Flux, and Regulation, Molecular Cell. 58 (2015) 699–706. https://doi.org/10.1016/j.molcel.2015.04.021.

[11] K. Cho, N.G. Mahieu, S.L. Johnson, G.J. Patti, After the feature presentation: technologies bridging untargeted metabolomics and biology, Current Opinion in Biotechnology. 28 (2014) 143–148. https://doi.org/10.1016/j.copbio.2014.04.006.

[12] R. Goodacre, Metabolomics of a superorganism, J Nutr. 137

(2007) 259S-266S. https://doi.org/10.1093/jn/137.1.259S.

[13] H.J. Issaq, Q.N. Van, T.J. Waybright, G.M. Muschik, T.D. Veenstra, Analytical and statistical approaches to metabolomics research, Journal of Separation Science. 32 (2009) 2183–2199. https://doi.org/10.1002/jssc.200900152.

[14] K. Saito, F. Matsuda, Metabolomics for Functional Genomics, Systems Biology, and Biotechnology, Annual Review of Plant Biology. 61 (2010) 463–489. https://doi.org/10.1146/annurev.arplant.043008.092035.

[15] X. Zhang, Y. Yap, D. Wei, G. Chen, F. Chen, Novel omics technologies in nutrition research, Biotechnology Advances. 26 (2008) 169–176. https://doi.org/10.1016/j.biotechadv.2007.11.002.

[16] E.J. Song, S.Md.E. Babar, E. Oh, Md.N. Hasan, H.-M. Hong, Y.S. Yoo, CE at the omics level: Towards systems biology – An update, ELECTROPHORESIS. 29 (2008) 129–142. https://doi.org/10.1002/elps.200700467.

[17] K. Saliminejad, H.R. Khorram Khorshid, S. Soleymani Fard, S.H. Ghaffari, An overview of microRNAs: Biology, functions, therapeutics, and analysis methods, J Cell Physiol. 234 (2019) 5451–5465. https://doi.org/10.1002/jcp.27486.

[18] M. Climent, G. Viggiani, Y.-W. Chen, G. Coulis, A. Castaldi, MicroRNA and ROS Crosstalk in Cardiac and Pulmonary Diseases, Int

J Mol Sci. 21 (2020) E4370. https://doi.org/10.3390/ijms21124370.

[19] Y. Xiao, J. Zhao, J.P. Tuazon, C.V. Borlongan, G. Yu, MicroRNA-133a and Myocardial Infarction, Cell Transplant. 28 (2019) 831–838. https://doi.org/10.1177/0963689719843806.

[20] Á. Sánchez-Illana, S. Thayyil, P. Montaldo, D. Jenkins, G. Quintás, C. Oger, J.-M. Galano, C. Vigor, T. Durand, M. Vento, J. Kuligowski, Novel free-radical mediated lipid peroxidation biomarkers in newborn plasma, Anal Chim Acta. 996 (2017) 88–97. https://doi.org/10.1016/j.aca.2017.09.026.

[21] Á. Sánchez-Illana, A. Núñez-Ramiro, M. Cernada, A. Parra-Llorca, E. Valverde, D. Blanco, M.T. Moral-Pumarega, F. Cabañas, H. Boix, A. Pavon, M. Chaffanel, I. Benavente-Fernández, I. Tofe, B. Loureiro, J.R. Fernández-Lorenzo, B. Fernández-Colomer, A. García-Robles, J. Kuligowski, M. Vento, HYPOTOP Study Group, Evolution of Energy Related Metabolites in Plasma from Newborns with Hypoxic-Ischemic Encephalopathy during Hypothermia Treatment, Sci Rep. 7 (2017) 17039. https://doi.org/10.1038/s41598-017-17202-7.

[22] A.D. Edwards, D.V. Azzopardi, Perinatal hypoxia-ischemia and brain injury, Pediatr Res. 47 (2000) 431–432. https://doi.org/10.1203/00006450-200004000-00003.

[23] M. Douglas-Escobar, M.D. Weiss, Hypoxic-ischemic encephalopathy: a review for the clinician, JAMA Pediatr. 169 (2015) 397–403. https://doi.org/10.1001/jamapediatrics.2014.3269.

[24] Á. Sánchez-Illana, J.D. Piñeiro-Ramos, J. Kuligowski, Small molecule biomarkers for neonatal hypoxic ischemic encephalopathy, Semin Fetal Neonatal Med. 25 (2020) 101084. https://doi.org/10.1016/j.siny.2020.101084.

[25] M. Quigley, N.D. Embleton, W. McGuire, Formula versus donor breast milk for feeding preterm or low birth weight infants, Cochrane Database Syst Rev. 7 (2019) CD002971. https://doi.org/10.1002/14651858.CD002971.pub5.

[26] D. Tudehope, M. Vento, Z. Bhutta, P. Pachi, Nutritional requirements and feeding recommendations for small for gestational age infants, J Pediatr. 162 (2013) S81-89. https://doi.org/10.1016/j.jpeds.2012.11.057.

[27] E. Villamor-Martínez, M. Pierro, G. Cavallaro, F. Mosca, B.W. Kramer, E. Villamor, Donor Human Milk Protects against Bronchopulmonary Dysplasia: A Systematic Review and Meta-Analysis, Nutrients. 10 (2018) 238. https://doi.org/10.3390/nu10020238.

[28] D. Poulimeneas, E. Bathrellou, G. Antonogeorgos, E. Mamalaki, M. Kouvari, J. Kuligowski, M. Gormaz, D.B. Panagiotakos, M. Yannakoulia, NUTRISHIELD Consortium, Feeding the preterm infant: an overview of the evidence, Int J Food Sci Nutr. 72 (2021) 4–13. https://doi.org/10.1080/09637486.2020.1754352.

[29] J. Meinzen-Derr, B. Poindexter, L. Wrage, A.L. Morrow, B. Stoll, E.F. Donovan, Role of human milk in extremely low birth weight infants' risk of necrotizing enterocolitis or death, J Perinatol. 29 (2009) 57–62. https://doi.org/10.1038/jp.2008.117.

[30] O. Ballard, A.L. Morrow, Human milk composition: nutrients and bioactive factors, Pediatr Clin North Am. 60 (2013) 49–74. https://doi.org/10.1016/j.pcl.2012.10.002.

[31] E. Bertino, G.V. Coppa, F. Giuliani, A. Coscia, O. Gabrielli, G. Sabatino, M. Sgarrella, T. Testa, L. Zampini, C. Fabris, Effects of Holder pasteurization on human milk oligosaccharides, Int J Immunopathol Pharmacol. 21 (2008) 381–385. https://doi.org/10.1177/039463200802100216.

[32] L.D.W. Arnold, The cost-effectiveness of using banked donor milk in the neonatal intensive care unit: prevention of necrotizing enterocolitis, J Hum Lact. 18 (2002) 172–177. https://doi.org/10.1177/089033440201800210.

[33] M.D. Mesa, B. Loureiro, I. Iglesia, S. Fernandez Gonzalez, E. Llurba Olivé, O. García Algar, M.J. Solana, M.J. Cabero Perez, T. Sainz, L. Martinez, D. Escuder-Vieco, A. Parra-Llorca, M. Sánchez-Campillo, G. Rodriguez Martinez, D. Gómez Roig, M. Perez Gruz, V. Andreu-Fernández, J. Clotet, S. Sailer, I. Iglesias-Platas, J. López-Herce, R. Aras, C. Pallás-Alonso, M.S. de Pipaon, M. Vento, M. Gormaz, E. Larqué Daza, C. Calvo, F. Cabañas, The Evolving Microbiome from Pregnancy to Early Infancy: A Comprehensive

Review, Nutrients. 12 (2020) E133. https://doi.org/10.3390/nu12010133.

[34] P.G. Radmacher, D.H. Adamkin, Fortification of human milk for preterm infants, Semin Fetal Neonatal Med. 22 (2017) 30–35. https://doi.org/10.1016/j.siny.2016.08.004.

[35] D. Escuder-Vieco, I. Espinosa-Martos, J.M. Rodríguez, N. Corzo, A. Montilla, P. Siegfried, C.R. Pallás-Alonso, L. Fernández, High-Temperature Short-Time Pasteurization System for Donor Milk in a Human Milk Bank Setting, Front. Microbiol. 9 (2018) 926. https://doi.org/10.3389/fmicb.2018.00926.

[36] M. Samánek, Z. Slavík, B. Zborilová, V. Hrobonová, M. Voríšková, J. Skovránek, Prevalence, treatment, and outcome of heart disease in live-born children: a prospective analysis of 91,823 live-born children, Pediatr Cardiol. 10 (1989) 205–211. https://doi.org/10.1007/BF02083294.

[37] M. Hamzah, H.F. Othman, A.M. Peluso, I. Sammour, H. Aly, Prevalence and Outcomes of Balloon Atrial Septostomy in Neonates With Transposition of Great Arteries, Pediatr Crit Care Med. 21 (2020) 324–331. https://doi.org/10.1097/PCC.0000000000002191.

[38] J. Villafañe, M.R. Lantin-Hermoso, A.B. Bhatt, J.S. Tweddell, T. Geva, M. Nathan, M.J. Elliott, V.L. Vetter, S.M. Paridon, L. Kochilas, K.J. Jenkins, R.H. Beekman, G. Wernovsky, J.A. Towbin, American College of Cardiology's Adult Congenital and Pediatric

Cardiology Council, D-transposition of the great arteries: the current era of the arterial switch operation, J Am Coll Cardiol. 64 (2014) 498–511. https://doi.org/10.1016/j.jacc.2014.06.1150.

[39] A. Nuñez-Ramiro, I. Benavente-Fernández, E. Valverde, M. Cordeiro, D. Blanco, H. Boix, F. Cabañas, M. Chaffanel, B. Fernández-Colomer, J.R. Fernández-Lorenzo, J. Kuligowski, B. Loureiro, M.T. Moral-Pumarega, A. Pavón, A. Sánchez-Illana, I. Tofé, D. Hervás, A. García-Robles, A. Parra-Llorca, M. Cernada, J. Martinez-Rodilla, S. Lorente-Pozo, R. Llorens, R. Marqués, M. Vento,
on behalf of the Hypotop Study Group, Topiramate plus Cooling for Hypoxic-Ischemic Encephalopathy: A Randomized, Controlled, Multicenter, Double-Blinded Trial, Neonatology. 116 (2019) 76–84. https://doi.org/10.1159/000499084.

[40] Policy Research Programme - Standard Information for Applicants, (n.d.). https://www.nihr.ac.uk/documents/policy-research-programme-standard-information-for-applicants/27427 (accessed May 18, 2021).

[41] A.C.C. Lee, N. Kozuki, H. Blencowe, T. Vos, A. Bahalim, G.L. Darmstadt, S. Niermeyer, M. Ellis, N.J. Robertson, S. Cousens, J.E. Lawn, Intrapartum-related neonatal encephalopathy incidence and impairment at regional and global levels for 2010 with trends from 1990, Pediatr Res. 74 Suppl 1 (2013) 50–72. https://doi.org/10.1038/pr.2013.206.

[42] G. Wassink, J.O. Davidson, S.K. Dhillon, K. Zhou, L. Bennet,

M. Thoresen, A.J. Gunn, Therapeutic Hypothermia in Neonatal Hypoxic-Ischemic Encephalopathy, Curr Neurol Neurosci Rep. 19 (2019) 2. https://doi.org/10.1007/s11910-019-0916-0.

[43] H.B. Sarnat, M.S. Sarnat, Neonatal encephalopathy following fetal distress. A clinical and electroencephalographic study, Arch Neurol. 33 (1976) 696–705. https://doi.org/10.1001/archneur.1976.00500100030012.

[44] N. Merchant, D. Azzopardi, Early predictors of outcome in infants treated with hypothermia for hypoxic-ischaemic encephalopathy, Dev Med Child Neurol. 57 Suppl 3 (2015) 8–16. https://doi.org/10.1111/dmcn.12726.

[45] F. Groenendaal, L.S. de Vries, Fifty years of brain imaging in neonatal encephalopathy following perinatal asphyxia, Pediatr Res. 81 (2017) 150–155. https://doi.org/10.1038/pr.2016.195.

[46] J. Shibasaki, N. Aida, N. Morisaki, M. Tomiyasu, Y. Nishi, K. Toyoshima, Changes in Brain Metabolite Concentrations after Neonatal Hypoxic-ischemic Encephalopathy, Radiology. 288 (2018) 840–848. https://doi.org/10.1148/radiol.2018172083.

[47] W.L.A. Lee, A.T. Michael-Titus, D.K. Shah, Hypoxic-Ischaemic Encephalopathy and the Blood-Brain Barrier in Neonates, Dev Neurosci. 39 (2017) 49–58. https://doi.org/10.1159/000467392.

[48] L. Bennet, L. Booth, A.J. Gunn, Potential biomarkers for

hypoxic–ischemic encephalopathy, Semin Fetal Neonatal Med. 15 (2010) 253–260. https://doi.org/10.1016/j.siny.2010.05.007.

[49] T.-W. Wu, B. Tamrazi, K.-H. Hsu, E. Ho, A.J. Reitman, M. Borzage, S. Blüml, J.L. Wisnowski, Cerebral Lactate Concentration in Neonatal Hypoxic-Ischemic Encephalopathy: In Relation to Time, Characteristic of Injury, and Serum Lactate Concentration, Front Neurol. 9 (2018) 293. https://doi.org/10.3389/fneur.2018.00293.

[50] R.C. Vannucci, R.M. Brucklacher, S.J. Vannucci, Glycolysis and Perinatal Hypoxic-Ischemic Brain Damage, DNE. 27 (2005) 185–190. https://doi.org/10.1159/000085991.

[51] N. Efstathiou, G. Theodoridis, K. Sarafidis, Understanding neonatal hypoxic-ischemic encephalopathy with metabolomics, Hippokratia. 21 (2017) 115–123.

[52] S.N. Reinke, B.H. Walsh, G.B. Boylan, B.D. Sykes, L.C. Kenny, D.M. Murray, D.I. Broadhurst, 1H NMR derived metabolomic profile of neonatal asphyxia in umbilical cord serum: implications for hypoxic ischemic encephalopathy, J Proteome Res. 12 (2013) 4230–4239. https://doi.org/10.1021/pr400617m.

[53] C.E. Ahearne, N.M. Denihan, B.H. Walsh, S.N. Reinke, L.C. Kenny, G.B. Boylan, D.I. Broadhurst, D.M. Murray, Early Cord Metabolite Index and Outcome in Perinatal Asphyxia and Hypoxic-Ischaemic Encephalopathy, Neonatology. 110 (2016) 296–302. https://doi.org/10.1159/000446556.

[54] N.M. Denihan, J.A. Kirwan, B.H. Walsh, W.B. Dunn, D.I. Broadhurst, G.B. Boylan, D.M. Murray, Untargeted metabolomic analysis and pathway discovery in perinatal asphyxia and hypoxic-ischaemic encephalopathy, J Cereb Blood Flow Metab. 39 (2019) 147–162. https://doi.org/10.1177/0271678X17726502.

[55] K. Sarafidis, N. Efstathiou, O. Begou, V. Soubasi, E. Agakidou, E. Gika, G. Theodoridis, V. Drossou, Urine metabolomic profile in neonates with hypoxic-ischemic encephalopa-thy, Hippokratia. 21 (2017) 80–84.

[56] S.K. Yum, C.-J. Moon, Y.-A. Youn, I.K. Sung, Changes in lactate dehydrogenase are associated with central gray matter lesions in newborns with hypoxic-ischemic encephalopathy, J Matern Fetal Neonatal Med. 30 (2017) 1177–1181. https://doi.org/10.1080/14767058.2016.1208745.

[57] M.-C. Chiang, R. Lien, S.-M. Chu, P.-H. Yang, J.-J. Lin, J.-F. Hsu, R.-H. Fu, K.-L. Lin, Serum Lactate, Brain Magnetic Resonance Imaging and Outcome of Neonatal Hypoxic Ischemic Encephalopathy after Therapeutic Hypothermia, Pediatr Neonatol. 57 (2016) 35–40. https://doi.org/10.1016/j.pedneo.2015.04.008.

[58] S. Shah, M. Tracy, J. Smyth, Postnatal Lactate as an Early Predictor of Short-Term Outcome after Intrapartum Asphyxia, Journal of Perinatology. 24 (2004) 16–20. https://doi.org/10.1038/sj.jp.7211023.

[59] D.M. Murray, G.B. Boylan, A.P. Fitzgerald, C.A. Ryan, B.P. Murphy, S. Connolly, Persistent lactic acidosis in neonatal hypoxic-ischaemic encephalopathy correlates with EEG grade and electrographic seizure burden, Arch Dis Child Fetal Neonatal Ed. 93 (2008) F183-186. https://doi.org/10.1136/adc.2006.100800.

[60] A.C. Beckstrom, P. Tanya, E.M. Humston, L.R. Snyder, R.E. Synovec, S.E. Juul, The perinatal transition of the circulating metabolome in a nonhuman primate, Pediatric Research. 71 (2012) 338–344. https://doi.org/10.1038/pr.2011.74.

[61] J. Kuligowski, R. Solberg, Á. Sánchez-Illana, L. Pankratov, A. Parra-Llorca, G. Quintás, O.D. Saugstad, M. Vento, Plasma metabolite score correlates with Hypoxia time in a newly born piglet model for asphyxia, Redox Biol. 12 (2017) 1–7. https://doi.org/10.1016/j.redox.2017.02.002.

[62] V.S. Anandi, B. Shaila, Evaluation of factors associated with elevated newborn 17-hydroxyprogesterone levels, J Pediatr Endocrinol Metab. 30 (2017) 677–681. https://doi.org/10.1515/jpem-2016-0459.

[63] K.R. Concepcion, L. Zhang, Corticosteroids and perinatal hypoxic-ischemic brain injury, Drug Discov Today. 23 (2018) 1718–1732. https://doi.org/10.1016/j.drudis.2018.05.019.

[64] S. Dong, Q. Zhang, D. Kong, C. Zhou, J. Zhou, J. Han, Y. Zhou, G. Jin, X. Hua, J. Wang, F. Hua, Gender difference in the effect

of progesterone on neonatal hypoxic/ischemic brain injury in mouse, Experimental Neurology. 306 (2018) 190–198. https://doi.org/10.1016/j.expneurol.2018.05.013.

[65] B.H. Walsh, D.I. Broadhurst, R. Mandal, D.S. Wishart, G.B. Boylan, L.C. Kenny, D.M. Murray, The Metabolomic Profile of Umbilical Cord Blood in Neonatal Hypoxic Ischaemic Encephalopathy, PLoS ONE. 7 (2012) e50520. https://doi.org/10.1371/journal.pone.0050520.

[66] U. Kariholu, P. Montaldo, T. Markati, P.J. Lally, R. Pryce, J. Teiserskas, N. Liow, V. Oliveira, A. Soe, S. Shankaran, S. Thayyil, Therapeutic hypothermia for mild neonatal encephalopathy: a systematic review and meta-analysis, Arch Dis Child Fetal Neonatal Ed. 105 (2020) 225–228. https://doi.org/10.1136/archdischild-2018-315711.

[67] A.J. Barkovich, B.L. Hajnal, D. Vigneron, A. Sola, J.C. Partridge, F. Allen, D.M. Ferriero, Prediction of neuromotor outcome in perinatal asphyxia: evaluation of MR scoring systems, AJNR Am J Neuroradiol. 19 (1998) 143–149.

[68] M. Rutherford, L.A. Ramenghi, A.D. Edwards, P. Brocklehurst, H. Halliday, M. Levene, B. Strohm, M. Thoresen, A. Whitelaw, D. Azzopardi, Assessment of brain tissue injury after moderate hypothermia in neonates with hypoxic–ischaemic encephalopathy: a nested substudy of a randomised controlled trial, Lancet Neurol. 9 (2010) 39–45. https://doi.org/10.1016/S1474-4422(09)70295-9.

[69] D. Broadhurst, R. Goodacre, S.N. Reinke, J. Kuligowski, I.D. Wilson, M.R. Lewis, W.B. Dunn, Guidelines and considerations for the use of system suitability and quality control samples in mass spectrometry assays applied in untargeted clinical metabolomic studies, Metabolomics. 14 (2018) 72. https://doi.org/10.1007/s11306-018-1367-3.

[70] ProteoWizard: Home, (n.d.). http://proteowizard.sourceforge.net/ (accessed May 19, 2021).

[71] K. Haug, K. Cochrane, V.C. Nainala, M. Williams, J. Chang, K.V. Jayaseelan, C. O'Donovan, MetaboLights: a resource evolving in response to the needs of its scientific community, Nucleic Acids Research. (2019) gkz1019. https://doi.org/10.1093/nar/gkz1019.

[72] C.A.S. <csmith at scripps.edu>, R.T. <rtautenh at gmail.com>, S.N. <sneumann at ipb-halle.de>, P.B. <hpbenton at scripps.edu>, C.C. <cjconley at ucdavis.edu>, J.R. <Johannes R. at eurac.edu>, M.W. <michael witting at helmholtz-muenchen.de>, xcms: LC-MS and GC-MS Data Analysis, (2021). https://doi.org/10.18129/B9.bioc.xcms.

[73] C. Kuhl, R. Tautenhahn, C. Böttcher, T.R. Larson, S. Neumann, CAMERA: An Integrated Strategy for Compound Spectra Extraction and Annotation of Liquid Chromatography/Mass Spectrometry Data Sets, (2011). https://doi.org/10.1021/ac202450g.

[74] J. Kuligowski, Á. Sánchez-Illana, D. Sanjuán-Herráez, M. Vento, G. Quintás, Intra-batch effect correction in liquid

chromatography-mass spectrometry using quality control samples and support vector regression (QC-SVRC), Analyst. 140 (2015) 7810–7817. https://doi.org/10.1039/c5an01638j.

[75] C.-C. Chang, C.-J. Lin, LIBSVM: A library for support vector machines, ACM Trans. Intell. Syst. Technol. 2 (2011) 27:1-27:27. https://doi.org/10.1145/1961189.1961199.

[76] Human Metabolome Database, (n.d.). https://hmdb.ca/ (accessed May 19, 2021).

[77] D. Broadhurst, R. Goodacre, S.N. Reinke, J. Kuligowski, I.D. Wilson, M.R. Lewis, W.B. Dunn, Guidelines and considerations for the use of system suitability and quality control samples in mass spectrometry assays applied in untargeted clinical metabolomic studies, Metabolomics. 14 (2018) 72. https://doi.org/10.1007/s11306-018-1367-3.

[78] J. Chong, O. Soufan, C. Li, I. Caraus, S. Li, G. Bourque, D.S. Wishart, J. Xia, MetaboAnalyst 4.0: towards more transparent and integrative metabolomics analysis, Nucleic Acids Res. 46 (2018) W486–W494. https://doi.org/10.1093/nar/gky310.

[79] L.W. Sumner, A. Amberg, D. Barrett, M.H. Beale, R. Beger, C.A. Daykin, T.W.-M. Fan, O. Fiehn, R. Goodacre, J.L. Griffin, T. Hankemeier, N. Hardy, J. Harnly, R. Higashi, J. Kopka, A.N. Lane, J.C. Lindon, P. Marriott, A.W. Nicholls, M.D. Reily, J.J. Thaden, M.R. Viant, Proposed minimum reporting standards for chemical analysis

Chemical Analysis Working Group (CAWG) Metabolomics Standards Initiative (MSI), Metabolomics. 3 (2007) 211–221. https://doi.org/10.1007/s11306-007-0082-2.

[80] L. Lehtonen, A. Gimeno, A. Parra-Llorca, M. Vento, Early neonatal death: A challenge worldwide, Semin Fetal Neonatal Med. 22 (2017) 153–160. https://doi.org/10.1016/j.siny.2017.02.006.

[81] A.C.C. Lee, N. Kozuki, H. Blencowe, T. Vos, A. Bahalim, G.L. Darmstadt, S. Niermeyer, M. Ellis, N.J. Robertson, S. Cousens, J.E. Lawn, Intrapartum-related neonatal encephalopathy incidence and impairment at regional and global levels for 2010 with trends from 1990, Pediatr Res. 74 Suppl 1 (2013) 50–72. https://doi.org/10.1038/pr.2013.206.

[82] J.J. Kurinczuk, M. White-Koning, N. Badawi, Epidemiology of neonatal encephalopathy and hypoxic-ischaemic encephalopathy, Early Hum Dev. 86 (2010) 329–338. https://doi.org/10.1016/j.earlhumdev.2010.05.010.

[83] F. Groenendaal, L.S. de Vries, Fifty years of brain imaging in neonatal encephalopathy following perinatal asphyxia, Pediatr Res. 81 (2017) 150–155. https://doi.org/10.1038/pr.2016.195.

[84] S. Lorente-Pozo, A. Parra-Llorca, I. Lara-Cantón, A. Solaz, J.L. García-Jiménez, F.V. Pallardó, M. Vento, Oxygen in the neonatal period: Oxidative stress, oxygen load and epigenetic changes, Semin Fetal Neonatal Med. 25 (2020) 101090.

https://doi.org/10.1016/j.siny.2020.101090.

[85] Q. Ma, L. Zhang, Epigenetic programming of hypoxic-ischemic encephalopathy in response to fetal hypoxia, Prog Neurobiol. 124 (2015) 28–48. https://doi.org/10.1016/j.pneurobio.2014.11.001.

[86] G.A. Nagana Gowda, D. Raftery, Biomarker Discovery and Translation in Metabolomics, Curr Metabolomics. 1 (2013) 227–240. https://doi.org/10.2174/2213235X113019990005.

[87] E. Locci, A. Noto, M. Puddu, G. Pomero, R. Demontis, C. Dalmazzo, A. Delogu, V. Fanos, E. d'Aloja, P. Gancia, A longitudinal 1H-NMR metabolomics analysis of urine from newborns with hypoxic-ischemic encephalopathy undergoing hypothermia therapy. Clinical and medical legal insights, PLoS One. 13 (2018) e0194267. https://doi.org/10.1371/journal.pone.0194267.

[88] A. Noto, G. Pomero, M. Mussap, L. Barberini, C. Fattuoni, F. Palmas, C. Dalmazzo, A. Delogu, A. Dessì, V. Fanos, P. Gancia, Urinary gas chromatography mass spectrometry metabolomics in asphyxiated newborns undergoing hypothermia: from the birth to the first month of life, Ann Transl Med. 4 (2016). https://doi.org/10.21037/atm.2016.11.27.

[89] J.D. Piñeiro-Ramos, A. Núñez-Ramiro, R. Llorens-Salvador, A. Parra-Llorca, Á. Sánchez-Illana, G. Quintás, N. Boronat-González, J. Martínez-Rodilla, J. Kuligowski, M. Vento, null The Hypotop Study Group, Metabolic Phenotypes of Hypoxic-Ischemic Encephalopathy

with Normal vs. Pathologic Magnetic Resonance Imaging Outcomes, Metabolites. 10 (2020). https://doi.org/10.3390/metabo10030109.

[90] S. Shankaran, S.A. McDonald, A.R. Laptook, S.R. Hintz, P.D. Barnes, A. Das, A. Pappas, R.D. Higgins, Eunice Kennedy Shriver National Institute of Child Health and Human Development Neonatal Research Network, Neonatal Magnetic Resonance Imaging Pattern of Brain Injury as a Biomarker of Childhood Outcomes following a Trial of Hypothermia for Neonatal Hypoxic-Ischemic Encephalopathy, J Pediatr. 167 (2015) 987-993.e3. https://doi.org/10.1016/j.jpeds.2015.08.013.

[91] Á. López-Gonzálvez, J. Godzien, A. García, C. Barbas, Capillary Electrophoresis Mass Spectrometry as a Tool for Untargeted Metabolomics, Methods Mol Biol. 1978 (2019) 55–77. https://doi.org/10.1007/978-1-4939-9236-2_5.

[92] Á. Sánchez-Illana, J.D. Piñeiro-Ramos, J.D. Sanjuan-Herráez, M. Vento, G. Quintás, J. Kuligowski, Evaluation of batch effect elimination using quality control replicates in LC-MS metabolite profiling, Anal Chim Acta. 1019 (2018) 38–48. https://doi.org/10.1016/j.aca.2018.02.053.

[93] C.A. Smith, E.J. Want, G. O'Maille, R. Abagyan, G. Siuzdak, XCMS: Processing Mass Spectrometry Data for Metabolite Profiling Using Nonlinear Peak Alignment, Matching, and Identification, Anal. Chem. 78 (2006) 779–787. https://doi.org/10.1021/ac051437y.

[94] T. Martínez-Sena, G. Luongo, D. Sanjuan-Herráez, J.V. Castell, M. Vento, G. Quintás, J. Kuligowski, Monitoring of system conditioning after blank injections in untargeted UPLC-MS metabolomic analysis, Scientific Reports. 9 (2019) 9822. https://doi.org/10.1038/s41598-019-46371-w.

[95] Á. Sánchez-Illana, D. Pérez-Guaita, D. Cuesta-García, J.D. Sanjuan-Herráez, M. Vento, J.L. Ruiz-Cerdá, G. Quintás, J. Kuligowski, Model selection for within-batch effect correction in UPLC-MS metabolomics using quality control - Support vector regression, Anal Chim Acta. 1026 (2018) 62–68. https://doi.org/10.1016/j.aca.2018.04.055.

[96] J. Kuligowski, Á. Sánchez-Illana, D. Sanjuán-Herráez, M. Vento, G. Quintás, Intra-batch effect correction in liquid chromatography-mass spectrometry using quality control samples and support vector regression (QC-SVRC), Analyst. 140 (2015) 7810–7817. https://doi.org/10.1039/c5an01638j.

[97] J. Cohen, Statistical power analysis for the behavioral sciences, 2nd ed, L. Erlbaum Associates, Hillsdale, N.J, 1988.

[98] Y. Benjamini, D. Drai, G. Elmer, N. Kafkafi, I. Golani, Controlling the false discovery rate in behavior genetics research, Behav Brain Res. 125 (2001) 279–284. https://doi.org/10.1016/s0166-4328(01)00297-2.

[99] B.J. Blaise, L. Schwendimann, V. Chhor, V. Degos, M.P. Hodson, G. Dallmann, M. Keller, P. Gressens, B. Fleiss, Persistently

Altered Metabolic Phenotype following Perinatal Excitotoxic Brain Injury, Dev Neurosci. 39 (2017) 182–191. https://doi.org/10.1159/000464131.

[100] M. Vento, J. Sastre, M.A. Asensi, J. Viña, Room-air resuscitation causes less damage to heart and kidney than 100% oxygen, Am J Respir Crit Care Med. 172 (2005) 1393–1398. https://doi.org/10.1164/rccm.200412-1740OC.

[101] D.W. Choi, Ionic dependence of glutamate neurotoxicity, J Neurosci. 7 (1987) 369–379.

[102] A. Villringer, U. Dirnagl, [Pathophysiology of cerebral ischemia], Z Arztl Fortbild Qualitatssich. 93 (1999) 164–168.

[103] A.A.-B. Badawy, S. Bano, Tryptophan Metabolism in Rat Liver After Administration of Tryptophan, Kynurenine Metabolites, and Kynureninase Inhibitors, Int J Tryptophan Res. 9 (2016) 51–65. https://doi.org/10.4137/IJTR.S38190.

[104] B. Heng, C.K. Lim, D.B. Lovejoy, A. Bessede, L. Gluch, G.J. Guillemin, Understanding the role of the kynurenine pathway in human breast cancer immunobiology, Oncotarget. 7 (2015) 6506–6520. https://doi.org/10.18632/oncotarget.6467.

[105] B. Widner, F. Leblhuber, D. Fuchs, Increased neopterin production and tryptophan degradation in advanced Parkinson's disease, J Neural Transm (Vienna). 109 (2002) 181–189.

https://doi.org/10.1007/s007020200014.

[106] M.F. Beal, W.R. Matson, K.J. Swartz, P.H. Gamache, E.D. Bird, Kynurenine pathway measurements in Huntington's disease striatum: evidence for reduced formation of kynurenic acid, J Neurochem. 55 (1990) 1327–1339. https://doi.org/10.1111/j.1471-4159.1990.tb03143.x.

[107] G.J. Guillemin, B.J. Brew, Implications of the kynurenine pathway and quinolinic acid in Alzheimer's disease, Redox Rep. 7 (2002) 199–206. https://doi.org/10.1179/135100002125000550.

[108] J.D. Piñeiro-Ramos, M.M. Cascant, A. Núñez-Ramiro, Á. López-Gonzálvez, Á. Solaz-García, A. Albiach-Delgado, J. Martínez-Rodilla, R. Llorens-Salvador, D. Sanjuan-Herraez, G. Quintás, C. Barbas, J. Kuligowski, M. Vento, Hypotop Study Group, Noninvasive monitoring of evolving urinary metabolic patterns in neonatal encephalopathy, Pediatr Res. 91 (2022) 598–605. https://doi.org/10.1038/s41390-021-01553-z.

[109] A.M. Mohr, J.L. Mott, Overview of microRNA biology, Semin Liver Dis. 35 (2015) 3–11. https://doi.org/10.1055/s-0034-1397344.

[110] R. Petri, J. Malmevik, L. Fasching, M. Åkerblom, J. Jakobsson, miRNAs in brain development, Exp Cell Res. 321 (2014) 84–89. https://doi.org/10.1016/j.yexcr.2013.09.022.

[111] Y. Liang, L. Wang, Inflamma-MicroRNAs in Alzheimer's

Disease: From Disease Pathogenesis to Therapeutic Potentials, Front Cell Neurosci. 15 (2021) 785433. https://doi.org/10.3389/fncel.2021.785433.

[112] V. Swahari, A. Nakamura, E. Hollville, H. Stroud, J.M. Simon, T.S. Ptacek, M.V. Beck, C. Flowers, J. Guo, C. Plestant, J. Liang, C.L. Kurtz, M. Kanke, S.M. Hammond, Y.-W. He, E.S. Anton, P. Sethupathy, S.S. Moy, M.E. Greenberg, M. Deshmukh, MicroRNA-29 is an essential regulator of brain maturation through regulation of CH methylation, Cell Rep. 35 (2021) 108946. https://doi.org/10.1016/j.celrep.2021.108946.

[113] E.A. Stevens, J.D. Mezrich, C.A. Bradfield, The aryl hydrocarbon receptor: a perspective on potential roles in the immune system, Immunology. 127 (2009) 299–311. https://doi.org/10.1111/j.1365-2567.2009.03054.x.

[114] K. Schroecksnadel, C. Winkler, C. Duftner, B. Wirleitner, M. Schirmer, D. Fuchs, Tryptophan degradation increases with stage in patients with rheumatoid arthritis, Clin Rheumatol. 25 (2006) 334–337. https://doi.org/10.1007/s10067-005-0056-6.

[115] R.M. Giusti, E.M. Maloney, B. Hanchard, O.S. Morgan, S.M. Steinberg, H. Wachter, E. Williams, B. Cranston, D. Fuchs, A. Manns, Differential patterns of serum biomarkers of immune activation in human T-cell lymphotropic virus type I-associated myelopathy/tropical spastic paraparesis, and adult T-cell leukemia/lymphoma, Cancer Epidemiol Biomarkers Prev. 5 (1996) 699–704.

[116] P.J. Birch, C.J. Grossman, A.G. Hayes, Kynurenic acid antagonises responses to NMDA via an action at the strychnine-insensitive glycine receptor, Eur J Pharmacol. 154 (1988) 85–87. https://doi.org/10.1016/0014-2999(88)90367-6.

[117] M.P. Heyes, Quinolinic acid in culture media used for in vitro neurotoxicology studies, Neurosci Lett. 145 (1992) 234–235. https://doi.org/10.1016/0304-3940(92)90030-b.

[118] M.N. Perkins, J.F. Collins, T.W. Stone, Isomers of 2-amino-7-phosphonoheptanoic acid as antagonists of neuronal excitants, Neurosci Lett. 32 (1982) 65–68. https://doi.org/10.1016/0304-3940(82)90230-0.

[119] C. Hilmas, E.F. Pereira, M. Alkondon, A. Rassoulpour, R. Schwarcz, E.X. Albuquerque, The brain metabolite kynurenic acid inhibits alpha7 nicotinic receptor activity and increases non-alpha7 nicotinic receptor expression: physiopathological implications, J Neurosci. 21 (2001) 7463–7473.

[120] J. Wang, N. Simonavicius, X. Wu, G. Swaminath, J. Reagan, H. Tian, L. Ling, Kynurenic acid as a ligand for orphan G protein-coupled receptor GPR35, J Biol Chem. 281 (2006) 22021–22028. https://doi.org/10.1074/jbc.M603503200.

[121] T.W. Stone, Subtypes of NMDA receptors, Gen Pharmacol. 24 (1993) 825–832. https://doi.org/10.1016/0306-3623(93)90155-q.

[122] M. Hokari, H.Q. Wu, R. Schwarcz, Q.R. Smith, Facilitated brain uptake of 4-chlorokynurenine and conversion to 7-chlorokynurenic acid, Neuroreport. 8 (1996) 15–18. https://doi.org/10.1097/00001756-199612200-00004.

[123] E.T. Chouchani, V.R. Pell, E. Gaude, D. Aksentijević, S.Y. Sundier, E.L. Robb, A. Logan, S.M. Nadtochiy, E.N.J. Ord, A.C. Smith, F. Eyassu, R. Shirley, C.-H. Hu, A.J. Dare, A.M. James, S. Rogatti, R.C. Hartley, S. Eaton, A.S.H. Costa, P.S. Brookes, S.M. Davidson, M.R. Duchen, K. Saeb-Parsy, M.J. Shattock, A.J. Robinson, L.M. Work, C. Frezza, T. Krieg, M.P. Murphy, Ischaemic accumulation of succinate controls reperfusion injury through mitochondrial ROS, Nature. 515 (2014) 431–435. https://doi.org/10.1038/nature13909.

[124] L.D. Lukyanova, Y.I. Kirova, E.L. Germanova, The Role of Succinate in Regulation of Immediate HIF-1α Expression in Hypoxia, Bull Exp Biol Med. 164 (2018) 298–303. https://doi.org/10.1007/s10517-018-3976-2.

[125] R. Tautenhahn, C. Böttcher, S. Neumann, Highly sensitive feature detection for high resolution LC/MS, BMC Bioinformatics. 9 (2008) 504. https://doi.org/10.1186/1471-2105-9-504.

[126] W. Yang, L. Chen, L. Xu, A.J. Bilotta, S. Yao, Z. Liu, Y. Cong, MicroRNA-10a Negatively Regulates CD4+ T Cell IL-10 Production through Suppression of Blimp1, J Immunol. 207 (2021) 985–995.

https://doi.org/10.4049/jimmunol.2100017.

[127] Y. Gui, H. Liu, L. Zhang, W. Lv, X. Hu, Altered microRNA profiles in cerebrospinal fluid exosome in Parkinson disease and Alzheimer disease, Oncotarget. 6 (2015) 37043–37053. https://doi.org/10.18632/oncotarget.6158.

[128] F. Li, X. Liang, Y. Chen, S. Li, J. Liu, Role of microRNA-93 in regulation of angiogenesis, Tumour Biol. 35 (2014) 10609–10613. https://doi.org/10.1007/s13277-014-2605-6.

[129] World Health Organization et al. - 2017 - Guideline..pdf, (n.d.). https://apps.who.int/iris/bitstream/handle/10665/259386/9789241550086-eng.pdf (accessed May 19, 2021).

[130] C.G. Victora, R. Bahl, A.J.D. Barros, G.V.A. França, S. Horton, J. Krasevec, S. Murch, M.J. Sankar, N. Walker, N.C. Rollins, Lancet Breastfeeding Series Group, Breastfeeding in the 21st century: epidemiology, mechanisms, and lifelong effect, Lancet. 387 (2016) 475–490. https://doi.org/10.1016/S0140-6736(15)01024-7.

[131] C.-Y. Boquien, Human Milk: An Ideal Food for Nutrition of Preterm Newborn, Front. Pediatr. 6 (2018). https://doi.org/10.3389/fped.2018.00295.

[132] R.J. Schanler, R.J. Shulman, C. Lau, Feeding strategies for premature infants: beneficial outcomes of feeding fortified human milk versus preterm formula, Pediatrics. 103 (1999) 1150–1157.

https://doi.org/10.1542/peds.103.6.1150.

[133] P.M. Sisk, C.A. Lovelady, R.G. Dillard, K.J. Gruber, T.M. O'Shea, Early human milk feeding is associated with a lower risk of necrotizing enterocolitis in very low birth weight infants, J Perinatol. 27 (2007) 428–433. https://doi.org/10.1038/sj.jp.7211758.

[134] A. Maayan-Metzger, S. Avivi, I. Schushan-Eisen, J. Kuint, Human milk versus formula feeding among preterm infants: short-term outcomes, Am J Perinatol. 29 (2012) 121–126. https://doi.org/10.1055/s-0031-1295652.

[135] B.R. Vohr, B.B. Poindexter, A.M. Dusick, L.T. McKinley, L.L. Wright, J.C. Langer, W.K. Poole, NICHD Neonatal Research Network, Beneficial effects of breast milk in the neonatal intensive care unit on the developmental outcome of extremely low birth weight infants at 18 months of age, Pediatrics. 118 (2006) e115-123. https://doi.org/10.1542/peds.2005-2382.

[136] E.B. Isaacs, B.R. Fischl, B.T. Quinn, W.K. Chong, D.G. Gadian, A. Lucas, Impact of breast milk on intelligence quotient, brain size, and white matter development, Pediatr Res. 67 (2010) 357–362. https://doi.org/10.1203/PDR.0b013e3181d026da.

[137] B.R. Vohr, B.B. Poindexter, A.M. Dusick, L.T. McKinley, R.D. Higgins, J.C. Langer, W.K. Poole, National Institute of Child Health and Human Development National Research Network, Persistent beneficial effects of breast milk ingested in the neonatal intensive care

unit on outcomes of extremely low birth weight infants at 30 months of age, Pediatrics. 120 (2007) e953-959. https://doi.org/10.1542/peds.2006-3227.

[138] Section on Breastfeeding, Breastfeeding and the use of human milk, Pediatrics. 129 (2012) e827-841. https://doi.org/10.1542/peds.2011-3552.

[139] M.A. Underwood, Human Milk for the Premature Infant, Pediatric Clinics of North America. 60 (2013) 189–207. https://doi.org/10.1016/j.pcl.2012.09.008.

[140] J.-C. Picaud, R. Buffin, Human Milk-Treatment and Quality of Banked Human Milk, Clin Perinatol. 44 (2017) 95–119. https://doi.org/10.1016/j.clp.2016.11.003.

[141] C. Peila, G.E. Moro, E. Bertino, L. Cavallarin, M. Giribaldi, F. Giuliani, F. Cresi, A. Coscia, The Effect of Holder Pasteurization on Nutrients and Biologically-Active Components in Donor Human Milk: A Review, Nutrients. 8 (2016). https://doi.org/10.3390/nu8080477.

[142] G. Weaver, E. Bertino, C. Gebauer, A. Grovslien, R. Mileusnic-Milenovic, S. Arslanoglu, D. Barnett, C.-Y. Boquien, R. Buffin, A. Gaya, G.E. Moro, A. Wesolowska, J.-C. Picaud, Recommendations for the Establishment and Operation of Human Milk Banks in Europe: A Consensus Statement From the European Milk Bank Association (EMBA), Front Pediatr. 7 (2019). https://doi.org/10.3389/fped.2019.00053.

[143] A. Wesolowska, E. Sinkiewicz-Darol, O. Barbarska, U. Bernatowicz-Lojko, M.K. Borszewska-Kornacka, J.B. van Goudoever, Innovative Techniques of Processing Human Milk to Preserve Key Components, Nutrients. 11 (2019). https://doi.org/10.3390/nu11051169.

[144] C. Gao, J. Miller, P.F. Middleton, Y.-C. Huang, A.J. McPhee, R.A. Gibson, Changes to breast milk fatty acid composition during storage, handling and processing: A systematic review, Prostaglandins Leukot Essent Fatty Acids. 146 (2019) 1–10. https://doi.org/10.1016/j.plefa.2019.04.008.

[145] D.L. O'Connor, S. Gibbins, A. Kiss, N. Bando, J. Brennan-Donnan, E. Ng, D.M. Campbell, S. Vaz, C. Fusch, E. Asztalos, P. Church, E. Kelly, L. Ly, A. Daneman, S. Unger, GTA DoMINO Feeding Group, Effect of Supplemental Donor Human Milk Compared With Preterm Formula on Neurodevelopment of Very Low-Birth-Weight Infants at 18 Months: A Randomized Clinical Trial, JAMA. 316 (2016) 1897–1905. https://doi.org/10.1001/jama.2016.16144.

[146] A. Parra-Llorca, M. Gormaz, Á. Sánchez-Illana, J.D. Piñeiro-Ramos, M.C. Collado, E. Serna, M. Cernada, A. Nuñez-Ramiro, A. Ramón-Beltrán, C. Oger, J.-M. Galano, C. Vigor, T. Durand, J. Kuligowski, M. Vento, Does Pasteurized Donor Human Milk Efficiently Protect Preterm Infants Against Oxidative Stress?, Antioxidants & Redox Signaling. 31 (2019) 791–799. https://doi.org/10.1089/ars.2019.7821.

[147] I. Beghetti, E. Biagi, S. Martini, P. Brigidi, L. Corvaglia, A. Aceti, Human Milk's Hidden Gift: Implications of the Milk Microbiome for Preterm Infants' Health, Nutrients. 11 (2019). https://doi.org/10.3390/nu11122944.

[148] A. Parra-Llorca, M. Gormaz, C. Alcántara, M. Cernada, A. Nuñez-Ramiro, M. Vento, M.C. Collado, Preterm Gut Microbiome Depending on Feeding Type: Significance of Donor Human Milk, Front. Microbiol. 9 (2018). https://doi.org/10.3389/fmicb.2018.01376.

[149] C. Milani, S. Duranti, F. Bottacini, E. Casey, F. Turroni, J. Mahony, C. Belzer, S. Delgado Palacio, S. Arboleya Montes, L. Mancabelli, G.A. Lugli, J.M. Rodriguez, L. Bode, W. de Vos, M. Gueimonde, A. Margolles, D. van Sinderen, M. Ventura, The First Microbial Colonizers of the Human Gut: Composition, Activities, and Health Implications of the Infant Gut Microbiota, Microbiol Mol Biol Rev. 81 (2017). https://doi.org/10.1128/MMBR.00036-17.

[150] S. Kurath-Koller, C. Moissl-Eichinger, G. Gorkiewicz, R. Kraschl, C. Kanduth, B. Hopfer, B. Urlesberger, B. Resch, Changes of intestinal microbiota composition and diversity in very low birth weight infants related to strategies of NEC prophylaxis: protocol for an observational multicentre pilot study, Pilot Feasibility Stud. 3 (2017). https://doi.org/10.1186/s40814-017-0195-y.

[151] M.M. Ulaszewska, C.H. Weinert, A. Trimigno, R. Portmann, C. Andres Lacueva, R. Badertscher, L. Brennan, C. Brunius, A. Bub, F.

Capozzi, M. Cialiè Rosso, C.E. Cordero, H. Daniel, S. Durand, B. Egert, P.G. Ferrario, E.J.M. Feskens, P. Franceschi, M. Garcia-Aloy, F. Giacomoni, P. Giesbertz, R. González-Domínguez, K. Hanhineva, L.Y. Hemeryck, J. Kopka, S.E. Kulling, R. Llorach, C. Manach, F. Mattivi, C. Migné, L.H. Münger, B. Ott, G. Picone, G. Pimentel, E. Pujos-Guillot, S. Riccadonna, M.J. Rist, C. Rombouts, J. Rubert, T. Skurk, P.S.C. Sri Harsha, L. Van Meulebroek, L. Vanhaecke, R. Vázquez-Fresno, D. Wishart, G. Vergères, Nutrimetabolomics: An Integrative Action for Metabolomic Analyses in Human Nutritional Studies, Mol Nutr Food Res. 63 (2019) e1800384. https://doi.org/10.1002/mnfr.201800384.

[152] M.X. Chen, S.-Y. Wang, C.-H. Kuo, I.-L. Tsai, Metabolome analysis for investigating host-gut microbiota interactions, J Formos Med Assoc. 118 Suppl 1 (2019) S10–S22. https://doi.org/10.1016/j.jfma.2018.09.007.

[153] E.B.-M. Daliri, S. Wei, D.H. Oh, B.H. Lee, The human microbiome and metabolomics: Current concepts and applications, Critical Reviews in Food Science and Nutrition. 57 (2017) 3565–3576. https://doi.org/10.1080/10408398.2016.1220913.

[154] I. Ten-Doménech, T. Martínez-Sena, M. Moreno-Torres, J.D. Sanjuan-Herráez, J.V. Castell, A. Parra-Llorca, M. Vento, G. Quintás, J. Kuligowski, Comparing Targeted vs. Untargeted MS2 Data-Dependent Acquisition for Peak Annotation in LC-MS Metabolomics, Metabolites. 10 (2020). https://doi.org/10.3390/metabo10040126.

[155] D. Kessner, M. Chambers, R. Burke, D. Agus, P. Mallick, ProteoWizard: open source software for rapid proteomics tools development, Bioinformatics. 24 (2008) 2534–2536. https://doi.org/10.1093/bioinformatics/btn323.

[156] H.P. Benton, E.J. Want, T.M.D. Ebbels, Correction of mass calibration gaps in liquid chromatography-mass spectrometry metabolomics data, Bioinformatics. 26 (2010) 2488–2489. https://doi.org/10.1093/bioinformatics/btq441.

[157] J.G. Caporaso, J. Kuczynski, J. Stombaugh, K. Bittinger, F.D. Bushman, E.K. Costello, N. Fierer, A.G. Peña, J.K. Goodrich, J.I. Gordon, G.A. Huttley, S.T. Kelley, D. Knights, J.E. Koenig, R.E. Ley, C.A. Lozupone, D. McDonald, B.D. Muegge, M. Pirrung, J. Reeder, J.R. Sevinsky, P.J. Turnbaugh, W.A. Walters, J. Widmann, T. Yatsunenko, J. Zaneveld, R. Knight, QIIME allows analysis of high-throughput community sequencing data, Nat Methods. 7 (2010) 335–336. https://doi.org/10.1038/nmeth.f.303.

[158] M.G.I. Langille, J. Zaneveld, J.G. Caporaso, D. McDonald, D. Knights, J.A. Reyes, J.C. Clemente, D.E. Burkepile, R.L. Vega Thurber, R. Knight, R.G. Beiko, C. Huttenhower, Predictive functional profiling of microbial communities using 16S rRNA marker gene sequences, Nature Biotechnology. 31 (2013) 814–821. https://doi.org/10.1038/nbt.2676.

[159] R. Caspi, R. Billington, L. Ferrer, H. Foerster, C.A. Fulcher, I.M. Keseler, A. Kothari, M. Krummenacker, M. Latendresse, L.A.

Mueller, Q. Ong, S. Paley, P. Subhraveti, D.S. Weaver, P.D. Karp, The MetaCyc database of metabolic pathways and enzymes and the BioCyc collection of pathway/genome databases, Nucleic Acids Res. 44 (2016) D471-480. https://doi.org/10.1093/nar/gkv1164.

[160] M. Kanehisa, Toward understanding the origin and evolution of cellular organisms, Protein Sci. 28 (2019) 1947–1951. https://doi.org/10.1002/pro.3715.

[161] L.W. Sumner, A. Amberg, D. Barrett, M.H. Beale, R. Beger, C.A. Daykin, T.W.-M. Fan, O. Fiehn, R. Goodacre, J.L. Griffin, T. Hankemeier, N. Hardy, J. Harnly, R. Higashi, J. Kopka, A.N. Lane, J.C. Lindon, P. Marriott, A.W. Nicholls, M.D. Reily, J.J. Thaden, M.R. Viant, Proposed minimum reporting standards for chemical analysis Chemical Analysis Working Group (CAWG) Metabolomics Standards Initiative (MSI), Metabolomics. 3 (2007) 211–221. https://doi.org/10.1007/s11306-007-0082-2.

[162] M. Shaffer, K. Thurimella, K. Quinn, K. Doenges, X. Zhang, S. Bokatzian, N. Reisdorph, C.A. Lozupone, AMON: annotation of metabolite origins via networks to integrate microbiome and metabolome data, BMC Bioinformatics. 20 (2019) 614. https://doi.org/10.1186/s12859-019-3176-8.

[163] -Venny-. Venn Diagrams for comparing lists. By Juan Carlos Oliveros., (n.d.). https://bioinfogp.cnb.csic.es/tools/venny_old/venny.php (accessed May 28, 2021).

[164] L.A. Papile, J. Burstein, R. Burstein, H. Koffler, Incidence and evolution of subependymal and intraventricular hemorrhage: a study of infants with birth weights less than 1,500 gm, J Pediatr. 92 (1978) 529–534. https://doi.org/10.1016/s0022-3476(78)80282-0.

[165] S. Li, Y. Park, S. Duraisingham, F.H. Strobel, N. Khan, Q.A. Soltow, D.P. Jones, B. Pulendran, Predicting Network Activity from High Throughput Metabolomics, PLOS Computational Biology. 9 (2013) e1003123. https://doi.org/10.1371/journal.pcbi.1003123.

[166] J. Bauer, J. Gerss, Longitudinal analysis of macronutrients and minerals in human milk produced by mothers of preterm infants, Clin Nutr. 30 (2011) 215–220. https://doi.org/10.1016/j.clnu.2010.08.003.

[167] N.R. García-Lara, D.E. Vieco, J. De la Cruz-Bértolo, D. Lora-Pablos, N.U. Velasco, C.R. Pallás-Alonso, Effect of Holder pasteurization and frozen storage on macronutrients and energy content of breast milk, J Pediatr Gastroenterol Nutr. 57 (2013) 377–382. https://doi.org/10.1097/MPG.0b013e31829d4f82.

[168] E. Bertino, G.V. Coppa, F. Giuliani, A. Coscia, O. Gabrielli, G. Sabatino, M. Sgarrella, T. Testa, L. Zampini, C. Fabris, Effects of Holder pasteurization on human milk oligosaccharides, Int J Immunopathol Pharmacol. 21 (2008) 381–385. https://doi.org/10.1177/039463200802100216.

[169] A. Coscia, C. Peila, E. Bertino, G.V. Coppa, G.E. Moro, O.

Gabrielli, L. Zampini, T. Galeazzi, F. Maccari, N. Volpi, Effect of holder pasteurisation on human milk glycosaminoglycans, J Pediatr Gastroenterol Nutr. 60 (2015) 127–130. https://doi.org/10.1097/MPG.0000000000000570.

[170] J.J. Hollanders, A.C. Heijboer, B. van der Voorn, J. Rotteveel, M.J.J. Finken, Nutritional programming by glucocorticoids in breast milk: Targets, mechanisms and possible implications, Best Pract Res Clin Endocrinol Metab. 31 (2017) 397–408. https://doi.org/10.1016/j.beem.2017.10.001.

[171] B. van der Voorn, M. de Waard, J.B. van Goudoever, J. Rotteveel, A.C. Heijboer, M.J. Finken, Breast-Milk Cortisol and Cortisone Concentrations Follow the Diurnal Rhythm of Maternal Hypothalamus-Pituitary-Adrenal Axis Activity, J Nutr. 146 (2016) 2174–2179. https://doi.org/10.3945/jn.116.236349.

[172] S.H. Ley, A.J. Hanley, D. Stone, D.L. O'Connor, Effects of pasteurization on adiponectin and insulin concentrations in donor human milk, Pediatr Res. 70 (2011) 278–281. https://doi.org/10.1203/PDR.0b013e318224287a.

[173] P.B. Untalan, S.E. Keeney, K.H. Palkowetz, A. Rivera, A.S. Goldman, Heat susceptibility of interleukin-10 and other cytokines in donor human milk, Breastfeed Med. 4 (2009) 137–144. https://doi.org/10.1089/bfm.2008.0145.

[174] R.A. Vass, E.F. Bell, T.T. Colaizy, M.L. Schmelzel, K.J.

Johnson, J.R. Walker, T. Ertl, R.D. Roghair, Hormone levels in preterm and donor human milk before and after Holder pasteurization, Pediatr Res. 88 (2020) 612–617. https://doi.org/10.1038/s41390-020-0789-6.

[175] D.J. Morris, A.S. Brem, Role of gut metabolism of adrenal corticosteroids and hypertension: clues gut-cleansing antibiotics give us, Physiological Genomics. 51 (2019) 83–89. https://doi.org/10.1152/physiolgenomics.00115.2018.

[176] S. Vincenzetti, V. Polzonetti, D. Micozzi, S. Pucciarelli, Enzymology of Pyrimidine Metabolism and Neurodegeneration, Curr Med Chem. 23 (2016) 1408–1431. https://doi.org/10.2174/0929867323666160411125803.

[177] D. van der Linde, E.E.M. Konings, M.A. Slager, M. Witsenburg, W.A. Helbing, J.J.M. Takkenberg, J.W. Roos-Hesselink, Birth prevalence of congenital heart disease worldwide: a systematic review and meta-analysis, J Am Coll Cardiol. 58 (2011) 2241–2247. https://doi.org/10.1016/j.jacc.2011.08.025.

[178] D.C. Bellinger, D. Wypij, M.J. Rivkin, D.R. DeMaso, R.L. Robertson, C. Dunbar-Masterson, L.A. Rappaport, G. Wernovsky, R.A. Jonas, J.W. Newburger, Adolescents with d-transposition of the great arteries corrected with the arterial switch procedure: neuropsychological assessment and structural brain imaging, Circulation. 124 (2011) 1361–1369. https://doi.org/10.1161/CIRCULATIONAHA.111.026963.

[179] J.M. Lim, T. Kingdom, B. Saini, V. Chau, M. Post, S. Blaser, C. Macgowan, S.P. Miller, M. Seed, Cerebral oxygen delivery is reduced in newborns with congenital heart disease, J Thorac Cardiovasc Surg. 152 (2016) 1095–1103. https://doi.org/10.1016/j.jtcvs.2016.05.027.

[180] L. Sun, C.K. Macgowan, J.G. Sled, S.-J. Yoo, C. Manlhiot, P. Porayette, L. Grosse-Wortmann, E. Jaeggi, B.W. McCrindle, J. Kingdom, E. Hickey, S. Miller, M. Seed, Reduced fetal cerebral oxygen consumption is associated with smaller brain size in fetuses with congenital heart disease, Circulation. 131 (2015) 1313–1323. https://doi.org/10.1161/CIRCULATIONAHA.114.013051.

[181] I.S. Park, S.Y. Yoon, J.Y. Min, Y.H. Kim, J.K. Ko, K.S. Kim, D.M. Seo, J.H. Lee, Metabolic Alterations and Neurodevelopmental Outcome of Infants with Transposition of the Great Arteries, Pediatr Cardiol. 27 (2006) 569–576. https://doi.org/10.1007/s00246-004-0730-5.

[182] M.E. van der Laan, E.A. Verhagen, A.F. Bos, R.M.F. Berger, E.M.W. Kooi, Effect of balloon atrial septostomy on cerebral oxygenation in neonates with transposition of the great arteries, Pediatr Res. 73 (2013) 62–67. https://doi.org/10.1038/pr.2012.147.

[183] D. Mukherjee, M. Lindsay, Y. Zhang, T. Lardaro, H. Osen, D.C. Chang, J.I. Brenner, F. Abdullah, Analysis of 8681 neonates with transposition of the great arteries: outcomes with and without Rashkind balloon atrial septostomy, Cardiol Young. 20 (2010) 373–380. https://doi.org/10.1017/S1047951110000296.

[184] G. Hiremath, G. Natarajan, D. Math, S. Aggarwal, Impact of balloon atrial septostomy in neonates with transposition of great arteries, J Perinatol. 31 (2011) 494–499. https://doi.org/10.1038/jp.2010.196.

[185] L. Terraneo, M. Samaja, Comparative Response of Brain to Chronic Hypoxia and Hyperoxia, Int J Mol Sci. 18 (2017) E1914. https://doi.org/10.3390/ijms18091914.

[186] I. Torres-Cuevas, A. Parra-Llorca, A. Sánchez-Illana, A. Nuñez-Ramiro, J. Kuligowski, C. Cháfer-Pericás, M. Cernada, J. Escobar, M. Vento, Oxygen and oxidative stress in the perinatal period, Redox Biol. 12 (2017) 674–681. https://doi.org/10.1016/j.redox.2017.03.011.

[187] K.A. Smith, G.B. Waypa, P.T. Schumacker, Redox signaling during hypoxia in mammalian cells, Redox Biology. 13 (2017) 228–234. https://doi.org/10.1016/j.redox.2017.05.020.

[188] V. Fanos, R. Pintus, A. Dessì, Clinical Metabolomics in Neonatology: From Metabolites to Diseases, Neonatology. 113 (2018) 406–413. https://doi.org/10.1159/000487620.

[189] Á. Sánchez-Illana, V. Shah, J.D. Piñeiro-Ramos, J.M. Di Fiore, G. Quintás, T.M. Raffay, P.M. MacFarlane, R.J. Martin, J. Kuligowski, Adrenic acid non-enzymatic peroxidation products in biofluids of moderate preterm infants, Free Radic Biol Med. 142 (2019) 107–112.

https://doi.org/10.1016/j.freeradbiomed.2019.02.024.

[190] G. Quintás, Á. Sánchez-Illana, J.D. Piñeiro-Ramos, J. Kuligowski, Chapter Six - Data Quality Assessment in Untargeted LC-MS Metabolomics, in: J. Jaumot, C. Bedia, R. Tauler (Eds.), Comprehensive Analytical Chemistry, Elsevier, 2018: pp. 137–164. https://doi.org/10.1016/bs.coac.2018.06.002.

[191] M.V. Johnston, W.H. Trescher, A. Ishida, W. Nakajima, Neurobiology of hypoxic-ischemic injury in the developing brain, Pediatr Res. 49 (2001) 735–741. https://doi.org/10.1203/00006450-200106000-00003.

[192] A. Fatemi, M.A. Wilson, M.V. Johnston, Hypoxic-ischemic encephalopathy in the term infant, Clin Perinatol. 36 (2009) 835–858, vii. https://doi.org/10.1016/j.clp.2009.07.011.

[193] Y. Teshima, M. Akao, R.A. Li, T.H. Chong, W.A. Baumgartner, M.V. Johnston, E. Marbán, Mitochondrial ATP-sensitive potassium channel activation protects cerebellar granule neurons from apoptosis induced by oxidative stress, Stroke. 34 (2003) 1796–1802. https://doi.org/10.1161/01.STR.0000077017.60947.AE.

[194] I. Millán, J.D. Piñero-Ramos, I. Lara, A. Parra-Llorca, I. Torres-Cuevas, M. Vento, Oxidative Stress in the Newborn Period: Useful Biomarkers in the Clinical Setting, Antioxidants (Basel). 7 (2018) E193. https://doi.org/10.3390/antiox7120193.

[195] A. Stincone, A. Prigione, T. Cramer, M.M.C. Wamelink, K. Campbell, E. Cheung, V. Olin-Sandoval, N.M. Gruning, A. Kruger, M.T. Alam, M.A. Keller, M. Breitenbach, K.M. Brindle, J.D. Rabinowitz, M. Ralser, The return of metabolism: biochemistry and physiology of the pentose phosphate pathway, Biological Reviews. 90 (2015) 927–963. https://doi.org/10.1111/brv.12140.

[196] E.M. Brekke, T.S. Morken, M. Widerøe, A.K. Håberg, A.-M. Brubakk, U. Sonnewald, The pentose phosphate pathway and pyruvate carboxylation after neonatal hypoxic-ischemic brain injury, J Cereb Blood Flow Metab. 34 (2014) 724–734. https://doi.org/10.1038/jcbfm.2014.8.

[197] A. Kuehne, H. Emmert, J. Soehle, M. Winnefeld, F. Fischer, H. Wenck, S. Gallinat, L. Terstegen, R. Lucius, J. Hildebrand, N. Zamboni, Acute Activation of Oxidative Pentose Phosphate Pathway as First-Line Response to Oxidative Stress in Human Skin Cells, Mol Cell. 59 (2015) 359–371. https://doi.org/10.1016/j.molcel.2015.06.017.

[198] M. Ralser, M.M. Wamelink, A. Kowald, B. Gerisch, G. Heeren, E.A. Struys, E. Klipp, C. Jakobs, M. Breitenbach, H. Lehrach, S. Krobitsch, Dynamic rerouting of the carbohydrate flux is key to counteracting oxidative stress, J Biol. 6 (2007) 10. https://doi.org/10.1186/jbiol61.

[199] Y.-P. Wang, L.-S. Zhou, Y.-Z. Zhao, S.-W. Wang, L.-L. Chen, L.-X. Liu, Z.-Q. Ling, F.-J. Hu, Y.-P. Sun, J.-Y. Zhang, C. Yang, Y. Yang, Y. Xiong, K.-L. Guan, D. Ye, Regulation of G6PD acetylation

by SIRT2 and KAT9 modulates NADPH homeostasis and cell survival during oxidative stress, EMBO J. 33 (2014) 1304–1320. https://doi.org/10.1002/embj.201387224.

[200] M. Akram, S.M. Ali Shah, N. Munir, M. Daniyal, I.M. Tahir, Z. Mahmood, M. Irshad, M. Akhlaq, S. Sultana, R. Zainab, Hexose monophosphate shunt, the role of its metabolites and associated disorders: A review, J Cell Physiol. (2019). https://doi.org/10.1002/jcp.28228.

[201] M.C.M. Vissers, A.B. Das, Potential Mechanisms of Action for Vitamin C in Cancer: Reviewing the Evidence, Front Physiol. 9 (2018) 809. https://doi.org/10.3389/fphys.2018.00809.

8. Annex. Supplementary figures and tables

A.1 Metabolic Phenotypes of Hypoxic-Ischemic Encephalopathy with Normal vs. Pathologic Magnetic Resonance Imaging Outcomes

Supplementary Table A.1.1 Annotation of altered metabolites. Note: blue stands for detected, but not altered; red stands for altered; IDs of annotated metabolites marked with a star have been verified with MS/MS data.

https://www.mdpi.com/2218-1989/10/3/109#supplementary

A.2 Non-invasive monitoring of evolving urinary metabolic patterns in Hypoxic-ischemic encephalopathy

Supplementary Table A.2.1 Normalized relative intensities of urinary metabolomic features acquired with three different analytical platform. https:www.nature.com/articles/s413900-021-01552-z#Sec16

Supplementary Table A.2.2 Metabolites detected in urine samples with the CE-TOFMS assay

Formula	Mass	RMT	Compound Name (Putative)
C2 H5 N O2	75,0323	0,74	Glycine
C3 H9 N O	75,069	0,60	Trimethylamine N-oxide
C4 H6 O2	86,0374	1,56	1,4-Lactone

Formula	Mass	RMT	Compound Name (Putative)
C3 H7 N O2	89,0481	0,80	Alanine
C4H9NO 2	103,063 6	0,71	3-Aminobutyric acid
C4 H9 N O2	103,063 5	0,94	N,N-Dimethylglycine
C5 H13 N O	103,099 7	0,62	Choline
C3 H7 N O3	105,042 8	0,87	Serine
C5 H9 N O2	115,063 2	0,93	L-Proline
C3 H7 N3 O2	117,054 8	0,74	Guanidinoacetate
C5 H11 N O2	117,078 8	0,96	Betaine
C5 H11 N O2	117,079 1	0,87	L-Valine/D-Norvaline
C3 H7 N O2 S	121,021 7	0,94	Cysteine
C6 H6 N2 O	122,047 8	0,68	Nicotinamide
C5 H8 N2 O2	128,058 8	0,78	5,6-Dihydrothymine
C5 H7 N O3	129,042 8	0,92	5-Oxoproline
C6 H11 N O2	129,079 1	0,89	Pipecolic acid
C6 H14 N2 O	130,110 3	0,75	N-Acetylputrescine
C5 H9 N O3	131,058 5	1,01	Trans 4 Hydroxy-L-proline
C4 H9 N3 O2	131,069 6	0,79	Creatine
C6 H13 N O2	131,094 3	0,89	Leucine / isoleucine
C5 H8 O4	132,042 7	1,58	Methylsuccinate/Deoxyribonolactone/Glutarate/Ethylmalonic acid
C5 H12 N2 O2	132,089 2	0,63	Ornithine
C5 H4 N4 O	136,039 3	1,00	Hypoxanthine
C7 H8 N2 O	136,063 6	0,66	1-Methylnicotinamide
C6 H6 N2 O2	138,043	0,74	Urocanate
C6 H8 N2 O2	140,058 8	0,73	Methylimidazoleacetic acid

Formula	Mass	RMT	Compound Name (Putative)
C7 H13 N O2	143,095	0,97	1- Aminocyclohexanecarboxylic acid
C7 H19 N3	145,156 5	0,43	Spermidine
C5 H10 N2 O3	146,069 1	0,92	L-Glutamine
C6 H14 N2 O2	146,104 8	0,64	L-Lysine
C5 H9 N O4	147,053 8	0,90	Glutamic acid
C5 H11 N O2 S	149,051 2	1,00	L-Methionine
C5 H5 N5 O	151,048 8	0,99	2-Hydroxyadenine
C5 H4 N4 O2	152,033 6	1,47	Xanthine/Alloxanthine
C7 H8 N2 O2	152,059 7	1,52	N1-Methyl-4-pyridone-5-carboxamide
C7 H8 N2 O2	152,058 3	1,42	N1-Methyl-2-pyridone-5-carboxamide
C8 H11 N O2	153,079 2	0,78	Dopamine/1-(4-Hydroxyphenyl)-2-aminoethanol/Vanillylamine
C6 H9 N3 O2	155,069 3	0,67	L-Histidine
C7 H16 N2 O2	160,121 1	0,65	N6-Methyl-L-lysine /Putreanine
C7 H15 N O3	161,105 3	0,76	Carnitine
C6 H10 O5	162,052 8	1,55	Glucosan/3-Hydroxyadipic acid/3-Hydroxy-3-methylglutarate/[FA hydroxy(6:0/2:0)] 2-hydroxy-Hexanedioic acid
C6 H14 N2 O3	162,100 7	0,66	DL-5-hydroxylysine
C6 H12 O5	164,067 8	1,55	6-Deoxy-L-galactose
C5 H11 N O3 S	165,047 2	0,99	L-Methionine S-oxide
C6 H7 N5 O	165,065 3	0,74	Methylguanine
C9 H11 N O2	165,079 1	0,94	Phenylalanine
C9 H13 N O2	167,094 5	0,75	3-Dehydroxycarnitine Adduct/1-(4-Hydroxyphenyl)-2-(methylamino)ethanol/Phenylephrine/3-Methoxytyramine
C5 H4 N4 O3	168,028 6	1,56	Urate
C7 H11 N3 O2	169,085 6	0,78	N(pi)-Methyl-L-histidine

Formula	Mass	RMT	Compound Name (Putative)
C7 H11 N3 O2	169,085 4	0,69	3-Methylhistidine
C6 H11 N3 O3	173,081 7	1,01	5-Guanidino-2-oxopentanoate
C6 H10 N2 O4	174,064 4	0,92	N-Formimino-L-glutamate
C6 H13 N3 O3	175,096 3	0,91	Citrulline
C6 H10 O6	178,048 6	1,58	Glucono-1,5-lactone
C6 H13 N O5	179,079 5	0,81	D-Glucosamine
C8 H8 N2 O3	180,054 2	1,21	Nicotinurate
C9 H11 N O3	181,074	0,96	Tyrosine
C9 H21 N3 O	187,168 4	0,59	N8-Acetylspermidine/N1-Acetylspermidine
C8 H16 N2 O3	188,116 3	0,86	N6-Acetyl-L-lysine/Glycyl-leucine
C9 H20 N2 O2	188,152 1	0,66	N6,N6,N6-Trimethyl-L-lysine
C10 H7 N O3	189,042 9	1,72	Kynurenate
C7 H14 N2 O4	190,094 3	0,98	meso-2,6-Diaminoheptanedioate
C6 H8 O7	192,027 3	1,62	Citrate/Isocitrate
C9 H10 N2 O3	194,069 4	0,88	4-Aminohippuric acid
C6 H12 O7	196,058 9	1,58	D-Gluconic acid/Galactonicacid/1-3-Dimethyluricacid/1-7-Dimethyluricacid
C8 H18 N4 O2	202,143	0,71	NG,NG-Dimethyl-L-arginine(ADMA)
C10 H26 N4	202,214 7	0,42	Spermine
C11 H12 N2 O2	204,089 8	0,94	Tryptophan
C10 H12 N2 O3	208,084 8	0,87	L-Kynurenine
C8 H10 N4 O3	210,075 2	1,56	1,3,7-Trimethyluric acid
C10 H19 N O4	217,131 6	0,78	Propanoyl-L-carnitine
C7 H14 N2 O4 S	222,068 2	0,87	L-Cystathionine
C9 H14 N4 O3	226,106 9	0,63	Carnosine

Formula	Mass	RMT	Compound Name (Putative)
C11 H20 N2 O3	228,1474	0,84	Leucyl-Proline
C11 H21 N O4	231,1473	0,83	Isobutyryl-L-carnitine/O-Butanoylcarnitine
C9 H11 N5 O3	237,0854	1,05	Biopterin
C6 H12 N2 O4 S2	240,0243	0,94	Cystine
C10 H16 N4 O3	240,1214	0,63	Homocarnosine/beta-Alanyl-N(pi)-methyl-L-histidine
C10 H15 N3 O5	257,1024	0,86	5-Methylcytidine
C11 H19 N O6	261,1231	0,87	Methylglutarylcarnitine
C13 H16 N2 O4	264,1111	1,58	Formyl-N-acetyl-5-methoxykynurenamine
C8 H16 N2 O4 S2	268,0559	0,96	Homocystine
C12 H21 N O6	275,1368	0,88	Glutarylcarnitine
C11 H21 N3 O5	275,1482	0,85	Epsilon-(gamma-Glutamyl)-lysine
C11 H15 N5 O4	281,1128	0,87	2'-O-Methyladenosine/1-Methyladenosine
C15 H27 N O4	285,1926	0,85	2-Octenoylcarnitine
C14 H30 N4 O2	286,2371	0,68	N1,N12-Diacetylspermine
C11 H17 N3 O6	287,1128	0,80	N-Ribosylhistidine
C14 H18 N2 O5	294,1224	1,07	Glutamylphenylalanine
C8 H15 N3 O5 S2	297,0464	0,84	L-Cysteinylglycinedisulfide
C11 H15 N5 O3 S	297,0913	0,87	5'-Methylthioadenosine
C11 H15 N5 O5	297,1073	1,03	1-methylguanosine
C11 H19 N O9	309,1061	1,67	N-Acetylneuraminate
C12 H17 N5 O5	311,1229	1,02	N2-N2-Dimethylguanosine
C17 H31 N O4	313,2222	0,88	9-Decenoylcarnitine
C12 H24 N2 O8	324,1538	0,78	Galactosylhydroxylysine

Formula	Mass	RMT	Compound Name (Putative)
C12 H22 O11	342,1172	1,55	Lactose
C17 H26 N6 O4	378,2026	1,57	Pentosidine
C14 H17 N5 O8	383,1081	1,19	Succinyladenosine
C18 H34 N2 O13	486,2068	0,86	Glucosylgalactosylhydroxylysine
C24 H42 O21	666,2217	1,56	Glycogen

Supplementary Table A.2.3 Amino acid quantification in urine samples

https:www.nature.com/articles/s413900-021-01552-z#Sec16

Supplementary Table A.2.4 Altered metabolites in urine samples from newborns with pathologic vs. normal MRI results.

https:www.nature.com/articles/s413900-021-01552-z#Sec16.

A.3 Targeted Metabolomics data and miRNA-seq assessment from HIE newborns during hypothermia treatment

No supplementary data.

A.4 Effect of donor human milk on host-gut microbiota and metabolic interactions in preterm infants

Supplementary Table A.4.1 Inclusion and exclusion criteria of preterm infants receiving OMM or DHM during hospitalization.

Inclusion criteria	Exclusion criteria
BW ≤1500 g and GA ≤32 weeks	GA >32 weeks or BW >1500 g
Enteral intake ≥150 mL/kg/day	Parents refuse to participate/sign informed consent
The principal nutrient received (OMM, DHM) was ≥80% of the total intake	Mixed breastfeeding
DHM from a maximum of two donors to one premature infant	Chromosomopathies
No additional treatments that could alter the microbiome (e.g. probiotics) or oxidative status (e.g. vitamin supplements)	Major malformations or surgery of the digestive tract

BW, birth weight; GA, gestational age.

Supplementary Table A.4.2 Molecular formula, KEGG ID and steroid hormones found in urine samples

RT [min]	*m/z*	Mol Formula	Species	*P*-value (FDR)	KEGG IDs
4.01	184.0976	C21H28O4	M+H[1+]	0.04	C05490
4.55	137.0966	C18H24O2	M+2H[2+]	0.04	C00951
4.88	551.2783	C27H46O4S	M+HCOOK[1+]	0.04	C18043
5.23	321.2061	C19H26O3	M+H2O+H[1+]	0.03	C05284, C05140, C05290, C05295, C05302
5.46	259.2063	C19H28O3	M-HCOOH+H[1+]	0.04	C05139, C05294, C18045, C18075
5.69	306.2143	C19H28O3	M(C13)+H[1+]	0.03	C05139, C05294, C18045, C18075
5.74	316.2351	C21H30O2	M(C13)+H[1+]	0.04	C00410
5.76	303.1955	C19H26O3	M+H[1+]	0.03	C05284, C05140, C05290, C05295, C05302
5.76	304.1994	C19H26O3	M(C13)+H[1+]	0.03	C05284, C05140, C05290, C05295, C05302
5.81	255.2106	C19H30O2	M-H4O2+H[1+]	0.03	C04295, C00523, C03917, C04373, C05293
6.04	287.2010	C19H26O2	M+H[1+]	0.03	C00280
6.05	269.1901	C19H28O3	M-H4O2+H[1+]	0.04	C05139, C05294, C18045, C18075
6.12	465.2484	C25H36O8	M+H[1+]	0.02	C11134
6.12	466.2519	C25H36O8	M(C13)+H[1+]	0.03	C11134
6.16	253.1956	C19H28O2	M-H4O2+H[1+]	0.04	C01227, C00674, C03772
6.16	297.2217	C21H32O3	M-H4O2+H[1+]	0.04	C05485, C04518, C05138, C18038, C18040
6.17	289.2165	C19H28O2	M+H[1+]	0.03	C01227
6.21	289.1803	C18H24O3	M+H[1+]	0.04	C05141, C05301
6.41	283.2426	C21H34O2	M-H4O2+H[1+]	0.05	C13712, C05480, C18041

Supplementary Table A.4.3 Molecular formula, KEGG ID and steroid hormones found in HM samples.

RT [min]	*m/z*	Mol Formula	Species	*P*-value (FDR)	KEGG IDs
0.30	547.2132	C25H34O9	M+HCOONa[1+]	0.02	C11131
3.44	337.2739	C21H34O2	M+H2O+H[1+]	0.03	C05480, C13712, C18041
3.90	311.2582	C19H32O2	M+H2O+H[1+]	0.014	C03852
4.17	245.2264	C21H32O2	M-C3H4O2+H[1+]	0.013	C01953, C03681, C05479
4.17	337.274	C21H34O2	M+H2O+H[1+]	0.03	C05480, C13712, C18041
4.73	339.2897	C21H36O2	M+H2O+H[1+]	0.02	C18042
4.90	339.2894	C21H36O2	M+H2O+H[1+]	0.04	C18042
5.03	337.2739	C21H34O2	M+H2O+H[1+]	0.02	C05480, C13712, C18041
5.04	245.2266	C21H32O2	M-C3H4O2+H[1+]	0.02	C01953, C03681, 05479
5.60	339.2897	C21H36O2	M+H2O+H[1+]	0.04	C18042

A.5 A reductive metabolic switch protects infants with congenital heart defect undergoing atrial septostomy against oxidative stress.

No supplementary data.

Articles included in the compendium

metabolites

MDPI

Article

Metabolic Phenotypes of Hypoxic-Ischemic Encephalopathy with Normal vs. Pathologic Magnetic Resonance Imaging Outcomes

José David Piñeiro-Ramos [1], Antonio Núñez-Ramiro [2], Roberto Llorens-Salvador [3], Anna Parra-Llorca [1], Ángel Sánchez-Illana [1], Guillermo Quintás [4,5], Nuria Boronat-González [2], Juan Martínez-Rodilla [1], Julia Kuligowski [1,*], Máximo Vento [1,2,†] and The HYPOTOP Study Group ‡

1 Neonatal Research Group, Health Research Institute Hospital La Fe, Avenida Fernando Abril Martorell 106, 46026 Valencia, Spain; jose_pineiro@iislafe.es (J.D.P.-R.); annaparrallorca@gmail.com (A.P.-L.); asanchezillana@gmail.com (Á.S.-I.); juan.martinez.rodilla@gmail.com (J.M.-R.); maximo.vento@uv.es (M.V.)
2 Division of Neonatology, University & Polytechnic Hospital La Fe, Avenida Fernando Abril Martorell 106, 46026 Valencia, Spain; aguillermo9nr@hotmail.com (A.N.-R.); nubogon@hotmail.com (N.B.-G.)
3 Division of Radiology and Imaging, University & Polytechnic Hospital La Fe, Avenida Fernando Abril Martorell 106, 46026 Valencia, Spain; llorens_rob@gva.es
4 Health & Biomedicine Unit, Leitat Technological Center, Parc Cientific Barcelona, 08028 Barcelona, Spain; gquintas@leitat.org
5 Unidad Analítica, Health Research Institute La Fe, Avenida Fernando Abril Martorell 106, 46026 Valencia, Spain
* Correspondence: julia.kuligowski@uv.es; Tel.: +34-961-246-661
† Senior author, Tel.: +34-961-245-688.
‡ The members of the HYPOTOP study group are listed in Appendix A.

Received: 11 February 2020; Accepted: 12 March 2020; Published: 14 March 2020

check for updates

Abstract: Hypoxic-Ischemic Encephalopathy (HIE) is one of the most relevant contributors to neurological disability in term infants. We hypothesized that clinical outcomes of newborns with (HIE) can be associated with changes at plasma metabolic level enabling the detection of brain injury. Plasma samples of a cohort of 55 asphyxiated infants who evolved to moderate/severe HIE were collected between birth and completion of therapeutic hypothermia (TH). Samples were analyzed employing a quantitative gas chromatography–mass spectrometry method for the determination of lactate and pyruvate and an untargeted liquid chromatography–time-of-flight mass spectrometry method for metabolic fingerprinting. Brain injury was assessed employing magnetic resonance imaging (MRI). A critical assessment of the usefulness of lactate, pyruvate, and pyruvate/lactate for outcome prediction was carried out. Besides, metabolic fingerprinting identified a dynamic perturbation of eleven metabolic pathways, including amino acid and purine metabolism, and the steroid hormone biosynthesis, in newborns with pathologic MRI outcomes. Although data suggest the usefulness of lactate and pyruvate monitoring during 72 h for discerning outcomes, only the steroid hormone biosynthesis pathway was significantly altered in early plasma samples (i.e., before the initiation of TH). This study highlights pathways that might potentially be targeted for biomarker discovery or adjuvant therapies to be combined with TH.

Keywords: liquid chromatography–time-of-flight mass spectrometry (LC-TOFMS); neonatal brain injury; perinatal asphyxia; untargeted metabolomics

1. Introduction

Hypoxic-Ischemic Encephalopathy (HIE) is the neurological consequence of impaired blood flow and/or gas exchange during birth [1]. Decreased cerebral perfusion and oxygenation trigger a sequence of acute cerebral metabolic alterations that characterize the primary energy failure phase of HIE. After resuscitation, the process undergoes a latent phase that lasts up to 6 h. This stage is followed by a secondary energy failure phase that enhances cerebral injury and may last for days, weeks, or even months [2].

HIE is one of the most relevant contributors to neurological disability in the pediatric age. In high-income countries, the incidence of HIE is around 1.6 per 1000 infants, while the risk is around 10-fold higher in low-income countries [3]. Therapeutic hypothermia (TH) initiated within 6 h of birth constitutes the standard of care for infants with moderate or severe HIE reducing mortality and improving neurodevelopmental outcome in survivors [4].

At present, no bedside test is available for an accurate and early diagnosis of HIE. In the delivery room, physicians rely on prenatal clinical information and serial Apgar scores with special emphasis on neurological assessment. In addition, cord blood gases, metabolic acidosis, and increased lactacidemia further reflect the severity of anaerobic metabolism [2]. The modified Sarnat staging system grades neonatal HIE according to the severity of the brain insult [5]. Later on, amplitude-integrated electroencephalography (aEEG) and/or multichannel EEG and cranial ultrasound will confirm the diagnosis [6]. Magnetic resonance imaging (MRI), including diffusion weighted imaging and spectroscopy, performed 5–7 days after birth, is the cornerstone for neurodevelopmental outcome prediction [7]. Particularly, time-dependent reductions in brain N-acetyl aspartate and creatinine concentrations at 18–96 h and 7–14 days are able to accurately predict adverse outcomes, whereas elevated cerebral lactate, glutamate, and glutamine concentrations have been found to be transient [8]. However, unstable neonates may not tolerate transport necessary for MRI or MRI scanning duration. Moreover, hypothermia may alter EEG recordings and limit its early predictive capacity [2].

HIE has been associated with damage to the integrity of the blood–brain barrier and, hence, brain injury could be reflected in peripheral blood samples [9]. In the search for blood biomarkers capable of determining the degree of brain injury and providing prognostic information, an array of different molecules has been proposed including neuronal tissue specific proteins, proteins involved in the pathogenesis of traumatic brain injury, excitatory amino acids, lipid peroxidation products, specific microRNAs, and inflammatory markers [2,6]. Despite the potential of these markers, few small pilot studies have validated their utility in the clinical practice [10] and none has been added to clinical guidelines [11].

Blood lactate, a hallmark of anaerobic metabolism, has been traditionally employed as surrogate marker for tissue hypoxia and/or ischemia. Pyruvate dehydrogenase controls the metabolic flux between the tricarboxylic acid cycle and glycolysis. Under hypoxic conditions, glucose is metabolized into lactate and exported to the extracellular compartment [12]. In infants with moderate/severe brain injury, a very strong correlation was found between serum and cerebral lactate concentrations at the basal ganglia, thalamus, and gray matter regions during TH [12]. It has been suggested that monitoring lactate could be useful for assessing the degree of HIE and even predict long-term neurodevelopmental outcomes [13]. However, these speculations were not based on adequately powered clinical studies.

Comprehensive metabolic phenotyping has been increasingly employed for identifying possible therapeutic targets, and the discovery of biomarkers to support treatment selection, patient stratification, and enhanced diagnosis [11]. However, metabolomics has only been scarcely used for progressing our understanding of the multilayer effects of HIE and TH on the newborn [14]. ^{1}H-nuclear magnetic resonance was used to characterize umbilical cord blood samples from infants with perinatal asphyxia or HIE compared to matched healthy controls, revealing significant changes in 18 metabolites [15]. A panel of four metabolites showed potential for predicting HIE severity according to Sarnat staging; however, it was not found to be superior to EEG or the Sarnat score for predicting neurodevelopmental outcome at three years of age [16]. Umbilical cord blood of a similar cohort of newborns with signs of

perinatal asphyxia and HIE as well as matched healthy controls was studied employing direct infusion Fourier-transform ion cyclotron resonance mass spectrometry (MS) [17]. Eight putatively annotated metabolites were identified to be significantly altered in newborns with HIE and four metabolites differentiated across severity grades of HIE based on continuous multichannel EEG monitoring at 24 h of life. In a longitudinal study involving six infants with mild/severe HIE, a specific metabolic profile was identified in urine samples as compared to healthy control subjects on Days 1 and 3 after birth [18].

The aim of this study was to elucidate dynamic metabolic changes in a cohort of newborn infants evolving to moderate/severe HIE undergoing TH in which hypoxia–ischemia-induced brain injury was assessed employing MRI. This study describes for the first time the evolution of the neonatal plasma metabolome of HIE covering the time period between birth and completion of TH treatment. The objectives of the present study were focused on preselecting disease-specific pathways at the phenotypic level that might be suitable for enabling an identification of those infants at risk of developing brain injury within the infants that qualify for hypothermia treatment as well as for monitoring the individual response to treatment and elucidating new potential therapeutic targets.

2. Results

2.1. Patient Characteristics

Population characteristics are shown in Table 1. There were only minor, non-significant differences between the control and the pathologic group, i.e., a higher proportion of males in the control group (59% vs. 42%) and higher proportion of C-section in the pathologic group (64% vs. 41%). Regarding the Sarnat staging, in the normal group, 86% of infants were initially identified as Sarnat 2, whereas, in the pathologic group, the proportion was 58% (p-value = 0.05). Although the analysis of the effect of topiramate vs. placebo was out of the scope of this study, the inclusion of a similar proportion of individuals from both treatment groups (p-value = 0.7) allowed compensating for the impact (confounder) of potential effects of pharmacological treatment on the metabolome.

Table 1. Clinical and demographic data of newborns.

Parameter	Normal (N = 22)	Pathologic (N = 33)	p-Value
Inborn	3 (14%)	8 (24%)	0.5
Maternal age (years)	34 (5)	33 (6)	0.4
Gestational age (weeks)	38.4 (37.3, 40.6)	39.0 (38.0, 40.6)	0.3
Gender (male, %)	13 (59%)	14 (42%)	0.3
Birth weight (g)	3265 (552)	3295 (697)	0.4
Length (cm)	51 (3)	51 (3)	0.4
Head circumference (cm)	34 (2)	34 (2)	0.3
Delivery mode (C-section)	9 (41%)	21 (64%)	0.2
Apgar score 1 min	2 (1, 4)	1 (1, 3)	0.6
Apgar score 5 min	4 (2, 5)	3 (1, 5)	0.3
Apgar score 10 min	5 (4, 6)	5 (4, 6)	1.0
Sarnat 2/Sarnat 3	19/3	19/14	0.05
pH UC	7.06 (0.27)	6.97 (0.17)	0.09
BE UC	−13 (10)	−16 (7)	0.2
pCO_2 (mmHg) UC	71 (33)	59 (33)	0.2
HCO_3 UC	15 (6)	13 (6)	0.2
Topiramate treatment (yes, %)	10 (45%)	17 (52%)	0.7
MR (days)	7 (5, 10)	7 (7, 10)	0.4

Note: Values are mean (SD), median (interquartile range), or n (%); p-values have been calculated employing the Student's t-test for unequal variances (α = 0.05), the Wilcoxon rank sum test (α = 0.05) or the χ^2-test (α = 0.05); UC, umbilical cord; BE, base excess; MR, magnetic resonance; inborn refers to infants born at the hospital where hypothermia treatment was carried out.

2.2. Plasma Lactate and Pyruvate Levels

The evolution of lactate and pyruvate plasma concentrations as well as lactate/pyruvate with time are shown in Figure 1. For lactate, as well as pyruvate, median concentrations at all studied time points were higher in newborns with pathologic MRI outcomes. To assess the potential of lactate, pyruvate, and lactate/pyruvate levels determined in blood before the initiation of TH and 24, 48, and 72 h after initiation of TH for predicting pathologic MRI outcomes, groups were compared employing the Wilcoxon rank sum test. Newborns with pathologic MRIs had significantly higher levels of lactate at 24 and 48 h as well as pyruvate at 72 h. Lactate/pyruvate did not show a clear trend with time and was not useful for discriminating between normal and pathologic MRI outcomes at any studied time point.

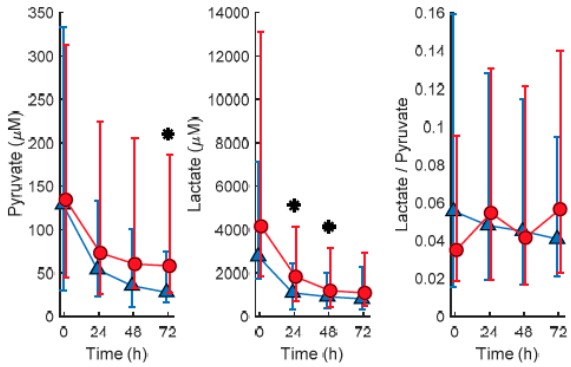

Figure 1. Evolution of pyruvate and lactate concentrations and lactate/pyruvate in plasma samples from newborns with normal (blue Δ and error bars are median and 25th and 75th percentile, respectively) and pathologic (red o and error bars are median and 25th and 75th percentile, respectively) MRI outcomes. Note: normal vs. pathologic at 0 h N = 13 and 23; at 24 h N = 20 and 30; at 48 h N = 22 and 28; and at 72 h N = 20 and 32, respectively; * indicates p-vales below 0.05 (Wilcoxon rank sum test) for comparing normal vs. pathologic MRI outcomes; blood samples were extracted at birth and at 24, 48, and 72 h after the administration of the first dose of medication/placebo.

2.3. Untargeted Metabolomic Analysis

Figure 2 shows the Principal Component Analysis (PCA) scores plot of plasma metabolomic analysis collected at the different time points. The strong impact of time on the plasma metabolome can be observed in direction of principal component (PC) 2 (9.5% of the total variance). Based on this observation, further data analysis was stratified by the sampling time point.

Figure 3 shows the number of features with different mean values (t-test, $\alpha = 0.05$) comparing normal vs. pathologic outcomes as determined by MRI. It can be observed that the number of altered features increases with time. Whereas 208 (2.6%) of the total of 8122 detected features showed different mean concentrations in blood before the initiation of TH, 24 h after the initiation of TH, already 491 (6.0%) were altered; 48 h and 72 h after the initiation of TH, this value further increased to 1228 (15.1%) and 1330 (16.4%), respectively. Furthermore, the pattern of affected metabolites shifted over time with only 65 of the altered features shared between blood before the initiation of TH and 24 h samples, 279 between 24 and 48 h samples, and 776 between 48 and 72 h samples. This indicates that the alteration of the metabolome in newborns with pathologic MRI outcomes rapidly changes at early time points and slowly stabilizes thereafter. In Figure 4, heat maps of the intensities of 2071 metabolic features that showed different distributions between normal and pathologic groups in at least one of the sampling times are depicted. Visual inspection of heat maps confirms an increase of HIE specific plasma metabolite patterns with time: whereas no clear patterns are observed from

metabolites detected in blood before the initiation of TH, differences are visible after 24 h and become more evident after 48 and 72 h.

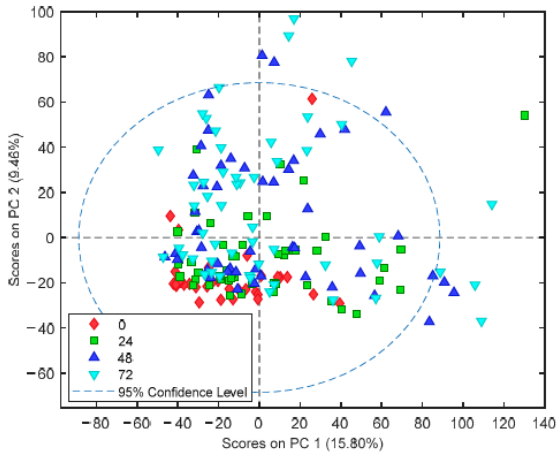

Figure 2. PCA scores plot of plasma metabolomic fingerprints. Note: Blood samples were extracted at birth and at 24, 48, and 72 h after the administration of the first dose of medication/placebo.

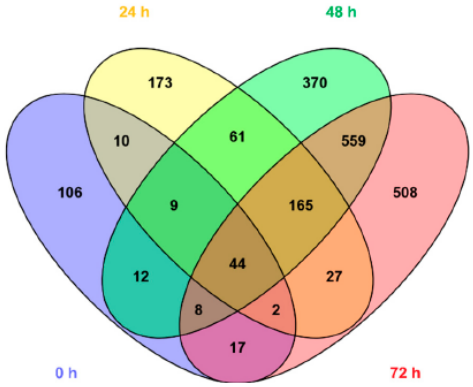

Figure 3. Venn diagram showing the overlap among altered metabolic features in plasma samples collected 0, 24, 48, and 72 h. Note: Blood samples were extracted at birth and at 24, 48, and 72 h after the administration of the first dose of medication/placebo.

Table 2 summarizes the metabolic pathways significantly altered in at least one of the studied time points and Table S1 shows the annotation of altered metabolites detected in plasma samples from newborns with HIE and normal vs. pathologic MRI outcomes. In line with previous observations, different pathways were affected in blood before the initiation of TH as compared to the remaining sampling times. Again, the number of altered pathways varies with time with three, two, five, and nine altered pathways in the first blood sample collected, and 24, 48, and 72 h after the initiation of TH,

respectively. In blood collected before the initiation of TH, purine, seleno amino acid metabolism, and steroid hormone synthesis were affected in newborns with pathologic MRI outcomes. Later, additional pathways mainly related to amino acid metabolism were altered. Only one metabolic pathway, i.e., steroid hormone biosynthesis, remained altered during the whole study period. Figure 5 shows the steroid hormone synthesis pathway and its intermediates highlighting metabolites detected and/or altered in this study at the four studied time points.

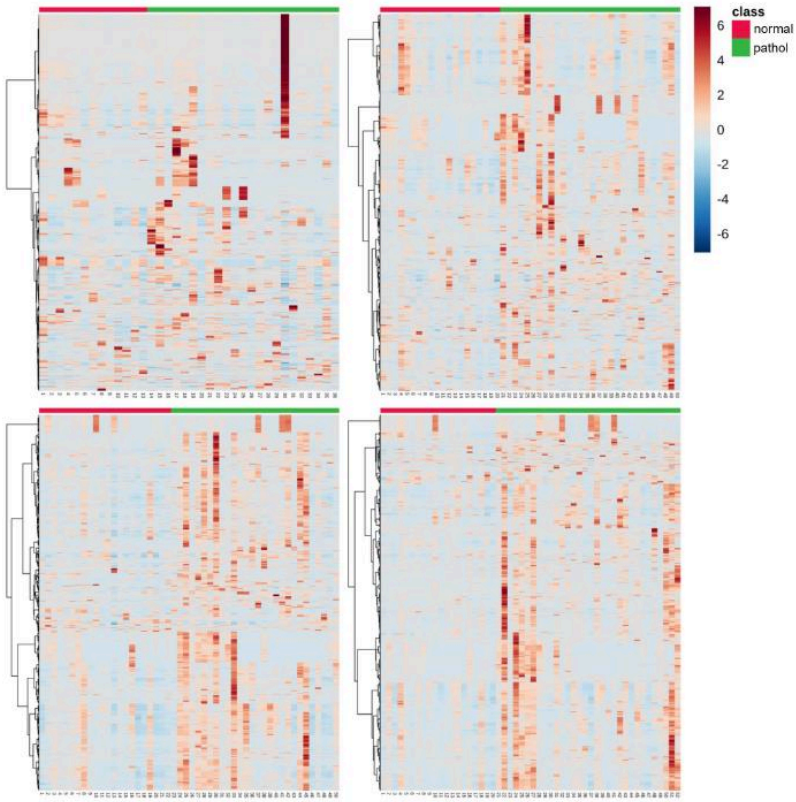

Figure 4. Heat maps of altered plasma metabolic features (N = 2071) in samples collected at: 0 h (top, left); 24 h (top, right); 48 h (bottom, left); and 72 h (bottom, right). Note: normal vs. pathologic at 0 h N = 13 and 23; at 24 h N = 20 and 30; at 48 h N = 22 and 28; and at 72 h N = 20 and 32, respectively; blood samples were extracted at birth and at 24, 48, and 72 h after the administration of the first dose of medication/placebo.

Table 2. Altered pathways in newborns suffering from HIE with pathologic MR outcomes.

Pathway	Total # of Metabolites	Hits (Total)	T0		T24		T48		T72	
			Hits (Sig)	Fisher's *p*-Value	Hits (Sig)	Fisher's *p*-Value	Hits (Sig)	Fisher's *p*-Value	Hits (Sig)	Fisher's *p*-Value
Alanine, aspartate, and glutamate metabolism	24	19	6	0.14	5	0.9	13	0.4	16	0.04
Arginine and proline metabolism	77	50	10	0.5	21	0.4	41	0.002	41	0.003
Caffeine metabolism	21	2	2	0.04	2	0.2	2	0.4	2	0.4
D-Glutamine and D-glutamate metabolism	11	7	1	0.8	3	0.6	7	0.03	7	0.04
Limonene and pinene degradation	59	7	2	0.4	1	1.0	4	0.7	7	0.04
Lysine biosynthesis	32	20	3	0.8	11	0.10	17	0.02	19	0.0013
Lysine degradation	47	32	7	0.4	17	0.07	21	0.4	28	0.002
Nitrogen metabolism	39	16	4	0.4	7	0.4	11	0.4	14	0.03
Phenylalanine metabolism	45	25	5	0.5	15	0.02	24	0.00009	21	0.02
Seleno amino acid metabolism	22	2	2	0.04	1	0.6	2	0.4	2	0.4
Steroid hormone biosynthesis	99	29	11	0.01	23	0.000009	25	0.004	25	0.006

Note: Results with a Fisher's *p*-value < 0.05 are gray-shaded.

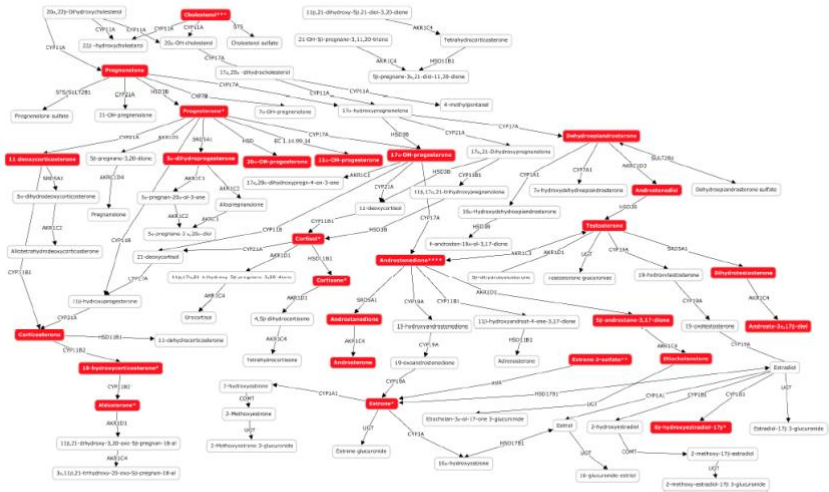

Figure 5. Altered metabolites of the steroid hormone biosynthesis pathway in plasma samples from newborns suffering from HIE at birth and 24, 48, and 72 h after the administration of the first dose of medication/placebo. Note: * altered only at 24, 48, and 72 h; ** altered only at 48 and 72 h; *** altered only at 48 h; **** altered only at 72 h.

3. Discussion

The HYPOTOP trial was designed to minimize shortcomings of single center trials, thus improving the generalizability of the observations. This is underpinned by the homogeneity of the clinical and demographic parameters between both study groups (normal vs. pathologic MRI outcome), as shown in Table 1. For the quantitative determination of lactate and pyruvate, a targeted gas chromatography–mass spectrometry (GC-MS) method was used, whereas untargeted fingerprinting was carried out using LC-TOFMS. For lactate and pyruvate concentrations in plasma samples collected before the initiation of TH, poor predictive values were found, whereas, during TH, lactate (24 and 48 h) and pyruvate (72 h) were able to discriminate between newborns with confirmed brain injury and normal outcomes, as shown in Figure 1. Optimum cut-off values from receiver operating characteristic (ROC) curves of 1.1 mM and 51.4 µM for lactate at 24 and 48 as well as pyruvate at 72 h, respectively, were obtained for the discrimination between both groups. The difference in concentration levels of lactate between newborns with normal and pathologic MRI outcomes decreased over time, whereas an increase was noted for pyruvate concentrations. Due to the high capacity for lactate transport into and out of the brain, blood lactate has been employed as surrogate marker for brain tissue hypoxia and/or ischemia. It has been demonstrated that serum lactate strongly correlates with cerebral lactate concentrations at the basal ganglia, thalamus, and gray matter regions measured during TH in newborns with moderate to severe brain injury [12]. In accordance with findings on blood lactate, the relative increase in serum lactate dehydrogenase concentrations between Days 1 and 3 was associated with central gray matter lesions [19]. Moreover, lactate and pyruvate concentrations were found to be elevated in plasma from newborns with HIE undergoing TH at 48 h as compared to a control group of healthy term infants [20] and serum lactate was significantly elevated at 72 h of life in newborns with poor neurodevelopmental outcomes [21]. Lactate levels acquired within the first hour of life in combination with serial measurements of lactate have been proposed as predictors of moderate/severe HIE [22] and prolonged time to normalization of serum lactate occurred in severe HIE with prolonged electrographic seizures [23]. In contrast, to date, no literature is available on blood pyruvate levels in newborn infants with HIE. In experimental studies, both concentrations of cerebral pyruvate and lactate were found to be elevated in hypoxia and hypoxia–ischemia [13].

A complementary analytical approach aimed at exploiting the potentials of untargeted metabolomic fingerprinting for enhancing the current understanding of the complex perturbations of hypoxia–ischemia on the individual, phenotypic level and its impact on the pathophysiology of HIE. The importance of repeated phenotypic monitoring should be highlighted as it is well known that HIE passes through different phases and TH induces a reduction in cerebral and whole-body metabolism [2]. Furthermore, the transition of the neonate from hypoxic in utero conditions to a relatively oxygen-rich environment induces changes in the metabolome. In an animal model, 23% of the detected metabolites showed a significant change in concentration when comparing umbilical cord blood to blood samples drawn until 72 h after birth [24]. In the present study, a clear effect of the time elapsed from birth until sample collection has been observed (see Figure 2), with the pattern of injury becoming more visible as time evolves (see Figure 3; Figure 4). This was further corroborated by the results of pathway analysis shown in Table 2 and Table S1, where an upward trend in the number of altered pathways with time was observed while the pattern of injury emerges during secondary energy failure.

We demonstrated that the early evolving blood metabolome provides useful information for the discrimination of newborns who will show pathologic MRI patterns after TH. In the first blood sample analyzed in this study, collected before initiation of TH, levels of two metabolites of the purine metabolism, i.e., xanthine and its derived nucleoside xanthosine, were found to be altered. Purine metabolism has been described repeatedly to be affected in animal experiments on hypoxia/reoxygenation [25] as well as newborns with HIE [17]. Interestingly, xanthine is an oxygen-dependent downstream product of hypoxanthine, which in turn is a hallmark of hypoxia and has been identified as a free radical generator, playing a key-role in oxidative stress-associated diseases of the newborn [25]. Furthermore, the steroid hormone biosynthesis pathway was affected

over the whole study period in newborns with HIE and pathological MRI outcomes, but became especially relevant during TH. In agreement with our observations (see Table S1), a significant increase of neonatal 17-hydroxyprogesterone levels has been reported in blood samples from infants suffering from birth asphyxia and neonatal seizures [26]. Although the influence of drugs administered for sedation, or antibiotics and vasopressor drugs cannot be ruled out, the observed effect might likely be linked to the response to stress and pain that inevitably triggers a hormonal response affecting epinephrine, norepinephrine, and cortisol levels. On the other hand, the use of hormones has been proposed as therapeutic drugs in the context of HIE. In experimental studies, the administration of glucocorticoids [27] and progesterone [28] ameliorated neonatal hypoxic-ischemic brain injury.

At later time points in samples collected during TH, a total of eight pathways involving amino acid metabolism, synthesis, and degradation have been observed to be perturbed when comparing between normal vs. pathologic groups. In the literature, several reports on the perturbation of amino acids in hypoxia and hypoxia–ischemia in experimental models and neonates can be found [14] and the accumulation of excitatory amino acids (glutamate and aspartate) in cerebral tissue during the acute phase as well as secondary energy failure have been extensively described [2]. In umbilical cord blood of newborns with HIE in comparison to a healthy control group, alanine, aspartate, and glutamate metabolism, as well as phenylalanine metabolism, were found to be altered [17] and changes in metabolite levels involved arginine and proline metabolism (i.e., proline [29]), nitrogen metabolism (i.e., phenylalanine [29] and tryptophan [17]), and phenylalanine metabolism (i.e., phenylalanine [29] and succinate [15–17]) were observed.

This study has some limitations. Although TH is a routine clinical practice, patients need to be transferred to level III NICUs to receive this treatment. Consequently, umbilical cord blood could not be collected from these patients. This is an intrinsic problem of studies on infants with HIE and the exclusion of outborn infants would dramatically increase the time needed for the recruitment of a representative number of subjects. In addition, this study does not include a healthy control group or newborns with asphyxia or classified as mild HIE (Sarnat 1), as only newborns subjected to hypothermia treatment were included. There is risk of adverse neurodevelopmental outcome of mild HIE newborns, but, up to now, there is no evidence to support cooling in these babies, and therefore we consider that the study of the metabolic fingerprint of those infants in correlation with the clinical outcomes would be of interest [30]. Furthermore, metabolomic coverage could be increased by taking advantage of complementary methods and analytical platforms. The use of complementary methodological approaches might help to achieve a more comprehensive view of the global effects of HIE on the plasma metabolome. Before the findings described in this study can be translated to the clinic, an exhaustive validation of the results is necessary involving the identification and quantification with primary standards following guidelines of regulators such as the U.S. Food & Drug Administration and European Medicines Agency.

We report the first metabolomic study involving human subjects and serial sample collections in HIE for modeling brain injury as confirmed with MRI. Herein, the time-dependent evolution of lactate and pyruvate levels in newborns with HIE undergoing TH is shown. Our data underpin the usefulness of blood lactate with a cut-off value of 1.1 mM between 24 and 48 h and pyruvate with a cut-off value of 51.4 μM at 72 h for anticipating favorable/unfavorable MRI outcomes. Although these findings need to be validated in independent cohorts, these biomarkers could be easily implemented within clinical routine care, as portable devices for point-of-care testing are commercially available. However, at very early sampling time points (before initiation of TH), the measurement of those parameters does not support outcome prediction. Metabolic pathway analysis revealed the time-dependent perturbation of several pathways. Purines (i.e., xanthine and xanthosine) were found to be altered in blood samples from newborns with pathologic MRI outcomes drawn before the initiation of TH and the steroid hormone biosynthesis pathway has been significantly altered during the whole study period comprising early samples collected shortly after birth and until completion of TH after 72 h. Hence, this study provides evidence of the usefulness of metabolites from both pathways as candidate biomarkers

to be evaluated in future clinical validation studies as they might allow an early prediction of central nervous system impairment reflected in an anatomic alteration detectable by MRI. In depth knowledge of metabolic alterations might furthermore support studies targeting the development of adjuvant therapies to be combined with TH, e.g., the administration of allopurinol and steroid hormones.

4. Materials and Methods

4.1. Study Approval

The study was approved by the Ethics Committee for Biomedical Research of the Health Research Institute La Fe (Valencia, Spain) and registered as EudraCT 2011-005696-17 under the abbreviation HYPOTOP. Informed consent was obtained from parents of all participants and all methods were performed in accordance with relevant guidelines and regulations.

4.2. Population

A cohort of 62 newborns enrolled in the HYPOTOP trial was included in this study according to pre-established inclusion and exclusion criteria. The HYPOTOP trial is a randomized, controlled, multicenter, double-blinded clinical trial aiming to assess the efficacy of topiramate vs. placebo in patients with HIE undergoing TH. A detailed description of the HYPOTOP trial including the study design and sample-size estimation can be found elsewhere [31].

4.3. Magnetic Resonance Imaging

MRI was performed between Days 4 and 8 after birth. It was carried out using a 3T magnet system (Signa Excite®, General Electric Healthcare, IL, USA) and always included 3D Gradient Echo T1 weighted MR images, coronal and axial Fast Spin Echo T2 weighted MR images, diffusion weighted images (b0 and b1000 values), and susceptibility weighted imaging. In most cases, single voxel MR spectroscopy in thalamus, white, and grey matter was acquired using PROBE sequence, as well as diffusion tensor imaging (32 directions). The score used to differentiate mild from moderate and severe HIE was based on the MR score described by Barkovich [32]. Acute hypoxic ischemic insult in basal ganglia and thalami (BGT) was classified as mild if focal injury with normal posterior limb of the internal capsule (PLIC) was seen; as moderate if multifocal BGT pattern and equivocal or normal PLIC was identified; and as severe when diffuse BGT patterns and abnormal PLIC was detected. To evaluate white matter injury as well as cortical injury, we defined mild injury when only periventricular white matter was involved and normal cortex was preserved, moderate when subcortical white matter and focal areas of cortical highlighting were identified, and severe when widespread abnormalities with extensive cortical involvement were described. MRI results were interpreted by experienced, blinded radiologists. Based on the results of MRI, patients were classified as "normal" ($N = 22$) or "pathologic" ($N = 33$) neuronal outcomes following the criteria explained elsewhere [33]. Seven patients were excluded from further analysis as no MRI results were available. Patient characteristics of the remaining 55 infants are shown in Table 1.

4.4. Blood Sampling, Processing and Storing

A 0.5 mL sample of whole blood was extracted at birth (umbilical cord blood, when available, or extracted as early as possible before the initiation of TH; $N = 36$) and at 24 ($N = 50$), 48 ($N = 50$), and 72 h ($N = 52$) after the administration of the first dose of medication or placebo from a peripheral vein using heparinized syringes (1% sodium heparin). Blood samples were centrifuged immediately at 1800× g and 20 °C during 10 min. Plasma was collected and stored at −80 °C until analysis.

In total, 188 samples were collected from 62 newborns with moderate or severe HIE. Patients were recruited at 13 sites following a stringent study protocol and written standard operating procedures to limit the probability of chance correlations due to bias, systematic errors, or flaws in the experimental design.

4.5. Analytical Methods

Sample analysis was centralized and performed by two blinded analytical chemists in randomized order.

4.5.1. Determination of Lactate and Pyruvate

The determination of lactate and pyruvate was carried out in plasma samples employing a two-step oximation–silylation procedure and a validated GC-MS method, employing a 6890 GC 5973N electron impact quadrupole MS system as described elsewhere [20].

4.5.2. Untargeted Metabolomic Analysis

Plasma samples were thawed on ice and homogenized on a Vortex S0200 mixer (LabNet, Edison, NJ, USA) during 10 s at maximum speed. Seventy-five microliters of cold (4 °C) CH_3OH were added to 25 µL of plasma and samples were centrifuged at 16,000 × *g* during 15 min at 4 °C. Eighty microliters of supernatant were collected and evaporated to dryness on a miVac centrifugal vacuum concentrator at room temperature and re-dissolved in 60 µL de H_2O:CH_3CN (0.1% *v/v* HCOOH) 95:5 containing phenylalanine-D_5, caffeine-D_9, leucine enkephalin, and reserpine, each at a concentration of 2 µM. Blank extracts were prepared by replacing whole blood with 500 µL of H_2O. A quality control (QC) sample was prepared by mixing 5 µL of each plasma sample and a total of 10 QC sample aliquots were processed as described for plasma samples.

Chromatographic separations were performed on an Agilent 1290 Infinity UHPLC chromatograph using a UPLC ACQUITY BEH C18 column (2.1 mm × 100 mm, 1.7 µm, Waters, Wexford, Ireland) and a flow rate of 400 µL min^{-1}. Autosampler and column temperatures were set to 4 and 40 °C, respectively, and an injection volume of 4 µL was used. Initial conditions of 98% of mobile phase A (H_2O (0.1% *v/v* HCOOH)) were kept for 0.5 min, followed by a linear gradient from 2% to 20% of mobile phase B (CH_3CN (0.1% *v/v* HCOOH)) in 3.5 min and from 20% to 95% B in 4 min. Conditions of 95% B were held for 1 min and a 0.25 min gradient was used to return to the initial conditions, which were held for 2.75 min.

Full-scan MS data between 100 and 1700 m/z with a scan frequency of 6 Hz (1274 transients/spectrum) were collected on an iFunnel quadrupole time-of-flight Agilent 6550 spectrometer operating in ESI^+ and TOF MS mode. The electrospray ionization parameters were set as follows: gas T, 200 °C; drying gas, 14 L min^{-1}; nebulizer, 37 psig; sheath gas T, 350 °C; sheath gas flow, 11 L min^{-1}. For automatic MS spectra re-calibration during analysis, a mass reference standard was introduced into the source via a reference sprayer valve using 149.02332 (background contaminant), 121.050873 (purine), and 922.009798 (HP-0921) *m/z* as references.

System suitability was checked employing a standard mixture containing internal standards. The analytical system was conditioned by injecting the QC extract 9 times at the beginning of the batch. Data acquired during system conditioning were discarded from data analysis. In total, 188 plasma sample extracts were analyzed in random order in a single analytical batch. QC samples were analyzed every 5th sample and twice at the beginning and end of the batch for assessment and correction of instrumental performance [34]. Furthermore, automated UHPLC-ESI(+)-QqTOF (MS/MS) analysis of the QC sample was performed using two collision energies (20 and 40 V) to support metabolite annotation. The blank extract was injected a total of 4 times and used for data clean-up with the aim of identifying signals from other than biological origin.

4.5.3. Statistics

Raw UHPLC-TOFMS data were converted into centroid mzXML format using ProteoWizard [35]. Metabolomics data have been deposited to the EMBL-EBI MetaboLights database with the identifier MTBLS1041 and the complete dataset can be accessed here [36]. A peak table was extracted using XCMS (version 3.4.2) [37] running in R (version 3.5). A total of 38014 features were initially detected

after peak detection, integration, chromatographic deconvolution, and alignment. The CAMERA [38] package was used for identifying peak groups and annotation of isotopes and adducts.

The obtained peak table was imported into MATLAB R2017b (Mathworks Inc., Natick, MA, USA) for further data processing and analysis. To reduce intra-batch variation, the Quality Control-Support Vector Regression algorithm [39] and the LIBSVM library [40] were applied using an ε–range of 2.5 to 7.5, a γ-range of 1 to 10^5. C was defined for each feature as the median value in QCs. Then, features detected in blanks (i.e., median peak area in QCs < 5 times the maximum value detected in blanks) and those with a RSD% in QC samples ≥20% were excluded. The final peak table contained 8122 features. Systematic identification of detected features was carried out by matching *m/z* values against the Human Metabolome Database (version 4.0) [41] with 5 ppm accuracy. To increase confidence in the identification, MS/MS fragmentation spectra were matched against reference spectra from HMDB and METLIN databases. Peak intensities of internal standards and QC samples were used for monitoring the instrumental response during data acquisition throughout the batch as described elsewhere [34,39].

MATLAB 2017b inbuilt functions as well as in-house written scripts (available from the authors upon reasonable request) and the PLS Toolbox 8.0 from Eigenvector Research Inc. (Wenatchee, WA, USA) were used for PCA, non-parametric Wilcoxon rank sum test, and *t*-test (α = 0.05, unequal variances). MetaboAnalyst (version 4.0) [42] was used for the construction of ROC curves, hierarchical clustering, and the generation of heat maps from auto scaled data employing Euclidean distance and Ward's method. As an input for pathway analysis, *t*-test *p*-values (α = 0.05, unequal variances) and fold changes were computed for each metabolic feature comparing normal and pathologic outcomes for each sampling time point separately. Pathway analysis was carried out using MetaboAnalyst with the "MS peaks to pathways" tool (mass accuracy = 5 ppm; *mummichog* algorithm with *p*-value cutoff set to the top 10% of peaks) and the Kyoto Encyclopedia of Genes and Genomes (KEGG) pathway library (*Homo sapiens*). Pathways with *p*-values from Fisher's exact *t*-test < 0.05 were considered as altered. Putative identifications based on *m/z* from pathway analysis were corroborated by manual inspection of raw data and MS/MS data when available ("level 2" identification as defined by The Metabolomics Standards Initiative [43]).

Supplementary Materials: The following are available online at http://www.mdpi.com/2218-1989/10/3/109/s1, Table S1: Annotation of altered metabolites. Note: Blue stands for detected, but not altered; red stands for altered; IDs of annotated metabolites marked with a star have been verified with MS/MS data.

Author Contributions: Conceptualization, M.V. and J.K.; methodology, M.V., G.Q., J.K., Á.S.-I., and J.D.P.-R.; software, G.Q., J.K., and J.D.P.-R.; validation, J.D.P.-R. and Á.S.-I.; formal analysis: J.M.-R., J.D.P.-R., and J.K.; investigation, A.N.-R., A.P.-L., N.B.-G., R.L.-S., Á.S.-I., J.D.P.-R., and the HYPOTOP study group; resources, G.Q., M.V., and J.K.; data curation, G.Q., J.M.-R., J.K., and J.D.P.-R.; writing—original draft preparation, J.K., J.D.P.-R., and G.Q.; writing—review and editing, M.V., Á.S.-I., and J.K.; visualization, J.K., J.D.P.-R., and G.Q.; supervision, J.K. and M.V.; project administration, J.K.; and funding acquisition, M.V. and J.K. All authors have read and agreed to the published version of the manuscript.

Funding: This research was funded by *Instituto de Salud Carlos III*, Ministry of Science and Innovation, Spain, grant numbers FI16/00380, CP16/00034, EC11-244, and PI17/00127.

Acknowledgments: The authors would like to express their gratitude to the parents and their newborns who participated in the study.

Conflicts of Interest: The authors declare no conflict of interest.

Appendix A

Members of the HYPOTOP Study Group: Isabel Izquierdo, Ana Gimeno, María Gormaz, Raquel Escrig, María Cernada, Marta Aguar, Ester Torres (Division of Neonatology, University and Polytechnic Hospital La Fe, Valencia, Spain); Isabel Benavente-Fernández (Division of Neonatology, University Hospital Puerta del Mar, Cádiz, Spain); Eva Valverde, Malaika Cordeiro (Division of Neonatology, University Hospital La Paz, Madrid, Spain); Dorotea Blanco (Division of Neonatology, University Hospital Gregorio Marañón, Madrid, Spain); Hector Boix (Department of Neonatology, University Hospital Vall d'Hebrón, Barcelona, Spain); Fernando Cabañas (Division of Neonatology, University

Hospital Quirónsalud Madrid, Madrid, Spain); Mercedes Chaffanel (Division of Neonatology, Regional University Hospital Málaga, Málaga, Spain); Belén Fernández-Colomer (Division of Neonatology, Central University Hospital of Asturias, Oviedo, Spain); Jose Ramón Fernández-Lorenzo (Division of Neonatology, University Hospital Complex of Vigo, Vigo, Spain); Begoña Loureiro (Division of Neonatology, University Hospital Cruces, Bilbao, Spain); Maria Teresa Moral-Pumarega (Division of Neonatology, University Hospital 12 de Octubre, Madrid, Spain); Antonio Pavón (Division of Neonatology, University Hospital Virgen del Rocío, Sevilla, Spain); and Inés Tofé (Division of Neonatology, University Hospital Reina Sofía, Córdoba, Spain).

References

1. Kurinczuk, J.J.; Barralet, J.H.; Redshaw, M.; Brocklehurst, P. Report to the Patient Safety Research Programme (Policy Research Programme of the Department Of Health). 2005. Available online: https://www.npeu.ox.ac.uk/downloads/files/reports/coNsEnsus-Monitoring-NE-Report.pdf (accessed on 14 March 2020).
2. Douglas-Escobar, M.; Weiss, M.D. Hypoxic-ischemic encephalopathy: A review for the clinician. *JAMA Pediatr.* **2015**, *169*, 397–403. [CrossRef] [PubMed]
3. Lee, A.C.C.; Kozuki, N.; Blencowe, H.; Vos, T.; Bahalim, A.; Darmstadt, G.L.; Niermeyer, S.; Ellis, M.; Robertson, N.J.; Cousens, S.; et al. Intrapartum-related neonatal encephalopathy incidence and impairment at regional and global levels for 2010 with trends from 1990. *Pediatr. Res.* **2013**, *74*, 50–72. [CrossRef] [PubMed]
4. Wassink, G.; Davidson, J.O.; Dhillon, S.K.; Zhou, K.; Bennet, L.; Thoresen, M.; Gunn, A.J. Therapeutic Hypothermia in Neonatal Hypoxic-Ischemic Encephalopathy. *Curr. Neurol. Neurosci. Rep.* **2019**, *19*, 2. [CrossRef] [PubMed]
5. Sarnat, H.B.; Sarnat, M.S. Neonatal encephalopathy following fetal distress. A clinical and electroencephalographic study. *Arch. Neurol.* **1976**, *33*, 696–705. [CrossRef] [PubMed]
6. Merchant, N.; Azzopardi, D. Early predictors of outcome in infants treated with hypothermia for hypoxic-ischaemic encephalopathy. *Dev. Med. Child Neurol.* **2015**, *57*, 8–16. [CrossRef]
7. Groenendaal, F.; de Vries, L.S. Fifty years of brain imaging in neonatal encephalopathy following perinatal asphyxia. *Pediatr. Res.* **2017**, *81*, 150–155. [CrossRef]
8. Shibasaki, J.; Aida, N.; Morisaki, N.; Tomiyasu, M.; Nishi, Y.; Toyoshima, K. Changes in Brain Metabolite Concentrations after Neonatal Hypoxic-ischemic Encephalopathy. *Radiology* **2018**, *288*, 840–848. [CrossRef]
9. Lee, W.L.A.; Michael-Titus, A.T.; Shah, D.K. Hypoxic-Ischaemic Encephalopathy and the Blood-Brain Barrier in Neonates. *Dev. Neurosci.* **2017**, *39*, 49–58. [CrossRef]
10. Bennet, L.; Booth, L.; Gunn, A.J. Potential biomarkers for hypoxic-ischemic encephalopathy. *Semin. Fetal Neonatal Med.* **2010**, *15*, 253–260. [CrossRef]
11. Sánchez-Illana, Á.; Piñeiro-Ramos, J.D.; Kuligowski, J. Small molecule biomarkers for neonatal hypoxic ischemic encephalopathy. *Semin. Fetal Neonatal Med.* **2020**, 101084. (In Press)
12. Wu, T.-W.; Tamrazi, B.; Hsu, K.-H.; Ho, E.; Reitman, A.J.; Borzage, M.; Blüml, S.; Wisnowski, J.L. Cerebral Lactate Concentration in Neonatal Hypoxic-Ischemic Encephalopathy: In Relation to Time, Characteristic of Injury, and Serum Lactate Concentration. *Front. Neurol.* **2018**, *9*, 293. [CrossRef] [PubMed]
13. Vannucci, R.C.; Brucklacher, R.M.; Vannucci, S.J. Glycolysis and Perinatal Hypoxic-Ischemic Brain Damage. *Dev. Neurosci.* **2005**, *27*, 185–190. [CrossRef] [PubMed]
14. Efstathiou, N.; Theodoridis, G.; Sarafidis, K. Understanding neonatal hypoxic-ischemic encephalopathy with metabolomics. *Hippokratia* **2017**, *21*, 115–123. [PubMed]
15. Reinke, S.N.; Walsh, B.H.; Boylan, G.B.; Sykes, B.D.; Kenny, L.C.; Murray, D.M.; Broadhurst, D.I. 1H NMR derived metabolomic profile of neonatal asphyxia in umbilical cord serum: Implications for hypoxic ischemic encephalopathy. *J. Proteome Res.* **2013**, *12*, 4230–4239. [CrossRef] [PubMed]
16. Ahearne, C.E.; Denihan, N.M.; Walsh, B.H.; Reinke, S.N.; Kenny, L.C.; Boylan, G.B.; Broadhurst, D.I.; Murray, D.M. Early Cord Metabolite Index and Outcome in Perinatal Asphyxia and Hypoxic-Ischaemic Encephalopathy. *Neonatology* **2016**, *110*, 296–302. [CrossRef]
17. Denihan, N.M.; Kirwan, J.A.; Walsh, B.H.; Dunn, W.B.; Broadhurst, D.I.; Boylan, G.B.; Murray, D.M. Untargeted metabolomic analysis and pathway discovery in perinatal asphyxia and hypoxic-ischaemic encephalopathy. *J. Cereb. Blood Flow Metab.* **2017**, *37*, 147–162. [CrossRef]

18. Sarafidis, K.; Efstathiou, N.; Begou, O.; Soubasi, V.; Agakidou, E.; Gika, E.; Theodoridis, G.; Drossou, V. Urine metabolomic profile in neonates with hypoxic-ischemic encephalopa-thy. *Hippokratia* **2017**, *21*, 80–84.
19. Yum, S.K.; Moon, C.-J.; Youn, Y.-A.; Sung, I.K. Changes in lactate dehydrogenase are associated with central gray matter lesions in newborns with hypoxic-ischemic encephalopathy. *J. Matern. Fetal Neonatal Med.* **2017**, *30*, 1177–1181. [CrossRef]
20. Sánchez-Illana, Á.; Núñez-Ramiro, A.; Cernada, M.; Parra-Llorca, A.; Valverde, E.; Blanco, D.; Moral-Pumarega, M.T.; Cabañas, F.; Boix, H.; Pavon, A.; et al. Evolution of Energy Related Metabolites in Plasma from Newborns with Hypoxic-Ischemic Encephalopathy during Hypothermia Treatment. *Sci. Rep.* **2017**, *7*, 17039. [CrossRef]
21. Chiang, M.-C.; Lien, R.; Chu, S.-M.; Yang, P.-H.; Lin, J.-J.; Hsu, J.-F.; Fu, R.-H.; Lin, K.-L. Serum Lactate, Brain Magnetic Resonance Imaging and Outcome of Neonatal Hypoxic Ischemic Encephalopathy after Therapeutic Hypothermia. *Pediatr. Neonatol.* **2016**, *57*, 35–40. [CrossRef]
22. Shah, S.; Tracy, M.; Smyth, J. Postnatal lactate as an early predictor of short-term outcome after intrapartum asphyxia. *J. Perinatol.* **2004**, *24*, 16–20. [CrossRef] [PubMed]
23. Murray, D.M.; Boylan, G.B.; Fitzgerald, A.P.; Ryan, C.A.; Murphy, B.P.; Connolly, S. Persistent lactic acidosis in neonatal hypoxic-ischaemic encephalopathy correlates with EEG grade and electrographic seizure burden. *Arch. Dis. Child. Fetal Neonatal Ed.* **2008**, *93*, F183–F186. [CrossRef] [PubMed]
24. Beckstrom, A.C.; Tanya, P.; Humston, E.M.; Snyder, L.R.; Synovec, R.E.; Juul, S.E. The perinatal transition of the circulating metabolome in a nonhuman primate. *Pediatr. Res.* **2012**, *71*, 338–344. [CrossRef] [PubMed]
25. Kuligowski, J.; Solberg, R.; Sánchez-Illana, Á.; Pankratov, L.; Parra-Llorca, A.; Quintás, G.; Saugstad, O.D.; Vento, M. Plasma metabolite score correlates with Hypoxia time in a newly born piglet model for asphyxia. *Redox Biol.* **2017**, *12*, 1–7. [CrossRef]
26. Anandi, V.S.; Shaila, B. Evaluation of factors associated with elevated newborn 17-hydroxyprogesterone levels. *J. Pediatr. Endocrinol. Metab.* **2017**, *30*, 677–681. [CrossRef] [PubMed]
27. Concepcion, K.R.; Zhang, L. Corticosteroids and perinatal hypoxic-ischemic brain injury. *Drug Discov. Today* **2018**, *23*, 1718–1732. [CrossRef]
28. Dong, S.; Zhang, Q.; Kong, D.; Zhou, C.; Zhou, J.; Han, J.; Zhou, Y.; Jin, G.; Hua, X.; Wang, J.; et al. Gender difference in the effect of progesterone on neonatal hypoxic/ischemic brain injury in mouse. *Exp. Neurol.* **2018**, *306*, 190–198. [CrossRef]
29. Walsh, B.H.; Broadhurst, D.I.; Mandal, R.; Wishart, D.S.; Boylan, G.B.; Kenny, L.C.; Murray, D.M. The Metabolomic Profile of Umbilical Cord Blood in Neonatal Hypoxic Ischaemic Encephalopathy. *PLoS ONE* **2012**, *7*, e50520. [CrossRef]
30. Kariholu, U.; Montaldo, P.; Markati, T.; Lally, P.J.; Pryce, R.; Teiserskas, J.; Liow, N.; Oliveira, V.; Soe, A.; Shankaran, S.; et al. Therapeutic hypothermia for mild neonatal encephalopathy: A systematic review and meta-analysis. *Arch. Dis. Child. Fetal Neonatal Ed.* **2020**, *105*, 225–228. [CrossRef]
31. Nuñez-Ramiro, A.; Benavente-Fernández, I.; Valverde, E.; Cordeiro, M.; Blanco, D.; Boix, H.; Cabañas, F.; Chaffanel, M.; Fernández-Colomer, B.; Fernández-Lorenzo, J.R.; et al. Topiramate plus Cooling for Hypoxic-Ischemic Encephalopathy: A Randomized, Controlled, Multicenter, Double-Blinded Trial. *Neonatology* **2019**, *116*, 76–84. [CrossRef]
32. Barkovich, A.J.; Hajnal, B.L.; Vigneron, D.; Sola, A.; Partridge, J.C.; Allen, F.; Ferriero, D.M. Prediction of neuromotor outcome in perinatal asphyxia: Evaluation of MR scoring systems. *AJNR Am. J. Neuroradiol.* **1998**, *19*, 143–149. [PubMed]
33. Rutherford, M.; Ramenghi, L.A.; Edwards, A.D.; Brocklehurst, P.; Halliday, H.; Levene, M.; Strohm, B.; Thoresen, M.; Whitelaw, A.; Azzopardi, D. Assessment of brain tissue injury after moderate hypothermia in neonates with hypoxic-ischaemic encephalopathy: A nested substudy of a randomised controlled trial. *Lancet Neurol.* **2010**, *9*, 39–45. [CrossRef]
34. Broadhurst, D.; Goodacre, R.; Reinke, S.N.; Kuligowski, J.; Wilson, I.D.; Lewis, M.R.; Dunn, W.B. Guidelines and considerations for the use of system suitability and quality control samples in mass spectrometry assays applied in untargeted clinical metabolomic studies. *Metabolomics* **2018**, *14*, 72. [CrossRef] [PubMed]
35. ProteoWizard. Available online: http://proteowizard.sourceforge.net (accessed on 14 March 2020).
36. MetaboLights. Available online: https://www.ebi.ac.uk/metabolights/MTBLS1041 (accessed on 14 March 2020).

37. LC-MS and GC-MS Data Analysis. Available online: https://bioconductor.org/packages/release/bioc/html/xcms.html (accessed on 14 March 2020).
38. Kuhl, C.; Tautenhahn, R.; Böttcher, C.; Larson, T.R.; Neumann, S. CAMERA: An Integrated Strategy for Compound Spectra Extraction and Annotation of Liquid Chromatography/Mass Spectrometry Data Sets. *Anal. Chem.* **2012**, *84*, 283–289. [CrossRef] [PubMed]
39. Kuligowski, J.; Sánchez-Illana, Á.; Sanjuán-Herráez, D.; Vento, M.; Quintás, G. Intra-batch effect correction in liquid chromatography-mass spectrometry using quality control samples and support vector regression (QC-SVRC). *Analyst* **2015**, *140*, 7810–7817. [CrossRef] [PubMed]
40. Chang, C.-C.; Lin, C.-J. LIBSVM: A Library for Support Vector Machines. *ACM Trans. Intell. Syst. Technol.* **2011**, *2*, 1–27. [CrossRef]
41. HMDB Version 4.0. Available online: http://www.hmdb.ca (accessed on 14 March 2020).
42. Chong, J.; Soufan, O.; Li, C.; Caraus, I.; Li, S.; Bourque, G.; Wishart, D.S.; Xia, J. MetaboAnalyst 4.0: Towards more transparent and integrative metabolomics analysis. *Nucleic Acids Res.* **2018**, *46*, W486–W494. [CrossRef]
43. Sumner, L.W.; Amberg, A.; Barrett, D.; Beale, M.H.; Beger, R.; Daykin, C.A.; Fan, T.W.-M.; Fiehn, O.; Goodacre, R.; Griffin, J.L.; et al. Proposed minimum reporting standards for chemical analysis Chemical Analysis Working Group (CAWG) Metabolomics Standards Initiative (MSI). *Metabolomics* **2007**, *3*, 211–221. [CrossRef]

Pediatric RESEARCH

www.nature.com/pr

CLINICAL RESEARCH ARTICLE

Noninvasive monitoring of evolving urinary metabolic patterns in neonatal encephalopathy

José David Piñeiro-Ramos[1], Mari Merce Cascant[1], Antonio Núñez-Ramiro[2], Ángeles López-Gonzálvez[3], Álvaro Solaz-García[1], Abel Albiach-Delgado[1], Juan Martínez-Rodilla[1], Roberto Llorens-Salvador[4], Daniel Sanjuan-Herraez[5,6], Guillermo Quintás[5,6], Coral Barbas[3], Julia Kuligowski[1], Máximo Vento[1,2] and on behalf of the Hypotop Study Group

BACKGROUND: Infants with moderate and severe neonatal encephalopathy (NE) frequently suffer from long-term adverse outcomes. We hypothesize that the urinary metabolome of newborns with NE reflects the evolution of injury patterns observed with magnetic resonance imaging (MRI).
METHODS: Eligible patients were newborn infants with perinatal asphyxia evolving to NE and qualifying for therapeutic hypothermia (TH) included in the HYPOTOP trial. MRI was employed for characterizing brain injury. Urine samples of 55 infants were collected before, during, and after TH. Metabolic profiles of samples were recorded employing three complementary mass spectrometry-based assays, and the alteration of detected metabolic features between groups was assessed.
RESULTS: The longitudinal assessment revealed significant perturbations of the urinary metabolome. After 24 h of TH, a stable disease pattern evolved characterized by the alterations of 4–8% of metabolic features related to lipid metabolism, metabolism of cofactors and vitamins, glycan biosynthesis and metabolism, amino acid metabolism, and nucleotide metabolism. Characteristic metabolomic fingerprints were observed for different MRI injury patterns.
CONCLUSIONS: This study shows the potential of urinary metabolic profiles for the noninvasive monitoring of brain injury of infants with NE during TH.

Pediatric Research _####################_; https://doi.org/10.1038/s41390-021-01553-z

IMPACT:

- A comprehensive approach for the study of the urinary metabolome was employed involving a semi-targeted capillary electrophoresis–time-of-flight mass spectrometry (TOFMS) assay, an untargeted ultra-performance liquid chromatography (UPLC)–quadrupole TOFMS assay, and a targeted UPLC-tandem MS-based method for the quantification of amino acids.
- The longitudinal study of the urinary metabolome identified dynamic metabolic changes between birth and until 96 h after the initiation of TH.
- The identification of altered metabolic pathways in newborns with pathologic MRI outcomes might offer the possibility of developing noninvasive monitoring approaches for personalized adjustment of the treatment and for supporting early outcome prediction.

INTRODUCTION

Perinatal asphyxia is defined as the interruption of blood flow and gas exchange to the fetus in the perinatal period. Prolonged hypoxia–ischemia can trigger a cascade of events leading to injury to vital organs, especially the brain (i.e., neonatal encephalopathy, NE). NE following birth asphyxia is a major cause of early neonatal death, cerebral palsy, or neurodevelopmental disability in term neonates, affecting ~0.5–1.5 per 1000 live births in high-income countries and ~1 million infants every year worldwide.[1–3] Magnetic resonance imaging (MRI), including diffusion-weighted imaging and spectroscopy performed between the fifth and seventh day after birth, has become the cornerstone for establishing the degree of brain injury and predicting neurodevelopmental outcome.[4] There is compelling evidence suggesting that perinatal asphyxia and the administration of supplemental oxygen may influence the brain at the molecular level by stimulating epigenetic modifications, including DNA methylation/demethylation, histone modifications, and miRNAs and epigenetic mechanisms, that may be involved in the development of a hypoxic/ischemic-sensitive phenotype.[5,6]

It has been observed that the combination of decreased cerebral perfusion and subsequent hypoxia triggers an evolving sequence of biochemical alterations that, lasting days, weeks, or even months, lead to anatomical and physiological injuries

[1]Neonatal Research Group, Health Research Institute La Fe, Valencia, Spain; [2]Division of Neonatology, University & Polytechnic Hospital La Fe, Valencia, Spain; [3]Centre for Metabolomics and Bioanalysis (CEMBIO), Universidad San Pablo-CEU, Madrid, Spain; [4]Division of Radiology and Imaging, University & Polytechnic Hospital La Fe, Valencia, Spain; [5]Health and Biomedicine, LEITAT Technological Center, Barcelona, Spain and [6]Unidad Analítica, Health Research Institute La Fe, Valencia, Spain
Correspondence: Julia Kuligowski (julia.kuligowski@uv.es)
A list of members and their affiliations appears in the Supplementary Information.

Received: 3 August 2020 Revised: 8 April 2021 Accepted: 10 April 2021
Published online: 05 May 2021

characterizing NE.[7,8] Therefore, a longitudinal biochemical assessment of NE is needed from birth until beyond the duration of therapeutic hypothermia (TH). NE has been associated with damage to the integrity of the blood–brain barrier, and therefore brain injury could be reflected in peripheral blood samples or other biofluids[9] theoretically enabling the implementation of noninvasive monitoring approaches. Metabolomics is a systems biology approach aiming at the holistic study of the complete pool of small molecules forming the metabolome of a biological sample. While metabolites are downstream products of the genome, transcriptome, and proteome, they reflect their interactions and the interaction with the environment, thereby providing a direct, dynamic, and meaningful read out of the biochemical status of a system closely related to its actual phenotype.[10] Literature reports on the use of metabolomics for the study of perinatal asphyxia in newborns with NE are highly encouraging, although the main scope has been the early diagnosis of NE based on the comparison of asphyxiated/NE infants to healthy control infants,[11–16] and metabolomics has only been scarcely used for progressing our understanding of the multilayer effects of NE and TH on the newborn.[16,17] Recently, the analysis of metabolic profiles of plasma samples collected between birth and until completion of TH enabled the identification of a dynamic perturbation of 11 metabolic pathways, including amino acid and purine metabolism, and the steroid hormone biosynthesis, in addition to pyruvate and lactate, in newborns with pathologic MRI outcomes.[18]

In this study, we hypothesized that the urinary metabolome of newborns with NE recorded during the first 96 h of life encompasses the evolution of the injury pattern of the brain that is evidenced by MRI outcomes. Hence, the goal of this study is to provide insight into metabolic alterations secondary to brain injury in a clinical cohort of newborn infants with NE undergoing TH, with the aim of generating a knowledge base for the future development of a noninvasive monitoring approach, supporting the prediction of long-term clinical outcomes.

METHODS

Study approval and population

The study was approved by the Ethics Committee for Biomedical Research of the Health Research Institute La Fe (Valencia, Spain) and registered under the acronym HYPOTOP (EudraCT 2011-005696-17). The HYPOTOP trial is a randomized, controlled, multicenter, double-blinded clinical trial for assessing the efficacy of topiramate vs. placebo in newborns, with NE undergoing TH. All methods were performed in accordance with relevant guidelines and regulations, and informed consent was obtained from legal representatives of enrolled infants. For a detailed description of the HYPOTOP trial, including the study design and the established inclusion and exclusion criteria, the reader is referred to the literature.[19] In this study, a sub-cohort of 55 newborns enrolled in the HYPOTOP trial was included.

Samples were collected from urinary catheters or using sterile cotton pads placed in the diaper following a standard operating procedure to avoid bias and systematic errors. Urine samples were collected before initiation of TH at 6 h, as well as 12, 24, 48, 72, and 96 h after the initiation of TH. Samples were aliquoted into three dry microcentrifuge tubes and stored immediately at −80 °C until analysis.

Magnetic resonance imaging

MRI was carried out using different high-field magnet systems between days 4 and 8 after birth. In all cases, 3D Gradient Echo T1-weighted MR images, axial Fast Spin Echo T2-weighted MR images, and diffusion-weighted images were acquired. The interpretation of MRI results was carried out by an experienced, blinded pediatric neuroradiologist, rating the extent of the injury in posterior limb internal capsule, basal ganglia, thalami, white matter, and cortex[20] and using a standardized score according to the National Institute of Child Health and Human Development (NICHD) Neonatal Research Network (NRN), discerning between injury patterns as described by Shankaran et al.[21].

Metabolomic fingerprinting of urine samples

Three complementary analytical approaches were employed for the analysis of metabolic fingerprints of urine samples to enhance metabolome coverage, i.e., (i) a semi-targeted capillary electrophoresis–time-of-flight mass spectrometry (CE–TOFMS) assay, (ii) an untargeted ultra-performance liquid chromatography–quadrupole time-of-flight mass spectrometry (UPLC–QTOFMS) assay, and (iii) a targeted UPLC-tandem MS (MS/MS)-based method for the quantification of amino acids. Results were normalized to creatinine concentrations and are made available as Supplementary Table 1.

Semi-targeted CE–TOFMS analysis. A total of 279 urine samples were thawed on ice and homogenized on a Vortex® mixer for 1 min. A total of 50 µL of the sample were mixed with 50 µL of 0.2 M formic acid containing 0.4 mM methionine sulfone (internal standard, IS). After homogenization on a Vortex® mixer for 5 min and centrifugation at 13,200 × *g* for 10 min at 4 °C, 60 µL of the supernatant were collected and mixed with 180 µL of cold methanol for 5 min. Samples were centrifuged at 13,200 × *g* for 15 min at 4 °C, and 200 µL of supernatant were transferred into microcentrifuge tubes and evaporated to dryness using a Speedvac concentrator. Finally, sample extracts were redissolved in 60 µL of 0.2 M formic acid, shaken for 5 min on a Vortex® mixer, and centrifuged at 2000 × *g* at 4 °C for 5 min. A total of 50 µL of supernatant were transferred to CE vials for analysis. Quality control (QC) samples were prepared by pooling 5 µL from each sample and processed applying the same procedure, as described for samples.

The analysis of urine samples was carried out by capillary electrophoresis–electrospray–time-of-flight MS (CE-ESI-TOFMS), using instrumental conditions described elsewhere.[22] Briefly, CE–ESI–TOFMS analysis was performed on an Agilent 7100 Capillary Electrophoresis system (Agilent Technologies, CA) coupled to an Agilent 6224 TOFMS instrument. The separation was performed on a fused silica capillary (Agilent; total length, 100 cm; i.d., 50 µm) in normal polarity with a background electrolyte composed of 1.0 M HCOOH solution in 10% CH_3OH (v/v). Samples were hydrodynamically injected at 50 mbar for 17 s followed by the injection of background electrolyte at 100 mbar for 10 s. The separation voltage applied was 30 kV with 25 mbar of internal pressure and the run time was 40 min. The sheath liquid (6 µL min^{-1}) composition was CH_3OH:H_2O (1:1, v/v) containing two reference masses (purine and HP-0921). The MS parameters used were: fragmentor 125 V, skimmer 65 V, octopole 750 V, nebulizer pressure 10 p.s.i., drying gas temperature at 200 °C, and flow rate 10 mL min^{-1}. The capillary voltage was 3500 V. Full-scan MS spectra from *m/z* 70 to 1000 were acquired in positive dual-ESI mode at a scan rate of 1.02 scan s^{-1}. MassHunter Workstation version B.06.01 controlled the CE–TOFMS system. The analysis of the samples was carried out in four batches of randomized samples. At the beginning of each batch, six QCs were injected for pre-sequence system conditioning, and a QC was injected every ninth sample to monitor the system performance. CE–TOFMS data processing using the Profinder software (B.06.00, Agilent) enabled the identification of 102 metabolites (Supplementary Table 2) in the urine sample set.

Untargeted UPLC–QTOFMS analysis. A total of 293 urine samples were prepared and analyzed by UPLC–QTOFMS assay, as described elsewhere.[23] Urine samples were randomly split into three analytical batches. Briefly, urine samples were thawed on ice, homogenized on a Vortex® mixer during 30 s, and centrifuged

(16,000 × *g* during 15 min at 4 °C). A total of 50 µL of supernatant were withdrawn and spiked with 50 µL of IS solution in 96-well plates containing phenylalanine-D_5 (Cambridge Isotopes Laboratory Inc., Andover, MA), caffeine-D_9 (Toronto Research Chemicals, Toronto, Ontario, Canada), leukine enkephalin (Sigma-Aldrich Química SA, Madrid, Spain), and reserpine (Sigma-Aldrich Química SA) in H_2O:CH_3OH (1:1, 0.1% v/v HCOOH) at concentrations ranging between 2 and 4 µM. Blanks were prepared by replacing urine with H_2O and a QC was prepared by mixing 5 µL of each final sample extract. The QC was split into three aliquots, each being measured in a single analytical batch to avoid additional freeze–thaw cycles. Sample extracts, blanks, and QCs were stored at −80 °C until analysis. Before analysis of each batch, sample extracts, blanks, and a QC aliquot were thawed on ice.

UPLC–QTOFMS analysis was performed on an Agilent 1290 Infinity UPLC chromatograph equipped with a UPLC BEH C18 (100 × 2.1 mm, 1.7 µm, Waters, Wexford, Ireland) column running a binary mobile phase gradient (mobile phase A: H_2O, 0.1% v/v HCOOH and mobile phase B: CH_3CN, 0.1% v/v HCOOHH), and acquiring full-scan MS data from 100 to 1700 *m/z* with a scan frequency of 6 Hz on an iFunnel QTOF Agilent 6550 spectrometer in the positive electrospray (ESI+) mode. The QC sample was injected ten times at the beginning of each batch for system conditioning, as well as after every five urine samples for the monitoring and control of the instrumental performance. The blank extract was injected twice, at the beginning and end of each batch.

The peak table was generated for each batch separately using XCMS (version 3.4.2) (https://bioconductor.org/packages/release/bioc/html/xcms.html) running in R (version 3.6.1), using the centWave method.[24] Intensity weighted *m/z* values of each feature were calculated using the wMean function and peak limits used for integration were found through descent on the Mexican hat filtered data. Peak grouping was carried out using the nearest method, and the fillPeaks method was applied to fill missing peak data.

All further calculations were carried out in MATLAB R2019b (Mathworks Inc., Natick, MA) using in-built, as well as in-house written scripts and functions and the PLS Toolbox 8.7 (Eigenvector Research Inc., Wenatchee). Blank samples were used to identify and remove features arising from contaminants and carryover with a ratio of median intensities in QCs and blanks <9.[25] The three data sets were aligned using *m/z* and RT tolerances of 50 mDa and 0.1 min, and a mzVsRT = 1. Within-batch effects were corrected for each batch separately employing the Quality Control-Support Vector Regression algorithm[23] and the LIBSVM library[26] method with an *ε*-range from 2.5 to 5, a *γ*-range from 1 to 10^5, and a *C*-interval of 50.[27,28] Between-batch effects were linearly corrected using the median values in QCs as reference.[23] UPLC-MS features with a relative intensity change across batches >5, and those with a *D*-ratio ≥ 20% in QCs after within and between-batch effect correction were classified as unreliable[29] and removed.

Quantitative amino acid profiling. A total of 237 urine samples were thawed on ice and homogenized on a Vortex S0200 mixer (LabNet, Edison, NJ) during 10 s. A total of 70 µL of water (Optima LC/MS grade, Fisher Scientific) were added to 5 µL of urine. Amino acid levels were quantified using a ultraderivation kit (AccQ Tag™ Ultra Derivatization Kit, Waters), following the manufacturer's protocol. Blanks were prepared by replacing the urine sample with water (Optima LC/MS grade). A QC was prepared by mixing 5 µL of each sample. Quantitative analysis of amino acids was performed employing a 1290 Infinity UPLC system from Agilent equipped with a UPLC CORTECS C18 column (150 × 2.1 mm, 1.6 µm) from Waters coupled to an Agilent 6460 triple quadrupole MS system operating in ESI+ mode. The flow rate was set to 500 µL min^{-1} running a binary gradient with 0.1% v/v HCOOH in H_2O and 0.1% v/v HCOOH in CH_3CN as mobile phase components. Column and autosampler were kept at 55 and 4 °C, respectively and the injection volume was 3 µL. Raw data were acquired and processed employing MassHunter Workstation (version B.07.00, Agilent). Missing values were imputed as 0.5 × LOQ of each compound. In Supplementary Table 3 a list of the parameters employed for amino acid quantification can be found.

Creatinine determination. Creatinine was quantified following the protocol of the Urinary Creatinine Detection Kit (Arbor Assays™, Ann Arbor, MI), employing a dilution factor of 1:4 and measuring the absorbance at 490 nm.

Data processing and statistics

Metabolic fingerprints were normalized to creatinine, $\log_{10}$ transformed, and pareto scaled. Between group comparisons of clinical and demographic variables were carried out employing the Student's *t* test for unequal variances ($\alpha = 0.05$), Wilcoxon rank-sum test ($\alpha = 0.05$), or χ^2-test ($\alpha = 0.05$), according to the underlying distribution. For determining differentially regulated metabolites or UPLC–QTOFMS features, as well as for comparing MRI outcomes at each time point, Student's *t* tests for unequal variances ($\alpha = 0.05$) were applied and fold change (FC) was calculated as the ratio of means between groups.

The standardized mean difference using the simplified Cohen equation to determine the pooled standard deviation[30] was calculated for each metabolite/metabolic feature at each of the six sample collection time points. Then, the Pearson correlation coefficient was calculated between the standardized mean difference and time and obtained FDR-adjusted *P* values were calculated.[31]

MetaboAnalyst (version 5.0)[32] was used for the generation of heatmaps from autoscaled data employing Euclidean distance and Ward's method. Pathway analysis was carried out using the *mummichog* algorithm (*P* value cutoff set to 0.05) with a *m/z* accuracy = 10 p.p.m. and the Kyoto Encyclopedia of Genes and Genomes (KEGG) pathway library (*Homo sapiens*). As an input, *t* test *P* values estimated assuming unequal variances between distributions, and FCs were computed for each metabolic feature comparing normal and pathologic outcomes. Pathways with gamma *P* values <0.05 were considered as significantly altered. The PLS Toolbox 8.7 (Eigenvector Research Inc., Wenatchee) was used for partial least squares (PLS) and PLS discriminant analysis (PLSDA) of autoscaled data. For *k*-fold cross validation, samples were distributed into folds by subject to prevent person-specific information crossover between the training folds and the test fold. Receiver operating characteristic (ROC) curves were constructed based on PLSDA predictions and cross validation results.

RESULTS

Patient characteristics

A total of 55 infants from the HYPOTOP cohort were included in this study. The characteristics of the studied population, including 55 newborns with NE undergoing TH are shown in Table 1. No significant differences between the control (i.e., normal neurological outcome) and pathologic groups were found in any of the collected anthropometric, clinical, or biochemical parameters. Furthermore, both groups were balanced in the proportion of infants receiving topiramate as adjuvant therapy.

Dynamics of the urinary metabolome

The urinary metabolome of newborns with NE was studied employing three complementary analytical methods, i.e., untargeted UPLC–QTOFMS, semi-targeted CE–TOFMS, and a targeted method for the determination of amino acids. Using UPLC–QTOFMS, a total of 293 urine samples were analyzed with

Table 1. Clinical and demographic parameters of newborns included in the multi-platform metabolomics study.

Parameter	Normal ($N = 22$)	Pathologic ($N = 33$)	P value
Inborn [%]	5 (23%)	6 (18%)	0.7
Maternal age (years) [mean ± s]	34 (4)	33 (6)	0.3
Gestational age (weeks) [median, IQR]	38.4 (37.4, 40.5)	39.0 (38.0, 40.6)	0.7
Gender (male/female)	11/11	17/16	0.9
Birth weight (g) [mean ± s]	3321 (566)	3258 (689)	0.7
Length (cm) [mean ± s]	52 (4)	50 (3)	0.3
Head circumference (cm) [mean ± s]	35 (1)	34 (2)	0.3
Delivery mode (C-section) [%]	9 (41%)	21 (64%)	0.1
Apgar score 1 min [median, IQR]	2 (1, 4)	1 (1, 3)	0.5
Apgar score 5 min [median, IQR]	4 (3, 5)	3 (1, 5)	0.1
Apgar score 10 min [median, IQR]	5 (5, 8)	5 (3, 6)	0.2
Sarnat 2/Sarnat 3	17/5	21/11	0.3
MRI score[a] [%]			
Score-0	22 (100%)	0 (0%)	
Score-1	0 (0%)	11 (33%)	
Score-2	0 (0%)	15 (45%)	
Score-3	0 (0%)	2 (6%)	
pH UC [mean ± s]	7.0 (0.3)	7.0 (0.2)	0.8
BE UC ($mEq\,L^{-1}$) [mean ± s]	−15 (10)	−15 (8)	0.8
pCO_2 UC (mmHg) [mean ± s]	67 (27)	63 (38)	0.7
HCO_3 UC ($mEq\,L^{-1}$) [mean ± s]	13 (4)	15 (8)	0.3
MR (days) [median, IQR]	8 (6, 10)	7 (7, 9)	1.0
Initiation of TH (h) [mean ± s]	34 (1.2)	34 (1)	0.7
Topiramate treatment (yes) [%]	10 (45%)	17 (52%)	0.7

[a]MRI scores assigned according to the National Institute of Child Health and Human Development (NICHD) Neonatal Research Network (NRN), as described by Shankaran et al.;[21] for five newborns from the pathologic group, no information on the degree of injury was available.

$N = 37$ collected before the initiation of TH and $N = 45$, $N = 54$, $N = 54$, $N = 54$, and $N = 49$ collected 12, 24, 48, 72, and 96 h, respectively, after the initiation of TH. After initial data preprocessing and filtering, 11,561 features were retained and used for further analysis. In case of CE–TOFMS, a total of 279 urine samples were analyzed with $N = 35$ collected before the initiation of TH and $N = 44$, $N = 52$, $N = 53$, $N = 53$, and $N = 42$ collected 12, 24, 48, 72, and 96 h, respectively, after the initiation of TH. A list of metabolites that were consistently detected in urine samples with the CE–TOFMS target assay can be found in Supplementary Table 2. Amino acids were quantified in 237 samples, $N = 27$ collected before the initiation of TH and $N = 40$, $N = 41$, $N = 47$, $N = 43$, and $N = 39$ collected 12, 24, 48, 72, and 96 h, respectively, after the initiation of TH (see Supplementary Table 3).

The longitudinal analysis of the metabolic fingerprint of infants with NE showed a dynamic behavior. Figure 1 (left) depicts the percentage of differentially expressed features and metabolites (t test P value < 0.05) after the initiation of TH, using the first urine samples collected as reference. The majority of detected signals showed a decreasing trend with time ranging between 16 and 59% at 12 and 96 h after the initiation of TH, respectively. Simultaneously, only between 0.08 and 1% were upregulated. Changes are most pronounced during the first 48 h after the initiation of TH, whereas rewarming (96 h) did not seem to have a strong impact. The effect of time is further represented in Fig. 2, where metabolite concentrations with a significant correlation with time are represented. In total, 43% of the features of the urinary metabolic fingerprint showed a significant correlation with time, and out of the correlated features, 53% tended to increase with time.

Perturbation of the urinary metabolome in infants with pathologic MRI outcome

Differences in the urinary metabolic fingerprints of infants with normal and pathologic MRI outcome were assessed throughout the first 96 h of life. As shown in Fig. 1 (right), the number of significantly altered metabolic features reaches a minimum at 12 h and ranges between 4 and 8% at the remaining time points (6 ± 2%). The proportion of upregulated features ranges between 0 and 0.2%, whereas the proportion of downregulated features was rising from 0.8% at 12 h to 7% at 96 h.

Figure 3 illustrates the metabolic pathways altered between newborn infants with pathologic and normal MRI outcomes. Significant alterations on the pathway level were found in urine samples collected at all studied time points. Pathways related to

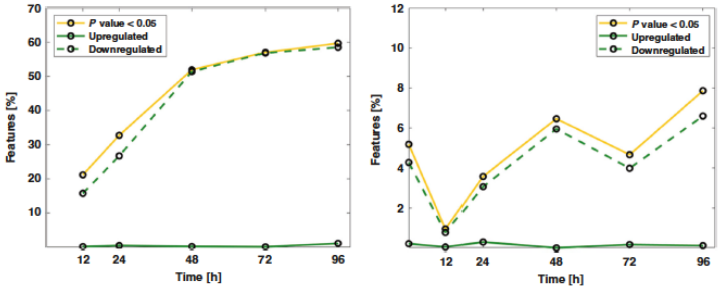

Fig. 1 Metabolic changes in urine samples from newborns with NE detected by multi-platform metabolomics. Left: % of significantly changing features (P value < 0.05) and % of upregulated and downregulated features at each time point during 96 h after initiating TH with respect to the first urine sample collected before the initiation of TH. Right: % of significantly changing features (P value < 0.05) and % of upregulated and downregulated features in urine samples from infants with vs. without brain injury, as detected by MRI.

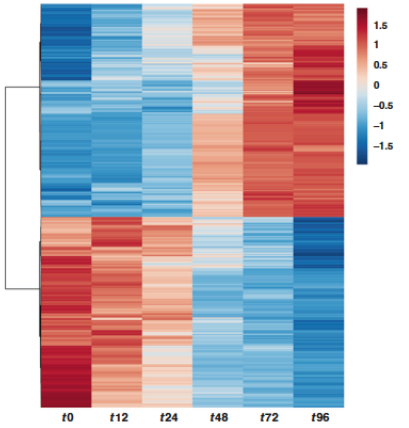

Fig. 2 Metabolic changes associated to time. Note: color represents standardized mean difference between time points; blue—metabolite levels lower than average, and red—metabolite levels higher than average. *P* values from Pearson correlation with time were computed, and significant metabolites after multiple testing correction are shown; heatmap calculated using Euclidean distance and Ward algorithm representing autoscaled features.

the amino acid and lipid metabolism were consistently identified to be affected in infants with pathologic MRI. Pathways related to the metabolism of cofactors and vitamins were altered during TH. Differences in pathways associated to xenobiotics biodegradation and metabolism were found repeatedly before, during and after TH. Carbohydrate metabolism and glycan synthesis and metabolism were altered during the first 24 h. Other pathways related to the metabolism of terpenoids and polyketides, and nucleotide and energy metabolism were affected transiently. Accordingly, Fig. 3 also shows the classes of changing metabolites, with "carboxylic acids and derivatives", "organooxygen compounds", "fatty acyls", "steroids and steroid derivatives", "indoles and derivatives", and "tetrapyrroles and derivatives" being the most prominent metabolite classes affected. A detailed list of identified altered metabolites is provided in Supplementary Table 4.

With the aim of defining a disease pattern in urine metabolic fingerprints, pathway analysis was repeated for all samples collected between 24 and 96 h after the initiation of TH together, as the differences between newborns with NE and pathologic vs. normal MRI outcomes in the metabolome became more stable (see Fig. 1). Pathway analysis confirmed the consistent alteration of ten pathways associated to amino acid and lipid metabolism, metabolism of cofactors and vitamins, glycan biosynthesis and metabolism, and nucleotide metabolism, as shown in Fig. 3. Using the metabolic features corresponding to metabolites included in those pathways as annotated by the mummichog algorithm (i.e., 398 features), a PLSDA model with four latent variables was computed for discerning between metabolic fingerprints of newborns with pathologic (Scores 1, 2, or 3) and normal MRI outcomes (Score-0) retrieved between 24 and 96 h after the initiation of TH. The significance of the model was confirmed by a permutation test (500 permutations) and ROC curves are shown in Fig. 4.

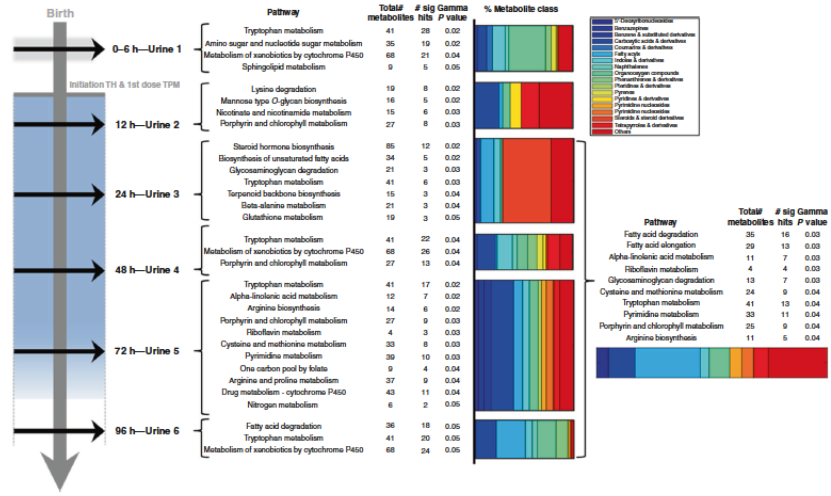

Fig. 3 Dynamic metabolic alterations detected in urine samples from infants with brain injury in comparison to infants without brain injury detected by MRI. Altered pathways and associated metabolites are shown for urine samples collected between birth and 96 h after the initiation of TH.

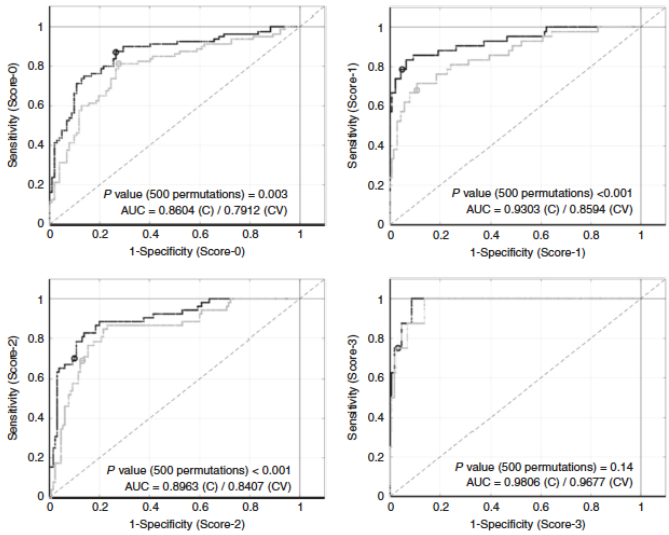

Fig. 4 Disease pattern of NE as reflected in the urinary metabolome between 24 and 96 h. ROC curves from a PLSDA model (four latent variables) for Score-0 (top, left), Score-1 (top, right), Score-2 (bottom, left), and Score-3 (bottom, right) calculated, using relative intensities of 398 metabolic features from altered metabolic pathways shown in Fig. 3. Note: black lines represent estimated PLSDA ROC curves (calibration set); gray lines represent estimated PLSDA ROC curves (cross validation); dashed lines represent 50% lines; and circles indicate model thresholds.

DISCUSSION

A severe hypoxic insult suffered in the perinatal period causes an imbalance of the homeostasis manifesting at a systemic level in the newborn. This perturbation can be readily monitored employing urinary metabolomics allowing to study dynamic changes of the phenotype over time. In this study, a continuously increasing proportion of altered metabolic features with time was detected affecting up to 59% of features (Fig. 1, left) and 43% of features showed a significant correlation with time (Fig. 2). The number of downregulated features was steadily increasing and higher than the number of upregulated features at all studied time points (Fig. 1, left). This observation is in good agreement with earlier literature reports on metabolomics studies involving the analysis of the urinary metabolome of NE infants over time,[15,17,33] reporting continuous changes during the neonatal period with some metabolites showing a relative increase in concentration, while others tended to decrease.

The main aim of this study was to search for a metabolic fingerprint able to discern urine samples from infants, which showed pathologic patterns during a subsequent MRI analysis from those with normal MRI results. This is the first study reporting distinct patterns in urinary metabolic fingerprints of newborns with NE and pathologic vs. normal MRI outcomes. The injury pattern showed a dynamic behavior. Initially detected differences between groups almost disappeared 12 h after the initiation of TH, which might reflect a partial recovery during the latent injury phase, and then became more evident again after 24 h of TH (Fig. 1, right).

To further elucidate the effect of brain injury on the metabolome, pathway analysis was employed. Pathway analysis aims to place the seemingly disjointed list of altered metabolites into a broader biological context by jointly assigning metabolites to relevant metabolic pathways, providing an interaction network that may identify centralized hubs, where metabolic pathways coincide or where bottlenecks may occur. Pathway alterations affecting between 3 and 11 pathways (Fig. 3) were detected across all studied time points, covering before and during TH, as well as after rewarming with some alterations being transient and others being detected consistently (e.g., tryptophan metabolism).

From the clinical perspective and with the aim of developing a monitoring approach the discovery of stable disease patterns is valuable. We found that a total of ten pathways were consistently altered in urine samples of infants with NE and pathologic MRI outcomes, when urine samples collected between 24 and 96 h after the initiation of TH were analyzed (Fig. 3). Seemingly, after a period of 24 h after the initiation of TH, biochemical alterations that evolve to anatomical lesions in the brain that are later detectable by MRI are mirrored in the urinary metabolome. Metabolites associated to the ten altered metabolic pathways were successfully employed to discern between newborns with different injury patterns (i.e., Scores 0, 1, 2, and 3) as shown by ROC curves in Fig. 4. Statistically highly significant models could be obtained for all comparisons, with exception of the model for the discrimination of Score-3, probably due to the limited number of samples, as only two infants showed the highest degree of brain injury. Hence, our data provides evidence of gradual changes detectable in urine samples, providing a knowledge base for the development of biomarkers that might support clinical monitoring compatible with TH in the future.

To the best of our knowledge, this study has analyzed and compared for the first time the evolution of the metabolome of newborns with NE and pathologic vs. normal MRI outcomes over time. The use of a representative control group of newborns with NE instead of healthy control newborns has facilitated the interpretation of the outcomes. Due to substantial differences in the experimental design between this study and previous results,[15,17,33] a detailed comparison of the outcomes was not possible. However, alterations of amino acids and associated pathways, including tryptophan metabolism and aminoacyl-tRNA biosynthesis,[17,33] had been reported. In umbilical cord blood samples from infants with NE vs. healthy control newborns, the terpenoids backbone biosynthesis pathway and, also a significant alteration of kynurenine, a metabolite from the tryptophan metabolism pathway, were identified.[14] Interestingly, in a mouse model with induced excitotoxic lesion, changes in amino acid metabolism in brain tissue were sustaining acute and delayed responses to injury.[34]

In a previous study, we analyzed the plasma metabolic fingerprints of the newborns included in this study.[18] Several metabolic pathways altered in urine (Fig. 3) were also found to be affected in plasma, i.e., arginine and proline metabolism (48 and 72 h in plasma vs. 72 h in urine), lysine degradation (72 h in plasma vs. 12 in urine), nitrogen metabolism (72 h in plasma and urine), and steroid hormone biosynthesis (0, 24, 48, and 72 h in plasma vs. 24 h in urine). Hence, the results from metabolic fingerprinting in plasma and urine samples are in good agreement, indicating that the development of brain injury secondary to asphyxia is broadly affecting metabolism.

This study has limitations. No newborns with asphyxia or classified as mild NE (Sarnat 1) were included. There is risk of adverse neurodevelopmental outcome of newborns with mild NE, but to date, there is no evidence to support cooling in these babies. Furthermore, as NE is frequently associated to a transient renal insufficiency secondary to proximal tubular necrosis with decreased urine output and creatinine clearance, hematuria, and proteinuria, analytical determinations might have been influenced by renal insufficiency especially in babies with severe NE.[35]

In summary, this is the first time that a dynamic perturbation of the urinary metabolome of newborns with NE undergoing TH, and showing pathologic and normal MRI outcomes is reported. Undoubtedly, TH significantly influences patient's metabolism. However, since TH has become a standard of care, our results truly reflect the clinical situation undergone by patients with moderate to severe NE. From birth and until completing 24 h of TH, the metabolic fingerprint experienced a gradual shift and a distinct disease pattern evolved. This disease pattern is characterized by the alteration of amino acid and lipid metabolism, metabolism of cofactors and vitamins, glycan biosynthesis and metabolism, and nucleotide metabolism. Although follow-up studies are required for further confirming the observations from this study, this new insight might be meaningful for patient monitoring in the NICU and for supporting early outcome prediction.

ACKNOWLEDGEMENTS

The authors would like to express their gratitude to the parents and their newborns who participated in the study. This work was supported by the *Instituto Carlos III*, Ministry of Economy and Competitiveness, Spain [grant numbers CD19/00037, CP16/00034, EC11-244, and PI17/00127].

AUTHOR CONTRIBUTIONS

J.K., M.V., and C.B. were responsible for the conception and design of the study; J.D.P.-R., M.M.C., A.A.-D., A.S.G., J.M.-R., R.L.S., A.L.-G., D.S.-H., and G.Q. acquired the data; J.K., G.Q., J.D.P.-R., M.M.C., and A.N.-R. analyzed and interpreted the data; J.K. drafted the article; C.B., G.Q., and M.V. revised the manuscript critically and all authors approved the final version of the manuscript.

ADDITIONAL INFORMATION

Supplementary information The online version contains supplementary material available at https://doi.org/10.1038/s41390-021-01553-z.

Competing interests: The authors declare no competing interests.

Consent statement: Legal representatives of all participants signed an informed consent form.

Publisher's note Springer Nature remains neutral with regard to jurisdictional claims in published maps and institutional affiliations.

REFERENCES

1. Kurinczuk, J. J., White-Koning, M. & Badawi, N. Epidemiology of neonatal encephalopathy and hypoxic-ischaemic encephalopathy. *Early Hum. Dev.* **86**, 329–338 (2010).
2. Lee, A. C. C. et al. Intrapartum-related neonatal encephalopathy incidence and impairment at regional and global levels for 2010 with trends from 1990. *Pediatr. Res.* **74**, 50–72 (2013).
3. Lehtonen, L., Gimeno, A., Parra-Llorca, A. & Vento, M. Early neonatal death: a challenge worldwide. *Semin. Fetal Neonatal Med.* **22**, 153–160 (2017).
4. Groenendaal, F. & de Vries, L. S. Fifty years of brain imaging in neonatal encephalopathy following perinatal asphyxia. *Pediatr. Res.* **81**, 150–155 (2017).
5. Ma, Q. & Zhang, L. Epigenetic programming of hypoxic-ischemic encephalopathy in response to fetal hypoxia. *Prog. Neurobiol.* **0**, 28–48 (2015).
6. Lorente-Pozo, S. et al. Oxygen in the neonatal period: oxidative stress, oxygen load and epigenetic changes. *Semin. Fetal Neonatal Med.* **25**, 101090 (2020).
7. Douglas-Escobar, M. & Weiss, M. D. Hypoxic-ischemic encephalopathy: a review for the clinician. *JAMA Pediatr.* **169**, 397–403 (2015).
8. Edwards, A. D. & Azzopardi, D. V. Perinatal hypoxia-ischemia and brain injury. *Pediatr. Res* **47**, 431–432 (2000).
9. Lee, W. L. A., Michael-Titus, A. T. & Shah, D. K. Hypoxic-ischaemic encephalopathy and the blood-brain barrier in neonates. *Dev. Neurosci.* **39**, 49–58 (2017).
10. Nagana Gowda, G. A. & Raftery, D. Biomarker discovery and translation in metabolomics. *Curr. Metabolomics* **1**, 227–240 (2013).
11. Walsh, B. H. et al. The metabolomic profile of umbilical cord blood in neonatal hypoxic ischaemic encephalopathy. *PLoS ONE* **7**, e50520 (2012).
12. Reinke, S. N. et al. 1H NMR derived metabolomic profile of neonatal asphyxia in umbilical cord serum: implications for hypoxic ischemic encephalopathy. *J. Proteome Res.* **12**, 4230–4239 (2013).
13. Ahearne, C. E. et al. Early cord metabolite index and outcome in perinatal asphyxia and hypoxic-ischaemic encephalopathy. *Neonatology* **110**, 296–302 (2016).
14. Denihan N. M. et al. Untargeted metabolomic analysis and pathway discovery in perinatal asphyxia and hypoxic-ischaemic encephalopathy. *J. Cereb. Blood Flow Metab.* **39**, 147–162 (2019).
15. Locci, E. et al. A longitudinal 1H-NMR metabolomics analysis of urine from newborns with hypoxic-ischemic encephalopathy undergoing hypothermia therapy. Clinical and medical legal insights. *PLoS ONE* **13**, e0194267 (2018).
16. Efstathiou, N., Theodoridis, G. & Sarafidis, K. Understanding neonatal hypoxic-ischemic encephalopathy with metabolomics. *Hippokratia* **21**, 115–123 (2017).
17. Noto, A. et al. Urinary gas chromatography mass spectrometry metabolomics in asphyxiated newborns undergoing hypothermia: from the birth to the first month of life. *Ann. Transl. Med.* **4**, 417 (2016).
18. Piñeiro-Ramos, J. D. et al. Metabolic phenotypes of hypoxic-ischemic encephalopathy with normal vs. pathologic magnetic resonance imaging outcomes. *Metabolites* **10**, 109 (2020).
19. Nuñez-Ramiro, A. et al. Topiramate plus cooling for hypoxic-ischemic encephalopathy: a randomized, controlled, multicenter, double-blinded trial. *Neonatology* **116**, 76–84 (2019).
20. Rutherford, M. et al. Assessment of brain tissue injury after moderate hypothermia in neonates with hypoxic-ischaemic encephalopathy: a nested substudy of a randomised controlled trial. *Lancet Neurol.* **9**, 39–45 (2010).
21. Shankaran, S. et al. Neonatal magnetic resonance imaging pattern of brain injury as a biomarker of childhood outcomes following a trial of hypothermia for neonatal hypoxic-ischemic encephalopathy. *J. Pediatr.* **167**, 987–993.e3 (2015).
22. López-González, Á., Godzien, J., García, A. & Barbas, C. Capillary electrophoresis mass spectrometry as a tool for untargeted metabolomics. *Methods Mol. Biol.* **1978**, 55–77 (2019).
23. Sánchez-Illana, Á. et al. Evaluation of batch effect elimination using quality control replicates in LC-MS metabolite profiling. *Anal. Chim. Acta* **1019**, 38–48 (2018).
24. Smith, C. A., Want, E. J., O'Maille, G., Abagyan, R. & Siuzdak, G. XCMS: processing mass spectrometry data for metabolite profiling using nonlinear peak alignment, matching, and identification. *Anal. Chem.* **78**, 779–787 (2006).

25. Martínez-Sena, T. et al. Monitoring of system conditioning after blank injections in untargeted UPLC-MS metabolomic analysis. *Sci. Rep.* **9**, 1–9 (2019).
26. Chang, C.-C. & Lin, C.-J. LIBSVM: a library for support vector machines. *ACM Trans. Intell. Syst. Technol.* **2**, 27:1–27:27 (2011).
27. Sánchez-Illana, Á. et al. Model selection for within-batch effect correction in UPLC-MS metabolomics using quality control - Support vector regression. *Anal. Chim. Acta* **1026**, 62–68 (2018).
28. Kuligowski, J., Sánchez-Illana, Á., Sanjuán-Herráez, D., Vento, M. & Quintás, G. Intra-batch effect correction in liquid chromatography-mass spectrometry using quality control samples and support vector regression (QC-SVRC). *Analyst* **140**, 7810–7817 (2015).
29. Broadhurst, D. et al. Guidelines and considerations for the use of system suitability and quality control samples in mass spectrometry assays applied in untargeted clinical metabolomic studies. *Metabolomics* **14**, 72 (2018).
30. Cohen, J. et al. *Statistical Power Analysis for the Behavioria Sciences* (Lawrence Erlbaum Associates, 1988).
31. Benjamini, Y. & Hochberg, Y. Controlling the false discovery rate: a practical and powerful approach to multiple testing. *J. R. Stat. Soc. Ser. B Methodol.* **57**, 289–300 (1995).
32. Chong, J. et al. MetaboAnalyst 4.0: towards more transparent and integrative metabolomics analysis. *Nucleic Acids Res.* **46**, W486–W494 (2018).
33. Sarafidis, K. et al. Urine metabolomic profile in neonates with hypoxic-ischemic encephalopa-thy. *Hippokratia* **21**, 80–84 (2017).
34. Blaise, B. J. et al. Persistently altered metabolic phenotype following perinatal excitotoxic brain injury. *Dev. Neurosci.* **39**, 182–191 (2017).
35. Vento, M., Sastre, J., Asensi, M. A. & Viña, J. Room-air resuscitation causes less damage to heart and kidney than 100% oxygen. *Am. J. Respir. Crit. Care Med.* **172**, 1393–1398 (2005).

Clinical Nutrition 40 (2021) 1296–1309

Contents lists available at ScienceDirect

Clinical Nutrition

journal homepage: http://www.elsevier.com/locate/clnu

Original article

Effect of donor human milk on host-gut microbiota and metabolic interactions in preterm infants

José David Piñeiro-Ramos [a], Anna Parra-Llorca [a, 1], Isabel Ten-Doménech [a, 1], María Gormaz [a, b], Amparo Ramón-Beltrán [b], María Cernada [b], Guillermo Quintás [c, d], María Carmen Collado [e], Julia Kuligowski [a, *], Máximo Vento [a, b, 2]

[a] Neonatal Research Unit, Health Research Institute Hospital La Fe, Avda Fernando Abril Martorell 106, 46026 Valencia, Spain
[b] Division of Neonatology, University & Polytechnic Hospital La Fe, Avda Fernando Abril Martorell 106, 46026 Valencia, Spain
[c] Health and Biomedicine, Leitat Technological Center, Carrer de la Innovació, 2, 08225 Terrassa, Spain
[d] Analytical Unit, Health Research Institute La Fe, Avda Fernando Abril Martorell 106, 46026 Valencia, Spain
[e] Instituto de Agroquímica y Tecnología de Alimentos (IATA-CSIC), Av. Agustin Escardino 7, 46980, Paterna, Spain

ARTICLE INFO

Article history:
Received 8 June 2020
Accepted 14 August 2020

Keywords:
Donor human milk (DHM)
Gut-microbiota
Own mother's milk (OMM)
Preterm infant
Untargeted metabolomics
Nutrition

SUMMARY

Background & aims: Human milk is the gold standard for infant nutrition. Preterm infants whose mothers are unable to provide sufficient own mother's milk (OMM), receive pasteurized donor human milk (DHM). We studied metabolic signatures of OMM and DHM and their effect on the interplay of the developing microbiota and infant's metabolism.

Methods: Metabolic fingerprinting of OMM and DHM as well as infant's urine was performed using liquid chromatography–mass spectrometry and the infant's stool microbiota was analyzed by 16S rRNA sequencing.

Results: Significant differences in the galactose and starch and sucrose metabolism pathways when comparing OMM and DHM, and alterations of the steroid hormone synthesis and pyrimidine metabolism pathways in urine were observed depending on the type of feeding. Differences in the gut-microbiota composition were also identified.

Conclusion: The composition of DHM differs from OMM and feeding of DHM has a significant impact on the metabolic phenotype and microbiota of preterm infants. Our data help to understand the origin of the observed changes generating new hypothesis: i) steroid hormones present in HM have a significant influence in the activity of the steroid hormone biosynthesis pathway in preterm infants; ii) the pyrimidine metabolism is modulated in preterm infants by the activity of gut-microbiota. Short- and long-term implications of the observed changes for preterm infants need to be assessed in further studies.

1. Introduction

Breastfeeding is regarded as the best nutrition in the first six months of life. Apart from providing nutritional elements needed for growth, known short and long-term benefits for the infant-mother dyad are numerous [1,2]. Progress in medical interventions has allowed to increase the survival of extremely low gestational age newborns and early infant nutrition has become a major player in improving clinical outcomes of survivors [3]. Human Milk (HM) is recommended for preterm infants based on an array of benefits provided to this highly vulnerable population [4–11].

Currently, pasteurized donor human milk (DHM) is preferred over premature infant formula for premature infants whose mothers are unable to provide an adequate supply of milk [12]. Most DHM is provided by women who have delivered at term and donate their milk in later stages of lactation from weeks to several months after delivery. In comparison to milk produced during the first weeks after delivery, milk donated in later stages of lactation is typically low in protein, fat, and other bioactive molecules [13]. The composition is further affected by the processing of expressed milk following stringent protocols applied

* Corresponding author.
E-mail addresses: julia.kuligowski@uv.es (J. Kuligowski), maximo.vento@uv.es (M. Vento).
[1] These authors have contributed equally.
[2] Senior authorship.

https://doi.org/10.1016/j.clnu.2020.08.013

Abbreviations

HM	human milk
GA	gestational age
DHM	donor human milk
NEC	necrotizing enterocolitis
OMM	own mother's milk
LC-QTOFMS	liquid chromatography–quadrupole time-of-flight mass spectrometry
IPA	isopropanol
MTBE	methyl tert-butyl ether
IS	internal standard
QC	quality control
OTU	operational taxonomic unit
PICRUSt	Phylogenetic Investigation of Communities by Reconstruction of Unobserved States
PCoA	Principal Coordinates Analysis
PERMANOVA	permutational multivariate analysis of variance
KEGG	Kyoto Encyclopedia of Genes and Genomes
FC	fold change
AMON	Annotation of Metabolite Origins via Networks
KO	KEGG Orthology identifier
IQR	interquartile range
FDR	false discovery rate
CI	confidence interval
SD	standard deviation
R	Pearson correlation coefficients
HMO	human milk oligosaccharide

in HM banks involving pasteurization, necessary for minimizing the potential to transmit infectious agents as well as freezing and long-term storage [14–16]. While the macronutrient composition remains relatively intact, several bioactive components, such as enzymes and immune cells are compromised or destroyed [17,18].

The use of DHM in comparison to the use of formula milk results in lower rates of weight gain, linear growth, and head growth, but it was shown that DHM might reduce the incidence of necrotizing enterocolitis (NEC) [19,20]. Beyond the assessment of clinical parameters, scientific evidence for the effects of DHM on preterm infants is scarce. Recently it was shown that despite pasteurization, DHM does not compromise the protection against oxidative stress in comparison to the use of own mother's milk (OMM) [21]. Furthermore, the study of the composition of the developing gut-microbiome of preterm infants depending on the type of nutrition was in the spotlight of clinical studies [22,23], as diseases such as NEC and neonatal sepsis have been linked to shifts in microbial dynamics and early gut-microbiota [24,25]. It was observed that DHM fed preterm infants showed differences in the microbial patterns as compared to OMM fed infants. However, changes in the bacterial composition between DHM and OMM fed infants were smaller than in comparison to formula fed infants [22].

The metabolome represents a complex milieu of compounds of different origins, including human metabolism, the diet, xenobiotics, as well as metabolites produced by bacteria residing in the human gut that may cross the intestinal barrier and hence, it allows to untangle the relationships between diet, metabolome and health status [26]. The usefulness of metabolomics for characterizing the functional status of host-gut microbiota interactions has been repeatedly described [27,28] and comprehensive approaches seek to monitor alterations in the microbiota and host co-metabolites to identify metabolic patterns associated to changes in the microbiota functionality [29].

We hypothesize that differences in the composition of pasteurized DHM in comparison to OMM have an impact on the physiological response of preterm infants at the phenotypic level, and more specifically on the host-gut microbiota metabolic interactions. The study of the composition of the gut-microbiota as well as the urinary metabolome of preterm infants exclusively consuming either DHM or OMM (i.e. ≥80% v/v of the total intake) aided by state-of-the art bioinformatics tools based on metabolic networks allowed to gain insight into their response to nutrition as well as the interaction between diet, microbiome and infant's metabolism.

2. Material and methods

2.1. Study population

A prospective, observational cohort study was conducted including consecutively admitted preterm infants born at ≤32 weeks of gestation and/or birth weight ≤1500 g in the Division of Neonatology of the University and Polytechnic Hospital La Fe (Valencia, Spain) during a 12 month period. Two groups were recruited according to the main feeding type accounting for ≥80% v/v of the nutritional intake with either OMM or DHM after achieving full enteral nutrition (150 mL/kg/day). Inclusion and exclusion criteria are listed in Supporting material Table 1. The study protocol was approved by the Ethics Committee for Biomedical Research of the Health Research Institute La Fe (Valencia, Spain) with approval number 2014/0247. All methods were performed in accordance with the relevant guidelines and regulations and written permission was obtained from legal representatives by signing an informed consent form.

The protocols of the Division of Neonatology strongly support breastfeeding. If necessary, DHM is administered under medical prescription as a supplement to preterm infants born below ≤32 weeks or ≤1500 g of birth weight. Also, in case mothers refuse to breastfeed, DHM is offered. DHM is collected, processed, and stored in milk banks. Milk bank guidelines recommend Holder pasteurization (62.5 °C, 30 min) to inactivate viral and bacterial agents [15]. Both, DHM and OMM are routinely fortified with HM fortifier (PreNAN FM 85, Nestle "R", Vevey, Switzerland), adding one gram per 25 mL of milk. The nutritional intake was prospectively monitored, but not modified for this observational study.

2.1.1. Maternal and infant biological samples

OMM (n = 15) was collected one month after preterm birth. DHM (n = 12) was provided by volunteers admitted after the routine screening and interview at the HM bank (Banco de Leche Materna at the Hospital Universitario y Politécnico La Fe).

Mothers expressed milk using breast milk pumps following a standard operating procedure employed routinely in the hospital and the HM bank. Before extraction, hands must be washed with soap and water and nipples are cleaned with water. The removable parts of the breast milk pump as well as the collection bottles are sterilized. Aliquots of DHM were collected after Holder pasteurization. OMM and DHM samples were agitated and 1 mL aliquots were collected in dry, 1.5 mL microcentrifuge tubes.

Urine samples were collected from infants exclusively receiving DHM (n = 20) or OMM (n = 20) one month after birth using sterile

cotton pads placed in the diaper. Cotton pads were retrieved after one hour and squeezed with a syringe. The process was repeated until a minimum volume of 1 mL was collected. Stool samples from preterm infants exclusively receiving OMM ($n = 18$) or DHM ($n = 18$) were collected directly from the diaper when full enteral nutrition was achieved. All samples (urine, HM, and stool) were stored at −80 °C until analysis.

2.2. Liquid chromatography–quadrupole time-of-flight mass spectrometry (LC-QTOFMS) metabolomic screening of urine and HM samples

2.2.1. Standards and reagents

Acetonitrile (CH_3CN), methanol (CH_3OH), and isopropanol (IPA), all LCMS grade, methyl tert-butyl ether (MTBE, reagent grade), ammonium acetate (≥98%), formic acid (HCOOH, >98%), reserpine (>99%), and leucine-encephaline (97%) were obtained from Sigma Aldrich Quimica SA (Madrid, Spain). Ultra-pure water (>18.2 MΩ) was generated using a Milli-Q Water Purification System (Merck Millipore, Darmstadt, Germany). Phenylalanine-D_5 (98%) and methionine-D_3 (98%) were purchased from Cambridge Isotopes Laboratory Inc. (Andover, MA, USA); caffeine-D_9 (98%) was from Toronto Research Chemicals (Toronto, Ontario, Canada); (15,15,16,16,17,17,18,18,18-D_9) oleic acid-D_9 (>99%) was purchased from Avanti Polar Lipids (Alabaster, AL, USA) and prostaglandin $F_{2\alpha}$-D_4 (≥98%, deuterated incorporation ≥99%) was purchased from Cayman Chemical Company (Ann Arbor, MI, USA).

2.2.2. HM preparation and analysis

Parameters employed for HM fingerprinting have been described elsewhere [30]. In summary, OMM and DHM samples were subjected to a single-phase extraction procedure by adding 175 μL of CH_3OH followed by 175 μL of MTBE [31] and 20 μL of supernatant were added to 80 μL of a CH_3OH:MTBE (1:1, v/v) solution.

Untargeted metabolomics analysis was carried out employing a 1290 Infinity UPLC system from Agilent Technologies (Santa Clara, CA, USA) equipped with a Kinetex C18 column (50 × 2.1 mm, 1.7 μm) from Phenomenex (Torrance, CA, USA) running a binary gradient with (5:1:4 IPA: CH_3OH:H_2O 5 mM ammonium acetate, 0.1% v/v HCOOH) and (99:1 IPA:H_2O 5 mM ammonium acetate, 0.1% v/v formic acid) as mobile phase components. Column and autosampler were kept at 55 and 4 °C, respectively and the injection volume was 4 μL. For detection, an Agilent 6550 iFunnel QTOF-MS system working in the ESI^+ mode was used in the range between 70 and 1700 m/z with automatic MS spectra recalibration during analysis. LC-QTOFMS data acquisition was carried out employing MassHunter Workstation (version B.07.00) from Agilent.

2.2.3. Urine preparation and analysis

Urine samples were thawed on ice and thoroughly shaken on a Vortex® mixer during 10 s followed by centrifugation at 16 000×*g* and 4 °C during 10 min. 50 μL of supernatant were added to 50 μL of an internal standard (IS) solution containing reserpine, phenylalanine-D_5, leucine-enkephalin, caffeine-D_9, and methionine-D_3 at 2 μM each in H_2O:CH_3CN (96:4, 0.1% HCOOH v/v) and transferred to a 96-well plate. A blank extract was prepared using water instead of urine and following the same procedure as described for urine samples. A pooled quality control (QC) sample was prepared by mixing 5 μL of each study sample. Metabolomic analysis was carried out employing a 1290 Infinity UPLC system from Agilent Technologies equipped with a UPLC BEH C18 column (100 × 2.1 mm, 1.7 μm) from Waters (Wexford, Ireland). The flow rate was set to 400 μL min^{-1} running a binary gradient with 0.1% v/v HCOOH in H_2O and 0.1% v/v HCOOH in CH_3CN as mobile phase components. All remaining analysis parameters were set as described for HM analysis.

2.2.4. QC procedures

Before LC-QTOFMS experiments, a system suitability check was carried out by analyzing a 2 μM IS solution to ensure that the retention times, peak area and shape values and mass accuracies were within laboratory defined limits. Eight QCs were injected prior to the study samples at the beginning of the analysis batch for conditioning of the LC-QTOFMS system. Data acquired during the analysis of those samples were discarded. The blank extract was injected twice, once during system conditioning and at the end of the measurement sequence to identify signals from other than biological origin and data clean-up [32]. The injection order of sample extracts was randomized. The QC was injected every 5 samples and twice at the beginning and end of the batch for assessment and correction of instrumental performance [33].

2.3. Microbiota analysis

The analysis of the fecal microbiota composition has been described elsewhere [22]. Briefly, total fecal DNA was isolated using the MasterPure Complete DNA & RNA Purification Kit (Epicentre, Madison, WI United States) and V3–V4 region 16S rRNA libraries were sequenced using a 2 × 300 bp paired-end run (MiSeq Reagent kit v3) on a MiSeq-Illumina (Illumina, San Diego, USA) platform.

2.4. Data processing and statistics

2.4.1. Metabolomics data pre-processing

The pre-processing pipeline for data acquired during the analysis of HM samples has been described elsewhere [30]. For urine, centroid LC-QTOFMS raw data were converted to mzXML format employing ProteoWizard [34] (http://proteowizard.sourceforge.net/). The selection of parameters for peak table extraction and alignment was based on the observed variation of retention times and m/z values of ISs. XCMS software (http://metlin.scripps.edu/xcms/) [35–37] and CAMERA [38] in R 3.6.1 were employed for the generation of peak tables. For data acquired from urine samples, the centWave method with the following settings was used for peak detection: m/z range = 70–1200, ppm = 15, peakwidth = (3 and 20), snthr = 6. A minimum difference in m/z of 0.01 Da was selected for overlapping peaks. Intensity-weighted m/z values of each feature were calculated using the wMean function. Peak limits used for integration were found through descent on the Mexican hat filtered data. Peak grouping was carried out using the "density" method using mzwid = 0.015 and bw = 6. Retention time correction was carried out using the "obiwarp" method. After peak grouping, the fillPeaks method with the default parameters was applied to fill missing peak data. Automatic integration was assessed by comparison to manual integration using IS signals. A total of 40,513 features were initially detected after peak detection, integration, chromatographic deconvolution, and alignment in urine samples.

Further data processing and statistical analysis were carried out in MATLAB 2017b (Mathworks Inc., Natick, MA, USA) using in-house written scripts (available from the authors) and the PLS Toolbox 8.7 (Eigenvector Research Inc., Manson, WA, USA). During data pre-processing and filtering of data from urine analysis, features with an intensity <800 AU and those with a mean peak area <9 × mean peak area in blank samples, were removed [33]. Intra-batch effect correction was performed using Quality Control-Support Vector Regression algorithm [39–41] and the LIBSVM library [42] with the following parameters: ε–range = 2–5%; γ-range = $1–10^5$; C interval = 50%. Finally, features with a %RSD in QC

samples >20% after QC-SVRC were removed from the peak table. Urinary metabolic data were normalized to the creatinine concentration in each urine sample quantified by the modified Jaffe method (DetectX® urinary creatinine detection kit, Arbor Assays, Ann Arbor, MI, USA) following the manufacturer's protocol and employing a dilution factor of 1:4 during sample preparation.

2.4.2. Microbiota data

Sequencing data were processed using a QIIME pipeline (version 1.9.0) [43] running in R. Operational taxonomic units (OTUs) tables with 97% identity were constructed and representative sequences were taxonomically classified based on the Greengenes 16S rRNA gene database (version 13.8). OTUs with detection frequency <20% across all samples were removed and predictive inferred functional analysis was performed using the Phylogenetic Investigation of Communities by Reconstruction of Unobserved States (PICRUSt) approach, as described elsewhere [44]. Alpha-diversity indices (Chao1 and Shannon, richness and diversity index, respectively), Principal Coordinate Analysis (PCoA) of beta diversity based on UNIFRAC distance (phylogenetic) and permutational multivariate analysis of variance (PERMANOVA) test with 999 permutations were obtained to show the significance between-groups.

2.4.3. Pathway analysis

Differences between OMM and DHM group were studied on the pathway level employing the "MS Peaks to Pathways" tool (version 2.0) available in MetaboAnalyst 4.0 [45] using a mass accuracy of 5 ppm, the *mummichog* algorithm with a *p*-value cut-off of 0.05, and the Kyoto Encyclopedia of Genes and Genomes (KEGG) *Homo Sapiens* pathway library [46,47]. As an input, a four column table was generated including *m/z*, RT, the *p*-values from a t-test comparing mean values between each group and accounting for unequal variances, and fold changes (FC) calculated as the ratio of medians between groups. Metabolites included within significantly altered pathways were annotated in LC-QTOFMS data from HM samples using the output retrieved from the *mummichog* algorithm ('level 3' identification as defined by The Metabolomics Standards Initiative [48]).

AMON (Annotation of Metabolite Origins via Networks) was used to integrate microbiome and metabolome data [49]. This tool produces a table indicating which compounds could be produced by the microbiome, the host, or both based on the provided lists of gut-microbiome and human KEGG Orthology identifiers (KOs). AMON was used to compute enrichment of KEGG pathways in the compounds that were detected via LC-QTOFMS based on the list of annotated KEGG compound IDs provided by *mummichog* and were predicted to be generated either by the fecal microbiome or the host metabolism. This calculation is performed for all KEGG pathways with at least one metabolite predicted to be produced by the input gene sets.

2.4.4. Statistical tests

Categorical variables were compared using Pearson's chi-squared test ($\alpha = 5\%$). Kolmogorov–Smirnov analysis was performed to test the normal distribution of the data. Continuous variables were expressed as mean ± standard deviation or medians with interquartile range (IQR) depending on underlying distributions and comparisons were carried out using the Student's t-test ($\alpha = 5\%$) for data following a normal distribution or alternatively the Wilcoxon rank-sum test ($\alpha = 5\%$). values were false discovery rate (FDR)-adjusted where indicated. Pearson correlation was used to assess correlations between variables. Venny 2.1.0 was used for generating the Venn diagram [50].

2.4.5. Data availability

Peak tables extracted from urine and HM LC-QTOFMS data are accessible via the Mendeley Data repository (https://data.mendeley.com/) under https://doi.org/10.17632/7tb4d66z7c.1 and https://doi.org/10.17632/fnzbxmkv83.1, respectively. Sequencing data from the preterm gut microbiota of the infants matching the individuals included in this study can be retrieved from GenBank Sequence Read Archive Database under project accession number PRJEB25948 [22].

3. Results

3.1. Clinical data

In this observational study, OMM samples from mothers of preterm infants ($n = 15$) as well as DHM samples ($n = 12$) provided by volunteers at the HM bank were analyzed. OMM samples were collected at 1 month of age. The time of sample collection of DHM samples was heterogeneous, since for each mother several aliquots were collected over time and pooled prior to pasteurization. In this study, the elapsed time between the first and last expression of a pooled DHM sample ranged between 9 and 72 days. The median value of this elapsed time was used to represent the time of collection with respect to the infants' age. As a result, time of collection of DHM samples ranged between 21 and 164 days after delivery with a median value of 87 days (83 IQR). With respect to GA the median (5th–95th percentile) in the OMM group was 29 (25–32) in comparison to 40 (27–41) for milk donors (DHM group).

20 preterm infants exclusively receiving OMM and 20 exclusively fed with DHM were enrolled. Table 1 displays the demographic, perinatal, clinical, and analytical data of the recruited infants grouped according to the type of feeding. No statistically significant differences (*p*-values >0.05) were observed between the study groups.

3.2. Metabolomic analysis of HM samples

Metabolic fingerprints of OMM and DHM consumed by the preterm infants included in this study were acquired employing an LC-QTOFMS platform retrieving a total of 7109 metabolic features after peak detection, deconvolution, integration, alignment, within-batch effect correction, and clean-up. For 1034 features (14.6%), significant differences in mean values of OMM and DHM groups (t-test, *p*-value <0.05) were found and for 21 and 199 features $\log_2$(FC) <−1 and >1, respectively, were detected. Metabolic network analysis was employed for a functional interpretation of the acquired metabolic profiles within relevant networks using the *mummichog* algorithm [52]. Pathway analysis detected 13 pathways with more than two significantly changing metabolites (see Table 2). Significant differences between DHM and OMM groups were found for galactose and starch and sucrose metabolism (*gamma p*-value < 0.05).

3.3. Preterm gut-microbiota

Gut-microbiota profiles differed between DHM and OMM groups as shown in Fig. 1. Significant differences in beta diversity were detected (PCoA, PERMANOVA *P*-value = 0.04), although alpha diversity indexes were not different between groups. Significantly higher abundances of Staphylococcaceae (*Staphylococcus* genus) and Pasteurellaceae members (Wilcoxon rank-sum test, *p*-value <0.05) were observed in the DHM group, but differences did not remain significant after FDR correction. Likewise, functional prediction of KEGG pathways identified changes in ten metabolic

Table 1
Characteristics of the study population (infants).

Parameter	OMM ($n = 20$)	DHM ($n = 20$)	p-value
Gender, n (%)			
Male	14 (70)	12 (60)	0.06
Female	6 (30)	8 (40)	
GA median (5–95% CI)	28 (27–29)	29 (28–30)	0.06
Antenatal steroids, n (%)	17 (85)	17 (85)	0.6
Birth weight (g), mean (SD)	1300 (300)	1400 (200)	0.9
Preeclampsia, n (%)	2 (10)	5 (25)	0.2
Chorioamnionitis, n (%)	5 (25)	2 (20)	0.2
Mode of birth, n (%)			
Vaginal	9 (45)	9 (45)	0.6
C-section	11 (55)	11 (55)	
Apgar 1 min, median (IQR)	8 (5–9)	8 (6–9)	0.5
Apgar 5 min, median (IQR)	10 (8–10)	9 (8–10)	0.4
Umbilical artery blood gases, mean (SD)	7.2 (0.3)	7.28 (0.07)	0.9
Days of oxygen supplementation, median (IQR)	0 (1.3)	0 (0)	0.2
Respiratory distress syndrome, n (%)	8 (40)	5 (25)	0.13
Apneic syndrome, n (%)	17 (85)	15 (75)	0.2
Mechanical ventilation, n (%)	5 (25)	4 (20)	0.7
Non-invasive ventilation, n (%)	18 (90)	18 (90)	0.06
Postnatal steroids, n (%)	1 (5)	0 (0)	n.a.
Antibiotics therapy, n (%)			
Pre/intra-partum	20 (100)	20 (100)	1.0
Post-partum	8 (40)	7 (35)	0.6
Necrotizing enterocolitis, n (%)	0 (0)	1 (5)	n.a.
Bronchopulmonary dysplasia, n (%)	1 (5)	1 (5)	0.6
Persistent ductus arteriosus, n (%)	9 (45)	3 (15)	0.10
Intra-periventricular hemorrhage ≥grade 2 (Papile's classification [51]), n (%)	6 (30)	0 (0)	n.a.

Note: CI, confidence interval; SD, standard deviation; IQR, interquartile range; categorical variables were compared using Pearson's chi-squared test ($\alpha = 0.05$). Kolmogorov–Smirnov analysis was performed to test the normal distribution of the data. Continuous variables were expressed as mean ± standard deviation or medians with interquartile range depending on underlying distributions and comparisons were carried out using the Student's t-test ($\alpha = 5\%$) for data following a normal distribution or alternatively the Wilcoxon rank-sum test ($\alpha = 5\%$).

Table 2
Altered pathways in DHM vs. OMM.

Pathway name	Hits (all)	Hits (sig)	p-value	*gamma* p-value
Galactose metabolism	5	5	0.0004	0.007
Starch and sucrose metabolism	4	4	0.002	0.03
Fructose and mannose metabolism	7	4	0.04	0.2
Tyrosine metabolism	4	3	0.03	0.2
Amino sugar and nucleotide sugar metabolism	5	3	0.07	0.3
Linoleic acid metabolism	6	3	0.12	0.4
Glycolysis/Gluconeogenesis	2	2	0.05	0.4
Ascorbate and aldarate metabolism	2	2	0.05	0.4
Neomycin, kanamycin and gentamicin biosynthesis	2	2	0.05	0.4
Inositol phosphate metabolism	2	2	0.05	0.4
Phosphatidylinositol signaling system	2	2	0.05	0.4
Lysine degradation	3	2	0.12	0.5
Biosynthesis of unsaturated fatty acids	14	4	0.4	0.6

Note: P-values from Fisher's exact t-test (p-value) and adjusted for permutations (*gamma* p-value); all detected pathways with at least 2 significantly altered features are reported.

pathways (p-values < 0.05) that were non-significant after FDR correction.

3.4. Metabolomic analysis of urine samples

Urinary metabolic fingerprints of preterm infants exclusively receiving DHM vs. OMM were recorded employing an LC-QTOFMS platform. Initial pre-processing of data identified 10,450 metabolic features after feature extraction and pre-processing. In this study, 849 features (8.1% of the total) showed significantly different mean values between both groups (t-test, p-value <0.05) with 21 and 343 features showing $\log_2$(FC) of <−1 and >1, respectively, when comparing DHM and OMM groups. A list of the detected metabolic pathways with at least two significantly altered metabolic features is shown in Table 3. From the 32 detected pathways, only the steroid hormone biosynthesis pathway and pyrimidine metabolism were found to be significantly altered in urine samples from preterm infants consuming DHM as compared to OMM (*gamma* p-value < 0.05).

Using the results of the *mummichog* algorithm, 331 features were tentatively assigned to steroid hormones belonging to the steroid hormone synthesis pathway (KEGG map00140). Between group comparison of their intensities (i.e. OMM vs DHM) showed that 19 features (see Supporting material Table 2) had significantly different mean values (FDR-adjusted p-value <0.05) and $|\log_2(FC)| > 1$ (see Fig. 2, left). Remarkably, for all 19 features, higher intensities were detected in the OMM group as compared to the DHM group (see Fig. 2, right). This result confirms the alteration of the steroid hormone synthesis pathway detected by pathway analysis in newborns receiving DHM vs. OMM.

Likewise, 101 (1.0%) features were tentatively annotated as metabolites included in the pyrimidine metabolism pathway. However, none of these features showed significant differences in

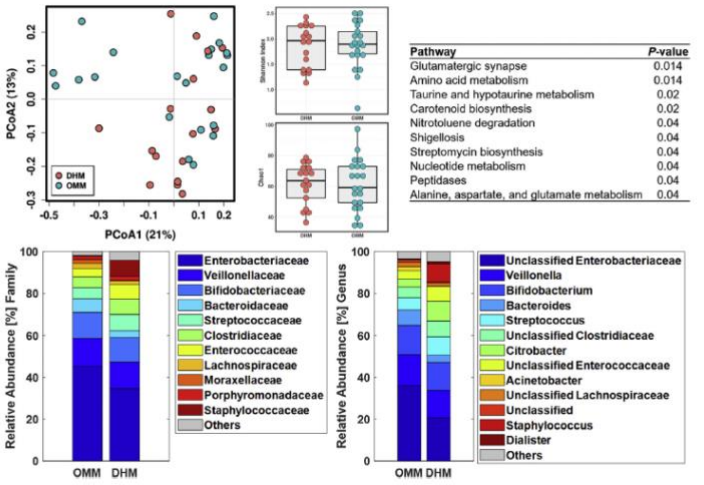

Pathway	*P*-value
Glutamatergic synapse	0.014
Amino acid metabolism	0.014
Taurine and hypotaurine metabolism	0.02
Carotenoid biosynthesis	0.02
Nitrotoluene degradation	0.04
Shigellosis	0.04
Streptomycin biosynthesis	0.04
Nucleotide metabolism	0.04
Peptidases	0.04
Alanine, aspartate, and glutamate metabolism	0.04

Fig. 1. Gut-microbiota profile of preterm infants exclusively receiving OMM and DHM. PCoA scores plot representing beta diversity relationships (top, left), alpha diversity (Shannon index) and richness (Chao1 index) (top, middle), functional predictions of KEGG pathways with significant differences between groups (top, right), and relative abundances at the family (bottom, left) and genus levels (bottom, right). OMM = light blue and DHM = orange (For interpretation of the references to colour in this figure legend, the reader is referred to the Web version of this article).

their mean intensities (FDR-adjusted *p*-value <0.05) and $|\log_2(FC)| > 1$. This indicates that alteration of pyrimidine metabolism is less evident than observed for the steroid hormone biosynthesis pathway, which agrees with the *gamma* *p*-values reported in Table 3 of 1.1E-08 vs. 0.04, respectively.

3.5. Integrative analysis of data from metabolomics and microbiota profiling

Integrative analysis of omics data was performed to elucidate the origin of observed pathway alterations in urine samples. The HM peak table was searched for metabolites of the steroid hormone biosynthesis pathway using tentative mummichog annotations. 73 unique features were assigned and out of those, 10 features (see Supporting material Table 3) showed significant differences in mean values and $|\log_2(FC)| > 1$ (see Fig. 3, left). Again, consistently higher intensities were detected in the OMM group as compared to the DHM group (see Fig. 3, right).

Figure 4 represents Pearson correlation coefficients (R) calculated between metabolic features annotated as steroid hormones in HM and urine. In HM samples, steroid hormone levels typically showed strong correlations with a median R = 0.9 (0.6–1.0 5th–95th percentile), whereas moderate correlation were found within urine samples (R = 0.5, 0.2–1.0 5th–95th percentile) as well as between urine and HM steroid levels (R = 0.38, 0.06–0.6 5th–95th percentile). Conversely, microbiota relative abundances overall did show weak correlations among them (R = −0.1, −0.2–0.7 5th–95th percentile) as well as with HM and urine steroid levels (R = 0.0, −0.3–0.6 5th–95th percentile and R = 0.0, −0.3–0.4 5th–95th percentile, respectively). However, some specific microbiota (i.e. *Blautia*, Unclassified Lachnospiraceae, and *Enterobacter*) were consistently correlated with steroid hormones in HM (R = 0.6, 0.6–0.6 5th–95th percentile).

Figure 5 depicts the steroid hormone biosynthesis pathway in which the altered metabolites annotated in urine and HM were highlighted for better visualization. It can be observed that metabolites found in HM and in urine were at close pathway distances. For example, pregnenolone was altered in HM samples, while direct downstream metabolites (i.e. 21-hydroxy-pregnenolone, 7α-hydroxy-pregnenolone, progesterone, 17α-hydroxy-pregnenolone) were altered in urine samples between DHM and OMM groups.

To explore whether the pathway alteration detected in urine samples could be caused by the activity of the gut-microbiome, an integrative approach (AMON) for the analysis of the gut-microbiome and metabolome data via networks was employed. This tool allows to gain insight on the metabolite origins, i.e. to determine the degree to which annotated compounds in the urinary metabolome of preterm infants may have been produced by bacteria present in fecal samples, the host, either, or neither. From 80 OTUs detected in fecal samples, PICRUSt predicted 6909 unique KOs. For representing the human gene content, the KEGG list of KOs in the human (*Homo sapiens*) genome was used. Altogether, from the 13,019 predicted KOs to be present in the gut microbiome and the human host, and with the information available in KEGG, it was predicted that these KOs produce 3746 compounds via 5463 reactions.

The employed metabolomics assay detected 10,450 metabolic features in urine samples from preterm infants. In total, 869 unique metabolites could be annotated by using the *mummichog* algorithm in the data set. Of these, 765 were predicted to be produced by enzymes in either human only or human and stool bacterial genomes while none of the detected metabolites was exclusively

Table 3
Altered pathways in urine samples from preterm infants consuming DHM vs. OMM.

Pathway name	Hits (all)	Hits (sig)	*p*-value	*gamma p*-value
Steroid hormone biosynthesis	96	43	4E-09	1.1E-08
Pyrimidine metabolism	24	10	0.013	0.04
Alanine, aspartate and glutamate metabolism	22	9	0.02	0.06
Glyoxylate and dicarboxylate metabolism	8	5	0.011	0.06
Nitrogen metabolism	7	4	0.04	0.2
Metabolism of xenobiotics by cytochrome P450	36	11	0.10	0.2
Linoleic acid metabolism	4	3	0.03	0.2
D-Glutamine and D-glutamate metabolism	10	4	0.13	0.3
Retinol metabolism	8	3	0.2	0.5
Arginine biosynthesis	13	4	0.3	0.5
Arachidonic acid metabolism	13	4	0.3	0.5
Drug metabolism – other enzymes	9	3	0.3	0.6
Biosynthesis of unsaturated fatty acids	4	2	0.2	0.6
Cysteine and methionine metabolism	22	5	0.5	0.7
Phenylalanine metabolism	34	7	0.6	0.7
Aminoacyl-tRNA biosynthesis	40	8	0.6	0.7
Phenylalanine, tyrosine and tryptophan biosynthesis	18	4	0.5	0.7
Butanoate metabolism	6	2	0.4	0.7
Valine, leucine and isoleucine degradation	14	3	0.6	0.8
Drug metabolism – cytochrome P450	29	5	0.7	0.9
Ubiquinone and other terpenoid-quinone biosynthesis	10	2	0.6	0.9
Tryptophan metabolism	66	11	0.8	0.9
Vitamin B6 metabolism	11	2	0.7	0.9
Pantothenate and CoA biosynthesis	11	2	0.7	0.9
Glycine, serine and threonine metabolism	12	2	0.7	0.9
Histidine metabolism	20	3	0.8	0.9
Purine metabolism	49	7	0.9	1.0
Folate biosynthesis	15	2	0.8	1.0
Tyrosine metabolism	64	9	0.9	1.0
Porphyrin and chlorophyll metabolism	16	2	0.9	1.0
Lysine degradation	18	2	0.9	1.0
Arginine and proline metabolism	38	2	1.0	1.0

Note: *P*-values from Fisher's exact t-test (*p*-value) and adjusted for permutations (*gamma p*-value); all detected pathways with at least 2 significantly altered features are reported.

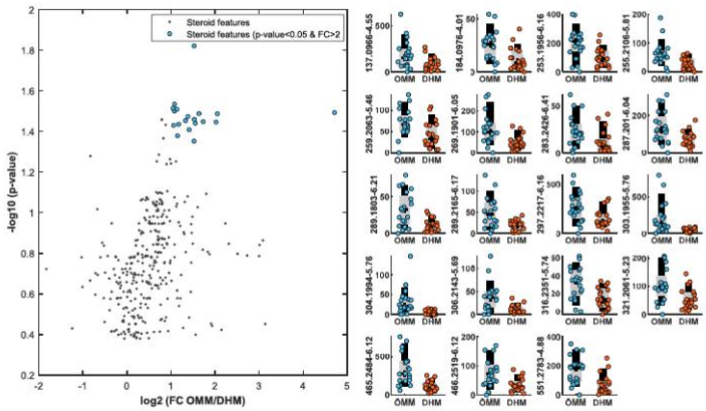

Fig. 2. Steroid hormone signals with different relative signal intensities found in urine samples from preterm infants exclusively receiving OMM or DHM.

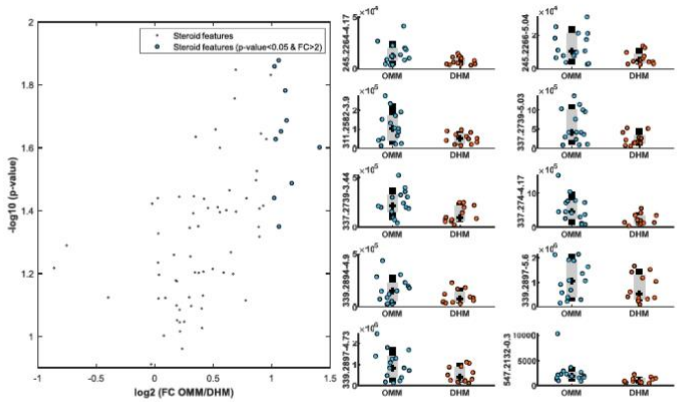

Fig. 3. Steroid hormone signals with different relative signal intensities found in OMM and DHM samples consumed by preterm infants.

attributed to the gene products of intestinal microbiota (see Fig. 6a). The remaining 104 metabolites were not predicted to be from the human or the gut-microbiome either.

The enrichment of pathways that can be produced by each input KO is tested relative to the full set of all compounds in that pathway for the detected human and bacterial metabolites. In total, the calculation was performed for 217 KEGG pathways that had at least one metabolite predicted to be produced by the provided gene sets. For 127 and 98 pathways, FDR adjusted p-values <0.05 and <0.01, respectively, were found in human and/or microbial metabolism (Fig. 6b). Clearly, the impact on the steroid hormone biosynthesis pathway can be ascribed to human metabolism rather than the microbiome with adjusted p-values of 0.0005 and 1.0, respectively. In case of pyrimidine metabolism, adjusted p-values of 0.0005 and 7×10^{-8} were obtained for host and microbiota, respectively. Hence, metabolites from the pyrimidine metabolism pathway are influenced by both, host and microbiome, although the impact was much more pronounced in case of bacterial metabolism. The metabolite origin within the pyrimidine metabolism pathway was further visualized in Fig. 7.

4. Discussion

This study assesses the impact of the administration of DHM in comparison to OMM on the microbiome profiles and metabolic fingerprints of preterm infants during the NICU stay. The comparison of the HM metabolome from DHM and OMM revealed differences in two pathways related to carbohydrate metabolism (see Table 2). The total carbohydrate concentration is higher in milk from mothers of preterm infants in comparison to full-term milk [53] and specifically lactose and human milk oligosaccharides (HMOs) have been found at significantly higher concentrations in preterm milk. In this study, DHM was mainly provided by mothers of term infants and therefore the observed alterations of metabolic pathways related to carbohydrates are consistent with results reported in the literature [53]. Furthermore, although HM carbohydrate contents, including the most abundant carbohydrate lactose and HMOs and glycosaminglycans, are not significantly reduced by Holder pasteurization [54–56], a significant decrease of lactose contents was reported under conditions of frozen storage of pasteurized milk at −20 °C [54]. Observed differences in carbohydrate metabolism might be especially relevant, as it has been reported that bioactive factors contained in HM, such as non-digestible HMOs, could possibly modulate the composition of microbial communities in the gut, selecting for beneficial bacteria, and are emerging as early mediators in the relationship between the development of the gut-microbiome in early life and clinical outcomes [23]. When assessing the composition of the gut-microbiome of preterm infants exclusively fed DHM in comparison to OMM (see Fig. 1), we observed subtle differences.

The impact of the changing milk composition and microbiome on the preterm infant was measured through the study of the urinary metabolome. Our results have unraveled the presence of significant differences in the metabolome (see Table 3) that may exert an influence upon specific aspects of preterm physiology of yet unknown short-and-long-term consequences. Specifically, we detected the alteration of the steroid hormone biosynthesis pathway and the pyrimidine metabolism in preterm infants exclusively receiving DHM in comparison to OMM.

Milk-borne hormones including glucocorticoids are postulated to play a role in the proliferation and differentiation of the intestinal epithelium and vertical transmission of glucocorticoids via HM has been described [57]. Hence, the possibility of attributing the changes in the preterm infant's metabolism to differences in the composition of DHM and OMM was explored. Metabolites of the steroid hormone biosynthesis pathway were found to decrease in infants consuming DHM (Fig. 2) and the same trend was observed in DHM as compared to OMM (Fig. 3) while no differences in antenatal or postnatal steroid administration were found between infants receiving DHM or OMM. Of note, changes in the hormonal environment in the mother giving birth preterm or term could explain the differences found [57,58]. However, further studies addressing this specific issue are needed. Interestingly, in our study, some of the metabolites that showed significantly different

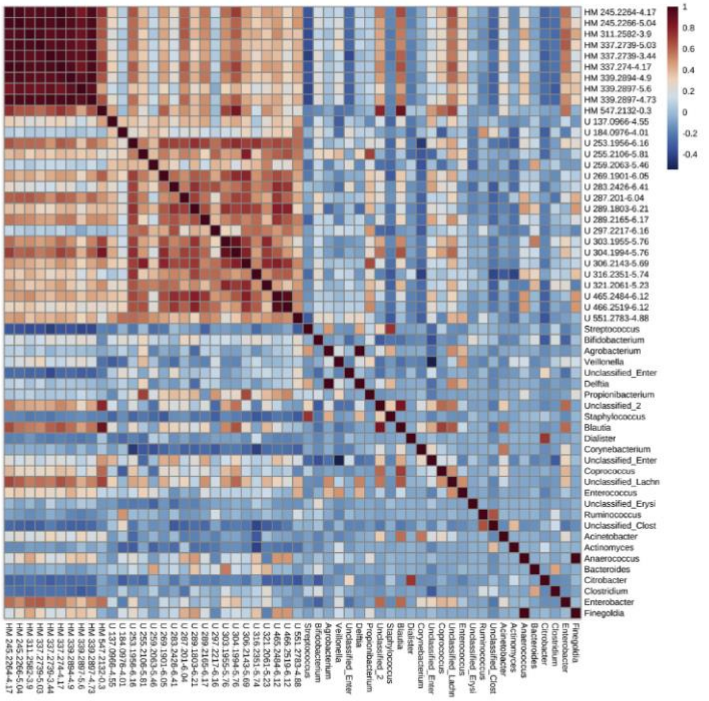

Fig. 4. Correlation coefficients of steroid hormones in urine and HM samples as well as microbiota profiles (genus level).

concentrations between DHM and OMM were direct precursors of metabolites altered in urine samples (see Fig. 5). It has been observed that HM glucocorticoid hormone levels follow the diurnal rhythm of maternal hypothalamus-pituitary-adrenal axis activity reflected in diurnal changes [58]. DHM is processed in batches as a pool from HM aliquots collected on different days and the collection time may vary between HM aliquots. Furthermore, administered DHM was subjected to Holder pasteurization. There is controversy about the stability of hormones during heat treatment [58–61] and comprehensive studies covering metabolites from the steroid hormone biosynthesis pathway are lacking.

We also explored the possibility of gut-microbiota to contribute to the observed changes in steroid hormone biosynthesis pathway in preterm infants fed with DHM vs. OMM. HM glucocorticoids might modify the intestinal microbiome and intestinal bacteria can metabolize steroid hormones and are possibly involved in metabolizing endogenous glucocorticoids [57,62]. In this study overall, weak correlations were observed within microbiota as well as between microbiota and HM and urine steroids. However, some specific microbiota, i.e. *Blautia*, Unclassified Lachnospiraceae, and *Enterobacter*, showed moderate, but consistent correlations ($R = 0.6$) across altered HM steroids between DHM and OMM groups (Fig. 4). Yet, relative abundances of these microbiota did not correlate with urine steroids.

The urinary metabolome gives a snapshot of the metabolic state of the preterm infant at one month of age. In addition, through the detection of bacterial (co-)metabolites it might mirror the activity of the gut-microbiota. To decipher the origin of observed metabolites, we applied a network-based approach. In our study, the majority of detected metabolites could be produced by both, host and gut-microbiota and none of the detected metabolites was exclusively assigned to bacteria. Pathway enrichment analysis of KEGG pathways in detected compounds indicates that alterations in the steroid hormone biosynthesis pathway are not related to bacterial metabolism (adjusted p-value $= 1$), but significantly affected by human metabolism (adjusted p-value $= 5 \times 10^{-4}$). This supports the hypothesis that changes between steroid levels in DHM and OMM might cause these changes observed in preterm infants. However, pyrimidine metabolism, the second pathway altered in

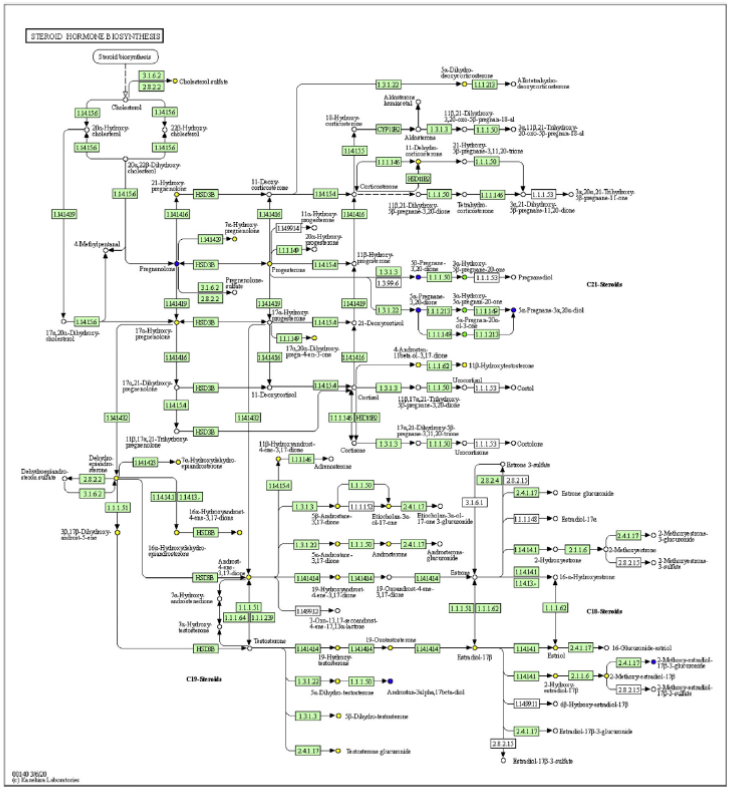

Fig. 5. Altered metabolites of the steroid hormone biosynthesis pathway detected in HM (blue), urine (yellow), or both (green) (For interpretation of the references to colour in this figure legend, the reader is referred to the Web version of this article).

the urinary metabolome of preterm infants, is significantly affected by both, bacterial and host metabolism (adjusted *p*-values of 7×10^{-8} and 5×10^{-4}, respectively) and hence, the metabolites of this pathway seem to be strongly influenced by the activity of the gut-microbiome. Pyrimidine metabolism could be the link between ingestion of OMM and improved neuro-developmental outcome at later stages, as it is tightly related to brain growth and metabolism. Cytidine and uridine act as precursors of the cytidine triphosphate used in the biosynthetic pathway of phosphatidylcholine and phosphatidylethanolamine via the Kennedy cycle [63]. Brain growth and exponential establishment of synaptic connections are essential in the neonatal period.

The study has some limitations. This is a pilot study and hence, the number of subjects included is limited requiring the validation of the reported findings in follow-up studies. However, the aim here was to test the feasibility of the study design and to provide a knowledge base for future studies. DHM samples were different from OMM in terms of GA as well as collection time. However, this resembles the characteristics of HM provided by HM banks. Furthermore, the metabolism of HM-specific compounds is not well-covered in KEGG pathways. Finally, AMON does not account for co-metabolism between the host and microbes which might be a limitation when combined with metabolomics data from urine samples, as many metabolites need to be transformed by human metabolism prior to their excretion.

In summary, this is, to the best of our knowledge, the first time that the interplay between DHM, preterm infant and the gut-microbiome has been comprehensively assessed. The results obtained indicated differences between DHM from a HM bank and OMM samples from mothers of preterm infants related to carbohydrate metabolism. Preterm infants exclusively receiving

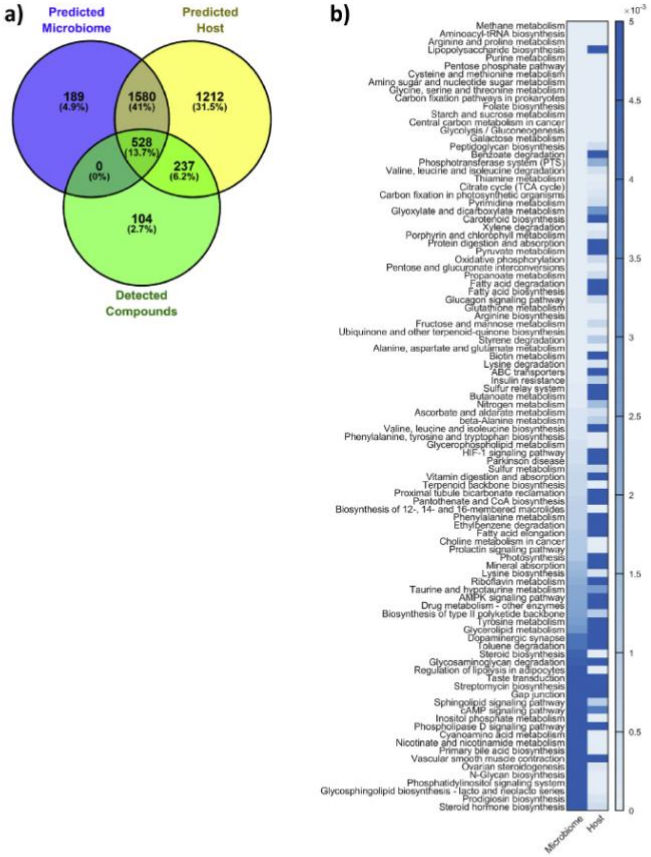

Fig. 6. Metabolic interactions of host-gut microbiota in preterm infants. Metabolites predicted to be produced by the gut-microbiome and the host as well as measured compounds (LC-QTOFMS) (a) and heatmap showing the adjusted *p*-values associated with a pathway enrichment analysis of KEGG pathways in compounds that were detected via untargeted LC-QTOFMS analysis of urine samples and were predicted to be generated by members of the fecal microbiota or the human host (b) Note: only pathways with adjusted *p*-values <0.01 in host and/or microbiome are shown to enhance visibility.

either DHM or OMM showed a clear alteration in urinary steroid hormone levels and the alteration of the pyrimidine metabolism between groups was detected. Our data help to understand the origin of the observed changes generating new hypothesis: i) steroid hormones present in HM have a significant influence in the activity of the steroid hormone biosynthesis pathway in preterm infants, either directly or through the modification of gut-microbiota; ii) the pyrimidine metabolism is modulated in preterm infants by the activity of gut-microbiota. Future studies making use of targeted approaches for the validation of the changes highlighted by pathway analysis are required, specifically focusing on the quantification of metabolites from the

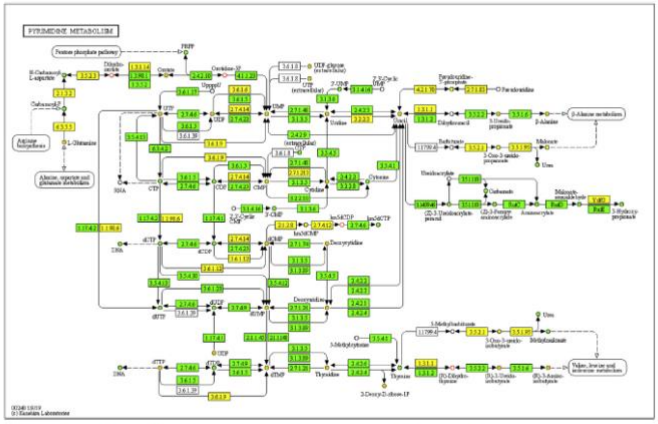

Fig. 7. Pyrimidine metabolism map (KEGG map00240) colored by putative origin of compounds (circles), and presence of the reaction (rectangles). Note: yellow indicates human origin, green indicates human or bacteria origin, and red outlined compounds that were detected by LC-QTOFMS (For interpretation of the references to colour in this figure legend, the reader is referred to the Web version of this article).

steroid hormone biosynthesis pathway in urine and HM and assessment of carbohydrate metabolism in HM. In addition, short- and long-term consequences of the observed changes in the neonatal period need to be evaluated. Finally, the findings of this study are of practical relevance as they might trigger alternative strategies for improving neonatal nutrition based on modifying the properties of DHM through the changes of guideline for DHM collection, targeted fortification and HM processing and storage.

Funding sources

This work was supported by the Instituto de Salud Carlos III, Ministry of Economy and Competitiveness, Spain [grant numbers CD19/00176, CM18/00165, and CP16/00034]; and the European Union's Horizon 2020 Research and Innovation Programme through the Nutrishield project (https://nutrishield-project.eu/) [Grant Agreement No 818110]. MCC would like to acknowledge the support from the European Research Council (ERC) Starting Grant [Grant Agreement No. 639226].

This paper reflects only the authors views; the funding sources are not liable for any use that may be made of the information contained therein and were not involved in the study design; the collection, analysis and interpretation of data; in the writing of the report; and in the decision to submit the article for publication.

Author contribution

MV, MG, MCC, and JK participated in Conceptualization and Funding acquisition; all authors participated in the Investigation and Methodology; JK, GQ, JDPR, and ITD were in charge of Visualization and Writing of the original draft; all authors participated in the reviewing and editing of the draft and approved the final version of the manuscript.

Conflict of interest

The authors declare that the research was conducted in the absence of any commercial or financial relationships that could be construed as a potential conflict of interest.

Acknowledgements

The authors are grateful to parents and their infants, as well as milk donors who agreed to participate in this study. The authors would like to thank K. Thurimella, M. Shaffer, and C. Lozupone for technical assistance with AMON.

Appendix A. Supplementary data

Supplementary data to this article can be found online at https://doi.org/10.1016/j.clnu.2020.08.013.

References

[1] Victora CG, Bahl R, Barros AJD, França GVA, Horton S, Krasevec J, et al. Breastfeeding in the 21st century: epidemiology, mechanisms, and lifelong effect. Lancet Lond Engl 2016;387:475–90. https://doi.org/10.1016/S0140-6736(15)01024-7.

[2] World Health Organization. Guideline: protecting, promoting and supporting breastfeeding in facilities providing maternity and newborn services. 2017.

[3] Boquien C-Y. Human milk: an ideal food for nutrition of preterm newborn. Front Pediatr 2018;6. https://doi.org/10.3389/fped.2018.00295.

[4] Schanler RJ, Shulman RJ, Lau C. Feeding strategies for premature infants: beneficial outcomes of feeding fortified human milk versus preterm formula. Pediatrics 1999;103:1150–7.

[5] Sisk PM, Lovelady CA, Dillard RG, Gruber KJ, O'Shea TM. Early human milk feeding is associated with a lower risk of necrotizing enterocolitis in very low birth weight infants. J Perinatol Off J Calif Perinat Assoc 2007;27:428–33. https://doi.org/10.1038/sj.jp.7211758.

[6] Meinzen-Derr J, Poindexter B, Wrage L, Morrow AL, Stoll B, Donovan EF. Role of human milk in extremely low birth weight infants' risk of necrotizing enterocolitis or death. J Perinatol Off J Calif Perinat Assoc 2009;29:57–62. https://doi.org/10.1038/jp.2008.117.

[7] Maayan-Metzger A, Avivi S, Schushan-Eisen I, Kuint J. Human milk versus formula feeding among preterm infants: short-term outcomes. Am J Perinatol 2012;29:121–6. https://doi.org/10.1055/s-0031-1295652.

[8] Vohr BR, Poindexter BB, Dusick AM, McKinley LT, Wright LL, Langer JC, et al. Beneficial effects of breast milk in the neonatal intensive care unit on the developmental outcome of extremely low birth weight infants at 18 months of age. Pediatrics 2006;118:e115–23. https://doi.org/10.1542/peds.2005-2382.

[9] Isaacs EB, Fischl BR, Quinn BT, Chong WK, Gadian DG, Lucas A. Impact of breast milk on intelligence quotient, brain size, and white matter development. Pediatr Res 2010;67:357–62. https://doi.org/10.1203/PDR.0b013e3181d026da.

[10] Vohr BR, Poindexter BB, Dusick AM, McKinley LT, Higgins RD, Langer JC, et al. Persistent beneficial effects of breast milk ingested in the neonatal intensive care unit on outcomes of extremely low birth weight infants at 30 months of age. Pediatrics 2007;120:e953–9. https://doi.org/10.1542/peds.2006-3227.

[11] Okamoto T, Shirai M, Kokubo M, Takahashi S, Kajino M, Takase M, et al. Human milk reduces the risk of retinal detachment in extremely low-birthweight infants. Pediatr Int 2007;49:894–7. https://doi.org/10.1111/j.1442-200X.2007.02483.x.

[12] American Academy of Pediatrics. Breastfeeding and the use of human milk. Pediatrics 2012;129:e827–41. https://doi.org/10.1542/peds.2011-3552.

[13] Underwood MA. Human milk for the premature infant. Pediatr Clin North Am 2013;60:189–207. https://doi.org/10.1016/j.pcl.2012.09.008.

[14] Picaud J-C, Buffin R. Human milk-treatment and quality of banked human milk. Clin Perinatol 2017;44:95–119. https://doi.org/10.1016/j.clp.2016.11.003.

[15] Peila C, Moro GE, Bertino E, Cavallarin L, Giribaldi M, Giuliani F, et al. The effect of Holder pasteurization on nutrients and biologically-active components in donor human milk: a review. Nutrients 2016;8. https://doi.org/10.3390/nu8080477.

[16] Weaver G, Bertino E, Gebauer C, Grovslien A, Mileusnic-Milenovic R, Arslanoglu S, et al. Recommendations for the establishment and operation of human milk banks in Europe: a consensus statement from the European Milk Bank Association (EMBA). Front Pediatr 2019;7:53. https://doi.org/10.3389/fped.2019.00053.

[17] Wesolowska A, Sinkiewicz-Darol E, Barbarska O, Bernatowicz-Lojko U, Borszewska-Kornacka MK, van Goudoever JB. Innovative techniques of processing human milk to preserve key components. Nutrients 2019;11. https://doi.org/10.3390/nu11051169.

[18] Gao C, Miller J, Middleton PF, Huang Y-C, McPhee AJ, Gibson RA. Changes to breast milk fatty acid composition during storage, handling and processing: a systematic review. Prostaglandins Leukot Essent Fatty Acids 2019;146:1–10. https://doi.org/10.1016/j.plefa.2019.04.008.

[19] O'Connor DL, Gibbins S, Kiss A, Bando N, Brennan-Donnan J, Ng E, et al. Effect of supplemental donor human milk compared with preterm formula on neurodevelopment of very low-birth-weight infants at 18 Months: a randomized clinical trial. JAMA 2016;316:1897–905. https://doi.org/10.1001/jama.2016.16144.

[20] Quigley M, Embleton ND, McGuire W. Formula versus donor breast milk for feeding preterm or low birth weight infants. Cochrane Database Syst Rev 2019;7:CD002971. https://doi.org/10.1002/14651858.CD002971.pub5.

[21] Parra-Llorca A, Gormaz M, Sánchez-Illana Á, Piñeiro-Ramos JD, Collado MC, Serna E, et al. Does pasteurized donor human milk efficiently protect preterm infants against oxidative stress? Antioxid Redox Signal 2019. https://doi.org/10.1089/ars.2019.7821.

[22] Parra-Llorca A, Gormaz M, Alcántara C, Cernada M, Nuñez-Ramiro A, Vento M, et al. Preterm gut microbiome depending on feeding type: significance of donor human milk. Front Microbiol 2018;9. https://doi.org/10.3389/fmicb.2018.01376.

[23] Beghetti I, Biagi E, Martini S, Brigidi P, Corvaglia L, Aceti A. Human milk's hidden gift: implications of the milk microbiome for preterm infants' health. Nutrients 2019;11:2944. https://doi.org/10.3390/nu11122944.

[24] Milani C, Duranti S, Bottacini F, Casey E, Turroni F, Mahony J, et al. The first microbial colonizers of the human gut: composition, activities, and health implications of the infant gut microbiota. Microbiol Mol Biol Rev MMBR 2017;81. https://doi.org/10.1128/MMBR.00036-17.

[25] Kurath-Koller S, Moissl-Eichinger C, Gorkiewicz G, Kraschl R, Kanduth C, Hopfer B, et al. Changes of intestinal microbiota composition and diversity in very low birth weight infants related to strategies of NEC prophylaxis: protocol for an observational multicentre pilot study. Pilot Feasibility Stud 2017;3. https://doi.org/10.1186/s40814-017-0195-y.

[26] Ulaszewska MM, Weinert CH, Trimigno A, Portmann R, Andres Lacueva C, Badertscher R, et al. Nutrimetabolomics: an integrative action for metabolomic analyses in human nutritional studies. Mol Nutr Food Res 2019;63:e1800384. https://doi.org/10.1002/mnfr.201800384.

[27] Chen MX, Wang S-Y, Kuo C-H, Tsai I-L. Metabolome analysis for investigating host-gut microbiota interactions. J Formos Med Assoc 2018. https://doi.org/10.1016/j.jfma.2018.09.007.

[28] Goodacre R. Metabolomics of a superorganism. J Nutr 2007;137:259S–66S. https://doi.org/10.1093/jn/137.1.259S.

[29] Daliri EB-M, Wei S, Oh DH, Lee BH. The human microbiome and metabolomics: current concepts and applications. Crit Rev Food Sci Nutr 2017;57:3565–76. https://doi.org/10.1080/10408398.2016.1220913.

[30] Ten-Doménech I, Martínez-Sena T, Moreno-Torres M, Sanjuan-Herráez JD, Castell JV, Parra-Llorca A, et al. Comparing targeted vs. untargeted MS2 data-dependent acquisition for peak annotation in LC–MS metabolomics. Metabolites 2020;10:126. https://doi.org/10.3390/metabo10040126.

[31] Villaseñor A, García-Perez I, Garcia A, Posma JM, Fernández-López M, Nicholas AJ, et al. Breast milk metabolome characterization in a single-phase extraction, multiplatform analytical approach. Anal Chem 2014;86:8245–52. https://doi.org/10.1021/ac501853d.

[32] Martínez-Sena T, Luongo G, Sanjuan-Herráez D, Castell JV, Vento M, Quintás G, et al. Monitoring of system conditioning after blank injections in untargeted UPLC-MS metabolomic analysis. Sci Rep 2019;9:1–9. https://doi.org/10.1038/s41598-019-46371-w.

[33] Broadhurst D, Goodacre R, Reinke SN, Kuligowski J, Wilson ID, Lewis MR, et al. Guidelines and considerations for the use of system suitability and quality control samples in mass spectrometry assays applied in untargeted clinical metabolomic studies. Metabolomics 2018;14:72. https://doi.org/10.1007/s11306-018-1367-3.

[34] Kessner D, Chambers M, Burke R, Agus D, Mallick P. ProteoWizard: open source software for rapid proteomics tools development. Bioinforma Oxf Engl 2008;24:2534–6. https://doi.org/10.1093/bioinformatics/btn323.

[35] Smith CA, Want EJ, O'Maille G, Abagyan R, Siuzdak G. XCMS: processing mass spectrometry data for metabolite profiling using nonlinear peak alignment, matching, and identification. Anal Chem 2006;78:779–87. https://doi.org/10.1021/ac051437y.

[36] Benton HP, Want EJ, Ebbels TMD. Correction of mass calibration gaps in liquid chromatography-mass spectrometry metabolomics data. Bioinforma Oxf Engl 2010;26:2488–9. https://doi.org/10.1093/bioinformatics/btq441.

[37] Tautenhahn R, Böttcher C, Neumann S. Highly sensitive feature detection for high resolution LC/MS. BMC Bioinf 2008;9:504. https://doi.org/10.1186/1471-2105-9-504.

[38] Kuhl C, Tautenhahn R, Böttcher C, Larson TR, Neumann S. CAMERA: an integrated strategy for compound spectra extraction and annotation of liquid chromatography/mass spectrometry data sets. Anal Chem 2012;84:283–9. https://doi.org/10.1021/ac202450g.

[39] Kuligowski J, Sánchez-Illana Á, Sanjuán-Herráez D, Vento M, Quintás G. Intra-batch effect correction in liquid chromatography-mass spectrometry using quality control samples and support vector regression (QC-SVRC). Analyst 2015;140:7810–7. https://doi.org/10.1039/c5an01638j.

[40] Sánchez-Illana Á, Pérez-Guaita D, Cuesta-García D, Sanjuan-Herráez JD, Vento M, Ruiz-Cerdá JL, et al. Model selection for within-batch effect correction in UPLC-MS metabolomics using quality control – support vector regression. Anal Chim Acta 2018. https://doi.org/10.1016/j.aca.2018.04.055.

[41] Sánchez-Illana Á, Piñeiro-Ramos JD, Sanjuan-Herráez JD, Vento M, Quintás G, Kuligowski J. Evaluation of batch effect elimination using quality control replicates in LC-MS metabolite profiling. Anal Chim Acta 2018;1019:38–48. https://doi.org/10.1016/j.aca.2018.02.053.

[42] Chang C-C, Lin C-J. LIBSVM: a library for support vector machines. ACM Trans Intell Syst Technol 2011;2:27:1–27:27. https://doi.org/10.1145/1961189.1961199.

[43] Caporaso JG, Kuczynski J, Stombaugh J, Bittinger K, Bushman FD, Costello EK, et al. QIIME allows analysis of high-throughput community sequencing data. Nat Methods 2010;7:335–6. https://doi.org/10.1038/nmeth.f.303.

[44] Langille MGI, Zaneveld J, Caporaso JG, McDonald D, Knights D, Reyes JA, et al. Predictive functional profiling of microbial communities using 16S rRNA marker gene sequences. Nat Biotechnol 2013;31:814–21. https://doi.org/10.1038/nbt.2676.

[45] Chong J, Soufan O, Li C, Caraus I, Li S, Bourque G, et al. MetaboAnalyst 4.0: towards more transparent and integrative metabolomics analysis. Nucleic Acids Res 2018;46:W486–94. https://doi.org/10.1093/nar/gky310.

[46] Caspi R, Billington R, Ferrer L, Foerster H, Fulcher CA, Keseler IM, et al. The MetaCyc database of metabolic pathways and enzymes and the BioCyc collection of pathway/genome databases. Nucleic Acids Res 2016;44:D471–80. https://doi.org/10.1093/nar/gkv1164.

[47] Kanehisa M. Toward understanding the origin and evolution of cellular organisms. Protein Sci 2019;28:1947–51. https://doi.org/10.1002/pro.3715.

[48] Sumner LW, Amberg A, Barrett D, Beale MH, Beger R, Daykin CA, et al. Proposed minimum reporting standards for chemical analysis Chemical Analysis Working Group (CAWG) Metabolomics Standards Initiative (MSI). Metabolomics Off J Metabolomic Soc 2007;3:211–21. https://doi.org/10.1007/s11306-007-0082-2.

[49] Shaffer M, Thurimella K, Quinn K, Doenges K, Zhang X, Bokatzian S, et al. AMON: annotation of metabolite origins via networks to integrate microbiome and metabolome data. BMC Bioinf 2019;20:614. https://doi.org/10.1186/s12859-019-3176-8.

[50] Oliveros JC. Venny. An interactive tool for comparing lists with Venn's diagrams. 2007.

[51] Papile LA, Burstein J, Burstein R, Koffler H. Incidence and evolution of subependymal and intraventricular hemorrhage: a study of infants with birth weights less than 1,500 gm. J Pediatr 1978;92:529–34. https://doi.org/10.1016/s0022-3476(78)80282-0.

[52] Li S, Park Y, Duraisingham S, Strobel FH, Khan N, Soltow QA, et al. Predicting network activity from high throughput metabolomics. PLoS Comput Biol 2013;9. https://doi.org/10.1371/journal.pcbi.1003123.

[53] Bauer J, Gerss J. Longitudinal analysis of macronutrients and minerals in human milk produced by mothers of preterm infants. Clin Nutr Edinb Scotl 2011;30:215–20. https://doi.org/10.1016/j.clnu.2010.08.003.
[54] García-Lara NR, Vieco DE, De la Cruz-Bértolo J, Lora-Pablos D, Velasco NU, Pallás-Alonso CR. Effect of Holder pasteurization and frozen storage on macronutrients and energy content of breast milk. J Pediatr Gastroenterol Nutr 2013;57:377–82. https://doi.org/10.1097/MPG.0b013e31829d4f82.
[55] Bertino E, Coppa GV, Giuliani F, Coscia A, Gabrielli O, Sabatino G, et al. Effects of Holder pasteurization on human milk oligosaccharides. Int J Immunopathol Pharmacol 2008;21:381–5. https://doi.org/10.1177/039463200802100216.
[56] Coscia A, Peila C, Bertino E, Coppa GV, Moro GE, Gabrielli O, et al. Effect of Holder pasteurisation on human milk glycosaminoglycans. J Pediatr Gastroenterol Nutr 2015;60:127–30. https://doi.org/10.1097/MPG.0000000000000570.
[57] Hollanders JJ, Heijboer AC, van der Voorn B, Rotteveel J, Finken MJJ. Nutritional programming by glucocorticoids in breast milk: targets, mechanisms and possible implications. Best Pract Res Clin Endocrinol Metab 2017;31:397–408. https://doi.org/10.1016/j.beem.2017.10.001.
[58] van der Voorn B, de Waard M, van Goudoever JB, Rotteveel J, Heijboer AC, Finken MJ. Breast-milk cortisol and cortisone concentrations follow the diurnal rhythm of maternal hypothalamus-pituitary-adrenal axis activity. J Nutr 2016;146:2174–9. https://doi.org/10.3945/jn.116.236349.
[59] Ley SH, Hanley AJ, Stone D, O'Connor DL. Effects of pasteurization on adiponectin and insulin concentrations in donor human milk. Pediatr Res 2011;70:278–81. https://doi.org/10.1203/PDR.0b013e318224287a.
[60] Untalan PB, Keeney SE, Palkowetz KH, Rivera A, Goldman AS. Heat susceptibility of interleukin-10 and other cytokines in donor human milk. Breastfeed Med Off J Acad Breastfeed Med 2009;4:137–44. https://doi.org/10.1089/bfm.2008.0145.
[61] Vass RA, Bell EF, Colaizy TT, Schmelzel ML, Johnson KJ, Walker JR, et al. Hormone levels in preterm and donor human milk before and after Holder pasteurization. Pediatr Res 2020:1–6. https://doi.org/10.1038/s41390-020-0789-6.
[62] Morris DJ, Brem AS. Role of gut metabolism of adrenal corticosteroids and hypertension: clues gut-cleansing antibiotics give us. Physiol Genomics 2019;51:83–9. https://doi.org/10.1152/physiolgenomics.00115.2018.
[63] Vincenzetti S, Polzonetti V, Micozzi D, Pucciarelli S. Enzymology of pyrimidine metabolism and neurodegeneration. Curr Med Chem 2016;23:1408–31. https://doi.org/10.2174/0929867323666160411125803.

antioxidants

MDPI

Article

A Reductive Metabolic Switch Protects Infants with Transposition of Great Arteries Undergoing Atrial Septostomy against Oxidative Stress

José David Piñeiro-Ramos [1], Otto Rahkonen [2], Virpi Korpioja [3], Guillermo Quintás [4,5], Jaana Pihkala [2], Olli Pitkänen-Argillander [2], Paula Rautiainen [6], Sture Andersson [7], Julia Kuligowski [1,*] and Máximo Vento [1,8,*]

1 Neonatal Research Unit, Health Research Institute Hospital La Fe, Avenida Fernando Abril Martorell 106, 46026 Valencia, Spain; josedavidpineiro@gmail.com
2 Department of Paediatric Cardiology, New Children's Hospital, University of Helsinki and Helsinki University Hospital, Box 347, Stenbäckinkatu 9, 00029 Helsinki, HUS, Finland; Otto.Rahkonen@hus.fi (O.R.); jaana.pihkala@hus.fi (J.P.); Olli.Pitkanen@hus.fi (O.P.-A.)
3 Department of Children and Adolescents, Oulu University Hospital, P.O. Box 23, FIN-90029 OYS, 90570 Oulu, Finland; korpiojavirpi@gmail.com
4 Health & Biomedicine Unit, Leitat Technological Center, Par Cientific Barcelona, 08028 Barcelona, Spain; gquintas@leitat.org
5 Analytical Unit, Health Research Institute La Fe, Avenida, Fernando Abril Martorell 106, 46026 Valencia, Spain
6 Department of Anaesthesia and Intensive Care, New Children's Hospital, Helsinki University Hospital and University of Helsinki, Stenbackinkatu 9, 00029 Helsinki, Finland; Paula.Rautiainen@hus.fi
7 Pediatric Research Center, New Children's Hospital, Helsinki University Hospital and University of Helsinki, Stenbackinkatu 9, 00029 Helsinki, Finland; sture.andersson@hus.fi
8 Division of Neonatology, University & Polytechnic Hospital La Fe, Avenida Fernando Abril Martorell 106, 46026 Valencia, Spain
* Correspondence: julia.kuligowski@uv.es (J.K.); maximo.vento@uv.es (M.V.); Tel.: +34-96-1246661 (J.K.); +34-96-1246603 (M.V.)

check for updates

Citation: Piñeiro-Ramos, J.D.; Rahkonen, O.; Korpioja, V.; Quintás, G.; Pihkala, J.; Pitkänen-Argillander, O.; Rautiainen, P.; Andersson, S.; Kuligowski, J.; Vento, M. A Reductive Metabolic Switch Protects Infants with Transposition of Great Arteries Undergoing Atrial Septostomy against Oxidative Stress. *Antioxidants* **2021**, *10*, 1502. https://doi.org/10.3390/antiox10101502

Academic Editor: Jacob V. Aranda

Received: 22 July 2021
Accepted: 16 September 2021
Published: 22 September 2021

Publisher's Note: MDPI stays neutral with regard to jurisdictional claims in published maps and institutional affiliations.

Abstract: Transposition of the great arteries (TGA) is one of the most common cyanotic congenital heart diseases requiring neonatal surgical intervention. Parallel circulations that result in impaired cerebral oxygen delivery already in utero may lead to brain damage and long-term neurodevelopmental delay. Balloon atrial septostomy (BAS) is often employed to mix deoxygenated and oxygenated blood at the atrial level. However, BAS causes a sudden increase in arterial blood oxygenation and oxidative stress. We studied changes in oxygen saturation as well as metabolic profiles of plasma samples from nine newborn infants suffering from TGA before and until 48 h after undergoing BAS. The plasma metabolome clearly changed over time and alterations of four metabolic pathways, including the pentose phosphate pathway, were linked to changes in the cerebral tissue oxygen extraction. In contrast, no changes in levels of lipid peroxidation biomarkers over time were observed. These observations suggest that metabolic adaptations buffer the free radical burst triggered by re-oxygenation, thereby avoiding structural damage at the macromolecular level. This study enhances our understanding of the complex response of infants with TGA to changes in oxygenation induced by BAS.

Keywords: transposition of the great arteries; balloon atrial septostomy; hypoxemia; metabolomics; oxidative stress; newborn; liquid chromatography-mass spectrometry (LC-MS)

1. Introduction

Transposition of the great arteries (TGA) is one of the most common cyanotic congenital heart diseases with an incidence of 0.3 per 1000 live births that requires surgical

intervention in the neonatal period [1]. In hearts with TGA, systemic and pulmonary circulations run in parallel rather than in serial. This results in significant hypoxemia clinically reflected as central cyanosis. Survival after birth is only possible if there is an adequate blood mixing between the two circulations. Most hypoxemic neonates with TGA benefit from early institution of prostaglandin E1 (PGE) for ductal patency. If hypoxemia persists despite prostaglandin E1 (PGE1) infusion, balloon atrial septostomy (BAS) is needed to increase systemic oxygenation by improving the mixing of deoxygenated and oxygenated blood at the atrial level. After stabilization, arterial switch operation (ASO) is performed in the neonatal period. Mortality of ASO is low in the current era, however, morbidity is high and neonates with TGA are at risk of impaired neurodevelopmental outcome. Thus, long-term follow-up demonstrates that 30–50% of school-aged children with TGA show some form of developmental delay [2].

The underlying mechanism of developmental delay is thought to be multifactorial and include prenatal and postnatal factors. Hence, fetal hypoxia due to decreased oxygen delivery has been implicated in the abnormal brain development seen in newborns with TGA [3]. Moreover, reduced fetal cerebral oxygen consumption in TGA neonates has been associated with smaller head circumference and brain volume than those of normal neonates [4]. In addition, postnatal factors such as postnatal chronic hypoxemia, open-heart surgery with deep hypothermic circulatory arrest, and balloon atrial septostomy (BAS) have also been considered responsible for brain injury [5]. BAS improves mixing of systemic and pulmonary circulation and leads to an immediate increase in arterial oxygen content. However, BAS does not allow for full normalization of systemic oxygenation preoperatively. Very little is known about the direct effect of BAS on the neonatal brain, on cerebral oxygenation and oxygen metabolism [6], and whether the rapid increase of oxygen delivery results in brain reperfusion injury in neonates with TGA [7,8].

In mammals, aerobic metabolism with the concourse of oxygen is the most efficient biological means to supply energy required to sustain life. Under anaerobic conditions, pyruvate is converted into L-lactate. Anaerobic metabolism is by far less energy efficient than aerobic metabolism. Hence, in the absence of oxygen, the energy consumed by neurons rapidly leads to an exhaustion of the ATP reserves [9]. Due to the high metabolic rate of the brain, survival is almost exclusively dependent on the energy generated by aerobic glycolysis. The lack of oxygen stores and the reduced glycolytic capacity compel brain tissue to rely entirely on a continuous supply of oxygen and glucose provided by cerebral perfusion. Under these circumstances, acutely or chronically reduced oxygen availability due to environmental or pathophysiological causes inevitably leads to alterations of the brain structure and function [10].

Incomplete reduction of oxygen leads to the formation of reactive oxygen species (ROS), some of which are free radicals (e.g., anion superoxide and hydroxyl radicals). These extremely short half-life metabolites are capable of damaging nearby cellular components such as proteins, lipids, carbohydrates or DNA [11]. Both, acute and chronic hypoxia, enhance the formation of ROS through mitochondrial uncoupling provoking oxidative stress (OS) [12]. In addition, during reoxygenation, the increased availability of oxygen causes the activation of oxidases such as nicotinamide adenine dinucleotide phosphate (NADPH) oxidase or xanthine oxidase, further increasing the formation of anion superoxide and nitric oxide [11]. Neurons are highly vulnerable to the deleterious effects of ROS generated during acute hypoxia and/or hyperoxia. ROS trigger specific pathways that lead to apoptosis, necrosis, and inflammation of vulnerable areas of the brain causing long term neurodevelopmental, motor, and cognitive impairment [10].

Blood lactate has been largely employed as a surrogate for tissue hypoxia and/or ischemia. However, exclusive monitoring of serum lactate has neither provided sufficient insight into the magnitude of brain hypoxia nor conferred reliable prognostic information regarding long-term neurodevelopmental impairment [13,14]. More recently, comprehensive metabolic fingerprinting characterized by the simultaneous measurement of hundreds

of metabolites from biological matrices has been increasingly employed for identifying predictive biomarkers or patient stratification [15].

In the present study we focused on the metabolic switch in infants with TGA after BAS. We performed serial analysis of lipid peroxidation byproducts as well as the plasma metabolome before and after BAS. This allowed us to study the impact of the rapid change in arterial blood oxygen content switching from a chronic hypoxic environment to an almost normoxic one, thus giving an insight into the dynamic hypoxia-related changes on the phenotypic level.

2. Materials and Methods

2.1. Study Population

We performed a prospective single center study to evaluate changes in cerebral oxygenation and metabolism before and for a period of 96 h following BAS in neonates with TGA. All patients with TGA admitted to Children's Hospital, Helsinki University Hospital, between 1 January 2015, and 1 June 2017, were considered for inclusion in the present study. Inclusion criteria included term gestational age and simple TGA without any significant associated heart defects (i.e., patients with ventricular septal defect were excluded). Reasons for failure to enroll included unavailability of parents for the consent process or parental refusal.

The study protocol was approved by the Ethics Committee of Helsinki University Hospital. All procedures were performed in accordance with relevant guidelines and regulations and written permission by signing an informed consent form or phone permission in urgent cases was obtained from legal representatives.

Data collected included peripheral oxygen saturation (SpO_2), mixed venous saturation, regional cerebral tissue oxygen saturation ($rcSO_2$) measured by near infrared spectroscopy (NIRS), heart rate, blood pressure, blood lactate levels, pH, base excess, and hemoglobin prior to and following BAS. Blood samples for metabolic analysis were collected from arterial cannula 5 min prior to and 5 min, 6 h, 24 h, 48 h, 72 h, and 96 h following BAS. At each timepoint, 1 mL of blood was collected into lithium heparin tubes, centrifuged, aliquoted, and stored at −70 °C. Differences during $rcSO_2$, preductal peripheral oxygen saturation, fractional tissue oxygen extraction (FTOE), and cerebral oxygen extraction (CEO_2) were analyzed prior to and following BAS. Cerebral oxygen extraction was estimated from the difference of SaO_2 and ScO_2 as ScO_2 is close to venous SO_2. FTOE was calculated as CEO_2/SaO_2. Information regarding medications used prior to and following BAS was collected from electronic patient records.

2.2. Analytical Procedures

2.2.1. Lipid Peroxidation Biomarkers

Biomarkers of lipid peroxidation were analyzed in 63 plasma samples following previously published procedures [16,17]. Deuterated internal standards (IS) ($PGF_{2\alpha}$-d4 and 15-F_{2t}-Isoprostane-d4) were purchased from Cayman Chemical Company (Ann Arbor, MI, USA). For sample processing, 100 µL of plasma were thawed on ice and 100 µL of KOH solution at 15% (*w/v*) were added. The mixture was incubated at 40 °C for 30 min. A volume of 3 µL of aqueous IS solution (20 µM) was added to hydrolyzed samples and diluted to 900 µL with H_2O:MeOH (85:15, 2.8% *v/v* HCOOH) solution. Then, the samples were mixed for 30 s at maximum speed and centrifuged at 16,000× *g* and 4 °C for 10 min. For clean-up and pre-concentration of the samples, an SPE procedure employing Discovery® DSC-18 SPE 96-well plates from Sigma Aldrich Química S.A (Madrid, Spain) was carried out. First, the stationary phase was equilibrated with 1 mL of MeOH and 1 mL of water. Then, the supernatant of the centrifuged and diluted sample was loaded followed by washing with 1 mL of H_2O (0.1% *v/v* HCOOH, pH 3) and 500 mL heptane. Finally, cartridges were dried with room air and the compounds of interest were eluted with 4 × 100 µL ethyl acetate. The eluate was evaporated using a miVac centrifugal vacuum concentrator (Genevac LTD, Ipswich, UK) and dissolved in 60 µL H_2O (0.1% *v/v* HCOOH, pH 3):CH_3OH (85:15 *v/v*).

An Acquity-Xevo TQS system from Waters (Milford, MA, USA) operating in negative electrospray ionization (ESI^-) mode was employed for UPLC-MS/MS analysis. A Waters BEH C_{18} column (2.1 mm × 100 mm, 1.7 µm, Waters, Wexford, Ireland) was used. Flow rate, column temperature, and injection volume were set at 450 µL min^{-1}, 45 °C, and 9 µL, respectively. A binary mobile phase H_2O (0.1% *v/v* HCOOH):CH_3CN (0.1% *v/v* HCOOH) gradient with a total runtime of 7.0 min was run as follows: from 0.0 to 0.1 min 15% *v/v* CH_3CN (0.1% *v/v* HCOOH) (mobile phase channel B); from 0.1 to 5.0 min % B increased up to 40%; from 5.0 to 6.0 min % B increased up to 75%; between 6.0 and 6.15 conditions were held constant at 75% B followed by the return to initial conditions (i.e., 15% B) between 6.15 and 6.25 min; conditions were maintained for 0.75 min for system re-equilibration. ESI interface conditions were selected as follows: capillary voltage was set to 2.9 kW; source and desolvation temperatures were 150 °C and 395 °C, respectively; and nitrogen cone and desolvation gas flows were 150 and 800 L h^{-1}, respectively. Parameters selected for determination of lipid peroxidation biomarkers are shown in Table 1.

Table 1. Mass spectrometric parameters and chromatographic windows employed for the lipid peroxidation biomarkers.

Analyte [p.d.u.]	RT [min]	Parent Ion (*m/z*)	Daughter Ion (*m/z*)	CE (eV)	Cone Voltage (V)
IsoPs	4.3–6.6	353.20	115.00	30	35
Di-homo-IsoPs	5.0–6.8	381.00	143.00	20	20
Di-homo-IsoFs	3.5–6.5	397.00	155.00	24	35
NeuroFs	2.70–6.50	393.00	193.00	20	35
IsoFs	2.1–6.60	369.20	115.00	20	45
NeuroPs	2.30–6.50	377.00	101.00	20	35

Note: IsoPs = isoprostanes. IsoFs = isofurans. NeuroFs = neurofurans. NeuroPs = neuroprostanes. RT stands of Retention times. CE stands of collision energy.

2.2.2. Untargeted Ultra-Performance Liquid Chromatography Coupled to Time-of-Flight Mass Spectrometry (UPLC-TOFMS) Metabolomic Analysis

Plasma samples were thawed on ice and homogenized on a Vortex mixer. 75 µL of cold acetonitrile were added to 25 µL of plasma, homogenized and kept on ice during 15 min followed by centrifugation at 16,000× *g* during 15 min at 4 °C. 80 µL of supernatant were collected and transferred to a 96 well plate, evaporated to dryness on a miVac centrifugal vacuum concentrator (Genevac LTD, Ipswich, UK) at room temperature and dissolved in 60 µL of an internal standard (IS) solution containing betaine-D_{11}, methionine-D_3, hypoxanthine-D_3, cystine-D_4, tyrosine-D_2, prostaglandin$F_{2\alpha}$-D_4, uridine-$C^{13}N^{15}$, reserpine, phenylalanine-D_5, leucine enkephalin, caffeine-D_9, and tryptophane-D_5 with purities ≥ 99% at a concentration of 1.5 µM in H_2O:CH_3CN (0.1% HCOOH) (95:5 *v/v*).

A QC sample was prepared by mixing 5 µL of each plasma sample and a total of three aliquots were processed alongside with the plasma samples applying the same procedures. A blank extract was prepared by using a heparinized syringe and 0.5 mL of ultrapure H_2O and processed as described for plasma samples.

For chromatographic separations, an Agilent Technologies (Santa Clara, CA, USA) 1290 Infinity UPLC chromatograph equipped with a UPLC ACQUITY BEH C18 column (2.1 mm × 100 mm, 1.7 µm, Waters, Wexford, Ireland) was employed. Autosampler and column temperatures were set to 4 and 40 °C, respectively. A flow rate of 400 µL min^{-1} and an injection volume of 4 µL were used. Separations were carried out keeping 98% of mobile phase A (H_2O, 0.1% *v/v* HCOOH) for 0.5 min, followed by a linear gradient from 2 to 20% of mobile phase B (CH_3CN, 0.1% *v/v* HCOOH) in 3.5 min and from 20 to 95% B in 4 min. Conditions of 95% B were maintained for 1 min and a 0.25 min gradient was used to return to the initial conditions, which were held until reaching 8.5 min.

Full-scan MS data were acquired between 100 and 1700 *m/z* with a scan frequency of 6 Hz (1274 transients/spectrum) on an iFunnel quadrupole time-of-flight (QTOF) Agilent 6550 spectrometer operating in the TOF MS mode. The following electrospray ionization settings were used: gas T, 200 °C; drying gas, 14 L min^{-1}; nebulizer, 37 psig; sheath gas

T, 350 °C; sheath gas flow, 11 L min^{-1}. A mass reference standard used for automatic MS spectra re-calibration during analysis was introduced into the source via a reference sprayer valve using the 149.02332 (background contaminant), 121.050873 (purine), and 922.009798 (HP-0921) *m/z*. MassHunter workstation from Agilent was employed for data acquisition and manual integration of ISs.

Before launching the analytical sequence, system suitability was checked employing a standard mixture containing ISs. The analytical system was conditioned by eight repeated injections of the QC at the beginning of the batch. Data acquired during system conditioning were discarded from data analysis. A total of 63 plasma sample extracts were analyzed in randomized order in a single analytical batch using the positive electrospray (ESI^+) mode. QC samples were analyzed every 6th sample and at the beginning and end of the batch for assessment and correction of instrumental performance [18]. The blank extract was injected a total of two times (once during system conditioning and once at the end of the batch) and used for data clean-up with the aim of identifying signals from other than biological origin. Subsequently, sample analysis was carried out in ESI^- mode repeating the same protocol described for the ESI^+ mode.

2.2.3. Data Processing and Statistical Analysis

ProteoWizard [19] (http://proteowizard.sourceforge.net (accessed on 20 September 2021)) software was used for conversion of raw UPLC-TOFMS data into centroid mzXML format. A peak table was extracted using XCMS (version 3.4.2) [20–22] (https://bioconductor.org/packages/release/bioc/html/xcms.html (accessed on 20 September 2021)) running in R (version 3.5). For peak detection, the centWave method was used as follows: ppm = 20, peakwidth = (4 and 25), snthresh = 10. For the resolution of overlapping peaks, a minimum *m/z* difference of 7.5 mDa was selected. For each extracted feature, the 'wMean' function was used for calculating intensity-weighted *m/z* values and peak limits used for integration were found through descent on the Mexican hat filtered data. For peak grouping the "nearest" method with mzVsRT = 1 and retention time (RT) and *m/z* tolerances of 6 s and 10 mDa, respectively, was used. Missing peak data was filled applying the fillPeaks method with the default parameters. A total of 18,582 and 13,479 features were initially detected after peak detection, integration, chromatographic deconvolution, and alignment in ESI^+ and ESI^- modes, respectively. The CAMERA [23] package was used for identifying peak groups and annotation of isotopes and adducts using the following settings: sigma = 6, perfwhm = 0.5, ppm = 20.

Peak integration accuracy was checked by comparing the generated peak table with areas obtained from manual integration of ISs. Peak intensities of ISs and QC samples were used for assessing the instrumental response during data acquisition throughout the batch as described elsewhere [24,25]. The Quality Control-Support Vector Regression (QC-SVR) algorithm [26] and the LIBSVM library [27] were used for correcting intra-batch variation using an ε–range of 2.5 to 7.5 and a γ-range of 1 to 10^5. C was defined for each feature as the median value in QCs. Then, features detected in blanks (<5× signal of the blank) and those with an RSD% in QC samples ≥20% were excluded. The final peak tables contained 3886 and 5600 features for ESI^+ and ESI^-, respectively, and were searched for molecular ion peaks of drugs and known drug metabolites that have been administered to infants, their isotope as well as Na and K adducts (*m/z* tolerance: 10 mDa). Metabolic features that were identified as drugs or their metabolites, isotopes and adducts were excluded from further data analysis.

MATLAB 2019b inbuilt functions as well as in-house written scripts (available from the authors upon reasonable request) and the PLS Toolbox 8.0 from Eigenvector Research Inc. (Wenatchee, WA, USA) were used for Principal Component Analysis (PCA) and the computation of Pearson correlations. For PCA, data sets generated in ESI^+ and ESI^- were concatenated. MetaboAnalyst (version 4.0) [28] was used for hierarchical clustering and the generation of heatmaps employing Euclidean distance and Ward's method (statistical analysis tool). Pathway analysis was carried out using MetaboAnalyst with the MS peaks

to pathways tool (mass accuracy = 10 ppm, mummichog algorithm with top 10% peaks *p*-value cut-off) in the 4-column format (*m/z*, RT, ionization mode, *p*-value of Pearson correlation between metabolic features and FTOE) and the Kyoto Encyclopedia of Genes and Genomes (KEGG) pathway library (*Homo sapiens*). Metabolomics data are available on Zenodo (https://zenodo.org/record/4495124#.YBpwoC1DkWp (2 February 2021)).

The non-parametric Wilcoxon rank-sum test was used for assessing changes in levels of biomarkers of lipid peroxidation over time. *p*-values from Spearman correlations were used for clinical data, where appropriate.

3. Results

3.1. Clinical Results

A total of 12 newborn infants fulfilled the study requirements. Out of these, one patient died, and two patients did not require BAS. The remaining 9 patients who underwent BAS, completed all analysis. Demographics and perinatal characteristics are detailed in Table 2. Six patients (50%) had prenatal diagnosis and nine patients (75%) underwent BAS due to low preductal saturation at the age 4.6 (± 2.7) hours. There was one early death prior to BAS. The patient was transferred from another central hospital with prostaglandin infusion but had extremely low preductal saturations (<30%), severe lactate acidosis, and was in pulseless electrical activity at the time of admission and care was withdrawn. Figure 1 describes evolving SpO_2, $rcSO_2$, FTOE, and CEO_2 before and after BAS. In the nine patients included in the study, the lowest preductal peripheral oxygen saturation (SpO_2) at admission had a median of 64.5% (range 39.0–92.0). Preductal SpO_2 increased from a median of 85.6% (range 62.0–90.6) before BAS to 89.1% (range 81.8–93.5) 6 h following BAS and 90.0% (range 85.2–93.6) 24 h following BAS. $rcSO_2$ at the same time points were 50.0% (range 35.0–70.0), 52.8% (range 36.4–72.5), 63.0% (range 48.2–74.1), and 69.2 (range 58.8–80.8), respectively. $rcSO_2$ correlated strongly with simultaneously measured SpO_2 (Spearman's r = 0.89, *p*-value < 0.001). CEO_2 increased after BAS (27.2–28.1) but both, CEO_2 and FTOE, decreased 24 h following BAS (see Figure 1). Complete recovery of cerebral oxygen saturation did not occur until 24 h after BAS.

Table 2. Patients' demographics and timing of postnatal clinical and analytical interventions.

Patients' Demographics	All Patients	BAS Patients
Patients recruited, N (%)	12 (100)	9 (100)
Gender, N (%)		
- Male	10 (83)	8 (89)
- Female	2 (17)	1 (11)
Balloon atrial septostomy, N (%)	9 (75)	9 (100)
Expired, N (%)	1 (8.3)	0 (0)
Prenatal diagnosis, N (%)	6 (50)	4 (44)
Gestational age, weeks (median, range)	39.5 (37.0–41.3)	39.9 (38.4–41.3)
Birth weight, kg (median, range)	3.4 (2.0–4.0)	3.5 (3.1–4.0)
Postnatal age, hours (median, range)		
- At the time of the first measured peripheral saturation	1.7 (0.5–13.2)	2.3 (0.5–6.7)
- At time of BAS		3.2 (2.0–9.1)
Saturation, % (median, range)		
- First peripheral saturation (SpO_2)	79 (51–91)	77 (56–88)
- Lowest peripheral saturation (SpO_2)	65 (39–86)	65 (39–86)
- First regional cerebral oxygen saturation ($rcSO_2$)	58 (37–79)	53 (37–79)
- 5-min post septostomy peripheral saturation (SpO_2)	86 (62–91)	86 (62–91)
Blood lactate, mmol/L (median, range)		
- Before BAS	3.2 (1.3–4.9)	3.6 (1.3–4.9)
- 5-min after BAS	2.7 (1.4–5.0)	3.3 (1.4–5.0)

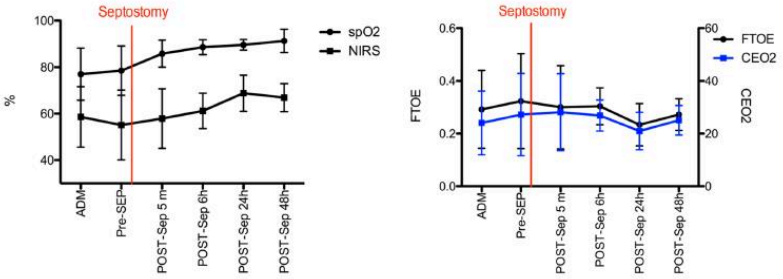

Figure 1. Evolution of SpO2, rcSO2 (**left**), FTOE, and CEO2 levels (**right**) before and after BAS. Black and blue lines and error bars are median and 25th and 75th percentile, respectively.

3.2. Lipid Peroxidation Biomarkers

Total di-homo-isoprostanes, di-homo-isofurans, and isoprostanes were excluded as these parameters were found <LOQ in all study samples. Figure 2 depicts relative responses of total neurofurans, isofurans, and neuroprostanes obtained over time. No significative changes over time were detectable (Wilcoxon rank sum test, p-values > 0.05). Furthermore, no strong (Pearson correlation coefficients > |0.5|) and significant correlations were found between isoprostanoid levels and FTOE.

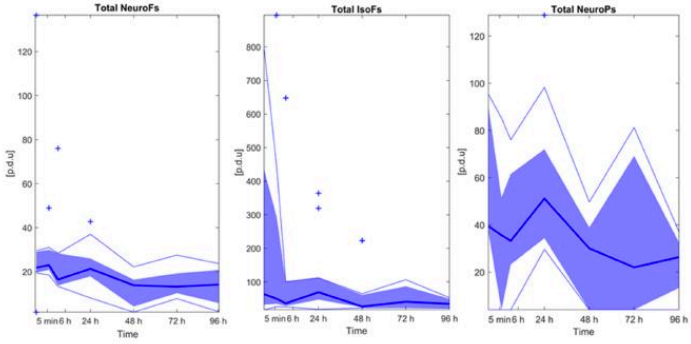

Figure 2. Isoprostanoid levels over time. Note: Bold blue lines correspond to median values, blue areas correspond to the interquartile range (1st and 3rd quartile), thin blue lines correspond to minimum and maximum values, and + correspond to outliers. Note: NeuroFs = neurofurans; IsoFs = isofurans; NeuroPs = neuroprostanes.

3.3. Effect of Time on the Plasma Metabolome

Figure 3 shows a PCA scores plot of the plasma metabolic fingerprint of infants before BAS and at different time points after BAS. The scores plot from PC1 vs. PC2 illustrates the impact of the sampling time point on the plasma metabolome. For most patients, a time-dependent shift towards lower scores on PC1 with increasing time after septostomy was observed. Even though the applied data analysis workflow included the removal of drug metabolites, this effect might, at least partially, be related to the employed medication and the procedure itself. Also, a high inter-individual variation can be noted.

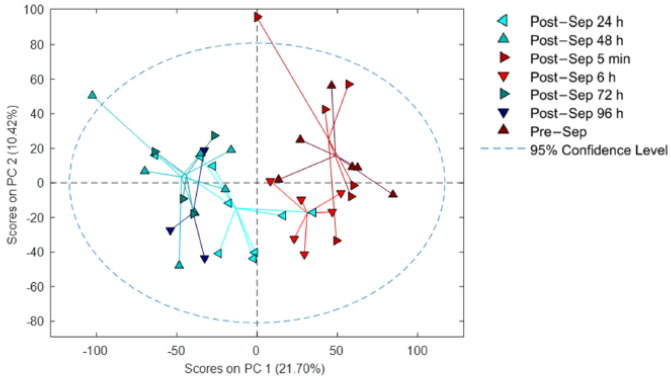

Figure 3. PCA results of samples collected before and at different time points after BAS. Note: Sep stands for septostomy.

3.4. Correlation of Metabolic Features with FTOE

FTOE reflects the balance between oxygen supply and consumption in tissue and can, therefore, be used as an indicator of inadequate tissue perfusion and oxygenation. We specifically focused on modelling the effects of metabolic changes in the plasma metabolome associated with FTOE. Pearson correlations for each metabolic feature with FTOE before and at different time points post-septostomy were calculated as shown in Figure 4. A panel of features with a significant association with FTOE (i.e., *p*-values from Pearson correlation < 0.05) was identified including both, positively (red dots, correlation coefficient > 0.5) and negatively (blue dots, correlation coefficient < −0.5) correlated features. Figure 5 shows a heatmap of the relative intensities of significantly correlated features. Two distinct clusters can be observed, with plasma fingerprints from samples collected before and 5 min as well as 6 h after BAS belonging to one cluster, and samples collected 24–96 h after BAS belonging to a second cluster. Most metabolic features in Figure 5 showed a decreasing trend in relative intensities when comparing cluster one to cluster two. Pathway analysis detected four significantly altered pathways associated with changing FTOE in infants with TGA undergoing BAS (see Table 3).

Table 3. Pathway alterations associated with changing FTOE in infants with TGA undergoing atrial septostomy.

Pathway Name	Compound Code (KEGG)	Pathway ID	# Hits	# Sig Hits	*p*-Value
Pentose phosphate pathway	C01801; C00672; C00121; C00121; C00257; C00257; C00258	map00030	7	7	0.00002
Pentose and glucuronate interconversions	C01068; C00181; C00259; C00310; C00312; C00379; C00532; C00379; C00532; C00379; C00379; C00532; C00257; C00257; C00029; C00052; C00191; C00618; C02266	map00040	11	7	0.003
Ascorbate and aldarate metabolism	C00137; C00029; C02670; C00191; C00800	map00053	8	5	0.013
Inositol phosphate metabolism	C00137; C00222; C00191	map00562	4	3	0.03

Note: Mummichog input: 10 ppm; *p*-value cut-off: 10%; KEGG database. #: stands for number (Number of hits, number of significant hits).

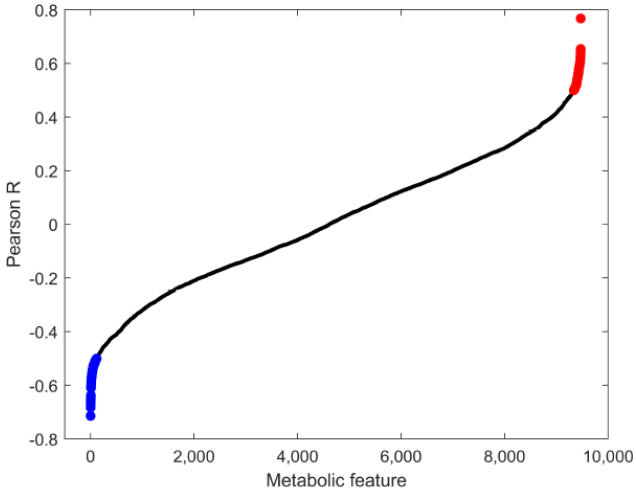

Figure 4. Pearson correlation coefficients between metabolic features and FTOE. Blue: features with p-values < 0.05 and correlation coefficients < −0.5; red: features with p-values < 0.05 and correlation coefficients > 0.5; black: all remaining features.

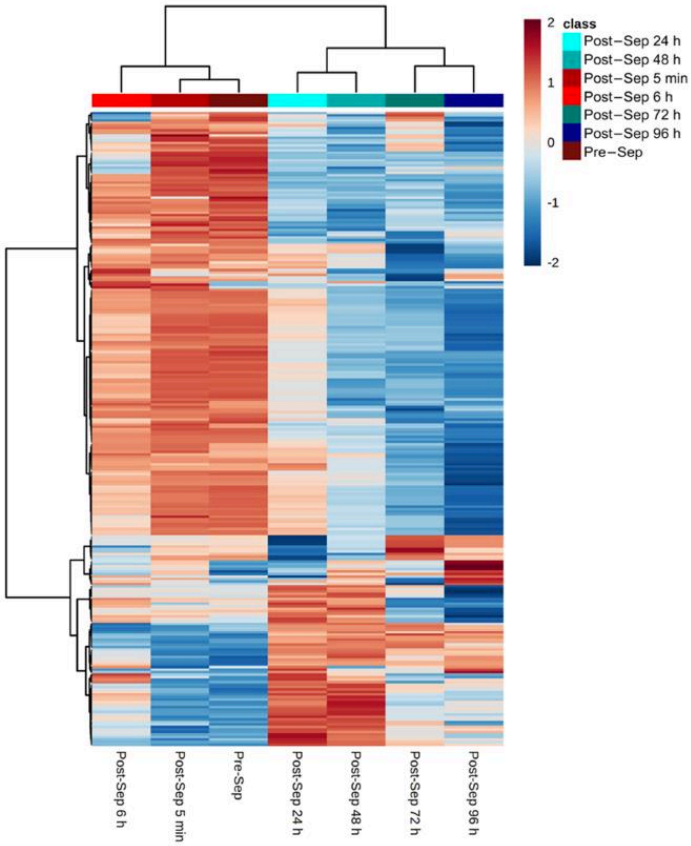

Figure 5. Relative intensities of metabolic features that correlate (i.e., *p*-value < 0.05 and |correlation coefficients| > 0.5) with FTOE. Note: color represents autoscaled relative intensities; blue—metabolite levels lower than average, and red—metabolite levels higher than average. *p*-values from Pearson correlation were computed and significantly correlating metabolites are shown; heatmap calculated using Euclidean distance and Ward algorithm.

4. Discussion

TGA is a severe congenital cardiac malformation that causes hypoxemia during fetal life and in the newborn period [1]. TGA has deleterious consequences on growth and development due to a deficient tissue oxygenation that especially affects the Central Nervous System [2,4]. We report the first metabolomic study involving neonates with TGA who underwent BAS. We performed a study on oxidative stress biomarkers as well as a comprehensive qualitative characterization of plasma metabolites before and after BAS.

BAS in TGA patients caused a rapid switch from hypoxia to normoxia. Preductal peripheral pulse oximetry saturation and $rcSCO_2$ increased rapidly after BAS while simultaneously FTOE decreased. As a result, brain oxygenation substantially improved (See Figure 1). Thereafter, changes in oxygenation plateaued. Complete recovery of cerebral oxygen saturation occurred only 24 h after BAS. A gradual change was observed in the metabolome, accordingly (See Figure 3). The provision of energy to satisfy metabolic demands of the brain is exclusively dependent on aerobic metabolism and oxygen deprivation caused by hypoxia and/or ischemia for just a few minutes may cause severe brain damage. Mitochondrial ROS production is regulated through tissue succinate levels and the activity of oxidases (NADPH oxidase, xanthine oxidase) [29]. During hypoxia and ulterior reoxygenation both, succinate levels and oxidase activation, generate a burst of ROS that directly damage tissue structure and function [29]. Moreover, the pro-oxidant imbalance provokes the activation of the caspase pathway and of transcription factor NF*k*B. Subsequently, programmed cell death and inflammation are triggered for hours, days, or even weeks. Consequently, there is an amplification of the initial area of brain injury that contributes to aggravate long-term neurological prognosis [30–32].

Isoprostanes and isofurans, but especially neuroprostanes and neurofurans are highly sensitive to oxidative stress related brain damage [33]. However, we did not observe changes in those compounds after BAS (See Figure 2). The attenuation of the expected pro-oxidant status after BAS suggests a pattern of metabolomic changes with a reducing profile. In this regard, post-BAS untargeted metabolomics evidenced a significant enhancement in the activity of the pentose phosphate pathway (PPP). The central role of the PPP has attracted more attention in recent years. Emerging evidence suggests that the PPP is tightly and meticulously controlled in cells and that its abnormal regulation leads to uncontrolled redox homeostasis [34]. The PPP has shown great versatility for *de novo* nucleotide biosynthesis via ribose-5-phosphate and adopts a simultaneous organization with glycolysis to produce NADPH. Nucleotide biosynthesis possibly participates in DNA damage repair. Our pathway analysis data revealed changes in the relative concentrations of 2-deoxy-D-ribose 1-phosphate (C00672), a precursor of ribose-5-phospate, and substrate of phosphoribosyl pyrophosphate (PRPP). This substrate is an essential compound of purine, pyridine, and histidine synthesis. NAPDH is a cofactor of glutathione reductase, an essential enzyme in the glutathione redox cycle that contributes to the reconversion of GSSG into GSH thus contributing to the normalization of the GSH/GSSG pair and the removal of ROS [35,36]. In this context, the pathway analysis data suggest an alteration of gluconic acid (C00257). The phosphorylation of this compound generates 6-phosphogluconate, an essential substrate in the oxidative branch of the PPP. Furthermore, alterations of other compounds such as ribitol-5-phosphate (C01068) and 2-deoxy-D-ribose (C00672) contribute as substrates for key PPP compounds. Indeed, the activity of the PPP is rapidly re-routed when cells are exposed to an oxidative burst. This response is exquisitely adjusted by cooperating of metabolic and gene regulatory mechanisms. Metabolic changes imply the inactivation of glycolytic enzymes which occurs immediately after the oxidant aggression thus blocking glycolysis [37]. Thereafter, the transcriptional response takes over and maintains higher PPP activity through up-regulation of enzymes and post-translational modifications including those which increase the activity of G6PDH [38]. Furthermore, to counteract mitochondrial ROS production under normal metabolic circumstances, but also during hypoxia or hypoxia-reoxygenation, steady NADPH production becomes essential as it represents the main electron donor for the generation of GSH that will provide electrons for the reduction of detrimental peroxides by glutathione peroxidase [34].

In addition, our results reveal the alteration of the pentose and glucuronate interconversion pathway, another key pathway in the homeostasis of metabolic pathways. The glucuronate pathway is an alternative pathway for the oxidative degradation of glucose without the production of ATP. Substrate compounds such as xylose (C00181), arabinose (C00259), arabitol (C00532), xylulose (C00312), UDP-glucose (C00029), glucuronic acid (C00191), dehydrogulonate (C00618), xylonolactone (C02266), and ribitol-5-phosphate

(C01068) were altered according to the reported pathway analysis data. Interestingly, in humans the synthesis of ascorbic acid is not feasible, therefore a substantial proportion of uridine diphosphate glucoronate (UDP-glucoronate) is converted into xylulose-5-phosphate which is further metabolized through the PPP to fuel NADPH production and promote the preservation of a reduced environment [39].

Finally, pathway analysis also showed an alteration of ascorbate and aldarate and inositol phosphate metabolism. The ability of ascorbate to donate electrons enables it to act as a free radical scavenger and to reduce higher oxidation states of iron to Fe^{2+}. Ascorbic acid is an important antioxidant in plasma, where it consumes oxygen free radicals. Erythrocytes have a high capacity to regenerate ascorbate from its two electron-oxidized form, dehydroascorbic acid. Intracellular dehydroascorbic acid is rapidly reduced to ascorbate by GSH in a direct chemical reaction, or indirectly with the concurrent action of glutaredoxin and thioredoxin reductases. Intracellular ascorbate can spare, and possibly recycle, alpha distocopherol in the erythrocyte membrane. In turn, alpha tocopherol protects the cell membrane from lipid peroxidation. The ability of erythrocytes to recycle ascorbate, coupled with the ability of ascorbate to protect alpha tocopherol in the cell membrane and in lipoproteins, provides a potentially important mechanism for preventing lipid peroxidative damage secondary to hypoxia or hypoxia-reoxygenation events [40].

We acknowledge limitations of our study. First, the number of subjects included is limited and some of the blood samples during BAS were not collected. We would like to stress the stringent inclusion criteria applied during patient recruitment and the low incidence of the condition. The present data provides evidence to justify large multi-center efforts for validating the current findings. Finally, we lack a control group of healthy infants for obvious ethical reasons.

5. Conclusions

In summary, this is a comprehensive metabolomic assessment of neonates with TGA. The results obtained suggest differences in oxygen supply and consumption in cerebral tissue during hypoxia and near-normoxia. The number of patients is limited, but the combined assessment of lipid peroxidation biomarkers and untargeted metabolomic screening of a cohort of infants with TGA undergoing BAS provides insightful information to understand the physiopathology of this complex disease. The metabolic switch after BAS causes oxidative stress. However, oxidative stress may at least be partially neutralized by the induction of different metabolic pathways but especially the PPP that supplies with reductive electrons. From a clinical point of view, although supplemental arterial oxygenation has limited effects on oxygenation in parallel circulation, our results suggest potential benefits of avoiding hyperoxia in patients undergoing BAS to prevent from attenuating the antioxidant effect inherent to the metabolic switch after septostomy.

Author Contributions: Conceptualization, O.R., M.V., and J.K.; Methodology, G.Q., J.K., O.R., and S.A.; Software, G.Q.; Validation, J.D.P.-R., G.Q., and J.K.; Formal Analysis, J.K., and J.D.P.-R.; Investigation, J.D.P.-R., G.Q., V.K., J.P., O.P.-A., and P.R.; Resources, M.V., G.Q., and J.K.; Data Curation, G.Q., J.D.P.-R.; Writing—Original Draft Preparation, M.V., and J.K.; Writing—Review & Editing, J.D.P.-R.; Visualization, J.D.P.-R., and J.K.; Supervision, S.A., M.V., and J.K.; Project Administration, S.A., M.V., and J.K.; Funding Acquisition, S.A., M.V., and J.K. All authors have read and agreed to the published version of the manuscript.

Funding: This research was funded by Instituto de Salud Carlos III [CP16/00034, PI17/00127, and PI20/00964], the RETICS funded by the PN 2018–2021 (Spain), ISCIII-Sub-Directorate General for Research Assessment and Promotion and the European Regional Development Fund (FEDER) [RD16/0022]; and the Foundation for Pediatric Research in Finland and Special Governmental Subsidy for Clinical Research.

Institutional Review Board Statement: The study was conducted according to the guidelines of the Declaration of Helsinki and approved by the Ethics Committee of Helsinki University Hospital (HUS §59/2015). The ethical approval number of the project is 123/13/03/03/2015.

Informed Consent Statement: Informed consent was obtained from all subjects involved in the study.

Data Availability Statement: Metabolomics data are available on Zenodo (https://zenodo.org/record/4495124#.YBpwoC1DkWp (2 February 2021)).

Acknowledgments: The authors would like to express their gratitude to the babies and their parents who enrolled their infants and gave their consent for this study.

Conflicts of Interest: The authors declare no conflict of interest.

References

1. Van der Linde, D.; Konings, E.E.M.; Slager, M.A.; Witsenburg, M.; Helbing, W.A.; Takkenberg, J.J.M.; Roos-Hesselink, J.W. Birth Prevalence of Congenital Heart Disease Worldwide: A Systematic Review and Meta-Analysis. *J. Am. Coll. Cardiol.* **2011**, *58*, 2241–2247. [CrossRef] [PubMed]
2. Bellinger, D.C.; Wypij, D.; Rivkin, M.J.; DeMaso, D.R.; Robertson, R.L.; Dunbar-Masterson, C.; Rappaport, L.A.; Wernovsky, G.; Jonas, R.A.; Newburger, J.W. Adolescents with D-Transposition of the Great Arteries Corrected with the Arterial Switch Procedure: Neuropsychological Assessment and Structural Brain Imaging. *Circulation* **2011**, *124*, 1361–1369. [CrossRef] [PubMed]
3. Lim, J.M.; Kingdom, T.; Saini, B.; Chau, V.; Post, M.; Blaser, S.; Macgowan, C.; Miller, S.P.; Seed, M. Cerebral Oxygen Delivery Is Reduced in Newborns with Congenital Heart Disease. *J. Thorac. Cardiovasc. Surg.* **2016**, *152*, 1095–1103. [CrossRef] [PubMed]
4. Sun, L.; Macgowan, C.K.; Sled, J.G.; Yoo, S.-J.; Manlhiot, C.; Porayette, P.; Grosse-Wortmann, L.; Jaeggi, E.; McCrindle, B.W.; Kingdom, J.; et al. Reduced Fetal Cerebral Oxygen Consumption Is Associated with Smaller Brain Size in Fetuses With Congenital Heart Disease. *Circulation* **2015**, *131*, 1313–1323. [CrossRef]
5. Park, I.S.; Yoon, S.Y.; Min, J.Y.; Kim, Y.H.; Ko, J.K.; Kim, K.S.; Seo, D.M.; Lee, J.H. Metabolic Alterations and Neurodevelopmental Outcome of Infants with Transposition of the Great Arteries. *Pediatr. Cardiol.* **2006**, *27*, 569–576. [CrossRef]
6. Van der Laan, M.E.; Verhagen, E.A.; Bos, A.F.; Berger, R.M.F.; Kooi, E.M.W. Effect of Balloon Atrial Septostomy on Cerebral Oxygenation in Neonates with Transposition of the Great Arteries. *Pediatr. Res.* **2013**, *73*, 62–67. [CrossRef]
7. Mukherjee, D.; Lindsay, M.; Zhang, Y.; Lardaro, T.; Osen, H.; Chang, D.C.; Brenner, J.I.; Abdullah, F. Analysis of 8681 Neonates with Transposition of the Great Arteries: Outcomes with and without Rashkind Balloon Atrial Septostomy. *Cardiol. Young* **2010**, *20*, 373–380. [CrossRef]
8. Hiremath, G.; Natarajan, G.; Math, D.; Aggarwal, S. Impact of Balloon Atrial Septostomy in Neonates with Transposition of Great Arteries. *J. Perinatol.* **2011**, *31*, 494–499. [CrossRef]
9. Hypoxic-Ischemic Encephalopathy: A Review for the Clinician | Cerebrovascular Disease | JAMA Pediatrics | JAMA Network. Available online: https://jamanetwork.com/journals/jamapediatrics/fullarticle/2118582 (accessed on 13 July 2020).
10. Terraneo, L.; Samaja, M. Comparative Response of Brain to Chronic Hypoxia and Hyperoxia. *Int. J. Mol. Sci* **2017**, *18*, 1914. [CrossRef]
11. Torres-Cuevas, I.; Parra-Llorca, A.; Sánchez-Illana, A.; Nuñez-Ramiro, A.; Kuligowski, J.; Cháfer-Pericás, C.; Cernada, M.; Escobar, J.; Vento, M. Oxygen and Oxidative Stress in the Perinatal Period. *Redox Biol.* **2017**, *12*, 674–681. [CrossRef]
12. Redox Signaling during Hypoxia in Mammalian Cells | Elsevier Enhanced Reader. Available online: https://reader.elsevier.com/reader/sd/pii/S2213231717302355?token=9F2B800D98BB8EAC354ADDF5283F82835DF2689AA00C41C7A45BC70C1B1C24E5567F1645B0354F153F5ECD84CE7FAF8E (accessed on 13 July 2020).
13. Piñeiro-Ramos, J.D.; Núñez-Ramiro, A.; Llorens-Salvador, R.; Parra-Llorca, A.; Sánchez-Illana, Á.; Quintás, G.; Boronat-González, N.; Martínez-Rodilla, J.; Kuligowski, J.; Vento, M.; et al. Metabolic Phenotypes of Hypoxic-Ischemic Encephalopathy with Normal vs. Pathologic Magnetic Resonance Imaging Outcomes. *Metabolites* **2020**, *10*, 109. [CrossRef]
14. Wu, T.-W.; Tamrazi, B.; Hsu, K.-H.; Ho, E.; Reitman, A.J.; Borzage, M.; Blüml, S.; Wisnowski, J.L. Cerebral Lactate Concentration in Neonatal Hypoxic-Ischemic Encephalopathy: In Relation to Time, Characteristic of Injury, and Serum Lactate Concentration. *Front. Neurol.* **2018**, *9*, 293. [CrossRef]
15. Fanos, V.; Pintus, R.; Dessì, A. Clinical Metabolomics in Neonatology: From Metabolites to Diseases. *NEO* **2018**, *113*, 406–413. [CrossRef] [PubMed]
16. Sánchez-Illana, Á.; Thayyil, S.; Montaldo, P.; Jenkins, D.; Quintás, G.; Oger, C.; Galano, J.-M.; Vigor, C.; Durand, T.; Vento, M.; et al. Novel Free-Radical Mediated Lipid Peroxidation Biomarkers in Newborn Plasma. *Anal. Chim. Acta* **2017**, *996*, 88–97. [CrossRef] [PubMed]
17. Sánchez-Illana, Á.; Shah, V.; Piñeiro-Ramos, J.D.; Di Fiore, J.M.; Quintás, G.; Raffay, T.M.; MacFarlane, P.M.; Martin, R.J.; Kuligowski, J. Adrenic Acid Non-Enzymatic Peroxidation Products in Biofluids of Moderate Preterm Infants. *Free Radic. Biol. Med.* **2019**, *142*, 107–112. [CrossRef]
18. Broadhurst, D.; Goodacre, R.; Reinke, S.N.; Kuligowski, J.; Wilson, I.D.; Lewis, M.R.; Dunn, W.B. Guidelines and Considerations for the Use of System Suitability and Quality Control Samples in Mass Spectrometry Assays Applied in Untargeted Clinical Metabolomic Studies. *Metabolomics* **2018**, *14*, 1–17. [CrossRef] [PubMed]
19. Kessner, D.; Chambers, M.; Burke, R.; Agus, D.; Mallick, P. ProteoWizard: Open Source Software for Rapid Proteomics Tools Development. *Bioinformatics* **2008**, *24*, 2534–2536. [CrossRef]

20. Smith, C.A.; Want, E.J.; O'Maille, G.; Abagyan, R.; Siuzdak, G. XCMS: Processing Mass Spectrometry Data for Metabolite Profiling Using Nonlinear Peak Alignment, Matching, and Identification. *Anal. Chem.* **2006**, *78*, 779–787. [CrossRef]
21. Benton, H.P.; Want, E.J.; Ebbels, T.M.D. Correction of Mass Calibration Gaps in Liquid Chromatography-Mass Spectrometry Metabolomics Data. *Bioinformatics* **2010**, *26*, 2488–2489. [CrossRef]
22. Tautenhahn, R.; Böttcher, C.; Neumann, S. Highly Sensitive Feature Detection for High Resolution LC/MS. *BMC Bioinform.* **2008**, *9*, 504. [CrossRef]
23. Kuhl, C.; Tautenhahn, R.; Böttcher, C.; Larson, T.R.; Neumann, S. CAMERA: An Integrated Strategy for Compound Spectra Extraction and Annotation of Liquid Chromatography/Mass Spectrometry Data Sets. *Anal. Chem.* **2012**, *84*, 283–289. [CrossRef]
24. Sánchez-Illana, Á.; Piñeiro-Ramos, J.D.; Sanjuan-Herráez, J.D.; Vento, M.; Quintás, G.; Kuligowski, J. Evaluation of Batch Effect Elimination Using Quality Control Replicates in LC-MS Metabolite Profiling. *Anal. Chim. Acta* **2018**, *1019*, 38–48. [CrossRef]
25. Quintás, G.; Sánchez-Illana, Á.; Piñeiro-Ramos, J.D.; Kuligowski, J. Chapter Six-Data Quality Assessment in Untargeted LC-MS Metabolomics. In *Comprehensive Analytical Chemistry*; Jaumot, J., Bedia, C., Tauler, R., Eds.; Data Analysis for Omic Sciences: Methods and Applications; Elsevier: Amsterdam, The Netherlands, 2018; Volume 82, pp. 137–164.
26. Kuligowski, J.; Sánchez-Illana, Á.; Sanjuán-Herráez, D.; Vento, M.; Quintás, G. Intra-Batch Effect Correction in Liquid Chromatography-Mass Spectrometry Using Quality Control Samples and Support Vector Regression (QC-SVRC). *Analyst* **2015**, *140*, 7810–7817. [CrossRef]
27. Chang, C.-C.; Lin, C.-J. LIBSVM: A Library for Support Vector Machines. *ACM Trans. Intell. Syst. Technol.* **2011**, *2*, 1–27. [CrossRef]
28. Chong, J.; Soufan, O.; Li, C.; Caraus, I.; Li, S.; Bourque, G.; Wishart, D.S.; Xia, J. MetaboAnalyst 4.0: Towards More Transparent and Integrative Metabolomics Analysis. *Nucleic Acids Res.* **2018**, *46*, W486–W494. [CrossRef]
29. Chouchani, E.T.; Pell, V.R.; Gaude, E.; Aksentijević, D.; Sundier, S.Y.; Robb, E.L.; Logan, A.; Nadtochiy, S.M.; Ord, E.N.J.; Smith, A.C.; et al. Ischaemic Accumulation of Succinate Controls Reperfusion Injury through Mitochondrial ROS. *Nature* **2014**, *515*, 431–435. [CrossRef]
30. Johnston, M.V.; Trescher, W.H.; Ishida, A.; Nakajima, W. Neurobiology of Hypoxic-Ischemic Injury in the Developing Brain. *Pediatr. Res.* **2001**, *49*, 735–741. [CrossRef]
31. Fatemi, A.; Wilson, M.A.; Johnston, M.V. Hypoxic-Ischemic Encephalopathy in the Term Infant. *Clin. Perinatol.* **2009**, *36*, 835–858. [CrossRef]
32. Teshima, Y.; Akao, M.; Li, R.A.; Chong, T.H.; Baumgartner, W.A.; Johnston, M.V.; Marbán, E. Mitochondrial ATP-Sensitive Potassium Channel Activation Protects Cerebellar Granule Neurons from Apoptosis Induced by Oxidative Stress. *Stroke* **2003**, *34*, 1796–1802. [CrossRef]
33. Millán, I.; Piñero-Ramos, J.D.; Lara, I.; Parra-Llorca, A.; Torres-Cuevas, I.; Vento, M. Oxidative Stress in the Newborn Period: Useful Biomarkers in the Clinical Setting. *Antioxidants* **2018**, *7*, 193. [CrossRef]
34. Stincone, A.; Prigione, A.; Cramer, T.; Wamelink, M.M.C.; Campbell, K.; Cheung, E.; Olin-Sandoval, V.; Grüning, N.-M.; Krüger, A.; Tauqeer Alam, M.; et al. The Return of Metabolism: Biochemistry and Physiology of the Pentose Phosphate Pathway. *Biol. Rev. Camb Philos Soc.* **2015**, *90*, 927–963. [CrossRef]
35. Brekke, E.M.; Morken, T.S.; Widerøe, M.; Håberg, A.K.; Brubakk, A.-M.; Sonnewald, U. The Pentose Phosphate Pathway and Pyruvate Carboxylation after Neonatal Hypoxic-Ischemic Brain Injury. *Biol. Rev.* **2014**, *34*, 724–734. [CrossRef]
36. Kuehne, A.; Emmert, H.; Soehle, J.; Winnefeld, M.; Fischer, F.; Wenck, H.; Gallinat, S.; Terstegen, L.; Lucius, R.; Hildebrand, J.; et al. Acute Activation of Oxidative Pentose Phosphate Pathway as First-Line Response to Oxidative Stress in Human Skin Cells. *Mol. Cell* **2015**, *59*, 359–371. [CrossRef]
37. Ralser, M.; Wamelink, M.M.; Kowald, A.; Gerisch, B.; Heeren, G.; Struys, E.A.; Klipp, E.; Jakobs, C.; Breitenbach, M.; Lehrach, H.; et al. Dynamic Rerouting of the Carbohydrate Flux Is Key to Counteracting Oxidative Stress. *J. Biol.* **2007**, *6*, 10. [CrossRef] [PubMed]
38. Wang, Y.-P.; Zhou, L.-S.; Zhao, Y.-Z.; Wang, S.-W.; Chen, L.-L.; Liu, L.-X.; Ling, Z.-Q.; Hu, F.-J.; Sun, Y.-P.; Zhang, J.-Y.; et al. Regulation of G6PD Acetylation by SIRT2 and KAT9 Modulates NADPH Homeostasis and Cell Survival during Oxidative Stress. *EMBO J.* **2014**, *33*, 1304–1320. [CrossRef]
39. Akram, M.; Shah, S.M.A.; Munir, N.; Daniyal, M.; Tahir, I.M.; Mahmood, Z.; Irshad, M.; Akhlaq, M.; Sultana, S.; Zainab, R. Hexose Monophosphate Shunt, the Role of Its Metabolites and Associated Disorders: A Review. *J. Cell. Physiol.* **2019**, *234*, 14473–14482. [CrossRef] [PubMed]
40. Vissers, M.C.M.; Das, A.B. Potential Mechanisms of Action for Vitamin C in Cancer: Reviewing the Evidence. *Front. Physiol.* **2018**, *9*, 809. [CrossRef] [PubMed]

9. Appendices

9.1 Information of the articles included in the compendium

9.1.1 Article 1

Metabolic Phenotypes of Hypoxic-Ischemic Encephalopathy with Normal vs. Pathologic Magnetic Resonance Imaging Outcomes. Piñeiro-Ramos JD, Núñez-Ramiro A, Llorens-Salvador R, Parra-Llorca A, Sánchez-Illana Á, Quintás G, Boronat-González N, Martinez Rodilla J, Kuligowski J, Vento M, The Hypotop Study Group. **Metabolites**. 2020 Mar 14;13(3):109. doi10.3390/metabo10030109.

9.1.2 Article 2

Noninvasive monitoring of evolving urinary metabolic patterns in neonatal encephalopathy. Piñeiro-Ramos JD, Núñez-Ramiro A, López-Gonzálvez Á, Solar-García A, Albiach-Delgado A, Martinez Rodilla J, Llorens-Salvador R, Sanjuan-Herraez D, Quintás G, Barbas C, Kuligowski J, Vento M, The Hypotop Study Group. **Pediatric Research.** 2021 May 5. doi: 10.1038/s41390-021-01553-z.

9.1.3 Article 3

Targeted Metabolomics data and miRNA-seq assessment from HIE newborns during hypothermia treatment. In progress.

9.1.4 Article 4

Effect of donor human milk on host-gut microbiota and metabolic interactions in preterm infants. Piñeiro-Ramos JD, Parra-Llorca A, Ten-Doménech I, Gormaz M, Ramón-Beltrán A, Cernada M, Quintás G, Collado MC, Kuligowski J, Vento M. **Clinical Nutrition**. 2021 Mar; 40(3):1296-1309. doi: 10.1016/j.clnu.2020.08.013.

9.1.5 Article 5

A reductive metabolic switch protects infants with transposition of great arteries undergoing atrial septostomy against oxidative stress. Piñeiro-Ramos JD, Rahkonen O, Korpioja V, Quintás G, Pihkala J, Pitkänen-Argillander O, Rautiainen P, Andersson S, Kuligowski J, Vento. **Antioxidants**. 2021 Sep 22:10(10):1502. doi: 10.3390/antiox10101502.

9.2 Articles published by the doctoral candidate not included in the compendium but directly associated with the present doctoral thesis

9.2.1 Scientific articles

Evaluation of batch effect elimination using quality control replicates in LC-MS metabolite profiling. Sánchez-Illana Á, Piñeiro-Ramos JD, Sanjuan-Herráez JD, Vento M, Quintás G, Kuligowski J. **Analytica Chimica Acta**. 2018 Aug 17; 1019-48. doi: 10.1016/j.aca.2018.02.053.

Adrenic acid non-enzymatic peroxidation products in biofluids of moderate preterm infants. Sánchez-Illana Á, Shah V, Piñeiro Ramos JD, Di Fiore JM, Quintás G, Raffay TM, MacFarlane PM, Martin RJ, Kuligowski J. **Free Radical Biology Medicine.** 2019 Oct;142:107 112. doi: 10.1016/j.freeradbiomed.2019.02.024. Epub 2019 Feb 25.

Does Pasteurized Donor Human Milk Efficiently Protect Preterm Infants Against Oxidative Stress? Parra-Llorca A, Gormaz M, Sánchez-Illana Á, Piñeiro-Ramos JD, Collado MC, Serna E, Cernada M, Nuñez-Ramiro A, Ramón-Beltrán A, Oger C, Galano JM, Vigor C, Durand T, Kuligowski J, Vento M. **Antioxidant Redox Signal**. 2019 Oct 10;31(11):791-799. doi: 10.1089/ars.2019.7821.

Current Practice in Untargeted Human Milk Metabolomics. Ten-Doménech I, Ramos-Garcia V, Piñeiro-Ramos JD, Gormaz M, Parra-Llorca A, Vento M, Kuligowski J, Quintás G. **Metabolites**. 2020 Jan 22;10(2):43. doi: 10.3390/metabo10020043.

Small molecule biomarkers for neonatal hypoxic ischemic encephalopathy. Sánchez-Illana Á, Piñeiro-Ramos JD, Kuligowski J. **Seminars in Fetal & Neonatal Medicine**. 2020 Apr;25(2):101084. doi: 10.1016/j.siny.2020.101084.

The Relationship between Oxidative Stress, Intermittent Hypoxemia, and Hospital Duration in Moderate Preterm Infants. Shah VP, Raffay Tm, Martin RJ, Vento M, Sánchez-Illana Á, Piñeiro-Ramos JD, Kuligowski J, Di Fiore JM. **Neonatology**. 2020;117(5):577-583. doi: 10.1159/000509038.

Oxidative stress biomarkers in the preterm infant. Sánchez-Illana Á, Piñeiro-Ramos JD, Ramos-Garcia V, Ten-Doménech I, Vento M, Kuligowski J. **Advances in Clinical Chemistry**. 2021;102:127-189. doi: 10.1016/bs.acc.2020.08.011.

Do Levels of Lipid Peroxidation Biomarkers Reflect the Degree of Brain Injury in Newborns? Mari Merce Cascant Vilaplana, Ángel Sánchez-Illana, José David Piñeiro-Ramos, Roberto Llorens-Salvador. Guillermo Quintás, Camille Oger, Jean-Marie Galano, Claire Vigor, Thierry Durand, Julia Kuligowski, Máximo Vento, HYPOTOP Study Group. **Antioxid Redox Signal**. 2021 Dec 10;35 (17):1467-1475. Doi:10.1089/ars.2021.0168.

9.2.2 Congress communications

Evolution of phospholipid synthesis related biomarkers in newborns with hypoxic ischemic encephalopathy, **poster, MetaboMeeting.** 11. – 13.12.2017, Birmingham, United Kingdom.

Metabolomic profile alterations of newborn with hypoxic-ischemic encephalopathy with pathologic cerebral magnetic resonance imaging outcomes, **comunicación oral, III Congreso Nacional de Jóvenes Investigadores en Biomedicina.** 24. – 26.04.2019, Valencia, Spain.

Urinary metabolomic profile of preterm infants fed with own mother's milk and donated human milk, **poster, II Congreso Nacional de Jóvenes Investigadores en Biomedicina.** 23. – 24.11.2017, Valencia, Spain.

Perfil metabólico urinario del recién nacido premature alimentado con leche maternal o leche materna donada, **comunicación oral, VI Congreso de Investigación Biomédica.** 7. – 9.02.2018

Effect of nutrition on host-gut microbiota metabolic interactions of preterm infants fed with own mother's milk and donated mother milk, **poster, Metabolomics.** 23. – 27.06.2019, The Hague, The Netherlands.

Effect of donor human milk on host-gut microbiota and metabolic interactions in preterm infants, **comunicación oral, V Jornada Nacional de Neonatología.** 15.10.2020, reunión virtual.

Metabolic switch of infants with congenital heart defect undergoing atrial septostomy, **poster, Metabolomics.** 27. – 29.10.2020.

9.3 Other scientific contributions authored by the doctoral candidate published during the development of the present doctoral

9.3.1 Scientific articles

On-Capillary Surface-Enhanced Raman Spectroscopy: Determination of Glutathione in Whole Blood Microsamples. Sánchez-Illana Á, Mayr F, Cuesta-García D, Piñeiro-Ramos JD, Cantareo A, Guardia M, Vento M, Lendl B, Quintás G, Kuligowski J. **Analytical Chemistry**. 2018 Aug 7;90(15):9093-9100. doi: 10.1021/acs.analchem.8b01492.

Fetal chronic hypoxia and oxidative stress in diabetic pregnancy. Could fetal erythropoietin improve offspring outcomes? Teramo K, Piñeiro-Ramos JD. **Free Radical Biology Medicine.** 2019 Oct;142:32-37. doi: 10.1016/j.freeradbiomed.2019.03.012. Epub 2019 Mar 18.

Protein Oxidation Biomarkers and Myeloperoxidase Activation in Cerebrospianl Fluid in Childhood Bacterial Meningitis. Rugemalira E, Roine I, Kuligowski J, Sánchez-Illana Á, Piñeiro-Ramos JD, Andersson S, Peltola H, Leite Cruzeiro M, Pelkonen T, Vento M. **Antioxidants**. 2019 Oct 1;8(10):441. doi: 10.3390/antiox8100441.

Effect of a Marathon on Skin Temperature Response After a Cold-Stress Test and Its Relationship With Perceptive, Performance, and Oxidative-Stress Biomarkers. Priego-Quesada JI. Pérez-Guarner A, Gandia-Soriano A, Oficial-Casado F, Galindo C, Cibrián Ortiz de Anda RM, Piñeiro-Ramos JD, Sánchez-Illana Á, Kuligowski J, Gomes Barbosa MA, Vento M, Salvador Palmer R. **International Journal of Sports**

Physiology and Performance. 2020 May 29;15(10):1467-1475. doi: 10.1123/ijspp.2019-0963.

Transcriptome profiles discriminate between Gram-positive and Gram-negative sepsis in preterm neonates. Cernada M, Pinilla-González A, Kuligowski J, Morales JM, Lorente-Pozo S, Piñeiro-Ramos JD, Parra-Llorca A, Lara-Cantón I, Vento M, Serna E. **Pediatric Research**. 2021 Mar 25. doi: 10.1038/s41390-021-01444-3.

High Oxygen Does Not Increase Reperfusion Injury Assessed with Lipid Peroxidation Biomarkers after Cardiac Arrest: A Post Hoc Analysis of The COMACARE Trial. Humaloja J, Vento M, Kuligowski J, Andersson S, Piñeiro-Ramos JD, Sánchez-Illana Á, Litonius E, Jakkula P, Hästbacka J, Bendel S, Tiainen M, Reinikainen, Skrifvars MB. **J Clin Med. 2021** Sep 17;10(18):4226. Doi:10.3390/jcm10184226.

Early molecular markers of ventilator-associated pneumonia in bronchalveolar lavage in preterm infants. Pinilla-Gonzalez A, Lara-Cantón I, Torrejón-Rodriguez L, Parra-Llorca A, Aguar M, Kuligowski J, Piñeiro-Ramos JD, Sánchez-Illana Á, Navarro AG, Vento M, Cernada M. **Pediatr Res**. 2022 Sep 7:1-7. Doi: 10.1038/s41390-022-02271-w.

9.4 Funding

Research employment contract within the project “Minimal invasive biomarkers for the personalized treatment of neonatal Hypoxic-Ischemic Encephalopathy (HIE)” Ref. CP16/00034. Instituto Carlos III. Duration: March 2017 – March 2020.

Research employment contract within the project “Fact-based personalized nutrition for the young (NUTRISHIELD)” Ref. 818110 (H2020-SFS-2018-IA). Duration March 2020 – September 2021.

9.5 Ethics committee approval

GENERALITAT VALENCIANA
CONSELLERIA DE SANITAT

AGÈNCIA VALENCIANA DE SALUT

La Fe
DEPARTAMENT DE SALUT

DICTAMEN DEL COMITÉ ÉTICO DE INVESTIGACIÓN CLÍNICA

Don Serafín Rodríguez Capellán, Secretario del Comité Ético de Investigación Clínica del **Hospital Universitario La Fe,**

CERTIFICA

Que este Comité, actuando en calidad de CEIC de referencia, ha evaluado en su sesión de fecha 06/03/2012, la propuesta del promotor para que se realice el estudio:

Nº EUDRACT: **2011-005696-17**
Código de protocolo del promotor: **1645-CI-058**
Versión/fecha del protocolo: **2.0/ 17/01/2012**
Hoja de información al paciente/sujeto (versión/fecha): 2.0/ 10/01/2012 PARA PADRES/TUTORES
Título: **Multicenter, randomized, blinded clinical study comparing early use of total body moderate hypothermia plus topiramate or placebo in asphyxiated newborn infants evolving to moderate-to-severe hypoxic ischemic encephalopathy.**
ENSAYO CLÍNICO, MULTICÉNTRICO ALEATORIZADO Y ENMASCARADO (CIEGO) CON TOPIRAMATO VERSUS PLACEBO PARA EL TRATAMIENTO DE RECIÉN NACIDOS CON ASFIXIA PERINATAL TRATADOS CON HIPOTERMIA MODERADA CORPORAL TOTAL
Promotor: **Instituto de Investigacion Sanitaria La Fe**

Que tomando en consideración las siguientes cuestiones:

- La pertinencia del estudio, teniendo en cuenta el conocimiento disponible, así como los requisitos del Real Decreto 223/2004, de 6 de febrero y las normas que lo desarrollan.
- Los requisitos necesarios de idoneidad del protocolo en relación con los objetivos del estudio, justificación de los riesgos y molestias previsibles para el sujeto, así como los beneficios esperados.
- El seguro o la garantía financiera previstos.
- El procedimiento para obtener el consentimiento informado, incluyendo la hoja de información para los sujetos, el plan de reclutamiento de sujetos y las compensaciones previstas para los sujetos por daños que pudieran derivarse de su participación en el ensayo.
- El alcance de las compensaciones económicas previstas y su posible interferencia con el respeto a los postulados éticos.

Y habiendo tenido en cuenta los informes recibidos de los CEIC implicados, emite un **DICTAMEN FAVORABLE** para la realización de dicho ensayo en España en los centros que se relacionan a continuación:

Hospital Universitario La Fe con el Dr. Maximo Vento Torres
Hospital Universitario La Paz con la Dra. Eva Valverde Nuñez
Hospital General De Asturias con el Dr. José López Sastre
Hospital De Cruces con el Dr. Adolfo Valls i Soler
Hospital Virgen Del Rocio con el Dr. Antonio Losada
Hospitals Vall D'Hebron con el Dr. Hector Boix Alonso
Hospital Universitario 12 De Octubre con la Dra. Mª Teresa Moral
Hospital Materno Infantil De Málaga con la Dra. Mª Mercedes Chaffanel Peláez
Hospital Reina Sofía con la Dra. Juana Guzman Cabañas

Que el CEIC del **Hospital Clínico Universitario de Valencia**, ha emitido un **dictamen desfavorable**, por lo que este estudio no se realizará en dicho hospital.

Que en dicha reunión se cumplieron los requisitos establecidos en la legislación vigente (Real Decreto 223/2004) para que la decisión del citado CEIC sea válida.

Instituto de Investigación Sanitaria La Fe

Instituto de Investigación Sanitaria La Fe
SALIDA
15 ENE. 2020
Nº 0020

Dra. Julia Kuligowski
Servicio de Perinatología

Valencia, 27 de diciembre de 2019.

Asunto: Autorización inicio de estudio.

Adjunto le remito copia de los Informes Científico y Ético de Investigación, en el que se acuerda informar **favorablemente** sobre el Proyecto de Investigación titulado *"Nutrición personalizada del niño prematuro (Personalized nutrition for the preterm infant)"*, por usted presentado.

A la vista de los dictámenes emitidos, dicho Proyecto, puede iniciarse y llevarse a cabo.

Atentamente,

Instituto de Investigación Sanitaria La Fe

Dr. Máximo Vento Torres
Director Científico

IIS La Fe | Avenida Fernando Abril Martorell, nº 106, Torre A, 7ª. 46026 Valencia
Tel.: (+34) 96 124 66 01 | Fax: (+34) 96 124 66 20 | info@iislafe.es | www.iislafe.es